The ribosomal RNA processing gene *nucleolar protein 9* (*nol9*) is essential for normal exocrine pancreas development in zebrafish

LAURE K.K.J. LAM HUNG

DOWNING COLLEGE

This work is submitted for the degree of Doctor of Philosophy

September 2013

Abstract

The ribosomal RNA processing gene *nucleolar protein 9* (*nol9*) is essential for normal exocrine pancreas development in zebrafish

Laure K.K.J. Lam Hung

Zebrafish are an excellent model organism for the study of development and disease, as they are amenable to genetic manipulation and imaging techniques. Genetic screens in zebrafish have identified several mutations in genes involved in pancreas development and research of these mutants has furthered our knowledge of pancreatic disorders and syndromes. A zebrafish mutant in *nucleolar protein 9* (*nol9*) gene, *nol9*^{sa1022}, was found to be associated with a pancreas phenotype in the Zebrafish Mutation Project (ZMP). The main aim of this thesis is to determine the role of *nol9* in pancreas development by studying the *nol9*^{sa1022} mutant. This study has demonstrated that the function of Nol9 is conserved between zebrafish and human. The characterisation of *nol9*^{sa1022} mutants revealed that the pancreas, liver and intestine failed to develop normally after 3 days post fertilisation and this was due to impaired cell proliferation for the exocrine pancreas. The development of the endocrine pancreas and all the other organs appeared unaffected. Interestingly, *las1l*^{sa674}, a zebrafish mutant allele of a Nol9-interacting protein with similar function, was also found to exhibit digestive organ defects. Although an up-regulation of Tp53-signalling pathway genes were detected through mRNA expression analysis of *nol9*^{sa1022} mutant, loss of function of Tp53 did not suppress the pancreatic defects suggesting the involvement of a Tp53-independent mechanism. To gain insight into the underlying biology of the mutants, the mRNA expression profiles of four rRNA processing mutants *nol9*^{sa1022}, *las1l*^{sa674}, *tti*^{s450} and *set*^{s453} were compared. This analysis revealed that differentially expressed genes in all four mutants were enriched for ribosome- and translation-related terms, consistent with the known functions of these proteins. Overall, the findings presented here demonstrate that the *nol9*^{sa1022} mutant is an ideal *in vivo* model to study the roles of rRNA in cell proliferation and digestive organ development and can benefit the field of ribosomopathies.

Declaration

This dissertation is the result of my own work and includes nothing which is the outcome of work done in collaboration except where specifically indicated in the text. This dissertation does not exceed the word limit set by the Biology Degree Committee.

Laure Lam Hung,
September 2013

Acknowledgements

I am indebted to my two supervisors, Dr Derek Stemple and Dr Inês Barroso for their continuous support and guidance over these last four years. I am extremely grateful to the Wellcome Trust Sanger Institute for their generous funding and for giving me this unique opportunity. I would like to thank all the members of my two teams T31 and T35 especially Steve, John, Ian, Neha, Ewa, Jenn, Eve, Chris, Sebastian, Rachel and members of the RSF for their help. I am thankful to my family and friends, especially Rachel, Esthel, Emeline, Nathalie, Matante Amine, Madushi, Jenn, Eve, Haixi, Blanca, Neha, Ewa, Cat and Sheila for their endless encouragement. Finally I would like to dedicate this thesis to my parents whose unwavering love and support have made this journey possible.

Table of Contents

Chapter 1 Introduction

1.1 Pancreas

The pancreas derives its name from the Greek roots ‘pan’ and ‘creas’ meaning ‘all’ and ‘flesh’ respectively. It is composed of two morphologically and functionally distinct cell populations (Figure 1-1). The endocrine compartment consists of hormone-secreting cells that aggregate to form the islets of Langerhans that are associated with blood vessels, neurons and connective tissue. The endocrine islet is composed of α-, β-, δ-, ε- and PP-cells that secrete glucagon, insulin, somatostatin, ghrelin and pancreatic polypeptide respectively into the bloodstream to regulate glucose homeostasis and nutrient metabolism. The exocrine component comprises of acinar cells that form clusters at the end of pancreatic ducts. Acinar cells secrete enzymes including proteases, lipases and nucleases and duct cells actively secrete bicarbonate ions, mucins and transport digestive enzymes towards the dudodenum (Pan and Wright, 2011; Slack, 1995).

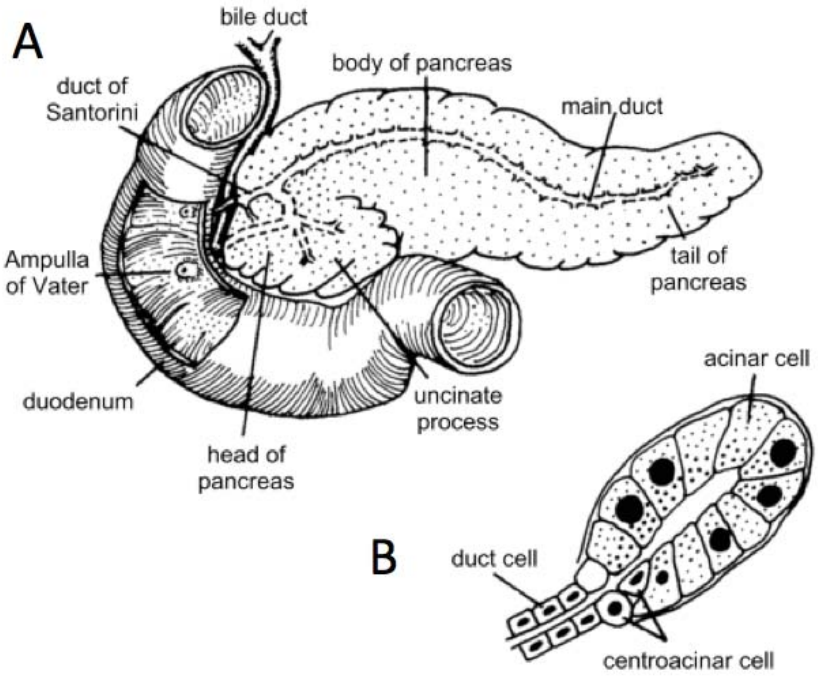

Figure 1-1 (A) Anatomy of the adult human pancreas, (B) Histology of a pancreatic acinus. Taken from Slack, 1995.

1.1.1 Pancreas development in humans

Most of the knowledge of pancreas development in mammals comes from studies in mice. However, human pancreas organogenesis largely resembles the process in the mouse. Pancreas formation starts with the regionalisation of the gut into distinct organ regions by a series of dorsoventral and anteroposterior patterning events. The endoderm evaginates forming the dorsal bud on the 26th day of gestation in humans (G26d) and approximately 9.5 days gestation in mice (E9.5). After 6 days in humans and approximately 12 hours in mice, the ventral bud emerges. The stalk region of the buds undergoes elongation while branching morphogenesis occur in the more apical region. As a consequence of gut rotation and dorsal bud elongation, the pancreatic buds come into contact and fuse at G37d to G42d in humans and E12 to E13 in mice. This causes the ducts of the ventral bud and the distal portion of the dorsal bud to fuse giving rise to the duct of Wirsung. The duct of the proximal portion of the dorsal bud remains as the duct of Santorini. Thereafter, the cellular architecture of the pancreas changes dramatically. A massive differentiation wave occurs and the three main pancreatic lineages are allocated. The number of endocrine cells particularly β-cells increases rapidly while acinar cell differentiation and rapid branching morphogenesis occur in the exocrine pancreas (Gittes, 2009; Pan and Wright, 2011).

1.1.2 Congenital disorders of the pancreas

Several congenital disorders and primary developmental anomalies of the pancreas have been described (Cano et al., 2007). They can be grouped into congenital developmental anomalies and primary malformations of the pancreas, congenital disorders with predominant secretory insufficiency, congenital disorders of pancreatic endocrine function and various other congenital diseases (Table 1-1). Since the zebrafish mutants that are being studied in this thesis show defects in development of the exocrine pancreas, I will describe the congenital disorders with predominant secretory insufficiency in more detail.

Entities	Genes
Developmental anomalies/malformations	
Pancreatic agenesis	*PDX1*/*IPF1*
Pancreatic and cerebellar agenesis	*PTF1A*
Pancreatic hypoplasia including congenital short pancreas	Unknown
Annular pancreas	Unknown
Pancreas divisum	Unknown
Pancreaticobiliary maljunction (common channel syndrome)	Unknown
Ectopic/heterotopic pancreas	Unknown
Congenital pancreatic cysts	
True pancreatic cysts	Unknown
Gastrointestinal duplication cysts	Unknown
Von Hippel-Lindau disease	*VHL*
Autosomal dominant polycystic kidney disease	*PKD1*, *PKD2*
Congenital secretory insufficiency	
Cystic fibrosis	*CFTR*
Shwachman-Diamond syndrome	*SBDS*
Johanson-Blizzard syndrome	*UBR1*
Pearson marrow-pancreas syndrome	mtDNA
Isolated enzyme deficiencies	*PRSS7*
Congenital disorders endocrine function	
Congenital hyperinsulinism and islet cell adenomatosis	*ABCC8*, *KCNJ11*, *GCK*, *HAD*, *INSR*, *GLUD1*
Transient neonatal diabetes mellitus	6q24 alterations, *ABCC8*
Permanent neonatal diabetes mellitus	*GCK*, *ABCC8*, *KCNJ11*
X-linked immunodysregulation, polyendocinopathy, and enteropathy syndrome	*FOXP3*
Miscellaneous	
Jeune syndrome	Unknown
Autosomal-recessive polycystic kidney disease	*PKHD1*
Beckwith-Wiedemann syndrome	11p15 alterations, *CDKN1C*, *H19*, *LIT1*
Renal-hepatic-pancreatic dysplasia	Unknown
Metabolic disorders	
Lipoprotein lipase deficiency	*LPL*
Apolipoprotein C-II deficiency	*APOC2*
Others	
Hereditary pancreatitis	*PRSS1*, (*SPINK1*)

Table 1-1 Congenital Pancreatic Disorders: Congenital developmental anomalies and primary malformations of the pancreas, congenital disorders with predominant secretory insufficiency, congenital disorders of pancreatic endocrine function and other congenital diseases affecting the pancreas and the genes mutated in the human disorder are shown. Taken from Cano et al., 2007.

1.1.2.1 Congenital disorders with predominant secretory insufficiency

Congenital disorders with predominant secretory insufficiency are rare and symptoms include loose and voluminous stools, excess fat in stools, abnormally low level of protein in the blood (hypoproteinemia) and failure to thrive. Exocrine pancreatic failure may manifest only after >90% of the exocrine cells are destroyed due to the high functional capacity of the exocrine pancreas (Stormon and Durie, 2002). Congenital pancreatic secretory insufficiency without diabetes results from either maturation defects or early-onset degeneration of acinar cells rather than an early developmental defect. In some conditions, the disease can progress to combined insufficiency of exocrine and endocrine pancreas.

Cystic fibrosis (CF; OMIM #219700) is the most common inherited cause of exocrine pancreatic insufficiency, with an incidence of approximately 1:2,500 (Roberts, 1990). The causative gene *cystic fibrosis transmembrane conductance regulator* (*CFTR)* was mapped by linkage analysis in the 1980s and encodes an epithelial chloride channel involved in electrolyte transport across epithelial cell membranes (Sheppard and Welsh, 1999). Only about 60% of CF patients have pancreatic insufficiency as newborns with most of the remaining patients losing pancreatic function over time (Waters et al., 1990). The pancreatic acinar tissue in CF is atrophic and pancreatic ducts are obstructed with secretory material. The basic pathogenesis is attributed to a progressive destruction of the pancreas possibly by viscous pancreatic secretions or other mechanisms (Freedman et al., 2000; Imrie et al., 1979).

Shwachman-Diamond syndrome (SDS; OMIM #260400) is the second most common cause of congenital exocrine pancreatic insufficiency, with an approximate incidence of 1:50,000 in the North American population (Cano et al., 2007; Narla and Ebert, 2010). It is an autosomal recessive ribosomopathy (Section 1.4.2), and in addition to the pancreatic defects, it is characterised by haematologic abnormalities most commonly an abnormally low number of neutrophils (neutropenia) and an increased risk of leukaemia. Other clinical features include short stature, skeletal abnormalities, a decrease in the number of red blood cells or a lower level of haemoglobin in blood (anaemia) and a relative decrease in number of platelets in blood (thrombocytopenia). Most SDS infants present signs and symptoms of exocrine pancreatic dysfunction which improves with age, with about 40-60% of patients no longer requiring enzyme supplements due to an improvement in digestive enzyme production (Mack et al., 1996). However, based on quantitative intubation techniques almost all SDS patients display a degree of exocrine pancreatic dysfunction (Ip et al., 2002). The SDS pancreas has

normal islets, ductal architecture and secretory function, but with few or no acinar cells and shows extensive fatty replacement (Cipolli, 2001; Jones et al., 1994). The pathogenesis of the exocrine defects is unknown but it is believed that the pancreatic acini either fail to mature properly or undergo very early degeneration rather than secondary acinar cell atrophy (Cipolli, 2001).

Linkage analysis of families with SDS revealed a disease-associated interval at 7q11 (Goobie et al., 2001; Popovic et al., 2002). Boocock *et al.* identified causal mutations in the gene *Shwachman-Bodian-Diamond syndrome* (*SBDS*) in that candidate region and these explain up to 90% of the cases. In addition, 75% of these mutations result from a gene conversion with *SBDSP,* an adjacent pseudogene that shares 97% homology with *SBDS* (Boocock et al., 2003). The SBDS protein is required for late cytoplasmic maturation of 60S ribosomal subunits and translational activation of ribosomes (Finch et al., 2011; Menne et al., 2007; Wong et al., 2011b). In mammalian cells, SBDS and elongation factor like 1 (EFL1) catalyse the removal of the assembly factor eukaryotic initiation factor 6 (eIF6) from late cytoplasmic pre-60S ribosomal subunits (Finch et al., 2011). Loss of *Sbds* in mice leads to early embryonic lethality (Zhang et al., 2006) whilst knockdown of *sbds* in zebrafish recapitulates the human phenotype: exocrine pancreatic insufficiency, neutropenia and skeletal defects (Provost et al., 2012).

Johanson-Blizzard syndrome (JBS; OMIM #243800) is a rare autosomal recessive disorder with an estimated incidence of 1:250,000 (Zenker et al., 2005). It is characterised by congenital pancreatic exocrine insufficiency and a typical facial appearance distinguished by absence or underdevelopment of the nasal wings. Short stature, scalp defects, deafness, absence of several permanent teeth (oligodontia), hypothyroidism, anorectal malformations and mental retardation may also be present (Al-Dosari et al., 2008). The pancreas of JBS infants has normal islets, ductal architecture and secretory function, but lacks acinar cells and shows replacement by fat and connective tissue (Jones et al., 1994). Early intrauterine destruction of acinar cells similar to prenatal onset pancreatitis could lead to the exocrine defects in JBS (Zenker et al., 2005). With age, the pancreatic disease progresses with a significant proportion of patients eventually developing diabetes.

Zenker *et al.* identified the causative gene *ubiquitin protein ligase E3 component n-recognin 1* (*UBR1*) by performing a genome-wide linkage scan in 7 affected families (Zenker et al., 2005). UBR1 protein is involved in the proteolytic pathway of the ubiquitin system

responsible for degradation of intracellular proteins. It is believed that an excess of non-degraded unidentified proteins leads to the pathogenesis observed in JBS. *Ubr*$^{-/-}$ mice display milder pancreatic abnormalities: impaired secretion of zymogen granules and increased susceptibility to pancreatic injury (Zenker et al., 2005; Zenker et al., 2006).

Pearson marrow-pancreas syndrome (OMIM #557000) is characterised by exocrine pancreatic dysfunction, anaemia with abnormal red blood cell precursors instead of healthy red blood cells (sideroblastic anaemia) and vacuolisation of precursors of the bone marrow. Pancreatic dysfunction manifestations are not always present in early childhood whilst haematologic symptoms often start in infancy. It is similar to Schwachman-Diamond syndrome but can be distinguished by their differing bone marrow morphology and pancreatic abnormalities; the pancreas is fibrotic in Pearson marrow-pancreas syndrome whilst the pancreas shows fatty replacement in SDS (Favareto et al., 1989). Pearson marrow-pancreas syndrome is caused by a single large deletion of several mitochondrial genes involved in oxidative phosphorylation suggesting that the pancreatic dysfunction results from an impaired energy supply in acinar cells (Rotig et al., 1989). The progression of the syndrome to a disease with overt muscle dysfunction, Kearns-Sayre syndrome has been reported (Rotig et al., 1995).

Various deficiencies of pancreatic enzymes have been described although they are very rare and the molecular defects have not yet been proven (Durie, 1996). Congenital pancreatic lipase deficiency results in excess fat in faeces (steatorrhea) (Sheldon, 1964). There have been reports of deficiency of colipase as well as both lipase and colipase (Hildebrand et al., 1982; Sjolund et al., 1991). Deficiency in pancreatic amylase can lead to diarrhoea in a starch-rich diet (Sjolund et al., 1991) whilst trypsinogen deficiency has been reported in children with growth failure, hypoproteinemia, diarrhoea and oedema (Townes, 1965). The few number of cases of isolated enzyme deficiencies suggests that the defect is usually compensated by alternative sources of lipolytic, glycolytic and proteolytic activities (Cano et al., 2007).

1.2 Zebrafish as a model organism

Danio rerio (Zebrafish) are teleosts of the cyprinid family in the Actinopterygii (ray-finned fish) class (Nüsslein-Volhard and Dahm, 2002). They are tropical freshwater fish that originated in the streams of the South-Eastern Himalayan region (Talwar and Jhingran, 1991). Their emergence as a vertebrate model organism that allowed both the application of genetic approaches and embryological methods started with the pioneering work of George Streisinger and his colleagues (Streisinger et al., 1981). Their seminal paper described a method to produce clones of homozygous diploid zebrafish and the first zebrafish mutation, *golden*, that produces a homozygous viable pigment phenotype. Subsequently, the University of Oregon zebrafish group provided a detailed description of zebrafish embryology (Kimmel et al., 1995) and isolated the first two developmental mutants, *cyclops* and *spadetail* that showed abnormal floor plate specification and defective trunk mesoderm respectively (Hatta et al., 1991; Ho and Kane, 1990; Molven et al., 1990). Since then, thousands of mutants have been characterised following the development of highly efficient mutagenesis methods and large-scale screens (Nüsslein-Volhard and Dahm, 2002).

Zebrafish is now an indispensable vertebrate model organism for studying embryo development and modelling of human diseases thanks to its numerous attractive features. *Ex utero* development and translucent embryos allow easy visualisation of internal organs. The development of embryos is rapid: all the common vertebrate specific body features including internal organs, compartmentalised brain, ears and eyes are observed after about 2 days post fertilization (d.p.f.). Zebrafish have high fecundity producing a brood size of hundreds of eggs, and have a relatively short generation time of 2-4 months, both characteristics important for genetic analyses. Adults can easily be maintained in a small space, with approximately five adult fish per litre (Nüsslein-Volhard and Dahm, 2002).

1.2.1 Zebrafish genome

A high-quality zebrafish genome, with complete annotation of protein-coding genes is important for the use of zebrafish as a model organism. It enables effective modelling of human diseases since the extent to which zebrafish and human genes are related can be determined, and it has accelerated the identification of mutants by allowing comparisons of mutated and normal sequences (Howe et al., 2013; Schier, 2013). In 2013, Howe *et al.* reported a high-quality zebrafish genome of 1.4 gigabases (Gb) on the Ensembl Zv9 assembly

(Howe et al., 2013). Zebrafish have 26,206 protein-coding genes (Collins et al., 2012), a number greater than any vertebrate previously sequenced. This is probably due to the zebrafish common ancestor undergoing the teleost-specific genome duplication (TSD), a second round of whole-genome duplication (WGD) (Meyer and Schartl, 1999). A comparison between human and zebrafish protein coding genes show that 71% of human genes have at least one zebrafish orthologue, a number which increases to 82% when only Online Mendelian Inheritance in Man (OMIM) genes are considered. This suggests a higher degree of conservation of disease-related genes compared to non-disease-related genes between humans and zebrafish.

1.2.2 Forward genetic approaches

Forward genetic screens involve screening a mutagenised population for a particular phenotype and subsequently identifying the causative gene. These screens have been carried out systematically in plants, flies and worms and have successfully identified numerous genes involved in embryogenesis. A smaller number of mammalian mutants have provided important insights into vertebrate development but identification of a large number is difficult because of intrauterine development and costly supporting research facilities. The remarkable advantages of the zebrafish and the success of the earliest zebrafish genetic screens (Kimmel, 1989) have encouraged large-scale genetic screens to be undertaken (Patton and Zon, 2001).

N-ethyl-N-nitrosurea (ENU) is an alkylating agent that induces random point mutations in the genome, with a preference for A->T transversions and AT->GC transitions (de Bruijn et al., 2009; Nolan et al., 2002). It was found to be the most efficient chemical mutagen in pre-meiotic germ cells in zebrafish making it suitable for large-scale mutagenesis screens (Mullins et al., 1994; Solnica-Krezel et al., 1994). The frequency at which ENU induces mutations is dosage dependent and a significant increase in mutation efficiency is observed when increasing the ENU concentration from 2.0 to 3.0 mM but concentrations significantly higher than 3.0 mM result in high lethality (Solnica-Krezel et al., 1994). An average germ line mutation load of one mutation every 175,000-250,000 base pairs can be achieved consistently by performing six weekly ENU treatments of varying concentrations (Kettleborough et al., 2011).

The groups at Boston (Driever et al., 1996) and Tübingen (Haffter et al., 1996) carried out the first zebrafish screens in which ENU-mutagenised males were outcrossed to wild-type

females to produce F1 offsprings. An F2 generation was raised from F1 sibling matings and subsequently incrossed to produce an F3 generation that contains homozygous induced mutations. The two screens altogether identified ~2000 developmental mutants representing more than 500 genes. These genes are involved in embryogenesis, gastrulation, pigmentation, body shape, haematopoiesis and development of the notochord, muscle, craniofacial skeleton, eye, ear, brain, cardiovascular and digestive organs. Positional cloning of several of these mutants has lead to a better understanding of developmental gene networks (Patton and Zon, 2001).

Insertional mutagenesis is also used in addition to chemical and radiation mutagenesis methods. A group led by Nancy Hopkins injected pseudotyped retroviruses with a genome based on Moloney murine leukemia virus ([M]MLV) and the envelope protein of Vesicular stomatitis Indiania virus (VSIV) into blastula-stage embryos (Gaiano et al., 1996; Lin et al., 1994). They had successfully infected the germ cells and found that insertion events were transmitted to their progeny. Although less efficient than ENU mutagenesis, insertional mutagenesis allows rapid identification of the mutated gene since each insertional event is tagged. A large-scale insertional mutagenesis screen was carried out and had identified 315 genes required for early vertebrate development (Amsterdam et al., 1999; Amsterdam et al., 2004; Golling et al., 2002).

1.2.3 Reverse genetic approaches

Reverse genetics investigate the function of a target gene by modifying its activity and studying the phenotypic consequences. As in forward genetic approaches, random mutagenesis has been the preferred method, since targeted knockout strategies were until recently inadequate in zebrafish. To identify induced mutations in a library of ENU-mutagenised zebrafish, the reverse genetic approach Targeting Induced Local Lesions IN Genomes (TILLING) has been used as an alternative to resequencing which is more laborious and expensive (Wienholds et al., 2003). TILLING, first described in *Caenorhabditis elegans* (Jansen et al., 1997) and *Arabidopsis thaliana* (McCallum et al., 2000), traditionally uses the plant endonuclease CEL1 (Oleykowski et al., 1998) to cleave heteroduplex DNA and analyse fragments to identify induced mutations. Using this approach, Wienholds *et al.* screened a library of 4608 ENU-mutagenised F1 fish for 16 genes and identified 255 mutations (Wienholds et al., 2003).

1.2.3.1 Zebrafish gene knockout resources

The Zebrafish Mutation Project (ZMP), previously known as the Zebrafish Mutation Resource, was launched in 2003 with aims to identify and phenotype disruptive mutations in every protein-coding gene in the zebrafish genome (Kettleborough et al., 2013). To identify mutant alleles, TILLING was used initially but was substituted by direct PCR-based resequencing of target genes (Kettleborough et al., 2011) and subsequently with whole-exome sequencing (Kettleborough et al., 2013). In brief, males are ENU mutagenised and outcrossed to create an F1 generation of carriers that are subjected to exome sequencing (Figure 1-2). Induced mutations are identified and their effect on protein coding is predicted using a modified version of the variant-calling pipeline of the 1000 Genomes Project (Abecasis et al., 2010; Abecasis et al., 2012). To take full advantage of this resource, it is important to screen for phenotypic consequences of disruptive mutations. Phenotypic analysis of homozygous nonsense and essential-splice mutations is carried out in a two-step, multi-allelic approach. The F1 individuals are outcrossed to produce an F2 family. In the first step, crosses of up to 12 pairs of F2 individuals are carried out and phenotypically normal F3 embryos are genotyped for disruptive mutations heterozygous in both parents. Homozygous mutations that are present in the expected Mendelian ratios are deemed to not cause a phenotype whereas if they are present in less than 25% of embryos, they are suspected to cause a phenotype. Secondly, the F2 adults that are heterozygous for any suspected causal mutation are incrossed and the morphological and behavioural phenotypes of the F3 embryos during the first 5 d.p.f. are examined. All phenotypes identified are genotyped for the suspected mutation, the mutation is documented as likely to be causal if over 90% of embryos are homozygous for the specific mutation whereas it is documented as being linked if less than 90% of embryos are homozygous. To date, ZMP has identified nonsense and essential splice site mutations in over 45% of all known protein-coding genes and has examined the phenotypic consequences of more than 1000 alleles. All mutant alleles and data generated by ZMP is available to the scientific community (http://www.sanger.ac.uk/Projects/D_rerio/zmp) (Dooley et al., 2013; Kettleborough et al., 2013). Alleles can be obtained from two international stock centres, the European Zebrafish Resource Center (http://www.itg.kit.edu/ezrc) and the Zebrafish International Resource Center (http://www.zebrafish.org/zirc). ZMP provides a resource to study developmental biology and human diseases and has been used in various studies including pancreas development (Arkhipova et al., 2012; Verbruggen et al., 2010; Wilfinger et al., 2013), heart development (de Pater et al., 2009), osteogenesis (Laue et al., 2008),

muscle development and associated disorders (Hinits et al., 2009; Knight et al., 2011; Lin et al., 2011; Powell and Wright, 2011) and haematopoietic disorders (Cvejic et al., 2008).

In addition to a library of ENU-mutagenised fish, Wang *et al*. reported the establishment of a pseudo-typed retrovirus mediated insertional library (Wang et al., 2007). So far, ~15000 [M]MLV proviral integrations have been mapped to 3054 genes, 0.5% of which have been rescued and characterised. Mutant lines are available to the scientific community through the Zebrafish International Resource Center (http://www.zebrafish.org/zirc) (Amsterdam et al., 2011; Varshney et al., 2013).

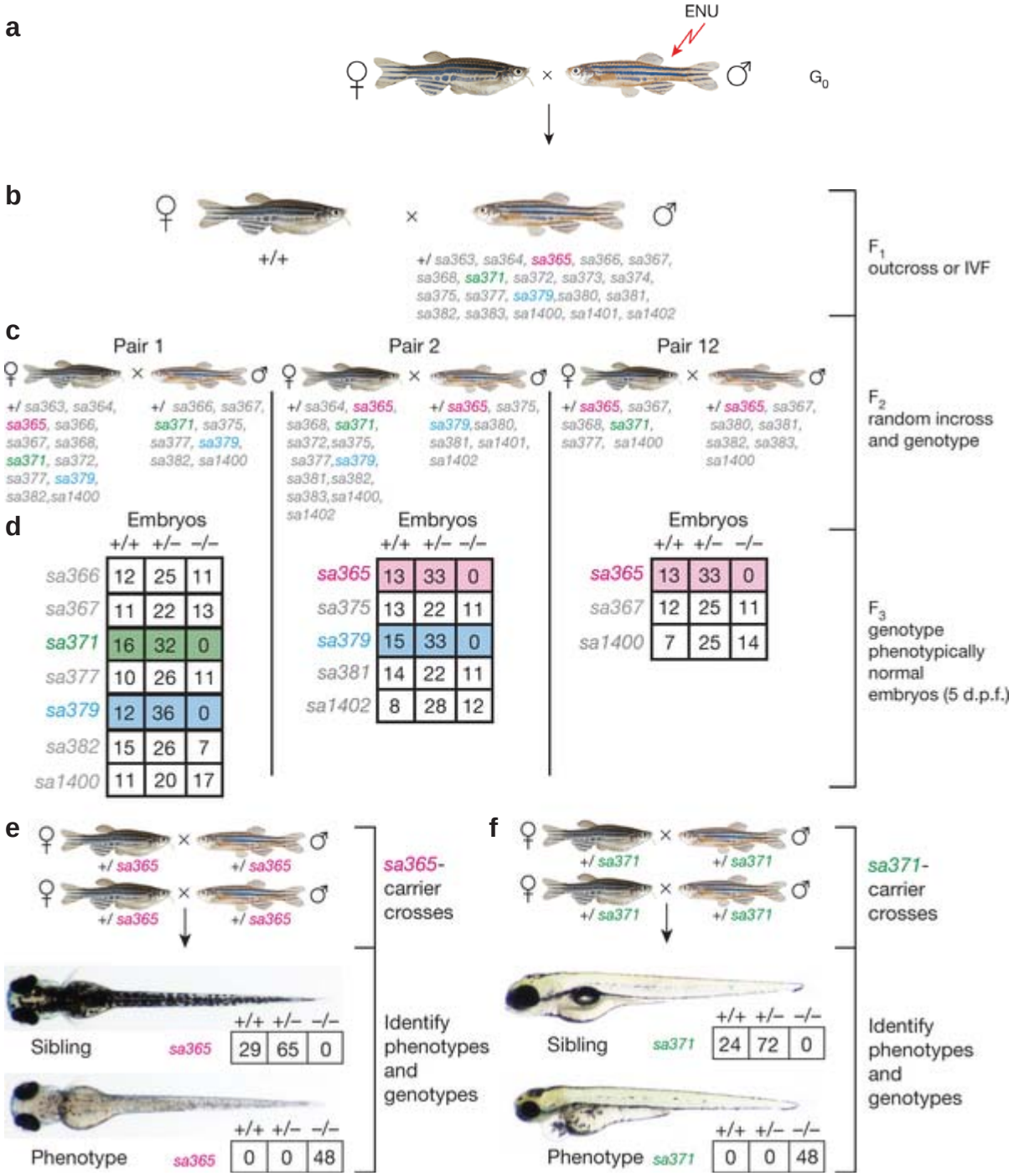

Figure 1-2 Zebrafish Mutation Project (ZMP) Phenotyping Pipeline. (a) G_0 males are ENU-mutagenised and outcrossed to create F_1 individuals and the induced mutations are identified by exome sequencing. (**b)** F_1 individuals are outcrossed or cryopreserved sperms are used in *in vitro* fertilisation (IVF) to produce an F_2 family. The induced disruptive mutations for one family are shown here. (**c**) F_2 individuals are incrossed and genotyped for induced mutations present in F_1 parents. (**d**) First round of phenotyping where 5 d.p.f. embryos of wild-type appearance are collected and genotyped for mutations present in both F_1 parents. Using a chi-squared test and a *p*-value cut-off of 0.05, the number of homozygous mutant embryos is assessed. Mutations that are homozygous in less than 25% of embryos are suspected to cause a phenotype. There are no homozygous embryos for alleles *sa365*, *sa371* and *sa379*. (**e**, **f**), Second round of phenotyping where F_2 adults heterozygous for suspected mutation are incrossed and embryos are phenotyped during the first 5 days and then genotyped. Embryos homozygous for *sa365* and *sa371* are phenotypic. Adapted from Kettleborough et al., 2013.

1.2.4 Transgenic approaches

The different techniques that can be used in zebrafish are summarised in Table 1-2. Transgenesis is an important technology that allows the study of a particular gene. The traditional method of generating transgenic fish involves DNA integration into the genome by injection of linearised or circular DNA plasmids or bacterial artificial chromosomes (BACs) into fertilised eggs. The germline transmission efficiency to the F1 generation is very low, 5-20%, with foreign DNA tending to integrate as concatemers with multiple tandem copies and potentially also causing chromosomal rearrangements. In addition, this repetitive DNA becomes susceptible to methylation over time leading to silencing of the transgene (Culp et al., 1991; Stuart et al., 1988; Thummel et al., 2006). To circumvent these problems, several new techniques have been developed with transposon-based methods being the most popular choice in zebrafish (Davidson et al., 2003; Kawakami et al., 2000).

DNA transposons are genetic elements that move or transpose by a 'cut and paste' mechanism and have been extensively studied in plants and invertebrates. The use of transposons as a genetic tool in vertebrates started with the application of the Sleeping Beauty (SB) transposon system in which the transposase is provided *in trans* and the key DNA cargo is flanked by transposon end sequences (Ivics et al., 1997). This transposon paradigm remains the primary approach employed today with 10 transposons from four different superfamilies (*TcI/Mariner*, *hAT*, *PIF/Harbinger*, *piggyBac*) available for use in vertebrates (Ni et al., 2008). *Tol2* and Sleeping Beauty transposon-based methods show efficient germline transmission in zebrafish (Davidson et al., 2003; Kawakami et al., 2000). Also, *Tol2*-mediated transgenes may not be subject to gene silencing effects since their expression persists through generations (Kawakami, 2007).

The high throughput nature of zebrafish allows transgenesis to be used as a screening tool to manipulate and probe the genome. Examples of this approach include insertional mutagenesis and gene trapping or enhancer detection (van Ruissen et al., 2005). Gene trapping is a high-throughput approach that introduces insertional mutations across a target genome and is widely used to generate knock-out mice (Mikkola and Orkin, 2005; Misra and Duncan, 2002). *Tol2* and Sleeping Beauty transposon-based methods have demonstrated to be suitable for gene trapping in zebrafish. Gene trap vectors whose principal element is a gene trapping cassette that consists of a reporter gene flanked by a 3' splice acceptor and a 5' transcriptional termination sequence are co-injected with transposase into zebrafish embryos

and result in inactivation of target genes and translation of the reporter gene (Kawakami et al., 2004; Kotani et al., 2006; Song et al., 2012a; Song et al., 2012b). Enhancer trapping uses insertion site context vectors to detect enhancers in the genome and has been extensively used in *Drosophila*. In zebrafish, Sleeping Beauty and *Tol2*-transposon based enhancer trapping methods have successfully identified enhancers (Balciunas et al., 2004; Fisher et al., 2006; Parinov et al., 2004).

1.2.4.1 Spatial and temporal control

Tissue-specific and inducible techniques allow spatial and temporal control of expression of a specific transgene and have been successfully used in various model organisms including mouse and zebrafish (Table 1-2). Many tissue-specific promoter elements have been identified in zebrafish and faithfully mimic the expression patterns of the endogenous gene for expression of a transgene in a specific tissue. To facilitate and provide tight spatial and temporal regulation of transgene expression, several genetic methods have been modified.

The yeast Gal4/UAS system consists of the yeast transcription activator protein Gal4 and the Upstream Activation Sequence (UAS), a Gal4-specific enhancer. Its versatility has been demonstrated in *Drosophila* and has been used to express genes in several model organisms, including zebrafish (Halpern et al., 2008). The Cre/LoxP system is an established genetic method to regulate transgene expression in mouse. Its utility in zebrafish was first demonstrated in 2005 (Langenau et al., 2005) and since then a number of Cre deleter zebrafish lines have been generated to achieve tissue-specific transgene expression (Feng et al., 2007; Langenau et al., 2007; Le et al., 2007; Pan et al., 2005; Thummel et al., 2005). Flp, another site-specific recombinase has been predominantly employed in *Drosophila*. It has also been used in mice and shown to function in zebrafish (Boniface et al., 2009; Wong et al., 2011a).

Several methods have been used to achieve temporal control. One method involves using a modified soldering iron to administer localised heat shock in adult fish with transgene expression regulated by a heat shock protein promoter but the utility of this approach is restricted by its inconsistency and limitation to superficial structures (Hardy et al., 2007). Influenced by the work on inducible Cre/LoxP system in mouse models, zebrafish researchers have used chimeric Cre recombinases to achieve temporal control (Metzger et al., 1995). Cre

fused to the mutated ligand-binding domain of estrogen receptor (Cre-ER^{T2}) show high ligand sensitivity and efficient inducible recombination (Feil et al., 1997; Indra et al., 1999). Site-specific recombination is induced by administration of tamoxifen or 4-hydroxy-tamoxifen, with fast recombination kinetics observed (Hans et al., 2009). The LexPR system is an inducible system developed in zebrafish and temporal control is achieved using the synthetic steroid, mifepristone (RU-486) (Emelyanov and Parinov, 2008; Nguyen et al., 2012). Huang *et al.* developed the tetracycline (Tet)-on system to induce heart-specific expression of GFP in adult fish. Doxycycline, a tetracycline derivative induces rapid and strong gene expression but inactivation of the transgene is very slow upon removal of doxycycline (Campbell et al., 2012; Huang et al., 2005).

1.2.5 Gene inactivation tools

Strategies have been developed to target specific genes by site-specific genome modification instead of relying on targeted genome modification based on large-scale forward genetic screens (Table 1-2). These include sequence-specific chimeric nucleases; i.e. zinc-finger nucleases (ZFNs), transcription activator-like effector nucleases (TALENs) and clustered regularly interspaced short palindromic repeats (CRISPR)/Cas-based RNA-guided Endonucleases (RGENs). ZFNs introduce double strand breaks (DSBs) at their target locus leading to insertion/deletion (indel) mutations mostly through error-prone non-homologous end joining (NHEJ) in zebrafish. ZFNs are chimeric proteins made up of a zinc finger DNA binding domain and a DNA cleavage domain derived from bacterial non-specific endonuclease FokI. ZFNs are assembled from multiple three-base recognition motifs comprising of about 30 amino acids. The main disadvantages of ZFNs are their complex manufacture due to nonintuitive ZFN binding rules and their diverse range of targeting efficacy. Despite these issues, ZFNs have been successfully used to generate dozens of zebrafish mutants (Urnov et al., 2010). TALENs are artificial restriction enzymes composed of a DNA binding domain of TALE proteins that are mainly found in the plant pathogen *Xanthomonas* and a DNA cleavage domain derived from FokI. TALENs consist of repeat modules of approximately 34 amino acids that are arranged into TAL effector arrays. Within each repeat module, a two-amino acid repeat variable di-residue (RVD) is responsible for one-to-one base pairing, with the four most commonly used RVDs binding preferentially to bases A, C, G or T. Like ZFNs, TALENs introduce double strand breaks but they are easier to design due to their simpler base recognition code and usually have higher targeting efficiency

and lower off-target effects. In addition, assembly of TALENs is rapid, taking less than a week, and is accessible to even small laboratories since the initiation of the entire platform is possible using clones from a single 96-well plate. Several groups have reported successful somatic and germline gene modifications using TALENs (Clark et al., 2011; Huang et al., 2012). The type II CRISPR/Cas system is derived from eubacteria and archaea and involves a complex of transactivating CRISPR RNA (tracrRNA), CRISPR RNA (crRNA) and Cas9 nuclease. Recently, Jinek *et al*. programmed the type II CRISPR system to target a specific genomic sequence using a guide RNA molecule: a chimera of tracrRNA- and crRNA-derived sequences connected by a four-base loop (Jinek et al., 2012). Using a similar chimeric guide RNA in zebrafish, mutations have been induced with efficiencies similar to ZFNs and TALENs. CRISPR gene editing system is faster and easier to produce than ZFNs or TALENs as it requires only a minimum of two plasmids one coding for *cas9* sequence and another one for a single unique guide RNA sequence. However, the off-target effects and germline efficiency remain to be determined (Blackburn et al., 2013; Hwang et al., 2013).

1.2.6 Gene knockdown tools

Gene knockdown tools have proved indispensable in developmental biology (Table 1-2). The established method to knock down specific target genes in eukaryotes is RNA interference (RNAi). RNAi, first identified in *Caenorhabditis elegans* is an endogenous gene-silencing mechanism involved in various biological processes such as transcriptional gene silencing, post-transcriptional regulation of gene expression and antiviral response (Lee et al., 1993; Plasterk, 2002; Wightman et al., 1993; Zamore, 2002). RNAi-based gene-silencing methods involve triggering the innate mechanism of cells by introducing small interference RNAs (siRNAs) or small hairpin RNAs (shRNAs) that are then processed by the enzyme Drosha to produce precursor microRNA-like molecules. These methods are routinely used in *Drosophila melanogaster*, human and mouse cell lines (Martin and Caplen, 2007). RNAi-mediated gene knockdown has been used in zebrafish but progress has been very slow with varying success rates and nonspecific toxicity observed in developing embryos (Kelly and Hurlstone, 2011). Instead, morpholino is the method of choice to knock down the gene of interest in zebrafish. It is a synthetic oligonucleotide made of a morpholine ring and is usually 25 bases long. It has the advantage of being completely resistant to nucleases, has excellent sequence specificity, generally good targetting predictability and high in-cell efficacy. It can either block translation by binding to the 5'UTR of a specific mRNA or interfere with pre-

mRNA processing steps, thereby modifying splicing and resulting in exon exclusion or intron inclusion (Summerton, 1999; Summerton and Weller, 1997). In addition, varying levels of gene knockdown can be achieved by controlling the dosage of the morpholino and the synergistic and counteractive effects of various genes can be studied by co-injecting several morpholinos. However, morpholino has two key disadvantages: firstly its effects are transient allowing only the study of early development and secondly it is known to produce off-target effects thereby complicating the interpretation of results (Eisen and Smith, 2008).

Techniques	Features
Transgenic methods	
Linearised/Circular DNA and BAC	• Simple procedure • Germline transmission is generally low 5-20% • Integrate as concatemers of many tandem copies and may cause chromosomal rearrangements • Transgene becomes methylated and silenced over time
Transposon-based (*Tol2*, Sleeping Beauty)	• Commonly used in various model organisms including zebrafish • Relative ease of manipulation and high germline transmission efficiency
Tissue-specific and Inducible methods	
Gal4/UAS system	• Highly successful in *Drosophila*, effective in mouse and functional in zebrafish • Variegated or diminished expression over time
Cre/LoxP & Cre-ER^{T2}	• Widely used in mouse and efficient in zebrafish • Efficacy of Cre-ER^{T2} in adult fish remains to be determined
Flp/FRT	• Widely used in *Drosophila* and moderately in mouse • Efficient but not established in zebrafish
LexPR	• First developed in zebrafish • Efficacy in adult fish not determined
Tet-On	• First developed in zebrafish • Rapid and strong gene expression but inactivation very slow
Gene inactivation methods	
ZFN	• Successful in various model organisms including zebrafish • Low germline efficacy with off-target effects observed • Difficult to design and production expensive and time-consuming
TALEN	• Effective in zebrafish • Moderate-high germline efficacy with very low off-target effects observed • Reasonable design and production affordable and rapid (<1 week)
CRISPR/Cas	• Functional in zebrafish • Germline efficacy and off-target effects remain to be determined (Initial results suggest similar germline efficacy to ZFN and TALEN) • Simple design and production inexpensive and very fast
Gene knockdown methods	
RNAi	• Successful and routinely used in mammalian cells • Progress slow in zebrafish • Varying success rates and off-target effects
Morpholino	• Method of choice in zebrafish • Highly specific and efficient • Transient knockdown and off-target effects

Table 1-2 Techniques used in zebrafish. Transgenic, tissue-specific and inducible, gene inactivation and knockdown methods and their different features are shown.

1.3 Zebrafish pancreas development

Zebrafish is an excellent model to study pancreas development for two main reasons. Firstly, the zebrafish and mammalian pancreas share similar anatomy and histology. The adult zebrafish pancreas contains several principal islets that are situated next to the gallbladder and additional smaller accessory islets embedded in the exocrine tissue situated in the intestinal mesentery. In both fish and mammals, the pancreatic islet is composed of a central core of insulin-producing β-cells that is surrounded by glucagon-producing α-cells, somatostatin-producing δ-cells and ghrelin-producing ε-cells (Argenton et al., 1999; Biemar et al., 2001; Devos et al., 2002). Enzyme-producing acinar cells surround the endocrine islets and are arranged into acini. A complex ductular network connects the exocrine cells to the intestine. In fish and mammals, the hepatic and main pancreatic ducts are joined at the site where they enter the intestine (Yee et al., 2005). Secondly, orthologous signalling pathways and transcription factors control pancreas development in zebrafish and mammals in a similar fashion.

Pancreas development in zebrafish, like other vertebrates, is a complex process comprising of three major developmental mechanisms. The first includes induction and pattern formation of the endoderm and defines the location of the pancreatic primordium within the endoderm. The second is the control of cell differentiation of pluripotent endodermal precursor cells into specialised pancreatic cells. The third involves morphogenesis of the pancreas and requires extensive rearrangements of cells and movements of whole organ parts resulting in the location, shape and cellular organisation of the pancreas (Gnugge et al., 2004).

1.3.1 Endoderm induction, patterning and regionalisation

The three primary germ layers, the endoderm, mesoderm and ectoderm form during gastrulation. The endoderm and mesoderm are thought to arise from the mesendoderm, a transient common precursor cell population. An evolutionarily conserved gene regulatory network consisting of Nodal growth factor signalling and downstream transcription factors controls the induction and commitment of mesendoderm to an endodermal lineage (Figure 1-3). After gastrulation, the naïve endoderm transforms into a primitive gut tube by a series of morphogenetic movements. The gut tube regionalises along both the anterior-posterior (A-P)

and dorsal-ventral (D-V) axes into foregut, midgut and hindgut domains. The basic organisation of the gut tube is conserved from fish to mammals (Zorn and Wells, 2009).

The endodermal germ layer derives from blastoderm cells that are mostly located in the dorsal half of the mid-blastula margin (Warga and Nusslein-Volhard, 1999). Both the yolk syncytial layer and the vegetal margin of the blastoderm secrete transforming growth factor beta (TGFβ) molecules (Rodaway et al., 1999). Nodal ligands, members of the TGFβ family, induce the endoderm and mesoderm in a concentration dependent manner; high levels promote endoderm development whilst lower levels promote mesoderm formation (Chen and Schier, 2001; Dougan et al., 2003; Thisse et al., 2000). Mid-blastula-stage marginal cells can give rise to both endoderm and mesoderm whilst late-blastula-stage marginal cells can give rise only to either endoderm or mesoderm. Notch (Kikuchi et al., 2004), Bone morphogenetic protein (BMP) and Fibroblast growth factor (FGF) (Poulain et al., 2006) signalling pathways are involved in segregation of the endoderm and mesoderm.

In the current model of zebrafish endoderm induction, nodal ligands encoded by *ndr1/squint* and *ndr2/cyclops* induce a common endo-mesodermal region (Figure 1-3). These ligands are expressed at the vegetal margin of the blastoderm and are antagonised by members of the Antivin/Lefty family (Agathon et al., 2001). Nodal signals act through Acvr1b/Taram-a receptors (Aoki et al., 2002b) and Oep co-receptors (Gritsman et al., 1999). This leads to intracellular phosphorylation of Smad2 proteins binding to Smad4 to form Smad2-Smad4 complex that translocates to the nucleus (Dick et al., 2000; Muller et al., 1999). Smad2-Smad4 complex interacts with additional cofactors: FoxH1/Fast1 (Pogoda et al., 2000; Sirotkin et al., 2000) and Mixer/Bon (Kikuchi et al., 2000) to activate target genes including three transcription factors: *mixer/bon* (Alexander and Stainier, 1999), *gata5/fau* (Reiter et al., 2001) and *og9x/mezzo* (Poulain and Lepage, 2002) leading to expression of *sox32*/*cas* (Alexander et al., 1999; Alexander and Stainier, 1999; Aoki et al., 2002a). Sox32 then induces the expression of *sox17*, the final determinant of endoderm specification (Alexander and Stainier, 1999). Several forkhead and homeobox transcription factors are also expressed in the endoderm including *foxa2* and *hhex* (Odenthal and Nusslein-Volhard, 1998; Wallace and Pack, 2003; Wallace et al., 2001). In addition, three maternal transcripts contribute to Nodal-dependent endoderm formation. Pou5fl/Spg maintains *sox32* expression in a positive feedback loop and interacts with Sox32 to specify mesoendodermal precursors to an endodermal identity inducing expression of *sox17* and *foxa2* (Lunde et al., 2004; Reim et

al., 2004). Eomesa interacts with both Mixer and Gata5 to induce expression of *sox32* (Bjornson et al., 2005) and Cdx1b regulates *foxa2* and possibly *gata5* expression during endoderm formation and digestive organ development (Cheng et al., 2008).

The next step in pancreas formation is the antero-posterior regionalisation of the digestive tube and is governed by the combined activity of several signalling pathways including Wnt, retinoic acid (RA), BMP, FGF and Hedgehog (Hh) (Figure 1-3) (Tiso et al., 2009).

Goessling *et al.* showed that during early somitogenesis, endodermal pattern formation requires suppression of Wnt signalling, but later in development Wnt activity alters endodermal fate with increased activity favouring liver growth over pancreas formation (Goessling et al., 2008). Stafford *et al.* studied the *neckless* mutant with disrupted Retinoic Acid (RA) synthetic enzyme (RALDH2) and demonstrated that RA signalling is required for specification of both the pancreas and the liver and that RA synthesised in the mesoderm acts as an instructive signal to induce precursors of the endocrine pancreas (Stafford and Prince, 2002; Stafford et al., 2006). The transcription factors Cdx4 and Cdx1a localise the pancreas by blocking pancreatic identity, possibly through RA inhibition in the posterior endoderm (Kinkel et al., 2008). Bmp2b signalling plays a role in endoderm patterning and controls the fate of bipotential hepatopancreatic progenitors whilst Bmp2a is required to specify the ventral pancreatic bud between 20 and 24 hours post fertilisation (h.p.f.) (Chung et al., 2008; Naye et al., 2012; Tiso et al., 2002). More recently, it was found that in early zebrafish developmental stages prostaglandin E2 (PGE2) synthesis favours liver over pancreatic cell fate by interacting with the bmp2b pathway but later in development PGE2 promotes both liver and pancreas outgrowth in zebrafish (Nissim et al., 2014)

FGF signalling is another pathway critical for pancreatic specification. At early stages, endodermal expression of *fgf24* stimulates the patterning of the pancreatic lateral plate mesoderm and subsequently both Fgf10 and Fgf24 induces ventral pancreas formation and represses the hepatic fate (Manfroid et al., 2007; Naye et al., 2012). Fgf10 refines the boundaries between the hepatopancreatic organs (liver, pancreas and gallbladder) and the ductal epithelium and inhibits the differentiation of the liver and proximal pancreas into hepatic and pancreatic cells respectively (Dong et al., 2007). Song *et al.* showed that both FGF and BMP act genetically upstream of RA signalling and that they direct pancreas formation through the hepactocyte nuclear factor 1 homeobox B (Hnf1b) pathway (Song et

al., 2007). Hnf1b controls the regionalisation and specification of the gut through proper expression of *pdx1* and *shh* (Sun and Hopkins, 2001). The Hnf1b and Wnt pathways were found to synergise in the specification of the ventrally derived hepatopancreas progenitors in studies of conditional loss of Wnt signalling in a hypomorphic *hnf1ba* zebrafish mutant (Lancman et al., 2013).

The Hedgehog (Hh) signalling pathway plays a critical role at two stages during pancreas development (Chung and Stainier, 2008; dilorio et al., 2002; Roy et al., 2001). At the start of gastrulation, Hh signalling is required for migration and differentiation of pancreas progenitors by inhibition of Bmp signalling (Tehrani and Lin, 2011). By the end of gastrulation, Hh acts antagonistically to RA in specification of the endocrine pancreas, although it still promotes differentiation of exocrine progenitor cells (Tehrani and Lin, 2011). The expression of *sonic hedgehog* (*shh*) in the second hedgehog-dependent step is regulated by Meis Homeobox 3 (Meis3) and pre-B-cell leukemia homeobox 4 (Pbx4) (dilorio et al., 2007). Histone deacetylase 1 (Hdac1) restricts foregut fates, promotes specification of the liver and exocrine pancreas and morphogenesis of the endocrine islet (Noel et al., 2008).

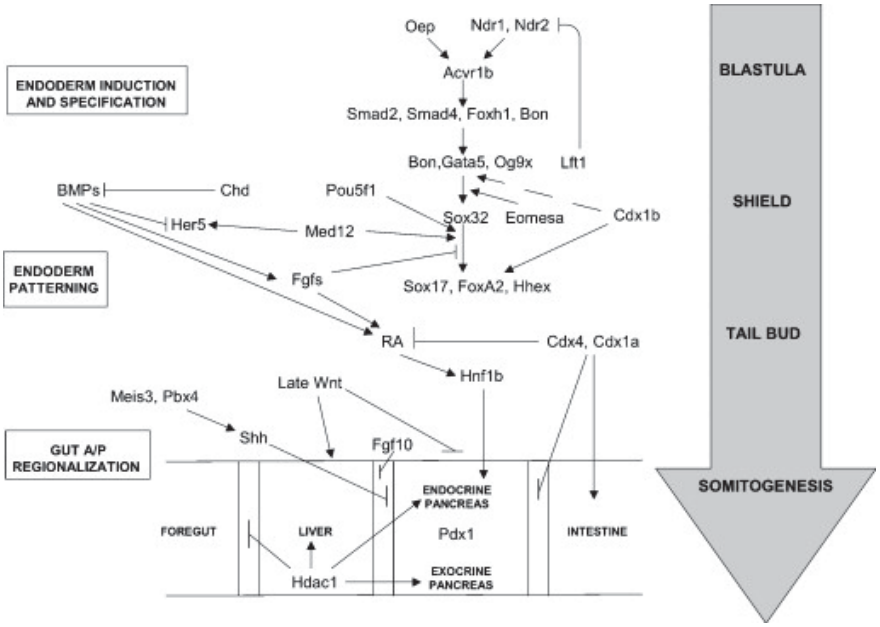

Figure 1-3 Integration of signalling cascades during zebrafish pancreas development. Nodal, Bmp, Fgf, RA, Wnt and Hh signalling pathways are involved in endoderm induction, specification and regionalisation at different embryonic stages (shown on the right) to define a Pdx1-positive pancreatic region within the developing gut tube. Taken from Tiso et al., 2009.

1.3.2 Morphogenesis of pancreas

In zebrafish pancreas morphogenesis, two contiguous areas of the gut bud sequentially and merge to form the definitive pancreas. Expression patterns of specific genes during early development have revealed that pancreatic precursors are already present before budding occurs. At 14 h.p.f., pancreatic precursors are first detected as two bilateral rows of cells adjacent to the midline, expressing *pancreatic and duodenal homeobox 1* (*pdx1*), a bipotential marker of intestinal bulb and pancreatic progenitor cells (Figure 1-4). Expression of endocrine markers *insulin, somatostatin* and *glucagon* are first detected at 15 h.p.f., 17 h.p.f. and 21 h.p.f. respectively. The bilateral group of cells begins to merge at 16 h.p.f. and by 18 h.p.f. is located in the midline, immediately dorsal to the yolk. At 24 h.p.f., the first pancreatic posterodorsal bud protrudes from the intestinal rod to form the primary islet (Argenton et al., 1999) (Biemar et al., 2001). Between 24 h.p.f. and 48 h.p.f., gut looping displaces the posterodorsal bud to right side and the gut to the left side. By 48 h.p.f., the first islet already has a similar organisation to its mammalian counterpart, with a core of β-cells surrounded by α- and δ-cells.

The second pancreatic anteroventral bud forms after 34 h.p.f. within the *pdx1*-expressing region of the ventral region of the gut tube and anteriorly to the main islet. Between 34 h.p.f. and 48 h.p.f., the second bud grows towards the first bud posteriorly and surrounds it, giving rise to exocrine tissue, pancreatic ducts and late-forming endocrine cells (Field et al., 2003a). *Trypsin*-positive cells surround *insulin*-positive cells in the head of the merged pancreas (Field et al., 2003a). *Carboxypeptidase A* and *elastase B*, two other exocrine-specific genes, are detected at 48 h.p.f. and 56 h.p.f. respectively (dilorio et al., 2002; Mudumana et al., 2004). The exocrine tissue continues to grow posteriorly along the intestine in parallel with the establishment of the intrahepatic ductal system (Wan et al., 2006). At 5 d.p.f., the zebrafish pancreas consists of a single islet with about 60 endocrine cells and exocrine acinar tissue with a branching ductal system connecting the pancreas to the gut. During postembryonic growth, the primary islet becomes bigger and smaller secondary islets are formed along the exocrine duct system resulting in several dozen secondary islets in adults (Chen et al., 2007; Pack et al., 1996; Parsons et al., 2009; Pauls et al., 2007; Yee et al., 2005).

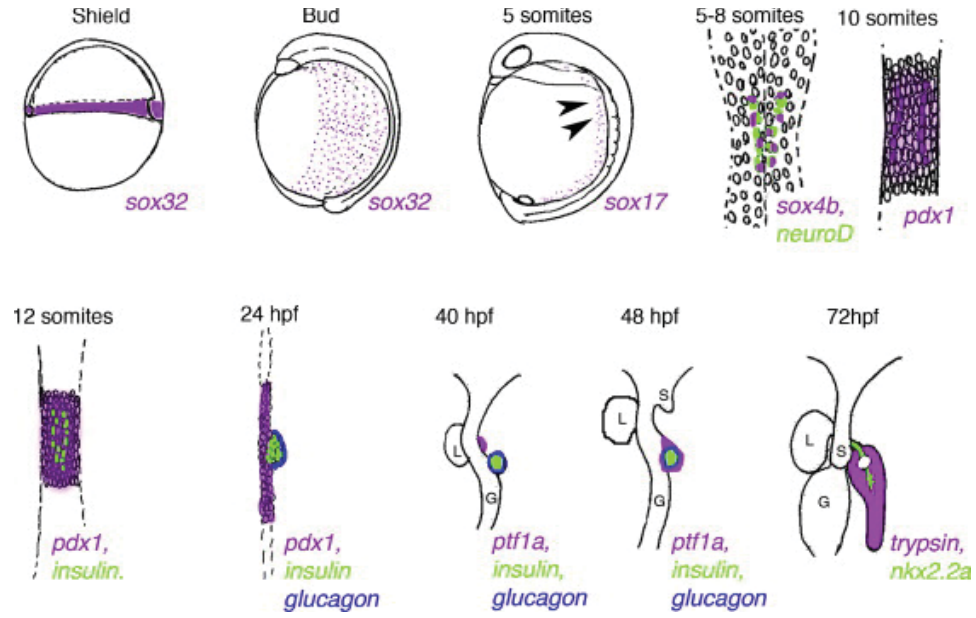

Figure 1-4 Zebrafish pancreas development. At the shield and bud stage, *sox32* is expressed. At the 5-somite stage, arrowheads indicate the *sox17*-positive endodermal area. At the 5-8 somite stages, *sox4b* and *neuroD* are the first genes expressed in the pancreatic primordium. At the 10-somite stage, two bilateral rows of cells express *pdx1*. At the 12-somite stage, *insulin* is detected. At 24 h.p.f., protrusion of the first pancreatic bud occurs with *glucagon* expression also detected. At 40 h.p.f., the second pancreatic bud is formed with *ptf1a* expression observed. At 48 h.p.f., the two buds have merged and at 72 h.p.f. growth of exocrine tissue, liver and gut is apparent. Lateral view dorsal to the right of embryos at shield, bud and 5-somite stages. Dorsal view anterior to the top of embryos at all other stages. L=liver, G=gut, S=swim bladder. Taken from Tiso et al., 2009.

1.3.3 Differentiation of pancreatic progenitor cells

Different signalling pathways and various transcription factors control the differentiation process of pancreatic cells. FGF and Notch signalling are two genetic pathways that are classically involved in cell fate decisions and differentiation from precursor cells. As previously mentioned, FGF appears to be involved in determining the fate towards ducts or organs during patterning and differentiation of the hepatopancreatic ductal system (Dong et al., 2007). Notch signalling is involved in cell fate decisions in both mammals and zebrafish (Appel et al., 1999; Artavanis-Tsakonas et al., 1999). Esni *et al.* showed that Notch signalling genes negatively regulate exocrine pancreatic differentiation in both mouse and zebrafish (Esni et al., 2004). Zebrafish *mindbomb* (*mib*) mutants, where Notch signalling is disrupted, displayed accelerated differentiation of the exocrine pancreas (Esni et al., 2004) (Table 1-3). Zecchin *et al*. determined that different Notch ligands of the Delta and Jagged families control temporally distinct phases of endocrine and exocrine cell type specification (Zecchin et al., 2007). Notch signalling also plays a role in secondary islet formation in zebrafish (Parsons et al., 2009; Wang et al., 2011). Parsons *et al.* showed that Notch inhibition induces loss of pancreatic Notch-responsive cells (PNCs) accompanied by precocious

secondary islet formation (Parsons et al., 2009). PNCs are progenitor cells that are associated with the pancreatic ductal epithelium and differentiate to form secondary islets, ducts and centroacinar cells later in development (Parsons et al., 2009; Wang et al., 2011). By using various transgenic lines the same group found that PNCs are derived from the ventral bud and are distinct from *ptf1a*-expressing pancreatic proegenitor cells (Wang et al., 2011). More recently, Huang *et al.* found that inhibition of RA signalling also induces secondary islet formation and that RA negatively regulates the differentiation of PNCs (Huang et al., 2014). In addition, G protein-coupled receptor (GPCR) signalling plays a role in clustering of endocrine progenitors into islets in both mouse and zebrafish (Serafimidis et al., 2011).

Transcription factors regulate the differentiation process at different stages (Figure 1-5). The pancreatic and duodenal homeobox 1 (Pdx1), homeobox Hb9 (Hlxb9) and pancreas transcription factor 1 subnit alpha (Ptf1a) specify pancreas progenitors at early stages. Subsequently the basic Loop-Helix-Loop factors neurogenin 3 (Ngn3) and neurogenic differentiation (NeuroD) induce the endocrine precursors and the homeodomain factors NKX-homeobox factor 2.2 (Nkx2.2) and 6.1 (Nkx6.1), Paired box 4 (Pax4) and 6 (Pax6) and aristaless related homebox (Arx) control the formation of the endocrine cells.

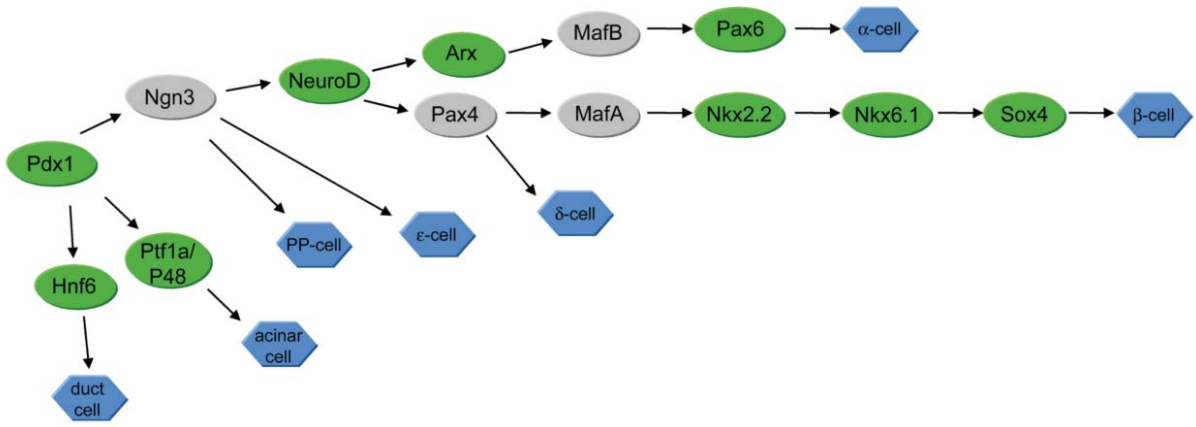

Figure 1-5 Diagram of transcription factors in mouse and zebrafish pancreatic cell differentiation. The lineages are based on data from mouse studies. The function of a transcription factor may not be conserved between mouse and zebrafish. Taken from Kinkel and Prince, 2009.

Pdx1 is one of the earliest specific markers of vertebrate endocrine and exocrine primordia (Milewski et al., 1998; Ohlsson et al., 1993). In zebrafish, *pdx1* expression starts at the 10-somite stage in the cells of the presumptive duodenum and pancreas (Biemar et al.,

2001). Studies of *pdx1* knockdown using morpholinos showed a reduction in exocrine and endocrine tissue with various endocrine cell types still present (Huang et al., 2001; Yee et al., 2001). These results suggest that Pdx1 is not required for specification but for differentiation of pancreatic cell types. Similarly in mice, the initial specification of the pancreatic buds is normal in *Pdx1* knockout embryos but further differentiation and morphogenesis of the pancreas are impaired (Ahlgren et al., 1997; Jonsson et al., 1994; Offield et al., 1996).

In mice, Hlxb9 is required for the development of the pancreas dorsal lobe but not for the initial phases of ventral bud formation (Harrison et al., 1999; Li et al., 1999). However, in zebrafish, morpholino knockdown of *hlxb9* showed that Hlxb9 is not required for early pancreas morphogenesis but is essential for β-cell differentiation (Wendik et al., 2004). Recently, it was found that within the endoderm Hlxb9 functions downstream of RA to promote β- and suppress α-cell fates in the endocrine pancreas progenitor lineage in zebrafish (Dalgin et al., 2011). In addition, Arkhipova *et al*. found that the zebrafish *hlxb9* enhancer is required and sufficient to regulate early expression in β-cells (Arkhipova et al., 2012). The simultaneous knockdown of Pdx1 and Hlxb9 using morpholinos in zebrafish lead to a near complete and persistent β-cell deficiency as opposed to early β-cell reduction and recovery after knockdown of either Pdx1 or Hlxb9 alone suggesting that Pdx1 and Hlxb9 cooperate in β-cell formation (Kimmel et al., 2011). In addition, they found that early-arising endocrine cells are already specified and their differentiation proceeds independently to *pdx1* whilst later-arising PNCs are mostly postmitotic and their differentiation is *pdx1*-dependent (Kimmel et al., 2011).

The transcription factor Ptf1a is required for converting intestinal to pancreatic lineages and for the development of acinar cells in mice (Kawaguchi et al., 2002; Krapp et al., 1998). Morpholino knockdown of *ptf1a* in zebrafish results in loss of exocrine pancreas with normal endocrine gene expression and islet morphology (Zecchin et al., 2004). By studying a *ptf1a* loss of function mutant and using morpholino knockdown, Dong *et al.* showed that high levels of Ptf1a promote exocrine fate but repress endocrine fate whereas low levels of Ptf1a promote endocrine fate (Dong et al., 2008). In addition, Hesselson *et al.* found that Ptf1a is essential in maintaining the pancreatic acinar cell fate by antagonising Ptf1a postembryonically (Hesselson et al., 2011). The *exocrine differentiation and proliferation factor* (*exdpf*) gene is a target of Ptf1a and morpholino knockdown of *expdf* resulted in loss or severe reduction of exocrine cells whilst the endocrine compartment appeared unaffected

(Jiang et al., 2008). The authors also found that *expdf* acts downstream of RA (Jiang et al., 2008). Another gene that was found to be involved in exocrine pancreas development is the Hlxb9-related factor Hlxb9la. Knockdown of *hlxb9la* using morpholino showed that Hlxb9la function in late morphogenesis of the exocrine pancreas (Wendik et al., 2004).

The differentiation of endocrine cells involves numerous transcription factors. Ngn3 was found to be required for specification of a common precursor for pancreatic endocrine cells α, β, δ and PP in mice (Gradwohl et al., 2000). Ngn3 has several downstream targets including NeuroD1 and Nkx2.2. NeuroD1 is a basic helix-loop-helix transcription factor and its loss of function in mice results in a reduction in β-cell number and arrested morphogenesis of the islet (Naya et al., 1997). Anderson *et al*. studied the network of Ngn3, Nkx2.2 and NeuroD1 in both mice and zebrafish and found that the transcriptional activity of *nkx2.2* is necessary to facilitate Ngn3 activation of NeuroD1 within the endocrine progenitor cell and also in maintaining *neurod1* expression in mature β-cells (Anderson et al., 2009a). However, Flasse *et al.* found that endocrine formation appeared normal in zebrafish *ngn3* null mutant embryos, but that endocrine cell differentiation is initiated by the basic helix-loop-helix factor Ascl1b and afterwards controlled by Neurod1 (Flasse et al., 2013). Nkx6.1 has been shown to act downstream of Nkx2.2 and is crucial for differentiation of α- and β-cells in mice and zebrafish (Binot et al., 2010; Henseleit et al., 2005; Sander et al., 2000). Another transcriptional target of Nkx2.2 is the L6 domain tetraspanin family member *tm4sf4* gene that acts in opposition to Nkx2.2 (Anderson et al., 2011).

Paired box 6 (Pax6) is a conserved transcription factor in vertebrates and plays an important role in the development of eye, brain and pancreas (Georgala et al., 2011; Sander et al., 1997; Shaham et al., 2012; St-Onge et al., 1997). Pax6 is involved in differentiation of endocrine cells: in mice, inactivation of *Pax6* lead to a severe reduction in β– and δ-cells, a near complete loss of α-cells and a significant increase of ε-cells (Heller et al., 2005; Heller et al., 2004; Sander et al., 1997; St-Onge et al., 1997) while a *pax6b* null mutant and *pax6b* morpholino injected zebrafish showed complete loss of β–cells, severe reduction of δ-cells, and a significant increase in ε-cell number (Verbruggen et al., 2010). Recently, Arkhipova *et al*. identified a cross-talk between Pax6b and Hlxb9 and showed that in zebrafish Pax6b is critical for maintenance but not induction of pancreatic *hlxb9* expression (Arkhipova et al., 2012). Another member of the Pax family, Pax4 has also been shown to play a role in pancreatic cell differentiation and act antagonistically to the transcription factor Arx. In both

mice and zebrafish, Pax4 acts opposite to Arx to modulate the number of pancreatic α-cells but Pax4 plays a crucial role only in β-cell differentiation in mice and not in zebrafish (Collombat et al., 2005; Collombat et al., 2003; Collombat et al., 2009; Djiotsa et al., 2012; Sosa-Pineda et al., 1997). The transcription factor Sox4b has also been shown to have a crucial function in generation of α-cells in zebrafish (Mavropoulos et al., 2005).

Besides Nkx2.2 and NeuroD1, Ngn3 has additional targets including the recently identified Rfx6 (Soyer et al., 2010). Rfx6 is a winged helix transcription factor that works in parallel with transcription factors NeuroD1, Pax4 and Arx during differentiation of islet cells. In zebrafish, *rfx6* is required for differentiation of cells expressing *glucagon*, *ghrelin* and *somatostatin* and for proper clustering of β-cells.

The LIM-Homeodomain (LIM-HD) transcription factor Isl1 is required for early pancreas morphogenesis and differentiation of the endocrine lineage. In mouse, Isl1 functions independently in exocrine and endocrine tissues (Ahlgren et al., 1997; Du et al., 2009; Liu et al., 2011; Liu et al., 2012). Zebrafish *isl1* mutants display a reduction in expression of endocrine hormones despite normal numbers of endocrine cells and smaller exocrine pancreas. In addition, combined knockdown of two or three *isl1/2* genes results in reduction of exocrine pancreas in a dose-dependent fashion. In zebrafish, *isl1* is important for endocrine cell maturation and *isl1* and *isl2* genes interact for expansion of the exocrine pancreas (Wilfinger et al., 2013).

Recently, Manfroid *et al*. found that the HMG box transcription factor *sox9b* gene plays a critical role in the development of the hepatopancreatic ductal system and the formation of secondary endocrine cells that are derived from pancreatic ducts (Manfroid et al., 2012). The *sox9b* mutants displayed disrupted ductal morphogenesis and differentiation and their β-cell recovery is highly compromised following β-cell ablation (Manfroid et al., 2012).

1.3.4 Role of ribosomal biogenesis genes in exocrine pancreas development

In recent years, several genes involved in ribosome biogenesis have been found to play a role in exocrine pancreas, intestine and liver development in zebrafish (Table 1-3). In 2003, Mayer and Fishman described *nil per os* (*npo*), a zebrafish mutant of *RNA-binding motif protein 19* (*rbm19*) that showed arrested morphogenesis and cytodifferentiation of the intestine and exocrine pancreas in a primordial state (Mayer and Fishman, 2003). The related yeast protein of Rbm19, Mrd1p mediates pre-rRNA processing (Jin et al., 2002). Chen *et al*. described a zebrafish mutant in the gene *digestive expansion factor* (*def*) as having hypoplastic digestive organs: pancreas, liver and intestine (Chen et al., 2005). Def is a member of a novel protein family that is conserved from yeast to human and forms part of the ribosomal small subunit (SSU) processome, a large ribonucleoprotein complex involved in pre-40S ribosome maturation (Charette and Baserga, 2010; Goldfeder and Oliveira, 2010; Harscoet et al., 2010). It was found that the isoform of *tp53*, Δ*113p53*, was selectively upregulated within the digestive organs and triggered expression of Tp53-responsive genes that lead to cell cycle arrest resulting in impaired growth of digestive organs (Chen et al., 2005). It was recently reported that Def is a nucleolar protein whose loss of function results in upregulation of Tp53 protein which accumulates in the nucleolus (Tao et al., 2013a). The authors showed that Def can lead to degradation of Tp53 protein, a process that is dependent on the activity of a cysteine protease, Calpain3 but independent of the proteasome pathway. In addition, adult transgenic fish lines with liver-specific over-expression of Def exhibited abnormal intrahepatic structure indicating that the levels of Def proteins must be controlled to maintain the structural integrity of the liver (Tao et al., 2013b).

Furthermore, Provost *et al*. described a zebrafish model of Shwachman-Diamond syndrome (Provost et al., 2012) in which morpholino knockdown of *sbds* recapitulated the developmental abnormalities characteristic of the human syndrome including pancreatic hypoplasia, skeletal defects and loss of neutrophils. Impaired expansion of *ptf1a*–expressing pancreatic progenitors was observed in *sbds* morphants. Loss of *tp53* by morpholino knockdown or by using *tp53* mutant lines fail to rescue the developmental defects observed in *sbds* knockdown thereby suggesting a Tp53-independent mechanism. Transcriptional profiling by microarray analysis and functional group analysis of differentially expressed genes revealed marked enrichment of genes involved in rRNA processing, ribosome biogenesis and translational initiation in *sbds*-deficient zebrafish. Loss of function studies of

two of these differentially expressed genes *ribosomal protein L3* (*rpl3*) and *pescadillo* (*pes*) also lead to impaired proliferation of pancreatic progenitor cells, a phenotype independent of Tp53 (Provost et al., 2012). The authors went on to study the role of other proteins of the large ribosomal subunits in pancreas development (Provost et al., 2013). They demonstrated that the *rpl* genes have a common expression pattern during development: in early embryos, their expression is initially widespread but afterwards become increasingly restricted to the endoderm. At 48 h.p.f., *rpl* genes were expressed at high levels in *ptf1a*-expressing progenitors within the pancreas. In *rpl23*^{hi2582} and *rpl6*^{hi3655b} mutants, *ptf1a*-expressing pancreatic progenitors failed to expand properly while in heterozygotes, these progenitors showed a recoverable delay in expansion. Knockdown of *tp53* failed to suppress the phenotype observed in *rpl23*^{hi2582} and *rpl6*^{hi3655b} mutant embryos suggesting a Tp53-independent mechanism (Provost et al., 2013).

Similarly, Boglev *et al.* described *titania* (*tti*^{s450}) that exhibited defects in intestine, pancreas, liver and craniofacial development (Boglev et al., 2013). It was identified in the ENU mutagenesis Liver^{plus} screen that was carried out on a transgenic line of zebrafish (*Tg(XlEef1a1:GFP)*^{s854}) expressing GFP specifically in the digestive organs (Field et al., 2003b; Ng et al., 2005; Ober et al., 2006). The *tti*^{s450} mutant harbours a nonsense mutation in *periodic tryptophan protein 2 homolog* (*pwp2h*), a gene encoding a small subunit processome component. Deficiency in *pwp2h* lead to impaired ribosome biogenesis due to a decreased production of mature 18S rRNA and 40S ribosomal subunit. The authors also found that autophagy was upregulated in intestinal epithelial cells of *tti*^{s450} mutants as a survival mechanism and this induction of autophagy was independent of the Tor and Tp53 pathways (Boglev et al., 2013).

More recently, Qin *et al.* identified and characterised a zebrafish mutant of *nucleolar protein with MIF4G domain 1* (*nom1*), a gene encoding a protein with a conserved role in 18S rRNA formation (Qin et al., 2014). The *nom1* mutants displayed defects in exocrine pancreas, intestine, liver and craniofacial development. The authors found that the pancreatic defect was due to impaired proliferation of *ptf1a*-expressing pancreatic progenitor cells and was independent of Tp53 activation. Whole transcriptome analysis by RNA-seq showed that both ribosome biogenesis and pre-mRNA splicing are perturbed in the *nom1* mutants.

Mutant	Gene	Gene Name	Phenotype	Reference
Early development				
heart and mind (*had*)	*atp1a1a.1*	ATPase, Na+/K+ transporting, alpha 1a polypeptide, tandem duplicate 1	Primary lateral *pdx1*-expressing pancreas primordia do not merge medially, perturbed endoderm morphogenesis	Shu et al., 2003
heart and soul (*has*)	*prkci*	protein kinase C, iota	Primary lateral *pdx1*-expressing pancreas de not merge	Field et al., 2003a
hnf1ba	*hnf1ba*	HNF1 homeobox Ba	Patterning of gut endoderm is disrupted, pancreas primordium does not differentiate	Sun and Hopkins, 2001
neckless (nls)	*aldh1a2*	aldehyde dehydrogenase 1 family, member A2	Pancreas primordium does not differentiate	Stafford and Prince, 2002
Endocrine pancreas				
angelina	*agl*	Unidentified	β-cells severely reduced	Kim et al., 2006
cheetah	*chee*	Unidentified	α-, β-, δ- cells scattered	Kim et al., 2006
dalmatian	*dal*	Unidentified	α-, β-, δ- cells scattered	Kim et al., 2006
floating head	*flh*		β-cells reduced	Biemar et al., 2001
knypek (*kny*)	*gpc4*	glypican 4	β-cells bilateral	Biemar et al., 2001
lazarus (*lzr*)	*pbx4*	pre-B-cell leukemia transcription factor 4	Anteriorly shifted endocrine pancreas	Popperl et al., 2000; dilorio et al., 2007
scarlet	*sle*	Unidentified	α-, β-, δ- cells scattered	Kim et al., 2006
schmalspur (*sur*)	*foxh1*	forkhead box H1	β-cells slightly reduced	Biemar et al., 2001
smoothened (*smo*)	*smo*	smoothened homolog (Drosophila)	Endocrine cells fail to develop	Roy et al., 2001; dilorio et al., 2002
sonic you (*syu*)	*shha*	sonic hedgehog a	Endocrine cells fail to develop	Roy et al., 2001; dilorio et al., 2002
spadetail	*tbx16*	T-box gene 16	β-cells bilateral or absent	Biemar et al., 2001
Exocrine Pancreas				
akreas	*ptf1a*	pancreas transcription factor 1 subunit alpha	Arrested growth of exocrine pancreas	Dong et al., 2008
apc	*apc*	adenomatous polyposis coli	Small exocrine pancreas	Goessling et al., 2008
daedalus (*dae*)	*fgf10a*	fibroblast growth factor 10a	Dysmorphic ductal system, ectopic endocrine cells	Manfroid et al., 2007; Dong et al., 2007
digestive expansion factor (*def*)	*def*	digestive expansion factor	Small exocrine pancreas	Chen et al., 2005; Tao et al., 2013a; Tao et al., 2013b
dnmt	*dnmt*	DNA methyltransferase 1	Degeneration of exocrine pancreas	Anderson et al., 2009b
donut	*met*	met proto-oncogene	Small exocrine pancreas	Anderson et al., 2013
ductjam (*dtj*)	*dtj*	unidentified	Small acini and dysmorphic ducts of exocrine pancreas	Yee et al., 2005

ducttrip (*dtp*)	*ahcy*	S-Adenosylhomocysteine hydrolase	Diminished acini and dysmoprhic ducts of exocrine pancreas	Yee et al., 2005; Matthews et al., 2009
earl grey (eal)	*sart3*	squamous cell carcinoma antigen recognised by T cells 3	Exocrine pancreas reduced or absent	Trede et al., 2007
flotte lotte (*flo*)	*ahctf1*	AT hook containing transcription factor 1	Small and degenerated exocrine pancreas	Yee et al., 2005; Davuluri et al., 2008
hdac1	*hdac1*	histone deacetylase 1	Small exocrine pancreas	Davuluri et al., 2008 Noel et al., 2008
ikarus	*fgf24*	fibroblast growth factor 24	Exocrine pancreas reduced	Manfroid et al., 2007
kras	*kras*	v-Ki-ras2 Kirsten rat sarcoma viral oncogene homolog	Arrested growth of exocrine pancreas	Park et al., 2008
mind bomb (*mib*)	*mib*	mind bomb	Premature exocrine differentiation	Esni et al., 2004
mitomess (*mms*)	*mms*	unidentified	Decreased zymogen and hypomorphic ducts of exocrine pancreas	Yee et al., 2005
nil per os (*npo*)	*rbm19*	RNA binding protein 19	Small exocrine pancreas	Mayer and Fishman, 2003
nom1	*nom1*	nucleolar protein with MIF4G domain 1	Small exocrine pancreas	Qin et al., 2014
pescadillo (*pes*)	*pes*	pescadillo	Small exocrine pancreas	Provost et al., 2012
piebald (*pie*)	*pie*	unidentified	Small and degenerated exocrine pancreas	Yee et al., 2005
rpl3	*rpl3*	ribosomal protein L3	Small exocrine pancreas	Provost et al., 2012
rpl6	*rpl6*	ribosomal protein L6	Small exocrine pancreas	Provost et al., 2012
rpl23	*rpl23*	ribosomal protein L23	Small exocrine pancreas	Provost et al., 2012
slimjim (slj)	*polr3b*	RNA polymerase III subunit 2	Small and degenerated exocrine pancreas	Yee et al., 2005; Yee et al., 2007
sweetbread (*swd*)	*swd*	unidentified	Small acini and hypomorphic ducts of exocrine pancreas	Yee et al., 2005
titania (*tti*)	*pwp2h*	periodic tryptophan protein 2 gene homolog (yeast)	Small exocrine pancreas	Boglev et al., 2013
Endocrine and Exocrine Pancreas				
minime	*mnm*	Unidentified	α-, β- cells scattered, β- cells reduced, exocrine pancreas reduced	Kim et al., 2006
peppershaker	*pps*	Unidentified	α-, β-, δ- cells scattered, exocrine pancreas disorganised	Kim et al., 2006
sea dragon	*sdr*	Unidentified	α-, β-, δ- cells reduced, duplicated exocrine pancreas	Kim et al., 2006

Table 1-3 Zebrafish mutations affecting pancreas development. Adapted from Gnugge et al., 2004, Kinkel and Prince, 2009 and Yee, 2010.

1.4 Ribosome

Since ribosomal biogenesis genes play a crucial role in exocrine pancreas development and Nol9 is involved in rRNA processing (Heindl and Martinez, 2010), I will briefly describe ribosomes, their biogenesis and function and ribosomopathies, human disorders where ribosome biogenesis or function is disrupted.

Ribosomes are essential to all organisms as a catalyst for protein synthesis and are required for cell survival, growth and differentiation. They are made up of both ribosomal ribonucleic acid (rRNA) and ribosomal proteins (RPs). The eukaryotic ribosome consists of two subunits: the 40S small subunit (SSU) and the 60S large subunit (LSU). The SSU is composed of a single rRNA (18S) and about 30 RPs, depending on the species whilst the LSU contains three rRNAs (5S, 5.8S, 25S) and about 45 RPs, varying between species (Panse and Johnson, 2010). The process of translation consists of three stages: initiation, elongation and termination, each requiring specific translation factors (Figure 1-6) (Walsh and Mohr, 2011). During the initiation step in eukaryotes, the 40S ribosome subunits bind to eukaryotic translation initiation factors, eIF1, eIF1a, the eIF3 complex, eIF5 and eIF2-GTP to form a 43S pre-initiation complex that is loaded with the initiator-methionine tRNA (Met-tRNA$_i$) in the P site. The multisubunit complex eIF4F, consisting of the cap-binding proteins eIF4E, eIF4G and eIF4A, positions the 43S complex onto the 5' end of a capped polyadenylated mRNA. The poly(A)-binding protein (PABP) recognises the polyadenylated 3' mRNA end and associates with the eIF4G resulting in a 'closed-loop' topology. The MNK kinase binds to eIF4G before phosphorylating eIF4E. After the 48S complex scans the mRNA and recognises the AUG start codon, the 60S subunit joins and triggers the release of the initiation factors (Jackson et al., 2010). During the elongation step, eEF1A•GTP delivers charged tRNAs to the 80S ribosome A site. After peptide-bond formation is catalysed by the 60S subunit, the eukaryotic elongation factor 2 (eEF2) translocates the 80S ribosome resulting in the deacetylated tRNA in the E site, the peptidyl-tRNA in the P site and a re-exposed A site (Herbert and Proud, 2007). During termination, the eukaryotic release factor 1 (eRF1) identifies the stop codon in the A site and stimulates the arrest of 80S and the release of the polypeptide. eRF3 frees eRF1 from the ribosome and the complex is dismantled by a group of initiation factors and nucleotide-hydrolysis by ABCE1, thus promoting the release of mRNA, tRNAs and the recycling of ribosomal subunits (Dinman and Berry, 2007).

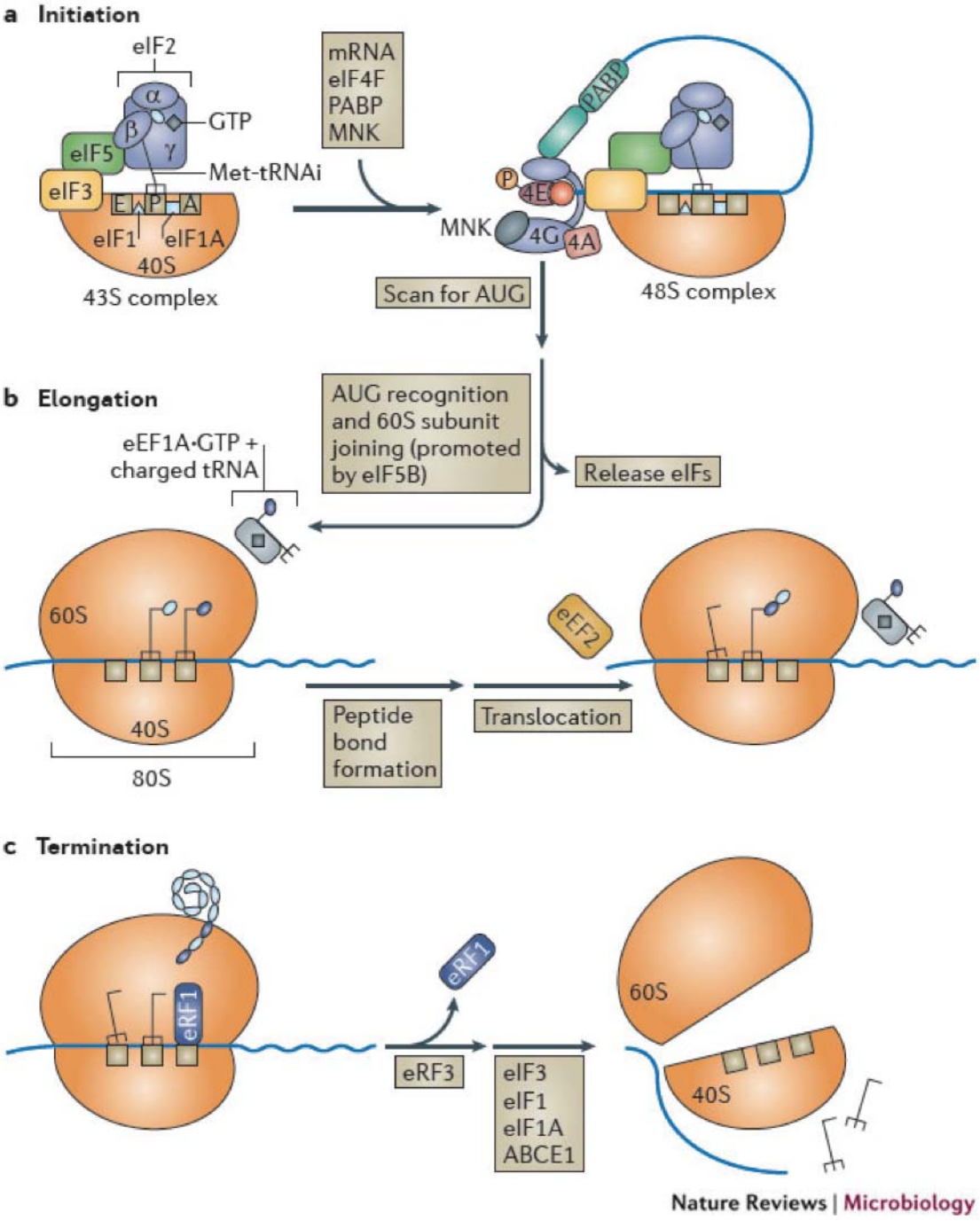

Figure 1-6 Overview of eukaryotic mRNA translation. The process of translation is divided into initiation, elongation and termination. During initiation (a), the 40S ribosome subunits bind to eukaryotic translation initiation factors, the initiator-methionine tRNA (Met-tRNA$_i$), the poly(A)-binding protein (PABP) and MNK to form the 48S complex that scans the mRNA. After AUG start codon recognition and joining of the 60S subunit, the initiation factors are released. During elongation (b), charged tRNAs are delivered by eEF1A•GTP and peptide-bond formation is catalysed by the 60S subunit. The 80S ribosome is then translocated by eukaryotic elongation factor (eEF2). During termination (c), the recognition of a stop codon by the eukaryotic release factor 1 (eRF1) initiates arrest of the 80S and the release of the polypeptide. eRF1 is released by eRF3 and the 80S complex is dismantled by several initiation factors and ABCE1-directed nucleotide hydrolysis resulting in subunit recycling. Taken from Walsh and Mohr, 2011.

1.4.1 Ribosome biogenesis

Ribosome biogenesis is an energy intensive and remarkably complex process that occurs at multiple cell sites. It utilises 60% of total cellular transcription in a growing yeast cell, with 2000 ribosomes synthesised every minute (Warner et al., 2001) whilst 7500 ribosomal subunits are made per minute in a mammalian HeLa cell (Lewis and Tollervey, 2000). It requires the coordinated action of all three RNA polymerase (RNAP I, II, III) and the synthesis of 4 rRNAs, 82 core RPs, more than 200 non-ribosomal proteins and approximately 70 small nucleolar RNAs (snoRNAs) (Panse and Johnson, 2010).

This multi-step process begins in the nucleolus with the RNAP I transcription of the ribosomal deoxyribonucleic acid (rDNA) units that are found in hundreds of copies as tandem repeats across the human genome (Figure 1-7). A single polycistronic 45S pre-rRNA is produced and subjected to several co-transcriptional modifications such as methylation and pseudo-uridylation by small nucleolar RNA-protein complexes (snoRNPs) (Lafontaine and Tollervey, 2006). Ribosomal Proteins (RPs) are synthesised in the cytoplasm and imported into the nucleus/nucleolus where they assemble on the nascent pre-rRNA in a hierarchical fashion. The resulting new structures recruit non-ribosomal *trans*-acting factors that are important in liberating mature RNAs from pre-rRNA precursors. Additional pre-rRNA processing involves removal of the flanking and internal spacer regions by a series of endo- and exo-nucleolytic cleavage events. Cleavage at site A2, the spacer region between the 18S and 5.8S rRNA results in the formation of pre-40S and pre-60S particles. The 5S rRNA is synthesised concurrently in the nucleoplasm by RNA pol III and is incorporated into the pre-60S subunit. Figure 1-8 and Figure 1-9 show the pre-ribosomal particles and non-ribosomal proteins including the ones mentioned in this thesis along the 40S (Figure 1-8) and the 60S assembly pathways (Figure 1-9) in *Saccharomyces cerevisiae* (Kressler et al., 2010).

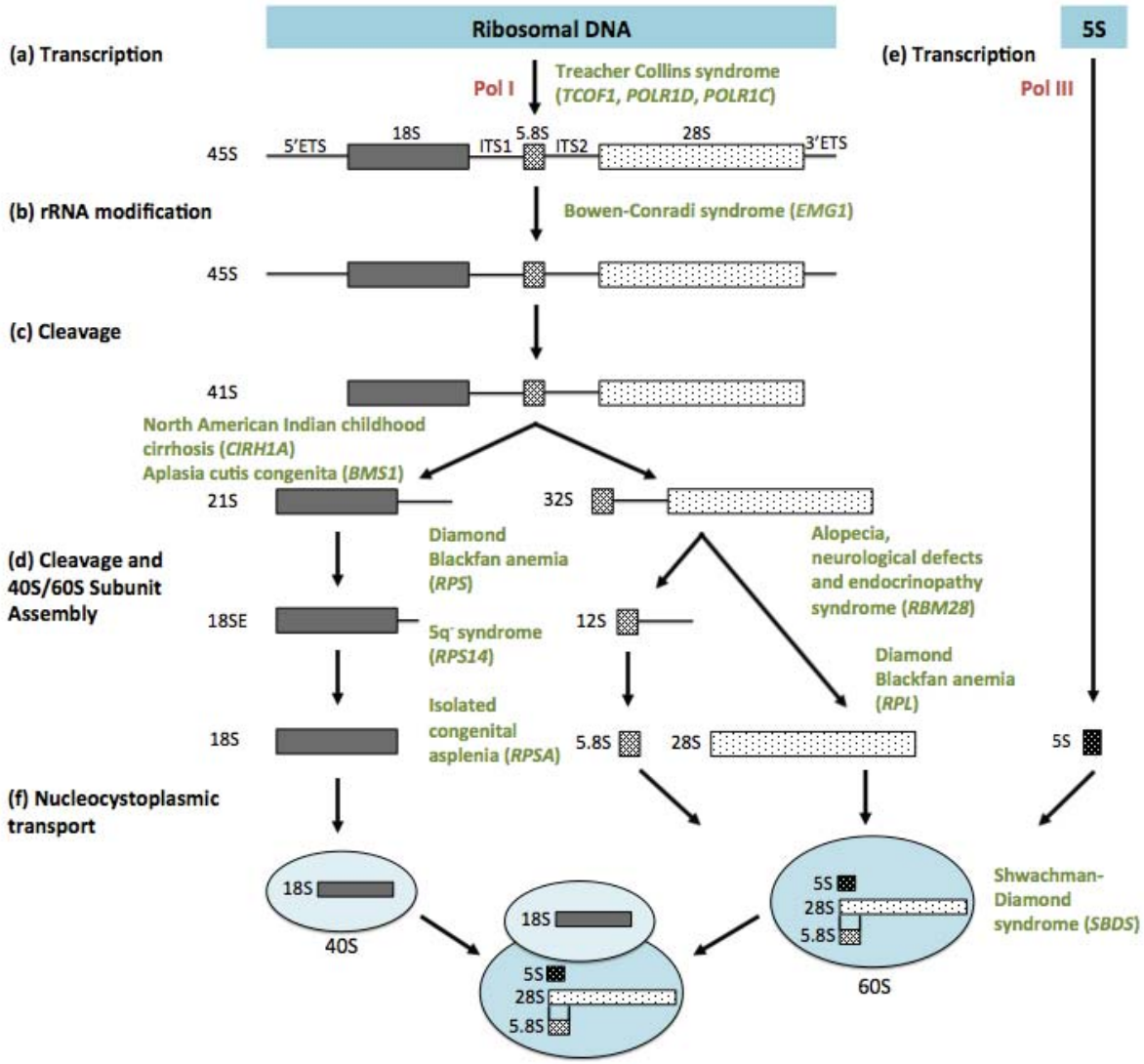

Figure 1-7 Simplified schematic of ribosome biogenesis and the stages which is affected in different ribosomopathies. Ribosome biogenesis starts with RNAP I transcription of rDNA (a) to produce a 45S pre-rRNA that is modified (b) and cleaved by exo- and endo-nucleases (c, d) to produce pre-40S rRNA (18S) and pre-60S rRNA (5.8S and 28S) particles. Ribosomal proteins assemble on the nascent pre-rRNA particles to form pre-40S and pre-60S particles (d). Meanwhile the 5S rRNA is transcribed by RNAP III and is incorporated into the pre-60S particles (e). The pre-ribosomal particles are exported to the cytoplasm (f) where final steps of maturation occur to produce translationally competent ribosomes. The names of the various ribosomopathies and their causative genes in brackets are shown. Adapted from Narla and Ebert, 2010 and Liu et al., 2013.

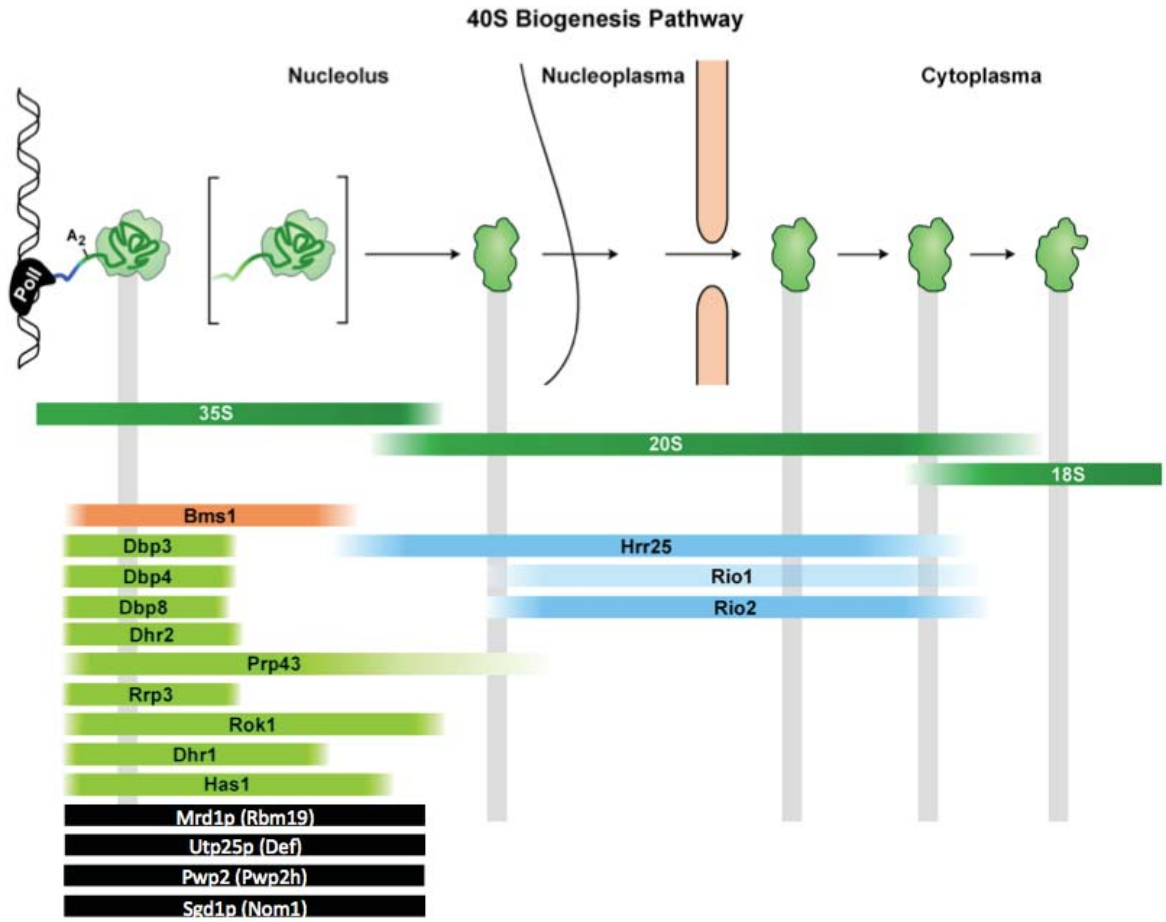

Figure 1-8 The 40S assembly pathway in *Saccharomyces cerevisiae*. The major 40S pre-ribosomal intermediates, their rRNAs (dark green), DExD/H-box ATPases (green), kinases (light blue) and GTPase (orange) are shown. The four proteins Mrd1p, Utp25p, Pwp2 and Sgd1p and their zebrafish orthologues in brackets (black) are mentioned in this thesis. The 35S pre-rRNA is transcribed by RNA Pol I and modified by snoRNPs. RPs and non-ribosomal factors assemble co-transcriptionally with the pre-rRNA and cleavage at site A2 generates the 20S pre-rRNA. The final rRNA processing occurs in the cytoplasm. Adapted from Kressler et al., 2010.

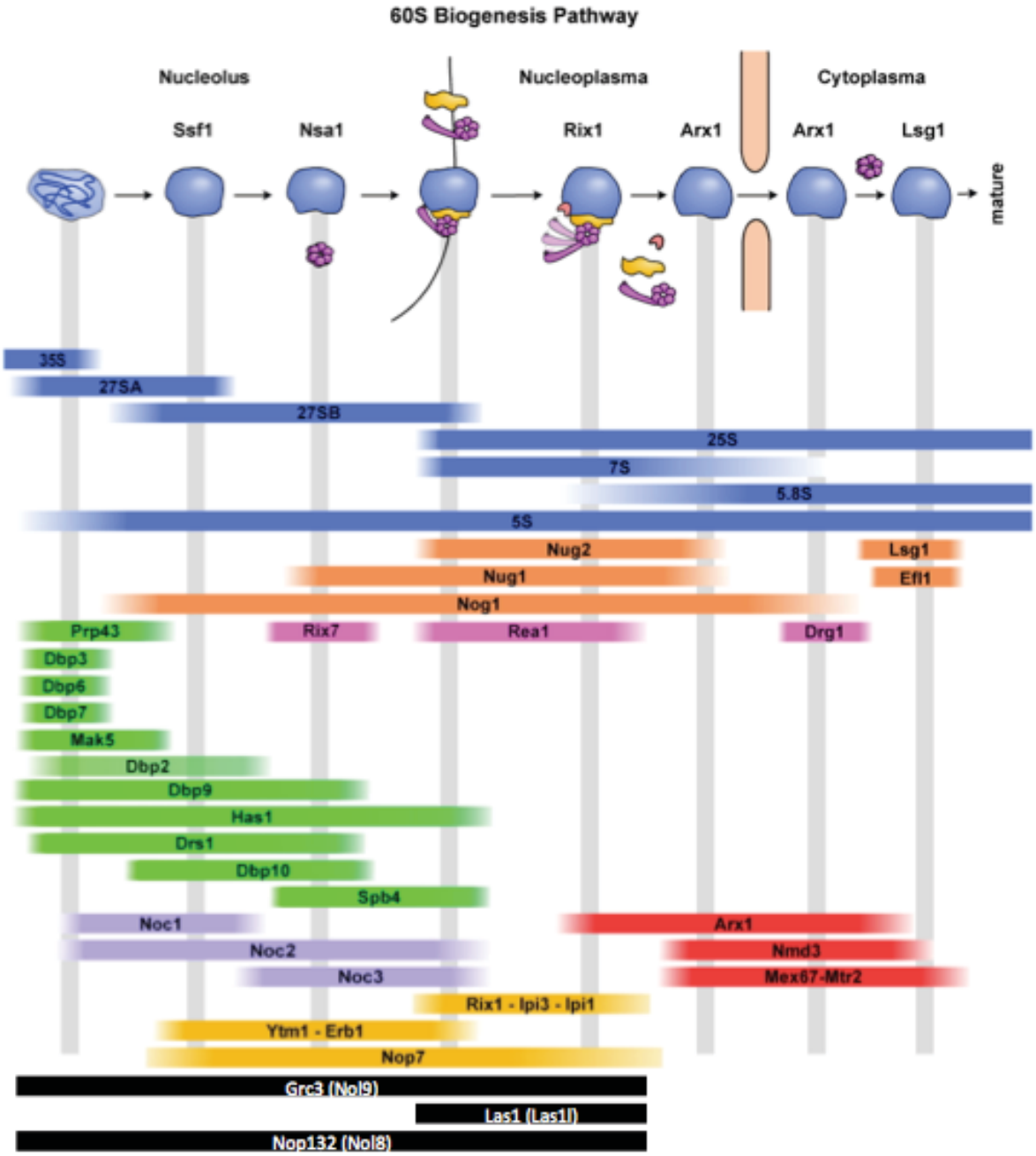

Figure 1-9 The 60S assembly pathway in *Saccharomyces cerevisiae*. The 60S pre-ribosomal intermediates, their rRNAs (blue), GTPases (orange, DexD/H-box, ATPases (green), AAA-type ATPases (pink), subcomplexes (purple/yellow) and export factors are shown. The proteins Grc3, Las1 and Nop132 and their zebrafish orthologues in brackets (black) are mentioned in this thesis. Adapted from Kressler et al., 2010.

The subsequent biogenesis and export pathways of pre-40S and pre-60S particles are independent. Pre-ribosomal particles are transported through the nuclear pore complex (NPC) to be released into the cytoplasm, where the final steps of maturation occur. Previously associated *trans*-acting and export factors are released from the pre-ribosomal particles and the final rRNA processing steps occur before the subunits can achieve translational competence (Liu et al., 2013; Panse and Johnson, 2010). Figure 1-10 shows the export of the pre-60S particles and the release of non-ribosomal factors in *Saccharomyces cerevisiae* (Kressler et al., 2010).

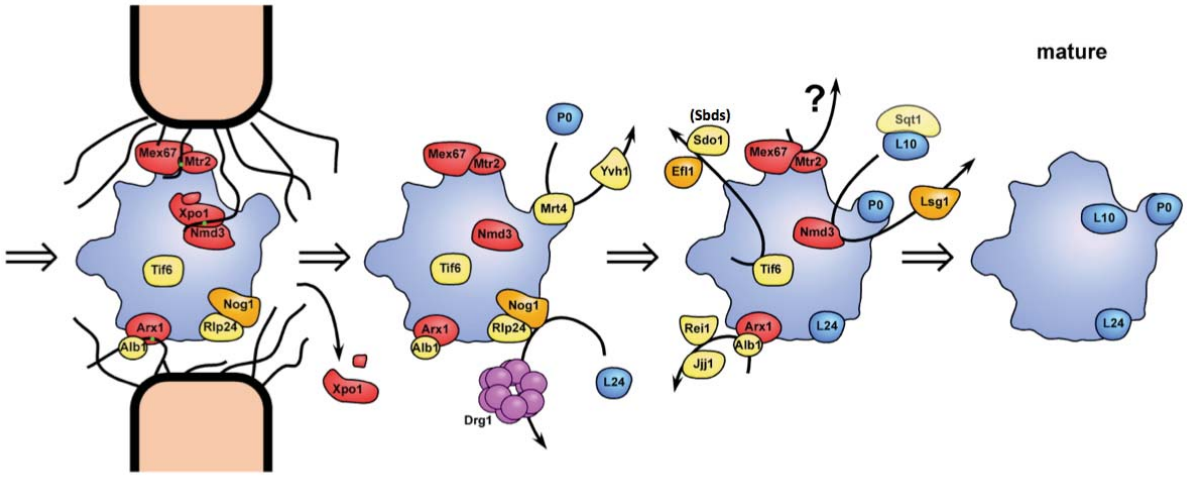

Figure 1-10 The export and maturation of pre-60S particles in *Saccharomyces cerevisiae*. The export factors (red), GTPases (orange), Drg1 AAA-ATPase (pink), other non-ribosomal factors (yellow) and ribosomal proteins (blue) are shown. Sdo1 and its zebrafish orthologue in bracket are mentioned in this thesis. Adapted from Kressler et al., 2010.

1.4.2 Ribosomopathies

Ribosomopathies consist of a group of disorders with defects in genes involved in ribosome biogenesis and function (Figure 1-7, Table 1-4). They show a wide range of symptoms, modes of inheritance and impaired molecular processes but there are some shared patterns between them. Firstly, most of the diseases are caused by haploinsufficiency or partial loss of protein expression suggesting that homozygous null mutations of genes involved in ribosome biogenesis are embryonic lethal. Secondly, even though there is no one symptom present in all diseases, shared clinical features between diseases are observed including defects in growth and development, haematological phenotypes such as anaemia and congenital anomalies such as thumb and craniofacial defects and susceptibility to cancer. The affected cell compartments show hypoplasia with decreased proliferation and increased apoptosis. Thirdly, a common cell death mechanism is probable since mutations in genes involved in ribosome biogenesis can activate the Tp53 pathway (Armistead and Triggs-Raine, 2014; Freed et al., 2010; Liu et al., 2013; Narla and Ebert, 2010).

The ribosomopathies that are inherited in an autosomal dominant fashion include Treacher Collins syndrome (TCS), Diamond Blackfan anemia (DBA), isolated congenital asplenia (ICAS) and aplasia cutis congenita (ACC). TCS (OMIM #606847 and #613717) and its autosomal recessive form (OMIM #248390) is characterised by craniofacial defects including abnormalities of the eyes, ears and facial bones including those of the cheek and lower jaw. In 1996, the Treacher Collins Syndrome Collaborative Group had identified five mutations in the Treacle gene (*TCOF1*) by positional cloning (The Treacher Collins Syndrome Collaborative Group, 1996) and currently the *TCOF1* database contains over 200 mutations including mostly nonsense, insertion, deletion and alternative splicing mutations (www.genoma.ib.usp.br/TCOF1_database). The protein Treacle has been shown to be essential for transcription of ribosomal DNA and is a component of the snoRNP complexes that plays a role in methylation of pre-rRNA transcripts (Gonzales et al., 2005; Valdez et al., 2004). Recently, mutations in genes *POLR1C* and *POLR1D* that encode shared subunits of RNA polymerase I and III have been identified as causing TCS (Dauwerse et al., 2011). By performing genome-wide copy number analysis, Dauwerse *et al*. identified a de novo deletion in *POLR1D* gene in an individual and subsequently detected 20 additional heterozygous mutations. They also sequenced the candidate gene *POLR1C* since it interacts strongly with

POLR1D and discovered compound heterozygous mutations in three patients (Dauwerse et al., 2011).

DBA (OMIM #105650, #610629, #612527, #612528, #612561, #612562, #612563, #613308, #613309, #614900, #615550 and #615909) is a congenital bone marrow failure syndrome and is characterised by large red blood cells due to low haemoglobin levels (macrocytic anaemia), abnormal decrease in immature red blood cells (reticulocytopenia), absence or selective decrease of erythroid precursors and increased risk of malignancy. In 40-62% of patients, additional physical abnormalities are present including cardiac defects, short stature and thumb abnormalities (Lipton and Ellis, 2009). The most commonly affected gene in DBA is *RPS19* (Draptchinskaia et al., 1999) but mutations in other ribosomal protein genes have also been found and include *RPS24* (Gazda et al., 2006), *RPS17* (Cmejla et al., 2007), *RPL35A* (Farrar et al., 2008), *RPL5* , *RPL11*, *RPS7* (Gazda et al., 2008), *RPS26*, *RPS10* (Doherty et al., 2010), *RPL26* (Gazda et al., 2012), *RPL15* (Landowski et al., 2013) and *RPS29* (Mirabello et al., 2014). In addition, causative mutations in the haematopoietic transcription factor gene *GATA1* have been found in patients with DBA (Ludwig et al., 2014; Parrella et al., 2014; Sankaran et al., 2012). More recently, Gripp *et al.* reported mutations in *RPS26*, *TSR2* and *RPS28* in patients that present with combining features of TCS and DBA (Gripp et al., 2014).

ICAS (OMIM #71400) is characterised by the absence of spleen with no other developmental defects at birth. Most affected individuals are susceptible to life-threatening bacterial infections (Mahlaoui et al., 2011). Recently, Bolze *et al.* identified heterozygous mutations in *ribosomal protein SA* (*RPSA*) in 18 patients from 8 families (Bolze et al., 2013). *RPSA* encodes a protein that is involved in pre-rRNA processing (O'Donohue et al., 2010) and is also a component of the small subunit (Ben-Shem et al., 2011).

ACC (OMIM #107600) is a non-syndromic disorder characterised by a congenital absence of skin usually on the scalp vertex (Nousbeck et al., 2008). Marneros identified the causative mutation of the autosomal dominant form of ACC in the ribosomal GTPase *BMS1* by genome-wide linkage analysis and exome sequencing (Marneros, 2013). The yeast orthologue of *BMS1*, *BMS1P* is required for the synthesis of the 18S rRNA precursors of the 40S ribosomal subunits (Gelperin et al., 2001).

Shwachman-Diamond syndrome (SDS), Bowen-Conradi syndrome (BCS), North American Indian childhood cirrhosis (NAIC) and alopecia, neurological defects and endocrinopathy (ANE) syndrome are amongst the autosomal recessive ribosomopathies. BCS (OMIM #211180) has been described mostly in the Hutterite population. It is a lethal and autosomal recessive syndrome characterised by pre- and post-natal growth retardation, smaller head circumference (microcephaly), slowed mental and physical processes (psychomotor delay) and multiple joint abnormalities (Bowen and Conradi, 1976). Armistead *et al.* (Armistead et al., 2009) recently reported a missense mutation in *EMG1*, one of 35 candidate genes in the interval mapped by linkage and haplotype analysis (Lamont et al., 2005). Emg1 is a putative methyltransferase and is involved in maturation of 18S rRNA and biogenesis of the 40S ribosomal subunit (Eschrich et al., 2002; Leulliot et al., 2008; Liu and Thiele, 2001).

NAIC (OMIM #604901) is found in the Ojibway-Cree population in Canada and manifests as neonatal jaundice, eventually leading to progressive destruction of the small bile ducts of the liver (biliary cirrhosis) (Betard et al., 2000). By genome-wide scan (Betard et al., 2000) and sequencing of candidate genes in the haplotype shared by all patients, a homozygous missense mutation (R565W) in the gene *CIRH1A* was reported to cause NAIC (Chagnon et al., 2002). Cirhin is a component of the small ribosomal subunit (SSU) processome t-UTP subcomplex and is required for processing of 18S rRNA and optimal rDNA transcription in both yeast and human cells (Gallagher et al., 2004; Prieto and McStay, 2007). Recently, Nol11 was found to interact with Cirhin and this interaction is partially disrupted by the R565W mutation implicating a role for *NOL11* in the pathogenesis of NAIC. Nol11 is also a component of the SSU processome and has similar function to Cirhin (Freed et al., 2012). *Cirh1a* knockout in mice was reported to be embryonic lethal whilst heterozygotes appeared to develop normally (Yu et al., 2009). Recently, a zebrafish model of NAIC was generated by morpholino knockdown of *cirh1a* (Wilkins et al., 2013). Cirhin-deficient 5 d.p.f. zebrafish larvae showed defects in biliary and canalicular morphology and hepatobiliary function (Wilkins et al., 2013).

ANE syndrome (OMIM #612079) is characterised by hair loss, microcephaly, mental retardation, progressive motor retardation and adrenal insufficiency. Nousbeck *et al.* identified a loss-of-function mutation in *RBM28* in a family with ANE syndrome by homozygosity mapping and candidate gene analysis (Nousbeck et al., 2008). *NOP4P*, the

yeast orthologue of *RBM28* is required for production of mature rRNA of the 60S ribosomal subunits (Sun and Woolford, 1994, 1997)

In contrast to the ribosomopathies described so far, a region that contains 40 genes in the long arm of chromosome 5 is deleted in the $5q^-$ syndrome (OMIM #153550) (Van den Berghe et al., 1974). $5q^-$ syndrome is a myelodysplastic syndrome (MDS) that shows ineffective production of non-lymphocyte blood cells and is characterised by macrocytic anaemia. *RPS14*, one of the genes deleted in the $5q^-$ region, was shown to be associated with the syndrome in an RNA interference-based functional screen (Ebert et al., 2008). Inactivating mutations in ribosomal protein genes in DBA is analogous to acquired haploinsufficiency for *RPS14* in $5q^-$ syndrome and contribute to the erythroid defects in both disorders.

Cartilage hair hypoplasia (CHH; OMIM #250460) and its variants anauxetic dysplasia (OMIM #607095) and metaphyseal dysplasia without hypotrichosis (OMIM #250460) (Bonafe et al., 2002; Ridanpaa et al., 2001; Thiel et al., 2005) and X-linked dyskeratosis congenita (X-DC; OMIM #305000) (Heiss et al., 1998) have initially been described as ribosomopathies. However the role of ribosome pathology in these two disorders is currently being challenged and therefore they will not be addressed in this chapter.

In general, the most surprising feature of ribosomopathies is that specific phenotypes in particular cell types are observed even though ribosomes are universally required for protein synthesis and ribosomal biogenesis proteins are ubiquitously expressed. The underlying mechanisms are not fully understood but the main hypothesis is that that highly proliferating tissues have a greater need for ribosomes and therefore are more severely affected than tissues with lower proliferating activity.

Ribosomopathies	Gene	Genetic Defect	Impaired Molecular Function	Clinical Features	References
Treacher Collins syndrome (TCS)	*TCOF1, POLR1D, POLR1C*	*TCOF1* and *POLR1D*: Autosomal Dominant *POLR1C:* Autosomal Recessive	Transcription of rDNA; *TCOF1* also involved in methylation of 18S rRNA	Cranofacial abnormalities	Shu et al., 2003, The Treacher Collins Syndrome Collaborative Group, 1996, Dauwerse et al., 2011.
Diamond Blackfan anemia (DBA)	*RPS19, RPS24, RPS17, RPL35A, RPL5, RPL11, RPS7, RPS10, RPS26, RPL26, RPL15, RPS29, GATA1*	Sporadic, autosomal dominant (40-45%)	Processing of pre-rRNA of 40S or 60S ribosomal subunit and proliferation/differentiation of haemopoietic progenitors	Macrocytic anaemia, cranofacial abnormalities,thumb abnormalities, short stature	Draptchinskaia et al., 1999, Gazda et al., 2006, Cmejla et al., 2007, Farrar et al., 2008, Gazda et al., 2008, Doherty et al., 2010, Gazda et al., 2012, Sankaran et al., 2012, Landowski et al., 2013, Ludwig et al., 2014, Mirabello et al., 2014, Parrella et al., 2014.
Treacher Collins syndrome and Diamond Blackfan anemia	*RPS26, TSR2, RPS28*	Autosomal Dominant	Processing of pre-rRNA of 40S ribosomal subunit	Macrocytic anaemia, cranofacial abnormalities	Gripp et al. 2014
Isolated congenital asplenia (ICAS)	*RPSA*	Autosomal Dominant	Component of 40S ribosomal subunit	Absence of spleen	Bolze et al., 2013
Aplasia cutis congenita (ACC)	*BMS1*	Autosomal Dominant	Ribosomal GTPase	Agenesis of skin, usually on scalp vertex	Marneros et al., 2013
Shwachman-Diamond syndrome (SDS)	*SBDS*	Autosomal Recessive	Maturation and export of 60S ribosomal subunit	Neutropenia/infections, pancreatic insufficiency, short stature	Boocock et al., 2003
Bowen-Conradi syndrome (BCS)	*EMG1*	Autosomal Recessive	Maturation of 40S ribosomal subunit	Growth retardation, psychomotor delay	Armistead et al., 2009
North American Indian childhood cirrhosis (NAIC)	*CIRH1A*	Autosomal Recessive	Maturation of 18S rRNA and rDNA transcription	Cirrhosis	Chagnon et al., 2002
Alopecia, neurological defects and endocrinopathy (ANE) syndrome	*RBM28*	Autosomal Recessive	Processing of pre-rRNA of 60S ribosomal subunit	Hair loss, microcephaly mental retardation, progressive motor retardation, adrenal insufficiency	Nousbeck et al., 2008
$5q^-$ syndrome	*RPS14*	Unknown	Maturation and export of 60S ribosomal subunit	Myelodysplastic syndrome, macrocytic anaemia	Van den Berghe et al., 1974

Table 1-4 Summary of ribosomopathies with details about the causative gene(s), genetic defect, impaired molecular function and clinical features. Adapted from Freed et al., 2010, Narla and Ebert 2010, Liu et al., 2013 and Armistead et al., 2014.

1.5 Thesis aims and objectives

The aim of this thesis is to characterise *nol9*^{sa1022} mutants in order to determine the function of Nol9 in zebrafish pancreas development and to provide insight into the mechanisms involved in rRNA processing mutants. To achieve this, the following objectives will need to be attained:

1. Confirm that *nol9* is the affected gene in *nol9*^{sa1022} mutant (Chapter 3)

Zebrafish mutants generated by ENU mutagenesis contain several disruptive mutations. To provide support that *nol9* is responsible for the pancreas phenotype in *nol9*^{sa1022} mutants, genotype-phenotype correlation and *nol9* morpholino knockdown was carried out in transgenic line *Tg(ins:mCherry)*^{jh2}*;Tg(ptf1a:EGFP)*^{jh1}.

2. Examine *nol9*^{sa1022} mutant for additional non-pancreatic defects (Chapter 3)

Zebrafish mutants of ribosomal biogenesis genes have defects in other organs including the intestine, liver and jaw. The *nol9*^{sa1022} mutant was analysed for those defects by staining and labelling using tissue-specific probes.

3. Identify the stage at which pancreas development is affected in *nol9*^{sa1022} mutant (Chapter 3)

It is important to determine the developmental stage at which pancreatic organogenesis is affected, i.e. during endoderm induction, specification of pancreas progenitor cells or proliferation of differentiated pancreatic cells. The pancreas development was studied using pancreatic-stage specific probes and the transgenic line *Tg(ins:mCherry)*^{jh2}*;Tg(ptf1a:EGFP)*^{jh1}.

4. Examine the formation of the endocrine pancreas namely the pancreatic islet and the secondary islets in *nol9*^{sa1022} mutant (Chapter 3)

The study of the endocrine pancreas is valuable since formation of the exocrine pancreas is impaired in *nol9*^{sa1022} mutant. The formation and differentiation of endocrine cells of the pancreatic islet was investigated using various antibodies and the formation of the secondary islets was examined using the Notch-inhibitor DAPT and the transgenic line *Tg(ins:mCherry)*^{jh2}*;Tg(ptf1a:EGFP)*^{jh1}.

5. Assess cell proliferation and cell death in *nol9*^{sa1022} mutant (Chapter 3)

Impaired cell proliferation and increased cell death can contribute to the defects in digestive organ development in *nol9*^{sa1022} mutant. Therefore the cell cycle of *nol9*^{sa1022} mutant was examined using flow cytometry analysis, cell proliferation rate and cell death of the exocrine pancreas of *nol9*^{sa1022} mutant were studied using Bromodeoxyuridine (BrdU) incorporation assay and terminal deoxynucleotidyl transferase dUTP nick end labelling (TUNEL) assay respectively.

6. Determine the expression pattern of *nol9* during zebrafish development (Chapter 3)

The expression pattern of *nol9* may help explain the tissue-specific defects observed in *nol9*^{sa1022} mutants and was examined using *in situ* hybridisation with a probe targeting the *nol9* gene.

7. Determine the function of Nol9 in rRNA processing and ribosome biogenesis in zebrafish (Chapter 3)

The human NOL9 protein has been shown to be involved in the processing of 28S rRNA of the large ribosomal subunit. The function of Nol9 in rRNA processing and ribosome biogenesis in zebrafish was determined by Northern blot analysis and polysome fractionation respectively.

8. Characterise *las1l*^{sa674}, a mutant in a Nol9-interacting protein (Chapter 4)

Assessment of the literature identified proteins that interact with Nol9 including LAS1-like (LAS1). The *las1l*^{sa674}, a mutant in the zebrafish orthologue of *LAS1L* was characterised using staining and the transgenic line *Tg(ins:mCherry)*^{jh2}*;Tg(ptf1a:EGFP)*^{jh1}.

9. Identify changes in gene expression in *nol9*^{sa1022} and *las1l*^{sa674} mutants (Chapter 5)

The mRNA expression profiles of *nol9*^{sa1022} and *las1l*^{sa674} mutants can reveal insight into the functions of *nol9* and *las1l* during development and was conducted using Differential Expression Transcript Counting Technique (DeTCT). The enrichment for gene ontology terms and pathways was carried out using the R topGO package and the Database for Annotation, Visualization and Integrated Discovery (DAVID).

10. Determine whether the mechanism involved in the pancreatic defects of *nol9*^{sa1022} mutants is Tp53-dependent or –independent (Chapter 5)

The Tp53 signalling pathway is known to function as a surveillance mechanism in response to defective ribosome biogenesis. It was determined whether the mechanism operating in *nol9*^{sa1022} and is Tp53-dependent or –independent by using a *tp53* loss of function mutant line and the transgenic line *Tg(ins:mCherry)*^{jh2}*;Tg(ptf1a:EGFP)*^{jh1}.

11. Compare the mRNA expression profiles of *nol9*^{sa1022} and *las1l*^{sa674} mutants with those of other rRNA processing mutants, *tti*^{s450} and *set*^{s453} (Chapter 5)

The mRNA expression profiles of *nol9*^{sa1022}, *las1l*^{sa674}, *tti*^{s450} and *set*^{s435} mutants were compared to identify shared genes and signalling pathways so as to help in deciphering the mechanism involved in the defective development of digestive organs of all four mutants.

Chapter 2 Materials & Methods

2.1 Zebrafish husbandry and genotyping

2.1.1 General husbandry

Adult zebrafish *nol9*$^{sa1022/+}$ and *las1l*$^{sa674/+}$ were kindly provided by the Wellcome Trust Sanger Institute (WTSI), Zebrafish Mutation Project, Hinxton, Cambridge. These adult zebrafish *nol9*$^{sa1022/+}$ were outcrossed to SAT wild-type and maintained as heterozygous lines. Fluorescent reporter lines *Tg(ins:mCherry)*^{jh2} (Pisharath et al., 2007) and *Tg(ptf1a:EGFP)*^{jh1} (Godinho et al., 2005), were kindly provided by Dr Elke Ober, MRC National Institute for Medical Research , Mill Hill, London . These two lines were incrossed to produce *Tg(ins:mCherry)*^{jh2}*;Tg(ptf1a:EGFP)*^{jh1}. The *tp53*^{zdf1} (Berghmans et al., 2005) was kindly provided by Dr Sebastian Gerety, Wellcome Trust Sanger Institute, Hinxton, Cambridge. The *nol9*$^{sa1022/+}$ adult zebrafish obtained from WTSI was outcrossed to *Tg(ins:mCherry)*^{jh2}*;Tg(ptf1a:EGFP)*^{jh1} and *tp53*$^{zdf1/+}$ to generate the lines *Tg(ins:mCherry)*^{jh2}*;Tg(ptf1a:EGFP)*^{jh1}*;nol9*$^{sa1022/+}$ and *nol9*$^{sa1022/+}$*;tp53*$^{zdf1/+}$ respectively. The *las1l*$^{sa674/+}$ was outcrossed to *Tg(ins:mCherry)*^{jh2}*;Tg(ptf1a:EGFP)*^{jh1} to produce *Tg(ins:mCherry)*^{jh2}*;Tg(ptf1a:EGFP)*^{jh1}*;las1l*$^{sa674/+}$. The *nol9*$^{sa1022/+}$*;tp53*$^{zdf1/+}$ was outcrossed to *Tg(ins:mCherry)*^{jh2}*;Tg(ptf1a:EGFP)*^{jh1} to generate the line *Tg(ins:mCherry)*^{jh2}*;Tg(ptf1a:EGFP)*^{jh1}*nol9*$^{sa1022/+}$*;tp53*$^{zdf1/+}$. All fish were maintained in accordance with regulations from the Institute and the Home Office.

For breeding purposes, adult males and females were placed in breeding tanks with a divider to separate the adults from the eggs. Embryos were collected and incubated in water containing and 2 mg/l methylene blue (Sigma). When stated, the embryos were maintained in water containing 0.18g/l sea salt and 0.002% Phenylthiourea (PTU, Sigma) in 0.18 g/l sea salt was added at 8-24 h.p.f. to inhibit melanocyte formation (Karlsson et al., 2001). All the embryos were raised at 28.5°C and staged according to Kimmel *et al.*, 1995 (Kimmel et al., 1995).

2.1.2 Genotyping of zebrafish embryos, larvae and adults

Genomic DNA was extracted using the Hot Shot method (described below) from whole embryos or fin clips and by Proteinase K digestion from embryos processed for whole-mount *in situ* hybridisation or immunohistochemistry. Genotyping was then performed by competitive allele-specific PCR (KASP) genotyping system (KBioscience).

Zebrafish, at least 3 months old, were anaesthetised in 0.02% 3-amino-benzoic acid ethyl ester (Sigma) before the tip of the tail fin was clipped and placed in individual well of a 96-well plate. They were individually kept until genotyping was completed. Whole zebrafish embryos were fixed at the appropriate stage in 100% methanol at -20°C overnight. Individual embryos were placed in wells of a 96-well plate and allowed to dry. Fin clips or whole embryos were digested in Hot Shot alkaline lysis buffer (25 mM NaOH, 0.2 mM EDTA) (50ul or 25ul respectively) at 95°C for 30 mins, followed by 5 mins on ice. An equal volume of Hot Shot neutralisation buffer (40mM Tris-HCl) was then added. DNA was diluted to a working concentration of 1.25-12.5 ng/µl.

Embryos processed for whole-mount *in situ* hybridisation and immunohistochemistry were placed in wells of 96-well plate and digested in 100 µg/ml of Proteinase K (Invitrogen) in lysis buffer (100 mM Tris-HCl, 200 mM NaCl, 0.2% SDS, 5 mM EDTA, pH 8) at 55°C overnight, with occasional vortexing to ensure complete disruption. Proteinase K was inactivated at 80°C for 30 mins. 50 µl isopropanol was added and plates were repeatedly inverted. DNA was precipitated by centrifugation at 4200rpm at 4°C for 30 mins. The DNA pellet was washed twice with 100 µl 70% ethanol, allowed to dry and resuspended in 25 µl of water to a working concentration of 1.25-12.5 ng/µl.

Genotyping was carried out using the competitive allele-specific PCR (KASP) genotyping system (KBioscience). 4 µl of DNA was pipetted into a black 96-well PCR plate followed (Bio-Rad) by 4 µl of PCR mix, according to the manufacturer's protocol (KBioscience). Plates were read using PHERAstar plus (BMG labtech) and analysed using the software KlusterCaller (KBioscience). Table 2-1 shows the sequences used for design of KASP assays by KBioscience to genotype *nol9*^{sa1022}, *las1l*^{sa674} and *tp53*^{zdf1}.

Gene	KASPar Sequences
nol9	GGTCATGTAGAAGTGCTGGGCTTCACCATAGAGGAGGGTCAACAGCCTTA[C/A]CCTSTG TTTTCACCACCGACCCACTGCCCGCTCACTATCACGGCCTTAGG
las1l	CTAACCACACCGCCAAAACAACGCAGATTCCGCCCACTGAGGAGCTCCAA[G/T]AGAAGY TGAGCACAGAAACTGTGCAGGAGAGGAACTYGGCTCTACAGGGA
tp53	ATTTTGCCTTATAATAGGAGGGTAATGTGAATCTAACCTGGCA[G/T]GTTTGGTGAAAGAA TCTTCTTCAGCTACATTACGACCTGAGGGGAGCAAAAA

Table 2-1 Sequences of *nol9*, *las1l* and *tp53* that was used to design KASP genotyping assays. Red shows mutation position with wild-type base followed by alternative base.

2.2 RNA extraction and DNAse treatment

RNA extraction was carried out on wild-type embryos at 1 d.p.f. and 2 d.p.f. for cDNA synthesis to generate *in situ* hybridisation RNA probes (Section 2.3.2), at 5 d.p.f. on mutant and wild-type siblings for Differential Expression Transcript Counting Technique (DeTCT; Section 2.6.1) and for cDNA synthesis to generate DIG-labelled probe for Northern blot analysis (Section 2.5.1).

Embryos were homogenised in 10 volumes of TRIzol® (Life Technologies), followed by a 5 minute incubation at room temperature. 0.2 ml chloroform per 1 ml TRIzol® reagent initially used, was added and mixed by vigorous shaking for 15 seconds. The tubes were spun at 12,000rpm at 4°C for 10 mins. RNA was precipitated from the aqueous phase by adding 0.5 ml isopropanol per 1 ml TRIzol® reagent initially used and mixed by repeated inversion. After 10 minute incubation at room temperature, the tubes were spun at 12,000rpm at 4°C for 10 mins. 1 ml 75% ethanol per 1 ml TRIzol® reagent initially used was added to wash the RNA pellet and the tubes were spun at 7500rpm at 4°C for 5 mins and this step was repeated. To dry the RNA pellet, the tubes were incubated at 37°C for 5-10 mins. 17µl RNAse-free water (Sigma) was added and incubated at 55°C for 10 mins. RNA was quantified on a NanoDrop ND-1000 Spetrophotometer (Thermo Scientific) and 1 µl was run on a 1% agarose (Invitrogen) gel in 1x Tris-acetate-EDTA (TAE) buffer (40mM Tris-acetate, 20mM acetic acid and 1mM EDTA).

For RNA used to make cDNA for RNA probes for *in situ* hybridisation (Section 2.3.2), DNase treatment of RNA was carried out using the DNA-free Kit (Life Technologies) according to the manufacturer's instructions.

For RNA used to make DeTCT libraries (Section 2.6.1), DNAse treatment was carried out as follows: RNAse-free water was added to make the volume up to 89 µl and 10 µl DNAse I Buffer (NEB) and 1µl DNase I (NEB) were added followed by a 10 minute

incubation at 37°C. 1 µl of 0.5M EDTA (Sigma) was added and the enzyme was heat inactivated at 75°C for 10 mins. 2 µl glycogen (Roche), 10 µl 3M NAOAc pH 5.2 (Sigma) and 300 µl 100% ethanol were added and the tubes were incubated at either -80°C for 1 hour or -20°C overnight. The RNA pellet was washed twice with freshly made 75% ethanol and dried at 37°C for 5 mins. The RNA was then dissolved in 9 µl RNAse-free water (Sigma) at 55°C for 5 mins.

2.3 RNA and protein expression detection

2.3.1 Embryo fixation

Embryos were fixed at the desired stage according to use. For *in situ* hybridisation, immunohistochemistry with specific antibodies and TUNEL assay, embryos and larvae were fixed in 4% paraformaldehyde (PFA) in phosphate-buffered saline (PBS; 135 mM NaCl, 1.3 mM KCl, 3.2 mM Na_2HPO_4, 0.5 mM KH_2PO_4, pH 7.4) at 4°C overnight. The embryos were then dehydrated in series of methanol in 1x PBST (PBS, 0.1% tween-20): 5 min in 25% (v/v) methanol; 5 min in 50% (v/v) methanol; and 5 min in 75% (v/v) methanol and washed and stored in 100% methanol at -20°C overnight or longer. For immunohistochemistry against Cytokeratin, larvae were fixed in 80% MeOH/20% dimethyl sulfoxide (DMSO) at 4°C overnight.

2.3.2 Whole-mount RNA *in situ* hybridisation

The probes for RNA *in situ* hybridisation were generated using a RT-PCR-based approach. The RNA was first reverse transcribed to cDNA, PCR was then performed using gene-specific primers with the antisense primer containing a T7-promoter sequence and finally *in vitro* transcription of the PCR product was carried out.

The cDNA synthesis was carried out using the Transcriptor High Fidelity cDNA synthesis Kit (Roche) according to the manufacturer's instructions. In brief, a 11.4 µl reaction containing 500ng of RNA and 1 µl of OligodT was incubated at 65°C for 10 mins. 4 µl of 5x Transcriptor High fidelity reaction buffer, 0.5 µl RiboLock Ribonuclease Inhibitor, 2 µl dNTPs, 1 µl 0.1M DTT and 1.1 µl Transcriptor High Fidelity Reverse Transcriptase were added and the reaction was incubated at 55°C for 2 hours.

The PCR was performed using the forward and reverse primers in Table 2-2. In a 30 µl reaction containing 5 µl of 1:20 wild-type cDNA generated, 15 µl JumpStart Taq Ready mix (Sigma) and 1 µl 10 µM primers were incubated and PCR was carried out under the following conditions:

1. 94°C for 2 mins;
2. 9 cycles of (94°C for 30 secs, 62°C (-0.5°C/cycle) for 30 secs, 72°C for 1.5 mins);
3. 31 cycles of (94°C for 30 secs, 58°C for 30 secs, 72°C for 1.5 mins) and
4. 72°C for 5 mins.

Gene	Primer Sequences
nol9	Forward: GACAATGAAAGTACACAAGGTTC Reverse: TAATACGACTCACTATAGGGTAACACTGCACGGTTCTTGG
foxa1	Forward: CATGACGAACAGCAGCATGA Reverse: GAAATTAATACGACTCACTATAGGCCGCTGGACTGCTCTCTCTT
gata6	Forward: CTGTCATGCGCAAACTGTCA Reverse: GAAATTAATACGACTCACTATAGG CGAAGTATCCGTTGGCATCA
pdx1	Forward: CCTTCCAGAGACACCCCAAC Reverse: GAAATTAATACGACTCACTATAGGCTGGTTGCCGTTGCATACAT
prox1	Forward: GAGCATCTAAGGGCCAAACG Reverse: GAAATTAATACGACTCACTATAGGGGTCCCTGGCTCTTTCCTCT
fabp2	Forward: GGCTCGGGGTAAAGTTAGGC Reverse: GAAATTAATACGACTCACTATAGG GGGCTGCCAATCATTAAAGC

Table 2-2 Forward and reverse primer sequences to generate probes for RNA *in situ* hybridisation

The *in vitro* transcription was carried out in a 20 µl reaction containing 1 µg of DNA template, 4 µl of 5 x Transcription Buffer (Fermentas), 1 µl RiboLock Ribonuclease Inhibitor (Fermetas), 1 µl of 0.1M DTT (Life Technologies), 2 µl of 10x DIG RNA labelling mix (Roche), 2 µl T7 RNA polymerase (Fermentas) and the tube was incubated at 37°C for 2 hours. 2 µl of DNase I (Fermetas) was added and incubated at 37°C for 15 min. The probes were cleaned up using Lithium Chloride precipitation Solution (Life Technologies) according to manufacturer's instructions. An equal volume of hybridisation buffer was added to the RNA probe and stored at –20°C.

Whole-mount RNA in situ hybridisation was performed using a protocol adapted from (Thisse and Thisse, 2008). The embryos were rehydrated through successive dilutions of methanol in 1x PBST: 5 min in 75% (v/v) methanol; 5 min in 50% (v/v) methanol; and 5 min in 25% (v/v) methanol and subsequently rinsed several times in PBST. The embryos were permeabilised using Proteinase K (Invitrogen; 10 µg/ml) according to the developmental stage: 1 d.p.f. – 5 mins, 2 d.p.f. – 10 mins, 3 to 4 d.p.f. – 30 mins and 5 d.p.f. - 45 mins. Embryos were then rinsed in PBST and fixed in 4% PFA in PBS at room temperature for 20

mins. The embryos were rinsed in PBST again before being placed in hybridisation buffer (50% formamide, 5x saline-sodium citrate buffer (SSC), 0.1% Tween-20, 150 µg/ml heparin, 5 mg/ml Ribonucleic acid from Torula yeast) at 68°C for 5 mins. The buffer was then replaced with fresh prewarmed hybridisation buffer and embryos were incubated at 68°C for 2 hours. The embryos were incubated in 200 µl of 1 µg/µl DIG-labelled RNA probes in hybridisation buffer at 68°C overnight. The embryos were washed with serial dilutions of hybridisation buffer in 2x SSC: 5 min in 75% (v/v) hybridisation buffer, 50% (v/v) hybridisation buffer, 25% (v/v) hybridisation buffer and 5 min in 2x SSC. The embryos were then washed twice in 0.2x SSC for 30 mins. The embryos were blocked in blocking solution (PBST, 2% goat serum, 2 mg/ml BSA) at room temperature for 2 hours on a rocker. The embryos were then incubated in an alkaline phosphatase-conjugated anti-digoxygenin antibody (Roche) diluted 1:2000 in blocking solution at 4°C overnight on a rocker. The embryos were then washed briefly in PBST and six times in PBST for 15 mins and then incubated with AP substrate nitro blue tetrazolium chloride (NBT)/5-bromo-4-chloro-3-indolyl phosphate toluidine salt (NBT/BCIP; Roche). The staining was stopped when required by rinsing in PBST for 10 mins and fixed in 4% PFA at room temperature for 20 mins. The embryos were then incubated for 15 mins in series of glycerol in PBS: 25% (v/v) glycerol, 50% (v/v) glycerol and subsequently washed in 100% glycerol and stored in 100% glycerol at 4°C.

2.3.3 Immunohistochemistry

Immunohistochemistry was used to study the endocrine pancreas development and cell differentiation and ducts of the exocrine pancreas. For immunohistochemistry against Carboxypeptidase-a and Cytokeratin, the fixed embryos were rehydrated through successive dilutions of methanol in 1x PBST: 5 min in 75% (v/v) methanol; 5 min in 50% (v/v) methanol; and 5 min in 25% (v/v) methanol. The larvae were digested with 0.1% collagenase (Sigma) in PBST for 30 mins. For immunohistochemistry, the larvae were then washed twice for 5 mins, then twice for 30 mins in PBS/0.1% Triton/0.2% BSA. They were then washed in blocking buffer (5% goat serum in PBS/0.1% Triton/0.2% BSA) for 1 hour and incubated in anti-Carboxypeptidase A1 antibody (Sigma) diluted 1:100 and anti-Cytokeratin (Santa Cruz Biotechnology) diluted 1:50 in blocking buffer at 4°C overnight. Larvae were then washed several times in PBS/0.1% Triton/0.2% BSA then once with blocking buffer before being incubated in Alexa-546 goat anti-rabbit (Invitrogen) diluted 1:1000 in blocking buffer at 4°C overnight. The larvae were washed several times before being mounted with Vectashield Mounting Media (Vector laboratories). For immunohistochemistry against Insulin, Glucagon, Somatostatin and Pdx1, embryos and larvae were deyolked before being incubated in blocking buffer (1% DMSO, 1% goat serum, 1% BSA and 1% Triton X-100 in 1X PBS) for at least 1 hour and incubated in primary antibodies in blocking buffer overnight 4°C overnight. The primary antibodies were polyclonal guinea pig anti-Insulin (Dako; 1:200), polyclonal rabbit anti-Somatostatin (Dako; 1:200), monoclonal mouse anti-Glucagon (Sigma; 1:1000) and polyclonal guinea pig anti-zebrafish Pdx1 (generous gift from Dr Chris Wright, Vanderbilt University, TN, USA; 1:200). Embryos/larvae were washed several times in PBST and incubated in blocking buffer for at least 1 hour before being incubated in secondary antibodies in blocking buffer at 4°C overnight. The secondary antibodies were diluted 1:1000 and included Alexa-594 goat anti-guinea pig (Invitrogen), Alexa-546 anti-rabbit (Invitrogen), Alexa-546 anti-mouse (Invitrogen) Alexa-660 anti-mouse (Invitrogen) and Alexa-680 anti-rabbit (Invitrogen). The larvae were washed several times before being mounted with Vectashield Mounting Media (Vector laboratories).

2.3.4 Microscopy

Images of live embryos and embryos subjected to whole mount RNA *in situ* hybridisation were taken using either the Leica DFC 450 CCD camera attached to LM80 dissecting microscope and Leica Application Suite software or a Leica DFC 420 CCD camera

attached to a Leica MZ16 FA dissecting microscope (Leica Microsystems, Germany) and Leica Application Suite software. Images of *Tg(ins:mCherry)*^{jh2}*;Tg(ptf1a:EGFP)*^{jh1}*;las1l*^{sa674}, *Tg(ins:mCherry)*^{jh2}*;Tg(ptf1a:EGFP)*^{jh1}*;nol9*^{sa1022} and embryos subjected to immunohistochemistry and TUNEL assay were taken using either the Leica DFC310 FX attached to Leica M205 FA microscope or the Leica TCS SP5/DM6000 confocal microscope with Leica Application Suite Advanced Fluorescence (v2.0.0 build 1934) software. The volume of the exocrine pancreas was measured from Z-stacks images with a 10 μm slice interval using the Measure Stacks plugin in the ImageJ64 software (National Institutes of Health (NIH), http://imagej.nih.gov/ij/). Photos were cropped and modified using the GIMP software.

2.4 Characterisation of loss of function mutants

2.4.1 Morpholino injections

1- to 2-cell stage embryos were injected with 4 ng of morpholino in 0.25% phenol red (Sigma). The translation blocking morpholino were designed and synthesised by Gene-Tools. The morpholino sequences were as follows: *nol9*: ACCTTGTGTACTTTCATTGTCATCC, std: CCTCTTACCTCAGTTACAATTTATA.

2.4.2 Inhibition of Notch-signalling

To study the secondary islet formation, the larvae were incubated in 100 μM of *N*-[*N*-(3,5-Difluorophenacetyl)-$_L$-alanyl]-*S*-phenylglycine *t*- butyl ester (DAPT, StressMarq) in egg water containing PTU from 3 d.p.f. until 5 d.p.f.

2.4.3 Flow cytometry analysis

Flow cytometry analysis was used to analyse the cell cycle of *nol9*^{sa1022} mutants and wild-type siblings. 80-100 larvae were incubated in 1 ml Accumax (Innovative Cell Technologies) at room temperature for 15 mins. Larvae were homogenized using a 1ml syringe and 21 and 25 gauge needle (Becton Dickinson). The tubes were spun at 1500rpm for 10 mins at 4°C. The pellet was washed with 1x PBS, strained through a 100μm nylon cell strainer (Fisher Scientific) and spun at 3000rpm for 3 mins. The pellet was fixed in 1% PFA at room temperature for 15 mins. The tubes were spun at 3000rpm for 3 mins and the pellet was fixed in cold 70% ethanol at 4°C for 2 hours. The tubes were spun at 3000rpm for 3 mins and resuspended and kept in 1 ml PBS at 4°C. For staining, the pellet was resuspended in 0.5 ml PBS containing 25 μg/ml propidium iodide (Sigma), 0.1 mg/ml RNase Type I, DNase free (Sigma), 0.002% Triton X-100 (Sigma) and 0.1% sodium citrate pH7.4 at 37°C for 40 mins in the dark. The tubes were spun at 3000rpm for 3 mins and the pellet was resuspended in 300 μl PBS. Cell analysis was carried out on BD LSRFortessa (BD Biosciences) and cell cycle measurements were performed using the program FlowJo v7.6.5.

2.4.4 Cell Proliferation

The BrdU assay was used for cell proliferation analysis. 4 d.p.f. larvae were chilled on ice for 15 mins before incubation in 10mM BrdU (Life Technologies) in egg water on ice for 20 min. The larvae were then incubated with pre-warmed egg water for 3 hours at 28°C. The

embryos were then fixed in 4% PFA at 4°C overnight. The larvae were washed 4 x 10 mins in PBST, 3 x 5 mins with ddH2O, 2 x 5 mins with 2N HCL, incubated in 2N HCL for 1 hour and washed 2 x 10 mins with 0.1% PBST and 1 x 10 mins in Tris-HCL pH 9.5. The larvae were incubated in blocking solution (10% FBS (Sigma), 1% DMSO, 0.1% Triton-X-1000 in 1X PBS) for 1 hour and incubated at 4°C overnight with monoclonal rat anti-BrdU (Abcam; 1:200). The larvae were washed several times in PBST and incubated in blocking solution for 1 hour before being incubated at 4°C overnight with anti-rat IgG-Cy3 conjugated (Millipore; 1:400). The larvae were washed several times before being mounted with Vectashield Mounting Media (Vector laboratories).

2.4.5 Cell Death

The TUNEL assay was used to detect apoptosis. The fixed embryos were rehydrated through successive dilutions of methanol in 1x PBST: 5 min in 75% (v/v) methanol; 5 min in 50% (v/v) methanol; and 5 min in 25% (v/v) methanol and the larvae were digested with 0.1% collagenase (Sigma) in PBST for 30 mins. The In Situ Cell Death Detection Kit, TMR red (Roche) was used according to the manufacturer's instructions.

2.4.6 Alcian blue staining

3 d.p.f. embryos and 5 d.p.f. larvae were rehydrated through successive dilutions of methanol in 1x PBST: 5 min in 75% (v/v) methanol; 5 min in 50% (v/v) methanol; and 5 min in 25% (v/v) methanol and subsequently rinsed several times in PBST. The embryos/larvae were stained overnight in solution containing 0.1% Alcian blue (Sigma) dissolved in 0.1N HCl. They were then rinsed twice in water and digested using 0.025% trypsin (Sigma) in a saturated solution of sodium tetraborate for 30 mins. The embryos/larvae were rinsed three times in water and transferred in series of glycerol in water: 25% (v/v) glycerol; 50% (v/v) glycerol and 75% (v/v) glycerol. The embryos and larvae were then imaged.

2.4.7 O-dianisidine staining

3 d.p.f. and 5 d.p.f. zebrafish were incubated for 30 mins in the dark with a solution containing 0.6 mg/ml o-dianisidine (Sigma), 11mM sodium acetate (pH 4.5), 43% ethanol (v/v) and 0.65% hydrogen peroxide. The embryos and larvae were subsequently washed in sterile water and transferred to 80% glycerol/20% water for imaging.

2.4.8 Statistical approaches

Student's *t*-test and Paired Student's *t*-test were used to compare the means of two populations in Statplus (AnalystSoft). A *p*-value cut-off of 0.05 was used to define statistical significance.

2.5 Study of rRNA processing and ribosome biogenesis

2.5.1 Bioanalyser & Northern Blot analysis

RNA from phenotypic and non-phenotypic larvae was analysed on the Agilent Bioanalyser 2100 according to the manufacturer's instructions. The Northern Blot analysis was carried out in collaboration with Dr Tobias Fleischmann. 1000 µg RNA from both phenotypic and non-phenotypic larvae was digested in 20 µl reaction in water: 0.5 µl RNAse H (NEB), 2 µl RNase H Buffer, with or without 2 µl of 100 µm oligo 5' GGTTCACGCCCTGTTGAAG 3' at 37°C for 15 mins. 20 µl of RNA was loaded on a 6% TBE/UREA gel (Life Technologies) using a Low Range RNA Ladder (NEB) and run for 1.5 hours at 180V in 1x TBE buffer. The gel was then stained with Sybr Safe stain (Invitrogen). The gel was blotted to Hybond-Nylon (Amersham) in 0.5x TBE buffer for 2 hours at 25 V.

The probe for Northern blot was generated using a RT-PCR-based approach and using the High Prime DNA Labeling and Detection Starter Kit II (Roche). The RNA was reverse transcribed as in Section 2.3.2 and purified using QIAquick Gel Extraction Kit (Qiagen), PCR was then performed using the primers 5' CGATGAAGAACGCAGCTAGC 3' and 5' CTGGCCTCGGAGATCGAC 3'. In a 50 µl reaction containing 5 µl 10x Buffer (Novagen), 5 µl 2mM dNTPs (Novagen), 3 µl $MgSO_4$ 1.5 µl (Novagen), 10 µM primers 2 µl cDNA generated and 1 µl KOD Hot Start DNA Polymerase (Novagen) were incubated and PCR was carried out under the following conditions

1. 95°C for 2 mins;
2. 25 cycles of (95°C for 20 secs, 56°C for 10 secs, 70°C for 15 secs);
3. Hold at 4°C

The DIG High Prime DNA Labeling and Detection Starter Kit II (Roche) was used according to the manufacturer's instructions for DNA labelling, hybridisation to the membrane, immunological detection and chemiluminescent signal detection. The signals was visualised using an X-ray film (Kodak).

2.5.2 Polysome fractionation

Polysome fractionation was carried out in collaboration with Dr Felix Weis. 50 phenotypic and non-phenotypic larvae were resuspended in lysis buffer (50mM Tris-HCl pH 7.4, 150mM potatssium acetate, 2.5 mM $MgCl_2$, 6 mM 2-Mercaptoethanol, 1 Tb/25ml

protease inhibitors (Roche), 0.1 mg/ml cycloheximide, 10% glycerol, 120 U/ml RNase inhibitors and 0.5% sodium deoxycholate) and sheared through 23G needle. The lysates were centrifuged at 16,100g for 20min at 4°C. The supernatant were loaded on a 500 µl sucrose cushion (35% in polysome profile buffer containing 50mM Tris-HCl pH 7.4, 80mM NaCl, 2.5 mM $MgCl_2$ and 6 mM 2-Mercaptoethanol) and centrifuged for 2 hours at 32,000 rpm at 4°C on a Beckman rotor TLA 120.2. The pellets were resuspended in 200 µl polysome profile buffer and cycloheximide. 100 µl of the solution were then loaded on 4 ml 10-45% sucrose gradient and unloaded using a Brandel gradient fractionator. A UV monitor (UV-1, Pharmacia) was used to detect the polysome profiles at A_{254} and a Labjack U3-LV data acquisition device with a LJTick-InAmp preamplifier was used to read the electronic outputs of the UV-1 monitor.

2.6 Differential Expression Transcript Counting Technique (DeTCT)

2.6.1 DeTCT Library preparation

DeTCT was developed by Dr John Collins and was used to study mRNA expression analyses of *nol9*^{sa1022}, *las1l*^{sa674}, *tti*^{s450} and *set*^{s453} mutants. For *nol9*^{sa1022} and *las1l*^{sa674}, six pairs of adult carriers were incrossed and for each pair, 25 mutant and 25 wild-type siblings were collected at 5 d.p.f. for RNA extraction (Section 2.2). For *tti*^{s450} and *set*^{s453}, the RNA of six biological replicates, i.e. 25 mutants and 25 wild-type siblings from six incrosses of adult carriers, were kindly provided Dr Joan Heath, Walter+Eliza Hall, Institute of Medical Research, Melbourne, Australia. DNAse treatment was carried out on all the RNA samples (Section 2.2).

The cDNA libraries were made as follows: 9µl of total RNA was fragmented by incubation in 10x Fragmentation Buffer (Ambion) at 70°C for 5 min s. The tube was immediately transferred to an ice bath and 1 µl of stop solution (Ambion) was added and the RNA was kept at 4°C. 62.5 µl Streptavidin Magnetic Beads (NEB) was added to 50 µl 1x Wash/binding buffer (0.5M NaCl, 20mM Tris-HCl pH 7.5, 1mM EDTA, Sigma) and applied to a magnet rack for 1 minute. The beads were washed twice in 100 µl 1x Wash/binding buffer before incubation in 100 µl 1x Wash/binding buffer containing 1 µl of 100µM 14bp polyT primer at room temperature for 5 mins on a tube rotator to allow polyT primer to bind to the beads (Figure 2-1 Step 1). The beads were then washed in 100 µl 1x Wash/binding buffer and then incubated in 50 µl 2x Wash/binding buffer (1M NaCl, 40mM Tris-HCL pH 7.5, 2mM EDTA; Sigma) together with 1 µl RNase Inhibitor (NEB) and fragmented RNA at room temperature for 20 mins on tube rotator. The beads were washed twice in 100 µl 1x Wash/binding buffer and once in 100 µl cold no EDTA/low salt buffer (0.15M NaCl, 20mM Tris-HCl pH 7.5; Sigma) before they were resuspended in 18.9 µl RNAse-free water (Sigma). 2.5 µl 10x T4 RNA ligase buffer (NEB), 1µl RNase Inhibitor (NEB), T4 PNK 3' phosphate minus (NEB) and 2.5µl 10mM ATP (NEB) were added and the reaction was incubated for 30 mins at 37°C. At room temperature, 10 µl 80% PEG (Promega) was added. 1.5 µl 10x T4 RNA ligase buffer (NEB), 1.5 µl 10mM ATP (NEB), 1 µl T4 RNA ligase (NEB) and 1 µl 10µM stRSSA4 primer (Table 2-3) were added and the reaction was incubated for 2 hours at 37°C (Figure 2-1 Step 2). 40 µl 2x Wash/binding buffer was added and incubated for 2 mins at room temperature. The beads were then washed twice with 100µl 1x Wash/binding buffer and once with 100µl cold no EDTA/low salt buffer before they were resuspended in 12 µl

RNase-free water (Sigma). The solution was incubated at 80°C for 2 mins and the poly(A) transcripts ligated to the partial Illumina adapter was eluted (Figure 2-1 Step 3).

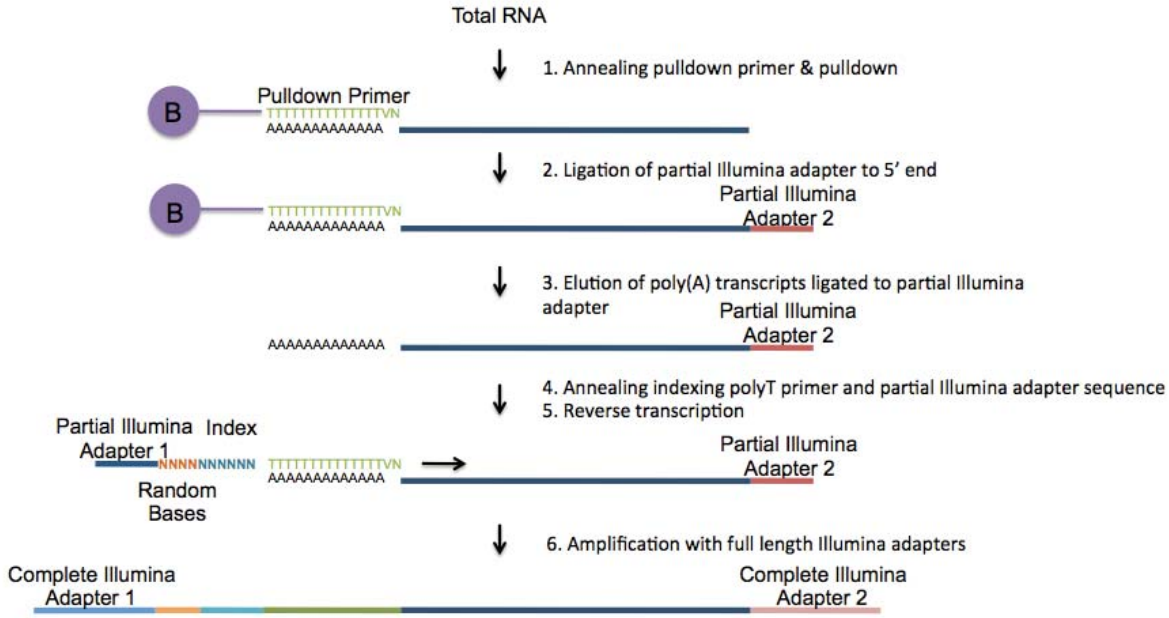

Figure 2-1 The DeTCT library preparation includes RNA extraction, pulldown of poly(A) transcripts, ligation of Illumina adapters and an indexing polyT primer, reverse transcription and amplification. (Dr John Collins, Personal Communication)

1 µl of specific tagged primer (Table 2-4) was added to the appropriate reaction tube, incubated at 70°C for 2 mins and immediately transferred to an ice bath (Figure 2-1 Step 4). For synthesis of first stranded cDNA: 4 µl 1 5xFS buffer (Invitrogen), 2 µl 0.1M DTT (Invitrogen), 1 µl 10mM dNTP (Invitrogen), 1 µl RNase Inhibitor (NEB) and 1 µl SuperScript II (Invitrogen) were added and incubated at 42°C for 1 hour (Figure 2-1 Step 5). The cDNA was cleaned using the QIAquick PCR Purification Kit (Qiagen) according to manufacturer's instructions and eluted in 38 µl EB Buffer (Qiagen). The PCR reaction was carried out in a 96-well PCR plate (Thermo Scientific) as follows: 2.5 µl 10x KOD polymerase buffer (Novagen), 2.5 µl 2mM dNTP (Novagen), 1 µl 25mM $MgSO_4$ (Novagen), 1 µl 10µM stSA.PCR.S.1+2 primer mix (Table 2-3), 0.5 µl KOD polymerase (Novagen) and 17.5 µl template or water. The following program was used on a PTC-225 Peltier Thermal Cycler (MJ Research): 94°C for 2 mins; 15 cycles of 94°C for 15 seconds, 60°C for 30 seconds, 68°C for 3 mins; and 68°C for 5 mins (Figure 2-1 Step 6). The PCR products were cleaned using the QIAquick PCR Purification Kit (Qiagen) according to manufacturer's instructions, eluted in 50 µl EB Buffer (Qiagen) and measured on an Eppendorf BioPhotometer. 5 µl of each sample and the PCR no template control were run on 1.5% agarose (Invitrogen) gel for

45 mins at 70 V in 1x TAE buffer. The DeTCT cDNA library was sequenced on an Illumina HISeq 2000 by the Wellcome Trust Sanger Institute Core Sequencing Facility.

Primer Name	Primer Sequence
stRSSA4	5' Am-CUCGGCAUUCCUGCUGAACCGCUCUUCCGAUCU 3’
stSAPCRS.1:	5' AATGATACGGCGACCACCGAGATCTACACTCTTTCCCTACACGA 3’
stSAPCRS.2:	5’ CAAGCAGAAGACGGCATACGAGATCGGTCTCGGCATTCCTGCTGAAC 3’

Table 2-3 Sequences of primers used in DeTCT library preparation

Sample	Primer Sequence
nol9_mu1	ACACTCTTTCCCTACACGACGCTCTTCCGATCTNNNNBGAGGCTTTTTTTTTTTTTTVN
nol9_wt1	ACACTCTTTCCCTACACGACGCTCTTCCGATCTNNNNBAGAAGTTTTTTTTTTTTTTVN
nol9_mu2	ACACTCTTTCCCTACACGACGCTCTTCCGATCTNNNNBCAGAGTTTTTTTTTTTTTTVN
nol9_wt2	ACACTCTTTCCCTACACGACGCTCTTCCGATCTNNNNBGCACGTTTTTTTTTTTTTTVN
nol9_mu3	ACACTCTTTCCCTACACGACGCTCTTCCGATCTNNNNBCGCAATTTTTTTTTTTTTTVN
nol9_wt3	ACACTCTTTCCCTACACGACGCTCTTCCGATCTNNNNBCAAGATTTTTTTTTTTTTTVN
nol9_mu4	ACACTCTTTCCCTACACGACGCTCTTCCGATCTNNNNBGCCGATTTTTTTTTTTTTTVN
nol9_wt4	ACACTCTTTCCCTACACGACGCTCTTCCGATCTNNNNBCGGCCTTTTTTTTTTTTTTVN
nol9_mu5	ACACTCTTTCCCTACACGACGCTCTTCCGATCTNNNNBAACCGTTTTTTTTTTTTTTVN
nol9_wt5	ACACTCTTTCCCTACACGACGCTCTTCCGATCTNNNNBACGGGTTTTTTTTTTTTTTVN
nol9_mu6	ACACTCTTTCCCTACACGACGCTCTTCCGATCTNNNNBCCAACTTTTTTTTTTTTTTVN
nol9_wt6	ACACTCTTTCCCTACACGACGCTCTTCCGATCTNNNNBAGCGCTTTTTTTTTTTTTTVN
las1l_mu1	ACACTCTTTCCCTACACGACGCTCTTCCGATCTNNNNBGAGGCTTTTTTTTTTTTTTVN
las1l_wt1	ACACTCTTTCCCTACACGACGCTCTTCCGATCTNNNNBAGAAGTTTTTTTTTTTTTTVN
las1l_mu2	ACACTCTTTCCCTACACGACGCTCTTCCGATCTNNNNBCAGAGTTTTTTTTTTTTTTVN
las1l_wt2	ACACTCTTTCCCTACACGACGCTCTTCCGATCTNNNNBGCACGTTTTTTTTTTTTTTVN
las1l_mu3	ACACTCTTTCCCTACACGACGCTCTTCCGATCTNNNNBGCCGATTTTTTTTTTTTTTVN
las1l_wt3	ACACTCTTTCCCTACACGACGCTCTTCCGATCTNNNNBCGGCCTTTTTTTTTTTTTTVN
las1l_mu4	ACACTCTTTCCCTACACGACGCTCTTCCGATCTNNNNBAACCGTTTTTTTTTTTTTTVN
las1l_wt4	ACACTCTTTCCCTACACGACGCTCTTCCGATCTNNNNBACGGGTTTTTTTTTTTTTTVN
las1l_mu5	ACACTCTTTCCCTACACGACGCTCTTCCGATCTNNNNBCCAACTTTTTTTTTTTTTTVN
las1l_wt5	ACACTCTTTCCCTACACGACGCTCTTCCGATCTNNNNBAGCGCTTTTTTTTTTTTTTVN
tti_mu1	ACACTCTTTCCCTACACGACGCTCTTCCGATCTNNNNBGAGGCTTTTTTTTTTTTTTVN
tti_wt1	ACACTCTTTCCCTACACGACGCTCTTCCGATCTNNNNBAGAAGTTTTTTTTTTTTTTVN
tti_mu2	ACACTCTTTCCCTACACGACGCTCTTCCGATCTNNNNBCAGAGTTTTTTTTTTTTTTVN
tti_wt2	ACACTCTTTCCCTACACGACGCTCTTCCGATCTNNNNBGCACGTTTTTTTTTTTTTTVN
tti_mu3	ACACTCTTTCCCTACACGACGCTCTTCCGATCTNNNNBCGCAATTTTTTTTTTTTTTVN
tti_wt3	ACACTCTTTCCCTACACGACGCTCTTCCGATCTNNNNBCAAGATTTTTTTTTTTTTTVN
set_mu1	ACACTCTTTCCCTACACGACGCTCTTCCGATCTNNNNBGCCGATTTTTTTTTTTTTTVN
set_wt1	ACACTCTTTCCCTACACGACGCTCTTCCGATCTNNNNBCGGCCTTTTTTTTTTTTTTVN
set_mu2	ACACTCTTTCCCTACACGACGCTCTTCCGATCTNNNNBAACCGTTTTTTTTTTTTTTVN
set_wt2	ACACTCTTTCCCTACACGACGCTCTTCCGATCTNNNNBACGGGTTTTTTTTTTTTTTVN
set_mu3	ACACTCTTTCCCTACACGACGCTCTTCCGATCTNNNNBCCAACTTTTTTTTTTTTTTVN
set_wt3	ACACTCTTTCCCTACACGACGCTCTTCCGATCTNNNNBAGCGCTTTTTTTTTTTTTTVN

Table 2-4 Sequences of primers used for different samples (Green, Red, Brown Random 4mer, Black tag 6bp, Pink 14bp PolyT).

2.6.2 DeTCT analysis

Dr Ian Sealy carried out the analysis of sequence data from DeTCT libraries of *nol9*^{sa1022}, *las1l*^{sa674}, *tti*^{s450} and *set*^{s453} mutants. The DeTCT analysis pipeline, written by Drs James Morris and Ian Sealy and available from https://github.com/iansealy/DETCT, was used. The sequencing data produces two sets of reads, the read 1 contains the random bases, the index tag, 14 T bases and the remaining is transcript-specific sequence whereas the read 2 is entirely transcript-specific sequence. The DeTCT analysis pipeline consists of the following steps:

1. FASTQ files are extracted from the BAM files;
2. The reads are trimmed: 21 bases are removed from the 3' ends of both read 1 and read 2 and the tag, random bases and polyT sequence are removed from the 5' end of read 1;
3. The reads are aligned to the Zv9 reference genome using the Burrows-Wheeler Aligner (BWA) software (Li and Durbin, 2009);
4. PCR duplicates are flagged using a modified version of the Picard suite's MarkDuplicates tool (available from https://github.com/iansealy/picard-detct);
5. The genome is divided into bins of 100 bases and the number of read 2s aligned in each bin are counted across all libraries;
6. Read peaks are probabilistically identified in the bin data using a Hidden Markov model (HMM). This provides a list of bins with associated read counts and probabilities;
7. Adjacent bins are joined together to make regions;
8. The 3' end associated with each region is identified by extracting the read 1s paired with read 2s within the region. The alignment of read 1 gives the 3' end position and the strand along with a read count;
9. The 3' ends are filtered for artefacts primed from genomic DNA rich in A bases and the 3' ends with the highest read counts are chosen;
10. The number of read 2s in each region for each experimental sample are used to produce count data;
11. The count data are used for differential expression analysis using DESeq (Anders and Huber, 2010). All regions with count sum below the 40th quantile are excluded. DESeq fits two models: one based only on sibling pairings and one based on sibling pairings and experimental condition (i.e. mutant or sibling) and compares which model explains the data best in order to produce a list of differentially expressed regions;

Each region is annotated with Ensembl gene information based on the nearest transcript to the 3' end.

2.6.3 Comparisons between *nol9*^{sa1022}, *las1l*^{sa674}, *tti*^{s450} and *set*^{s453} mutants

The total number of reads for libraries of three pairs of mutant and wild-type siblings of *nol9*^{sa1022}, *las1l*^{sa674}, *tti*^{s450} and *set*^{s453} mutants was normalised to a total read count of 26 M reads using Picard DownsampleSam tool. The steps 4-12 from the DeTCT analysis pipeline (Section 2.6.2) were carried out and the list of differentially expressed regions were filtered to include only the regions that are within 100 bases to the nearest 3' end Ensembl gene. This list was then filtered to include regions that are statistically significant at a DESeq adjusted *p*-value of 0.05 (Benjamini-Hochberg procedure for multiple testing) and the list of regions were sorted for unique genes to produce a list of statistically significant differentially expressed genes. The Ensembl Gene IDs of the statistically significant differentially expressed genes of *nol9*^{sa1022}, *las1l*^{sa674}, *tti*^{s450} and *set*^{s453} mutants were then compared using the tool VENNY (http://bioinfogp.cnb.csic.es/tools/venny/index.html).

2.6.4 Gene ontology enrichment analysis

Dr Ian Sealy carried out the enrichment analysis for Gene Ontology (GO) terms in *nol9*^{sa1022}, *las1l*^{sa674}, *tti*^{s450} and *set*^{s453} mutants using the R topGO package (Alexa et al., 2006). First, the whole list of regions produced by the DESeq-based pipeline was sorted for unique genes and their corresponding highest adjusted *p*-values were considered. The enrichment analysis was performed using the *elim* method and the Kolomogorov-Smirnov like test was used as the test statistic. The statistically significant GO term was defined as having a Ks-value of less than 0.01.

To identify the GO terms that were enriched between *nol9*^{sa1022}, *las1l*^{sa674}, *tti*^{s450} and *set*^{s453} mutants, the statistically significant GO terms (K-S value less than 0.01) of all four mutants were compared using the tool VENNY (http://bioinfogp.cnb.csic.es/tools/venny/index.html).

2.6.5 KEGG pathways enrichment analysis

For enrichment of KEGG pathways in *nol9*^{sa1022}, *tti*^{s450} and *set*^{s453} mutants, the Database for Annotation, Visualization and Integrated Discovery (DAVID) was used (Dennis et al., 2003; Huang da et al., 2009b) (http://david.abcc.ncifcrf.gov). First, the list of differentially expressed regions that was generated by the DESeq-based pipeline was sorted for unique genes to produce a background list of 11170 genes for *nol9*^{sa1022}, 10527 for *tti*^{s450} and 10535 for *set*^{s453} mutants. The list of statistically significant differentially expressed regions (DESeq adjusted *p*-value less than 0.05) was sorted for unique genes to produce a list of 566 for *nol9*^{sa1022}, 730 for *tti*^{s450} and 607 for *set*^{s453} mutants of statistically significant differentially expressed genes. The statistically significant differentially expressed genes were then compared to the respective background list using the DAVID functional annotation tool.

Chapter 3 Characterisation of *nol9*^{sa1022} mutants

3.1 Introduction

The Zebrafish Mutation Project (ZMP) aims to create a disruptive mutation in every protein-coding gene in the zebrafish genome and to study the phenotypic consequences of such alleles (Kettleborough et al., 2013). During the phenotypic analysis of offspring from incrosses of F2 *nol9*$^{sa1022/+}$, *nol9*$^{sa1022/sa1022}$ (abbreviated as *nol9*^{sa1022}) mutation was found to be associated with a pancreas phenotype (Figure 1-2). The pancreas of *nol9*^{sa1022} larvae was not visible at 5 days post fertilisation (d.p.f.). The ZMP founder fish carry on average seven nonsense mutations, four essential splice and 111 non-synonymous mutations in their exomes that are induced by ENU mutagenesis (Kettleborough et al., 2013). In order to reduce the number of background mutations, I outcrossed the F2 *nol9*$^{sa1022/+}$ adults to SAT wild-type zebrafish.

The *nucleolar protein 9* (*nol9*) gene has three Zv9 Ensembl transcripts: nol9-001, nol9-201 and nol9-002 (Figure 3-1 A). The nol9-001 and nol9-201 are each comprised of 2897 and 2506 bases, respectively, and each have 12 exons encoding a protein of 713 amino acids whilst the nol9-002 is a smaller transcript of 845 bases encoding a protein of 175 amino acids (Figure 3-1 A, B). The NOL9 proteins of human (ENSP00000366934) and mouse (ENSMUSP00000081133) and Nol9 protein in zebrafish (ENSDARP00000123267) are conserved especially in two domains known as *Molybdopterin guanine dinucleotide synthesis protein B* (*MobB*) and *Pre-mRNA cleavage complex II protein* (*Clp1*) (Figure 3-1 B). The zebrafish Nol9 protein has 34% and 30% identical amino acids compared to human and mouse NOL9, respectively. The *nol9*^{sa1022} mutant fish have a C to A mutation in exon 2 converting amino acid 195 from a Tyrosine into a stop codon (Figure 3-1 A, B).

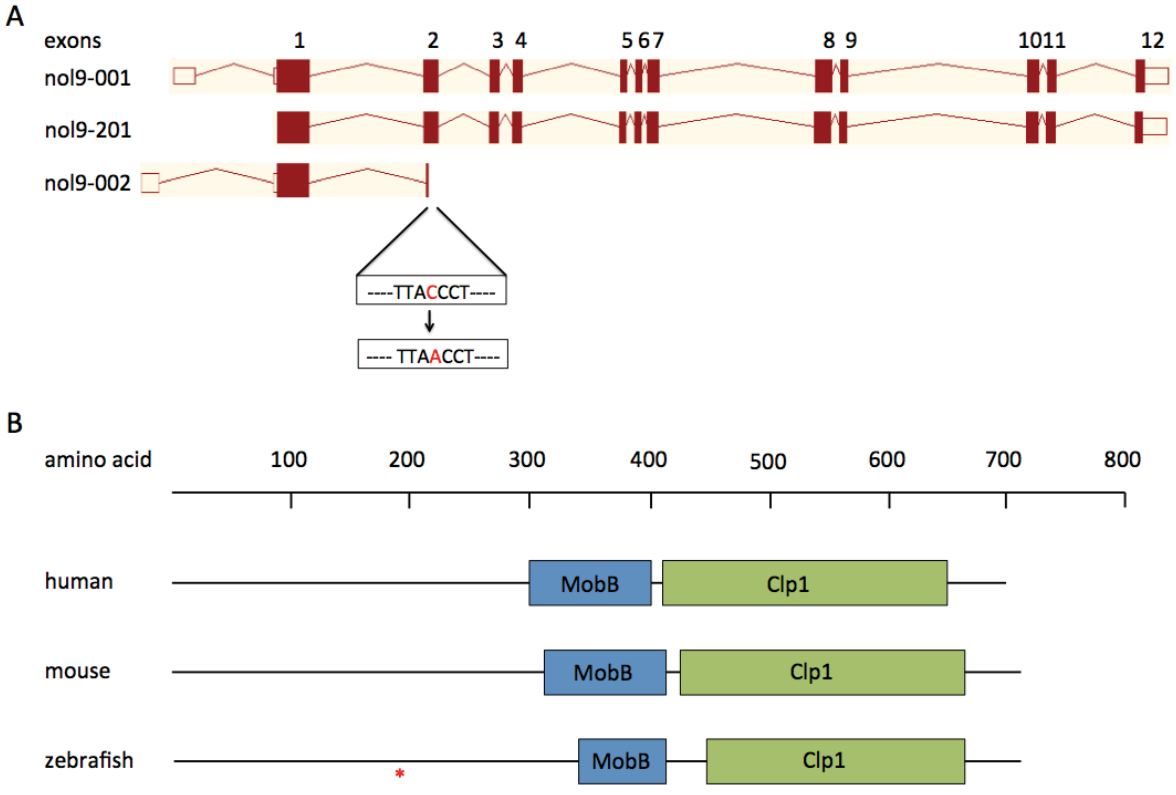

Figure 3-1 Diagram of *nol9* gene and Nol9 protein. (A) The zebrafish *nol9* gene has three Ensembl transcripts nol9-001, nol9-201 and nol9-002. The *nol9*^{sa1022} is a nonsense mutation in exon 2 of transcripts nol9-001 and nol9-201 converting the codon TAC (Tyrosine) into TAA (stop codon). The diagrams were taken from Ensembl. Exons are shown as boxes and introns are shown as lines. (B) The human, mouse and zebrafish Nol9 proteins are conserved. Boxes show the protein domains and * indicates the location of the *nol9*^{sa1022} mutation.

The human NOL9 protein is a polynucleotide 5'-kinase involved in ribosome biogenesis (Heindl and Martinez, 2010). It is a non-ribosomal protein that is required for the efficient generation of the large ribosomal subunit rRNAs, 5.8S and 28S and for the synthesis of the 60S ribosomal subunit (Heindl and Martinez, 2010). As mentioned in Chapter 1, the role of ribosome biogenesis in zebrafish pancreas development has been recognised in recent years. To increase our understanding of this subject, I first aimed to provide further evidence that the *nol9* mutation was causative of the observed pancreas phenotype by phenotyping and genotyping offspring of *nol9*$^{sa1022/+}$ adult, and by recapitulating the pancreas phenotype by morpholino knockdown of *nol9*. Secondly, given that other ribosome biogenesis mutants, including *nil per os* (*npo*) (Mayer and Fishman, 2003), *digestive expansion factor* (*def*) (Chen et al., 2005), *titania* (*tti*) (Boglev et al., 2013) and *nucleolar protein with MIF4G domain 1* (*nom1*) (Qin et al., 2014) also showed defects in the development of the liver and intestine, I aimed to determine whether these organs also showed morphological abnormalities in *nol9*^{sa1022} mutants. Thirdly, I aimed to identify the stage at which the development of the digestive organs is affected by using endodermal markers and developmental markers specific to the pancreas, liver and intestine. Fourthly, I aimed to examine the formation and differentiation of endocrine cells and the formation of secondary islets in *nol9*^{sa1022} mutants. To understand the mechanism of the hypoplastic pancreas phenotype, I studied the cell cycle in *nol9*^{sa1022} mutants, cell proliferation and death of the exocrine pancreas in *nol9*^{sa1022} mutants. As anaemia and craniofacial dysmorphology are common features of ribosomopathies and the zebrafish mutants *npo, def, tti* and *nom1* all exhibit abnormal jaws, I also examined the jaw morphology and erythrocyte development of *nol9*^{sa1022} mutants. The expression pattern of *nol9* during development was then investigated as the expression of *nol9* in the affected organs could help explain the tissue specific defects observed in *nol9*^{sa1022} mutants. Lastly, the functions of Nol9 in rRNA processing and ribosome biogenesis were studied using Northern blotting and polysome fractionation to determine whether Nol9 function is conserved in zebrafish.

3.2 Results

3.2.1 Gross morphology of *nol9*^{sa1022} mutants

The *nol9*^{sa1022} mutants appeared normal up to 4 days post fertilisation (d.p.f.) but at 5 d.p.f. they could be distinguished from wild-type siblings under a dissecting microscope (Figure 3-2). The *nol9*^{sa1022} larvae had fewer folds in their intestine, they had a smaller liver and pancreas and the swim bladders failed to inflate in the majority of larvae. They had no other obvious morphological defects. Thirty 5 d.p.f. phenotypic mutants and thirty wild-type siblings were further grown, by day 10, all the phenotypic *nol9*^{sa1022} mutants had died. These data suggest that *nol9* is involved in the development of digestive organs and that defective development of digestive organs likely underlies the early lethality in *nol9*^{sa1022} mutants.

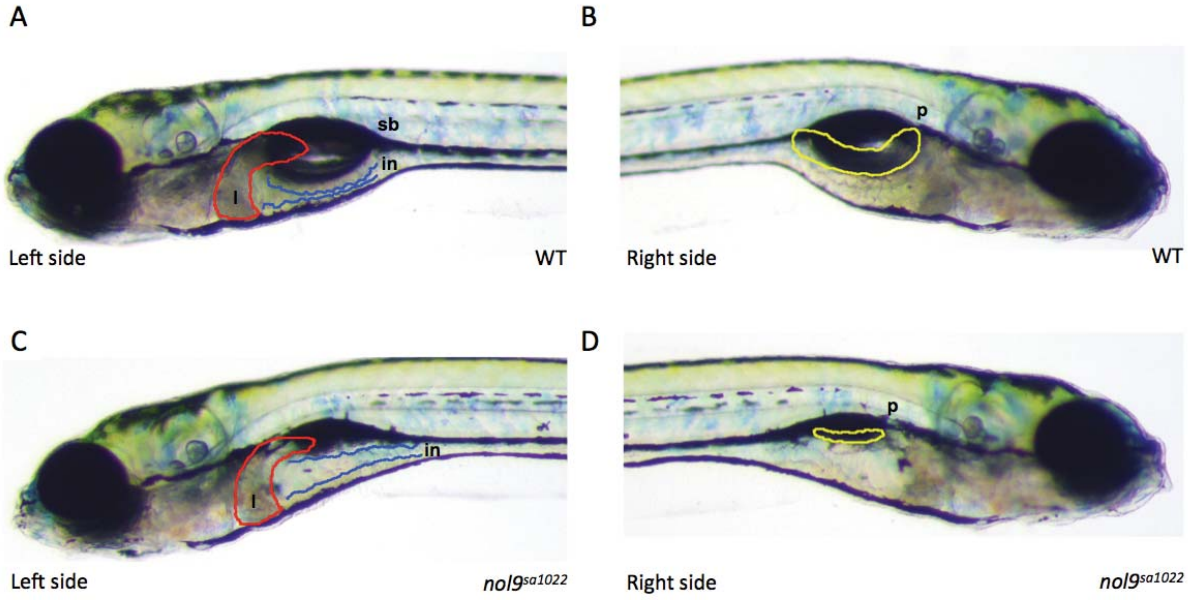

Figure 3-2 The digestive organs of *nol9*^{sa1022} mutants are underdeveloped. (A-D) Bright-field images of 5 d.p.f. wild-type and mutant larvae. (A,C) Left side view of wild-type (A) and *nol9*^{sa1022} larvae (C) showing that *nol9*^{sa1022} mutants have fewer intestinal folds (in; blue), a smaller liver (l; red) and generally uninflated swim bladder (sb) compared to wild-type siblings. (B,D) Right side view of wild-type (B) and *nol9*^{sa1022} larvae (D) showing that *nol9*^{sa1022} mutants have a smaller pancreas (p; yellow) compared to wild-type siblings. (WT) wild-type; (l) liver; (in) intestine; (sb) swim bladder; (p) pancreas.

3.2.2 The *nol9*^{sa1022} mutants have smaller exocrine pancreas

The pancreas of *nol9*^{sa1022} mutants appeared smaller than wild-type siblings under the dissecting microscope. In order to confirm this phenotype and to facilitate the study of pancreas development in *nol9*^{sa1022} mutants, the F2 *nol9*$^{sa1022/+}$ were outcrossed to the transgenic line *Tg(ins:mCherry)*^{jh2}*;Tg(ptf1a:EGFP)*^{jh1} (Pisharath et al., 2007) that expresses mCherry in the pancreatic islet and EGFP in the exocrine pancreas. At 5 d.p.f., the *ptf1a*-positive area of *nol9*^{sa1022} larvae appeared considerably smaller than that of wild-type siblings although the *insulin*-positive area appeared similar in size and shape in *nol9*^{sa1022} and wild-type larvae (Figure 3-3 A, B, Section 2.3.4). The mean volume of *ptf1a*-expressing region of *nol9*^{sa1022} mutants (n=8) is statistically significantly smaller than that of wild-type siblings (n=15), 0.0005 mm^3 and 0.00209 mm^3 respectively (Student's *t*-test, $p = 5.05 \times 10^{-11}$) (Figure 3-3 C, Section 2.3.4). These results demonstrate that the development of the exocrine pancreas is impaired in *nol9*^{sa1022} mutants.

To determine whether the *nol9*^{sa1022} mutation is causative of the small exocrine pancreas phenotype, incrosses of *Tg(ins:mCherry)*^{jh2}*;Tg(ptf1a:EGFP)*^{jh1}*;nol9*$^{sa1022/+}$ were phenotyped at 5 d.p.f based on the size of the *ptf1a*-expressing region and subsequently genotyped (Section 2.1.2). All larvae with a smaller area of *ptf1a*-positive cells were *nol9*$^{sa1022/sa1022}$ (n=36), whereas larvae with normal area of *ptf1a*-positive cells were either *nol9*$^{sa1022/+}$ (n=95) or *nol9*$^{+/+}$ (n=34) (Figure 3-3 D, E). This data indicates that the exocrine pancreas phenotype follows a Mendelian pattern of recessive inheritance and that the *nol9* mutation is linked to the small exocrine pancreas phenotype.

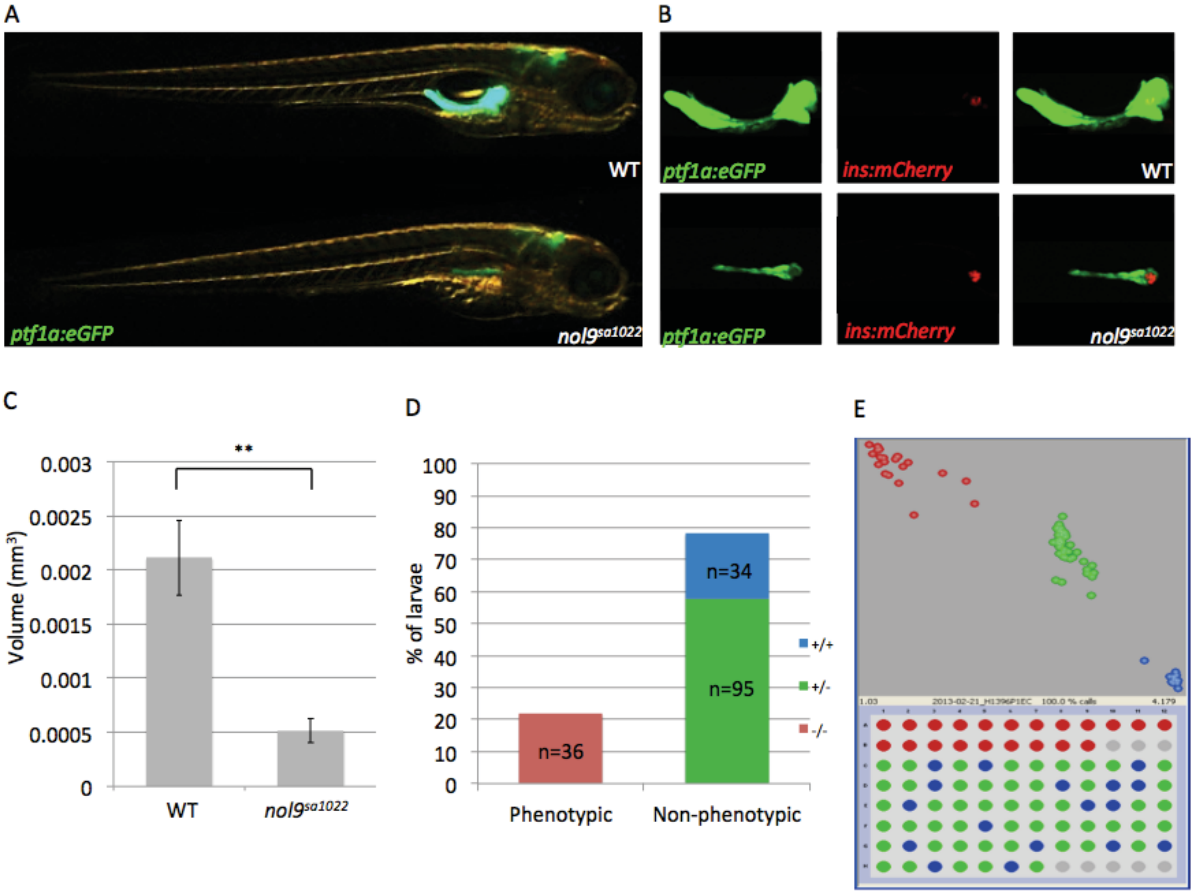

Figure 3-3 The *nol9*^{sa1022} mutation is causative of the exocrine pancreas phenotype. (A) Right side view of 5 d.p.f. *Tg(ins:mCherry)*^{jh2}*;Tg(ptf1a:EGFP)*^{jh1} larvae demonstrating that mutants appear to have a smaller *ptf1a*-positive area compared to wild-type siblings. (B) Confocal images of 5 d.p.f. *Tg(ins:mCherry)*^{jh2}*;Tg(ptf1a:EGFP)*^{jh1} larvae showing that mutants have a smaller *ptf1a*-positive area but normal *ins*-positive area compared to wild-type siblings. (C) The volume of *ptf1a*-expressing region of *nol9*^{sa1022} mutants (n=8) is significantly smaller than wild-type siblings (n=15). Data is represented as the mean ± SD, Student's *t*-test **p<0.01. (D) Graph showing the percentage of phenotypic and non-phenotypic larvae that are homozygous mutant (-/-, red), heterozygous (+/-, green) or homozygous wild-type (+/+, blue) for *nol9*^{sa1022} mutation. (E) Representative image of KASPar genotyping. Phenotypic larvae are in the first two rows and non-phenotypic larvae are in the remaining six rows. The genotype of homozygous mutant, heterozygous and homozygous WT larvae are shown as red, green and blue dots respectively. (WT) wild-type.

3.2.3 Knockdown of *nol9* results in smaller exocrine pancreas

To confirm that the *nol9* mutation is causative of the exocrine pancreas phenotype, *nol9* was knocked down using antisense morpholino oligonucleotide. An ATG morpholino was designed against the translation start site of *nol9* (Section 2.4.1). Wild-type *Tg(ins:mCherry)^{jh2};Tg(ptf1a:EGFP)^{jh1}* embryos were injected with either 4ng *nol9* ATG MO or 4ng standard control morpholino (std MO) (Eisen and Smith, 2008) and treated with phenothiourea (PTU) to inhibit pigmentation and aid in visualising pancreas development. At 4 d.p.f., the *nol9* ATG MO-injected larvae appeared morphologically normal compared to std MO-injected larvae although they sometimes displayed pericardial oedema (Figure 3-4 A). This is consistent with *nol9^{sa1022}* mutants also not displaying any obvious morphological defects at 4 d.p.f. The area of *ptf1a*-positive region appeared smaller in ATG MO-injected larvae compared to std MO-injected larvae whereas the *insulin*-positive signal appeared similar in both ATG MO and std MO-injected zebrafish (Figure 3-4 B, C). Three independent morpholino experiments were carried out and in total, 130 and 169 embryos were injected with std MO and *nol9* MO respectively (Figure 3-4 D). There was a statistically significant difference in the percentage of *nol9* ATG MO-injected, 56.28% and std MO-injected larvae, 5.75% that had a smaller pancreas relative to that of uninjected larvae (Student's *t*-test, p = 0.00359). Likewise, the percentage of larvae that had similar pancreatic size to uninjected larvae was statistically significantly different between *nol9* ATG MO-injected (29.52%) and std MO-injected groups (89.34%) according to the Student's *t*-test (p = 0.00683). There was no statistically significant difference in the percentage of severely delayed larvae in *nol9* ATG MO (14.2%) and std MO-injected (4.44%) zebrafish. This data suggests that knockdown of *nol9* results in smaller exocrine pancreas. To further support this, the pancreatic volume of uninjected, std MO-injected and ATG MO-injected larvae was measured from two independent experiments (Figure 3-4 E, Section 2.3.4). The mean volume of *ptf1a*-expressing region of 4 d.p.f. uninjected (n=20, 0.000609 mm^3) and std MO-injected (n=19, 0.000577 mm^3) larvae was not statistically significantly different from each other (Student's *t*-test, p = 0.555). However, the mean volume of *ptf1a*-expressing region of ATG MO-injected larvae (n=25), 0.000388 mm^3 was significantly smaller than that of uninjected and std MO-injected larvae, with a Student's *t*-test *p*-value of 0.00004 and 0.0000494 respectively. Altogether these results demonstrate that morpholino knockdown of *nol9* recapitulates the *nol9^{sa1022}* phenotype and substantiates the hypothesis that deficiency of *nol9* results in a small exocrine pancreas.

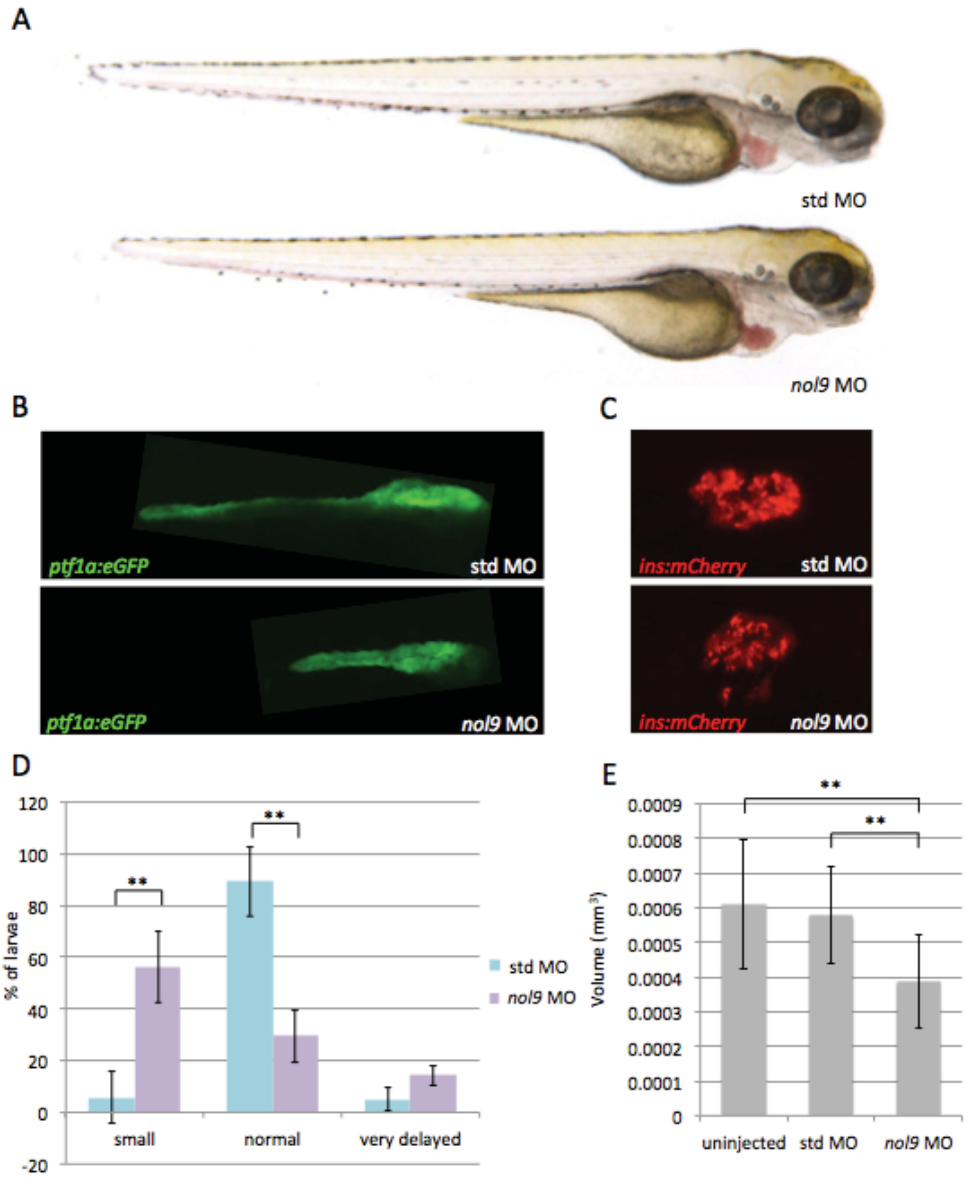

Figure 3-4 Knockdown of *nol9* results in small exocrine pancreas. (A) Right side view of 4 d.p.f. PTU-treated *Tg(ins:mCherry)*^{jh2}*;Tg(ptf1a:EGFP)*^{jh1} fish. The *nol9* ATG MO-injected fish appear morphologically normal compared to std MO-injected fish. (B-C) Representative maximum intensity projection images of a z series of confocal sections through morphants showing that *nol9* MO-injected larvae have a smaller *ptf1a*-positive area (B) compared to std MO-injected larvae whereas the *insulin*-positive signals (C) appear similar in both morphants. (D) Graph showing the percentage of *nol9* MO-injected (n=169) and std MO-injected (n=130) fish from three independent experiments with smaller or normal pancreatic size compared to uninjected larvae and the percentage of larvae that are very delayed. Data is represented as the mean ± SD, Student's *t*-test **p<0.01. (E) Graph showing the volume of *ptf1a*-expressing region of uninjected (n=20), std MO-injected (n=19) and *nol9* MO-injected (n=25) larvae from two independent experiments. Data is represented as the mean ± SD, Student's *t*-test **p<0.01. (std MO) standard control morpholino; (*nol9* MO) *nol9* translation blocking morpholino.

3.2.4 Early development of digestive organs is normal in *nol9*^{sa1022} mutants

The development of zebrafish pancreas consists of different stages including endoderm induction and patterning, cell differentiation of endodermal precursors into specialised pancreatic cells and morphogenesis of the pancreas (Gnugge et al., 2004). To determine the developmental stage at which the pancreas development is impaired in *nol9*^{sa1022} mutants, I first studied the endoderm formation in *nol9*^{sa1022} mutants. This was carried out by examining the expression of the genes *foxa1* (Odenthal and Nusslein-Volhard, 1998) and *gata6* (Wallace et al., 2001), which are expressed in the endodermal lineage during early development of digestive organs. Offspring from an incross of *nol9*$^{sa1022/+}$ carriers were first subjected to whole mount *in situ hybridisation* (ISH) using probes against *foxa1* and *gata6* at 1 d.p.f. and 2 d.p.f. and subsequently genotyped for the *nol9*^{sa1022} mutation (Figure 3-5, Sections 2.1.2 and 2.3.2). At 1 d.p.f., all offspring (n=31) from an incross of *nol9*$^{sa1022/+}$ expressed *foxa1* in the midline and in the pharyngeal endoderm. Six out of these 31 embryos were *nol9*^{sa1022} mutants (Figure 3-5 A). Similarly, all the 1 d.p.f. embryos subjected to *gata6* ISH (n=17) expressed *gata6* in the midline including four that were *nol9*^{sa1022} mutants (Figure 3-5 B). These results indicate that the endodermal layer had formed an endodermal rod in *nol9*^{sa1022} mutants. At 2 d.p.f., all 31 offspring from an incross of *nol9*$^{sa1022/+}$ showed normal expression patterns of *foxa1* including 11 that were *nol9*^{sa1022} mutants (Figure 3-5 C). In addition, all the 2 d.p.f. offspring examined showed similar expression patterns of *gata6* and 15 out of these 56 embryos were *nol9*^{sa1022} mutants (Figure 3-5 D). These results reveal that the formation of the pancreas and liver primordia and gut looping proceed normally in *nol9*^{sa1022} mutants. Overall, the expressions of *foxa1* and *gata6* in *nol9*^{sa1022} mutants demonstrate that the development of digestive organs is normal in *nol9*^{sa1022} mutants before 2 d.p.f., indicating that *nol9* is not involved in the early morphogenesis of the endoderm-derived organs.

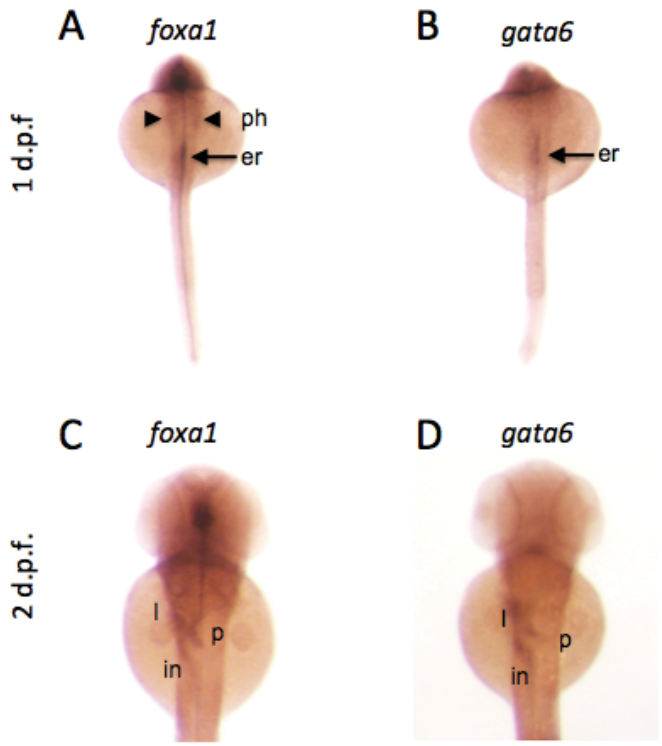

Figure 3-5 Early development of digestive organs is normal in *nol9*^{sa1022} mutants. (A-D) Whole mount *in situ hybridisation* using RNA probes against endoderm marker *foxa1* and *gata6*. Dorsal view with anterior to the top. (A-B) Representative image of all 1 d.p.f. offspring from an incross of *nol9*$^{sa1022/+}$ showing normal expression of *foxa1* (A) and *gata6* (B) in the endodermal rod (er; arrow). The pharyngeal endoderm (ph; arrowhead) also expresses *foxa1* (A). (C-D) Representative image of all 2 d.p.f. offspring from an incross of *nol9*$^{sa1022/+}$ showing expression of *foxa1* (C) and *gata6* (D) in the pancreas (p), liver (l) and intestine (in); (er) endodermal rod; (ph) pharyngeal endoderm; (l) liver; (p) pancreas; (in) intestine.

3.2.5 Expansion growth of the exocrine pancreas and formation of pancreatic ducts are impaired in *nol9*^{sa1022} mutants

To look more specifically at the development of the pancreas, I studied the expression of *pdx1* in 2 d.p.f. offspring from an incross of *nol9*$^{sa1022/+}$ zebrafish and subsequently genotyped the embryos (Figure 3-6 A, Sections 2.1.2 and 2.3.2). All the offspring (n=25) expressed *pdx1* in the pancreatic primordium including nine that were *nol9*^{sa1022} mutants. This data indicates that formation of pancreatic buds proceeds normally in *nol9*^{sa1022} mutants and supports our model that *nol9* is not required for pancreas development before 2 d.p.f.

In order to identify the developmental time point at which pancreas development is affected in *nol9*^{sa1022} mutants, offspring from an incross of *Tg(ins:mCherry)*^{jh2}*;Tg(ptf1a:EGFP)*^{jh1}*;nol9*$^{sa1022/+}$ were phenotyped at either 2, 3, 4 or 5 d.p.f and thereafter genotyped for the *nol9*^{sa1022} mutation (Sections 2.1.2). All 2 d.p.f. (n=24) offspring including seven *nol9*^{sa1022} mutants had formed the pancreatic head comprising of an *insulin*-expressing pancreatic islet surrounded by *ptf1a*-expressing exocrine tissue (Figure 3-6 B). At 3 d.p.f., the pancreatic islet had expanded and the *ptf1a*-expressing region had grown posteriorly in all the 20 embryos studied including four that were *nol9*^{sa1022} mutants (Figure 3-6 C). At 4 d.p.f., the *ptf1a*-positive exocrine pancreas of *nol9*^{sa1022} mutants (n=6) appeared smaller than wild-type siblings (n=14) whereas the *insulin*-positive pancreatic islet was indistinguishable in mutants and wild-type siblings (Figure 3-6 D). At 5 d.p.f., the expansion of the *ptf1a*-expressing region seen in wild-type siblings (n=16) was not visible in *nol9*^{sa1022} mutants (n=6), although the pancreatic islets appeared similar in mutants and wild-type siblings (Figure 3-6 E). These results reveal that the exocrine pancreas in *nol9*^{sa1022} mutants fails to expand normally between 3 and 4 d.p.f. and that this expansion defect is detectable through 5 d.p.f.

To determine whether cell differentiation was normal in the exocrine pancreas of *nol9*^{sa1022} mutants, I studied the production of Carboxypeptidase-a (Cpa), an exocrine pancreatic enzyme by immunohistochemistry (Figure 3-6 F, Section 2.3.3). Cpa was detected in both *nol9*^{sa1022} mutants and wild-type siblings although the Cpa-positive area appeared smaller in mutants compared to wild-type siblings. Overall, these results suggest that the defect in *nol9*^{sa1022} mutants is due to impaired expansion growth rather than impaired cell differentiation of the exocrine pancreas.

Since the expansion of acinar cells of the exocrine pancreas is impaired in *nol9*^{sa1022} mutants, the pancreatic ducts in *nol9*^{sa1022} mutants were examined by immunohistochemistry using an antibody against Cytokeratin labelling the pancreatic ductular epithelia (Figure 3-6 G, Section 2.3.3). At 5 d.p.f., the Cytokeratin-labelled pancreatic ducts of wild-type siblings were highly branched whereas pancreatic ducts were not apparent in *nol9*^{sa1022} mutants. This observation demonstrates that *nol9* is required for the formation of pancreatic ducts in zebrafish.

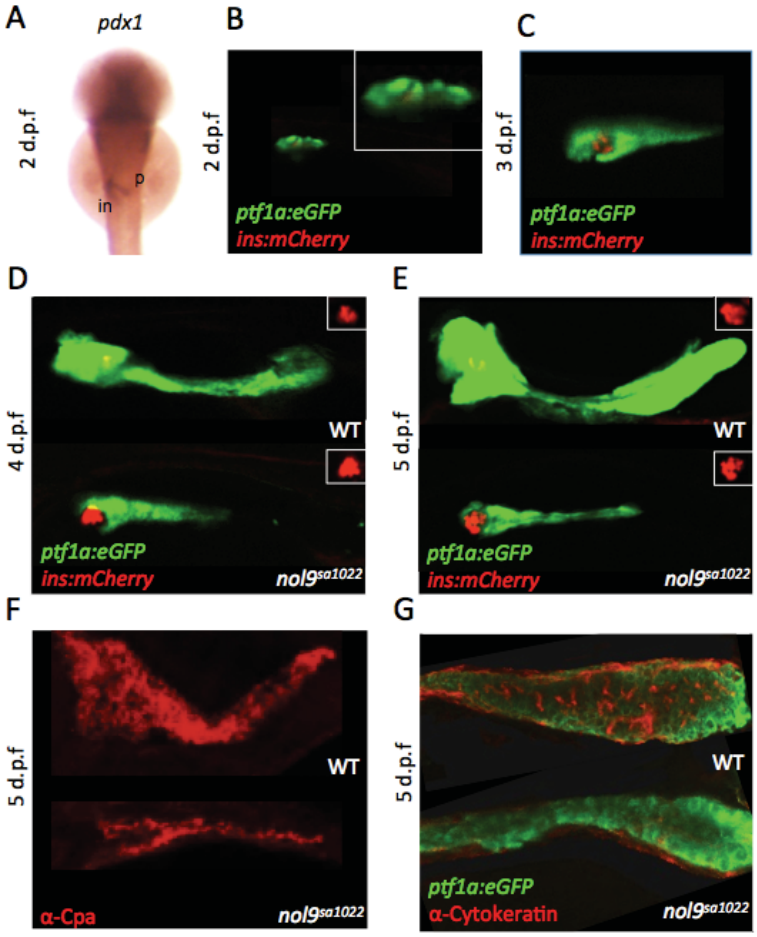

Figure 3-6 Expansion of exocrine pancreas and pancreatic duct formation is impaired in *nol9*^{sa1022} mutants. (A) Dorsal view with anterior to the top. Representative image of 2 d.p.f. offspring from an incross of *nol9*$^{sa1022/+}$ subjected to whole mount *in situ* hybridisation using RNA probes against the pancreas marker *pdx1*. The pancreatic (p) bud forms from the intestine (in). (B-E) 2 d.p.f to 5 d.p.f offspring from an incross of *Tg(ins:mCherry)*^{jh2}*;Tg(ptf1a:EGFP)*^{jh1}*;nol9*$^{sa1022/+}$. (B) Representative image of 2 d.p.f. embryo expressing *insulin* and *ptf1a* (magnified in boxed area). (C) Representative image of 3 d.p.f. embryo showing that the *insulin*- and *ptf1a*-positive region has grown in mutants and wild-type siblings. (D-E) At 4 d.p.f. (D) and 5 d.p.f. (E), the *ptf1a*-expressing exocrine pancreas is smaller in mutants compared to wild-type siblings whereas the *insulin*-expressing pancreatic islet (shown in boxed area) is similar in size in mutants and wild-type siblings. (F) Confocal images of 5 d.p.f. mutants and wild-type siblings subjected to immunohistochemistry using Carboxypeptidase-a (Cpa) antibody. The Cpa-positive area appears smaller in mutants compared to wild-type siblings. (G) Representative maximum intensity projection images of confocal stacks of 5 d.p.f. larvae from an incross of *Tg(ins:mCherry)*^{jh2}*;Tg(ptf1a:EGFP)*^{jh1}*;nol9*$^{sa1022/+}$ expressing only EGFP and subjected to immunohistochemistry using antibody against Cytokeratin. The pancreatic ducts are not apparent in *nol9*^{sa1022} mutants and is in contrast to the ductal network labelled in wild-type siblings. (WT) wild-type; (p) pancreas; (in) intestine.

3.2.6 Pancreatic endocrine cells are formed and are differentiated in *nol9*^{sa1022} mutants

As the *nol9*^{sa1022} mutants appeared to have similar *insulin*-expressing area as wild-type siblings, the pancreatic endocrine cells were studied at earlier stages by immunohistochemistry on offspring from an incross of *Tg(ins:mCherry)*^{jh2}*;Tg(ptf1a:EGFP)*^{jh1}*;nol9*$^{sa1022/+}$ adults (Figure 3-7, Section 2.3.3). At 2 d.p.f., *nol9*^{sa1022} mutants (n=16) and wild-type siblings (n=25) had similar levels of Pdx1 that labelled both the pancreatic islet and the exocrine tissue, and the area of Glucagon α-cells in *nol9*^{sa1022} mutants was indistinguishable from that in wild-siblings (Figure 3-7 A-D). In addition, *nol9*^{sa1022} mutants (n=4) showed a comparable area of Insulin-producing β-cells as wild-type siblings (n=24) (Figure 3-7 E). Moreover, the area of Somatostatin-producing δ-cells was similar between *nol9*^{sa1022} mutants (n=10) and wild-type siblings (n=22) (Figure 3-7 F). These results suggest that before 2 d.p.f., the formation and differentiation of endocrine cells proceed normally in *nol9*^{sa1022} mutants. At 4 d.p.f., the area of *ins:mcherry* cells is comparable between *nol9*^{sa1022} mutants (n=14) and wild-type siblings (n=15) (Figure 3-7 G, J). Similarly, the area of Somatostatin-producing and Glucagon-producing cells is not distinguishable between *nol9*^{sa1022} mutants (n=13 for Somatostatin and Glucagon) and wild-type siblings (n=13 for Somatostatin and n=16 for Glucagon) (Figure 3-7 H, K, I, L). These data suggest that the pancreatic endocrine cells of *nol9*^{sa1022} mutants continue to develop normally. Altogether, these observations indicate that the pancreatic endocrine cells form and differentiate into α-, β- and γ- cells in *nol9*^{sa1022} mutants and that the loss of *nol9* does not impair the development of the pancreatic islet.

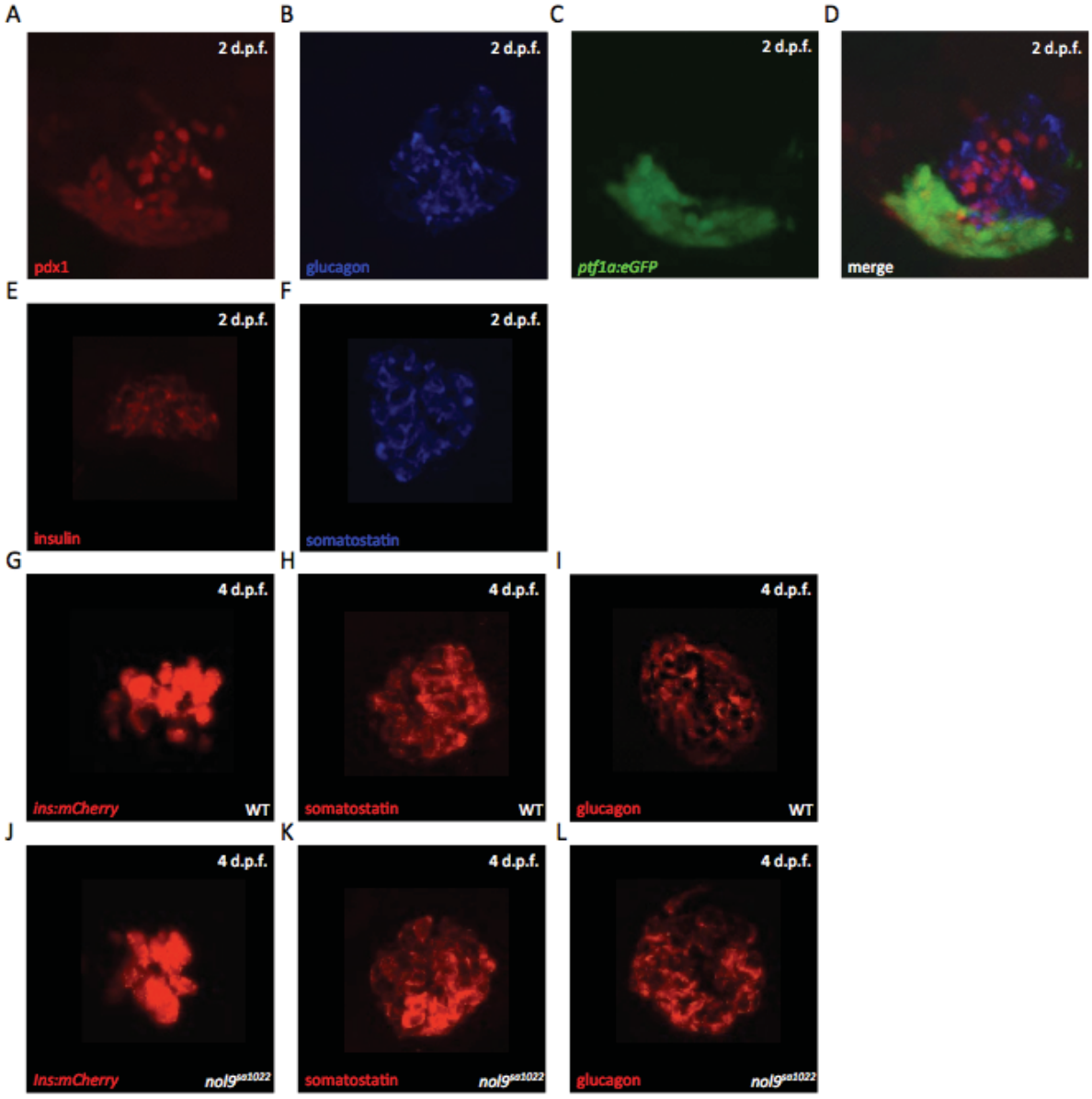

Figure 3-7 Formation and differentiation of pancreatic endocrine cells proceed normally in *nol9*^{sa1022} mutants. (A-L) Offspring from an incross of *Tg(ins:mCherry)*^{jh2}*;Tg(ptf1a:EGFP)*^{jh1}*;nol9*$^{sa1022/+}$; A-F, H, I, K and L express *EGFP* only and have been subjected to immunohistochemistry. (A-D) Representative image of 2 d.p.f. embryo showing presence of Pdx1-producing cells (A), Glucagon-producing cells (B), *ptf1a*-expressing cells (C) and a merged image (D). (E-F) Representative image of 2 d.p.f. offspring showing Insulin- (E) and Somatostatin- (F) producing cells. (G-L) 4 d.p.f. larvae showing comparable levels of *insulin* expression (G, J), Somatostatin (H, K) and Glucagon (I, L) between *nol9*^{sa1022} mutants (J, K, L) and wild-type siblings (G, H, I). (WT) wild-type.

3.2.7 Secondary islets cells expressing *insulin* are present in *nol9*^{sa1022} mutants

In order to study secondary islet formation in *nol9*^{sa1022} mutants, offspring from an incross of *Tg(ins:mCherry)*^{jh2}*;Tg(ptf1a:EGFP)*^{jh1}*;nol9*$^{sa1022/+}$ were incubated from 3 to 5 d.p.f. in egg water containing PTU with either 100 μM of Notch inhibitor *N*-[*N*-(3,5-difluorophenacetyl)-L-alanyl]-*S*-phenylglycine *t*-butyl ester (DAPT), Dimethyl sulfoxide (DMSO) or left untreated (Figure 3-8, Section 2.4.2). At 5 d.p.f., the percentage of untreated *nol9*^{sa1022} mutants and wild-type siblings that had *insulin*-positive secondary islets were 57.9% (11 out of 19) and 33.3% (5 out of 15) respectively (Figure 3-8 A, B). For DMSO-treated larvae, 31.3% (5 out of 16) *nol9*^{sa1022} mutants and 37.5% (6 out of 16) wild-type siblings had *insulin*-expressing secondary islets. The percentage of DAPT-treated *nol9*^{sa1022} mutants and wild-type siblings that had secondary islets were 71.4% (10 out of 14) and 72.4% (21 out of 29) respectively, both higher than DMSO-treated and untreated larvae. This data suggests that DAPT increases the percentage of larvae with secondary islets in both *nol9*^{sa1022} mutants and wild-type siblings. The mean number of secondary islets was 0.79 and 0.47 for untreated *nol9*^{sa1022} mutants and wild-type siblings respectively (Figure 3-8 C). The DMSO-treated *nol9*^{sa1022} mutants and wild-type siblings also had the same mean number of secondary islets of 0.625. Similarly, the mean number of secondary islets for DAPT-treated larvae was higher compared to DMSO-treated and untreated larvae (1.5 for *nol9*^{sa1022} mutants and 1.79 for wild-type siblings). The mean number of secondary islets in wild-type siblings in DAPT treatment was statistically significantly higher than that in DMSO treatment (Student's *t*-test, $p = 0.015$) and without treatment (Student's *t*-test, $p = 0.005$). The mean number of secondary islets in *nol9*^{sa1022} mutants in DAPT treatment was not statistically significantly different from that in DMSO treatment (Student's *t*-test, $p = 0.065$) or without treatment (Student's *t*-test, $p = 0.088$). These results indicate that the mean number of secondary islets in *nol9*^{sa1022} mutants is similar to wild-type siblings when left untreated or treated with DAPT or DMSO. Overall, this experiment demonstrates that secondary islet cells expressing *insulin* are formed in *nol9*^{sa1022} mutants and that together with results from the previous section suggest that the *nol9* mutation does not impair the development of the endocrine pancreas.

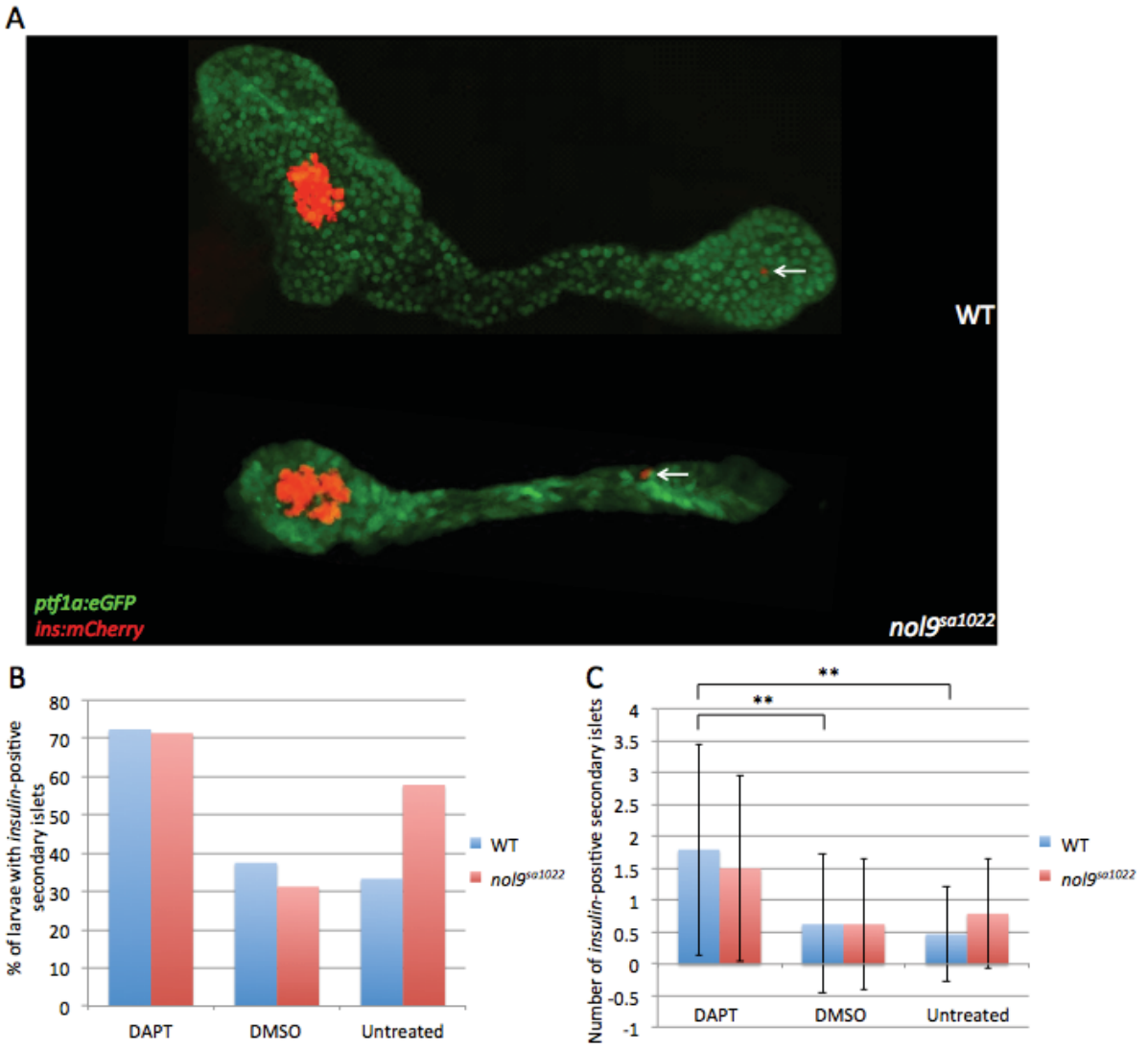

Figure 3-8 Secondary islet cells expressing *insulin* are formed in *nol9*^{sa1022} mutants. (A) Representative maximum intensity projection images of confocal stacks of 5 d.p.f. larvae from an incross of *Tg(ins:mCherry)*^{jh2}*;Tg(ptf1a:EGFP)*^{jh1}*;nol9*$^{sa1022/+}$ showing presence of *insulin*-positive secondary islets (arrow) in both *nol9*^{sa1022} mutants and wild-type siblings. (B) Graph showing the percentage of 5 d.p.f. untreated, DMSO-treated or DAPT-treated *nol9*^{sa1022} mutants and wild-type siblings that displayed *insulin*-positive secondary islets. (C) Graph showing the mean number of *insulin*-positive secondary islets of untreated, DMSO-treated or DAPT-treated *nol9*^{sa1022} mutants and wild-type siblings. Data is represented as the mean ± SD, Student's *t*-test **p<0.01. (WT) wild-type.

3.2.8 Expansion growths of liver and intestine are impaired in *nol9^{sa1022}* mutants

The endodermally-derived organs liver and intestine were found to be underdeveloped in *nol9^{sa1022}* mutants under the dissecting microscope. To examine the development of the liver, I studied the expression of *prospero homeobox protein 1* (*prox1*), an early hepatocyte marker (Glasgow and Tomarev, 1998), in offspring from an incross of *nol9$^{sa1022/+}$* from 2 d.p.f. to 4 d.p.f. and then genotyped them for the *nol9^{sa1022}* mutation (Sections 2.1.2 and 2.3.2). All 2 d.p.f embryos (n=26) expressed *prox1* in the liver primordium, including two that were *nol9^{sa1022}* mutants (Figure 3-9 A). At 3 d.p.f., all the offspring showed normal expression of *prox1* in the liver and seven of all the 37 offspring studied were *nol9^{sa1022}* mutants (Figure 3-9 B). At 4 d.p.f. however, the *nol9^{sa1022}* mutants (n=9) could be distinguished from wild-type siblings (n=26) as having a smaller *prox1*-expressing region (Figure 3-9 C). This data suggests that *nol9* is not required for the initiation and budding of the liver but for its expansion between 3 and 4 d.p.f.

The development of the intestine of *nol9^{sa1022}* mutants was followed by studying the expression of the intestinal epithelium marker *fatty acid binding protein 2* (*fabp2*) in offspring from *nol9$^{sa1022/+}$* zebrafish at 3 d.p.f. and 4 d.p.f (Andre et al., 2000) (Sections 2.1.2 and 2.3.2). All 3 d.p.f. offspring expressed *fabp2* in the foregut and nine out of 49 embryos studied were *nol9^{sa1022}* mutants (Figure 3-9 D). At 4 d.p.f., the *nol9^{sa1022}* mutants (n=11) showed a smaller *fabp2*-expressing region compared to wild-type siblings (n=22) (Figure 3-9 E). This data suggests that the *nol9^{sa1022}* mutation does not abolish cell differentiation in the intestine but instead affects the expansion growth of the intestine between 3 and 4 d.p.f.

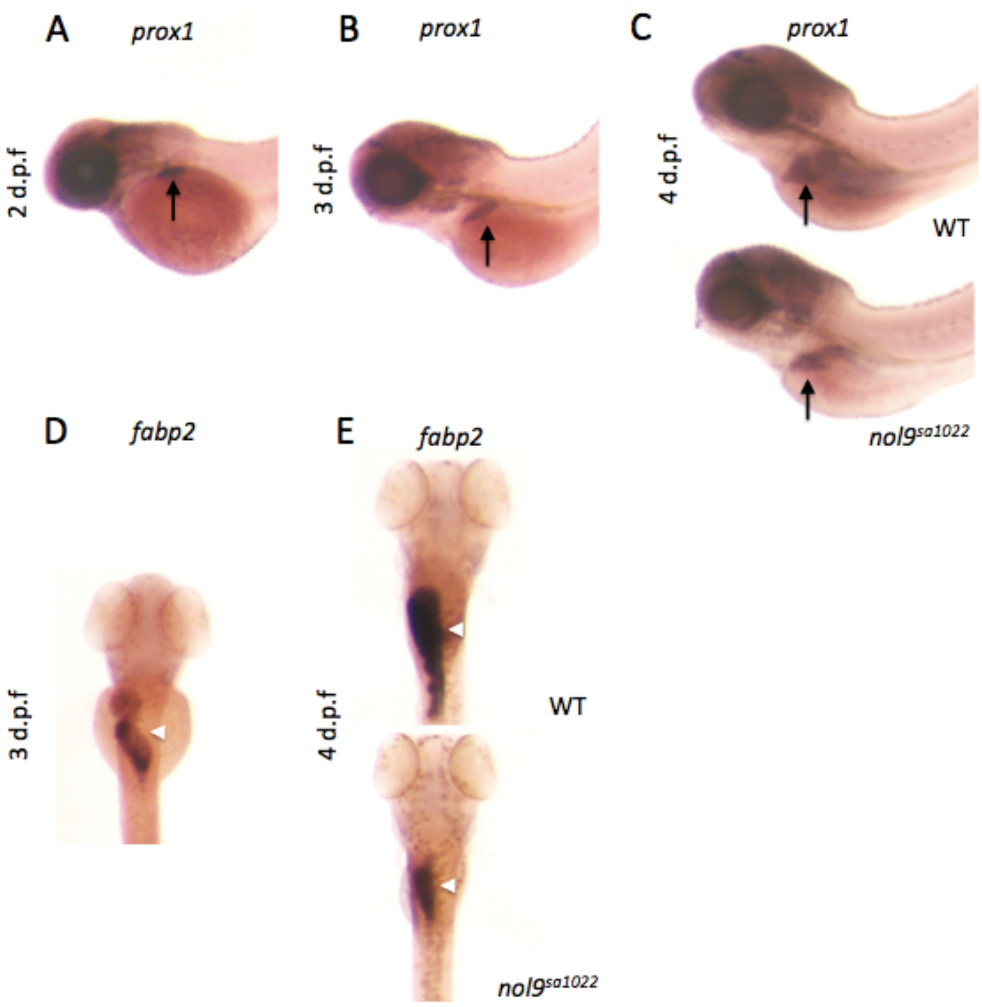

Figure 3-9 Expansion growths of liver and intestine are impaired in *nol9*^{sa1022} mutants. (A-E) Whole mount *in situ* hybridisation using RNA probes against *prox1* (A-C) and *fabp2* (D-E) on offspring from incross of *nol9*$^{sa1022/+}$ zebrafish. (A-C) Lateral view with anterior to the left. (A-B) Representative image of 2 d.p.f. (A) and 3 d.p.f. (B) offspring showing expression of *prox1* in the liver (arrow). (C) At 4 d.p.f., *nol9*^{sa1022} mutants have a smaller *prox1*-expressing region (arrow) compared to wild-type siblings. (D-E) Dorsal view with anterior to the top. (D) Representative image of 3 d.p.f. offspring showing expression of *fabp2* in the intestine (arrowhead). (E) 4 d.p.f. *nol9*^{sa1022} mutants have a smaller *fabp2*-positive region compared to wild-type siblings. (WT) wild-type.

3.2.9 The *nol9*^{sa1022} mutants have different proportion of cells in *G1*, *S* and *G2* phases of cell cycle

The expansion defects of digestive organs in *nol9*^{sa1022} mutants could be explained by two different hypotheses. Firstly, the proliferation of cells of digestive organs may be impaired in *nol9*^{sa1022} mutants. Secondly, there may be an increase in cell death in the digestive organs. To study cell proliferation of *nol9*^{sa1022} mutants, I first analysed the cell cycle of *nol9*^{sa1022} mutants by flow cytometry with propidium iodide to measure the proportion of cells in different phases of the cell cycle (Section 2.4.3). Four biological replicates of 5 d.p.f. *nol9*^{sa1022} mutants and wild-type larvae pairs were obtained with an equal number of larvae (70-100) for each pair. There was a significant increase in the percentage of cells in *G1* phase in *nol9*^{sa1022} mutants (97.1%) compared to wild-type siblings (95.5%) according to the Student's *t*-test ($p = 2.5\text{x}10^{-6}$) (Figure 3-10). This was accompanied by a significant decrease in the percentage of cells in *S* phase in *nol9*^{sa1022} mutants (1.6%) compared to wild-type siblings (2.6%, Student's *t*-test, $p = 2.5\text{x}10^{-5}$). The percentage of cells in *G2* phase in mutants (1.3%) was significantly smaller than those in wild-type siblings (1.8%, Student's *t*-test, $p = 6.3\text{x}10^{-5}$). These results indicate that cell proliferation is impaired in *nol9*^{sa1022} mutants and could contribute to the defective expansion of digestive organs.

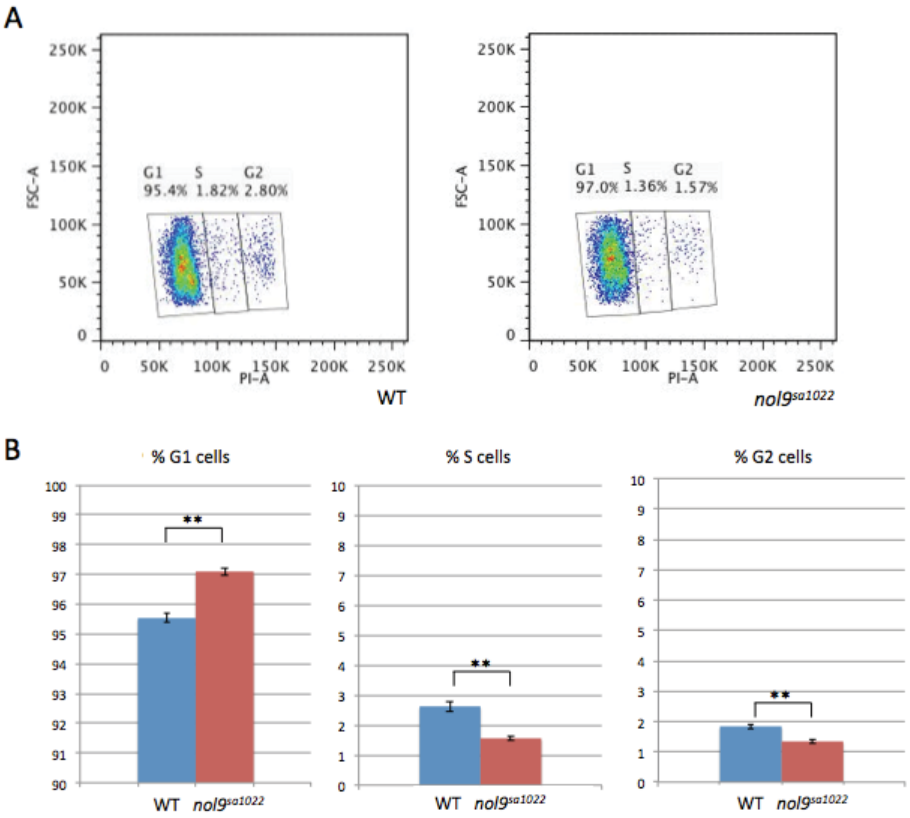

Figure 3-10 Cell cycle analysis of 5 d.p.f. *nol9*^{sa1022} mutants and wild-type siblings. (A) Representative scatter plots of propidium iodide (PI) staining versus forward scatter (FSC) of cells from wild-type (left) and *nol9*^{sa1022} mutant (right). (B) Graph of proportion of cells in G1, S and G2 cell cycle phases in wild-type and *nol9*^{sa1022} mutants. Data from four biological replicates is represented as the mean ± SD, Student's *t*-test **p<0.01. (WT) wild-type.

3.2.10 The pancreas of *nol9*^{sa1022} mutants show impaired cell proliferation

In order to examine cell proliferation in the pancreas of *nol9*^{sa1022} mutants, I measured 5-bromo-2'-deoxyuridine (BrdU) incorporation in 4 d.p.f. larvae from an incross of *Tg(ins:mCherry)*^{jh2}*;Tg(ptf1a:EGFP)*^{jh1}*;nol9*$^{sa1022/+}$ expressing only EGFP and not mCherry (Figure 3-11, Section 2.4.4). The mean number of *ptf1a*-expressing cells that were positive for BrdU was statistically significantly smaller in *nol9*^{sa1022} mutants, 19.33 (n=9) than that in wild-type siblings, 44.14 (n=7) according to the Student's *t*-test, $p = 0.00011$ (Figure 3-11 A, B, E). In contrast, the mean number of cells that were positive for BrdU in the spinal cord region above the vent is not statistically significantly different in *nol9*^{sa1022} mutants, 78.3 (n=3) and wild-type siblings, 78 (n=3) (Student's *t*-test, $p = 0.972$) (Figure 3-11 C, E). Similarly, the mean number of BrdU-positive cells in the spinal cord near the tail is comparable in *nol9*^{sa1022} mutants, 55.3 (n=3) and wild-type siblings, 55 (n=6) (Student's *t*-test, $p = 0.709$) (Figure 3-11 D, E). These results indicate that the proliferation rate of pancreatic exocrine cells is reduced in *nol9*^{sa1022} mutants and that impaired cell proliferation contributes to the expansion defect of the pancreas in *nol9*^{sa1022} mutants.

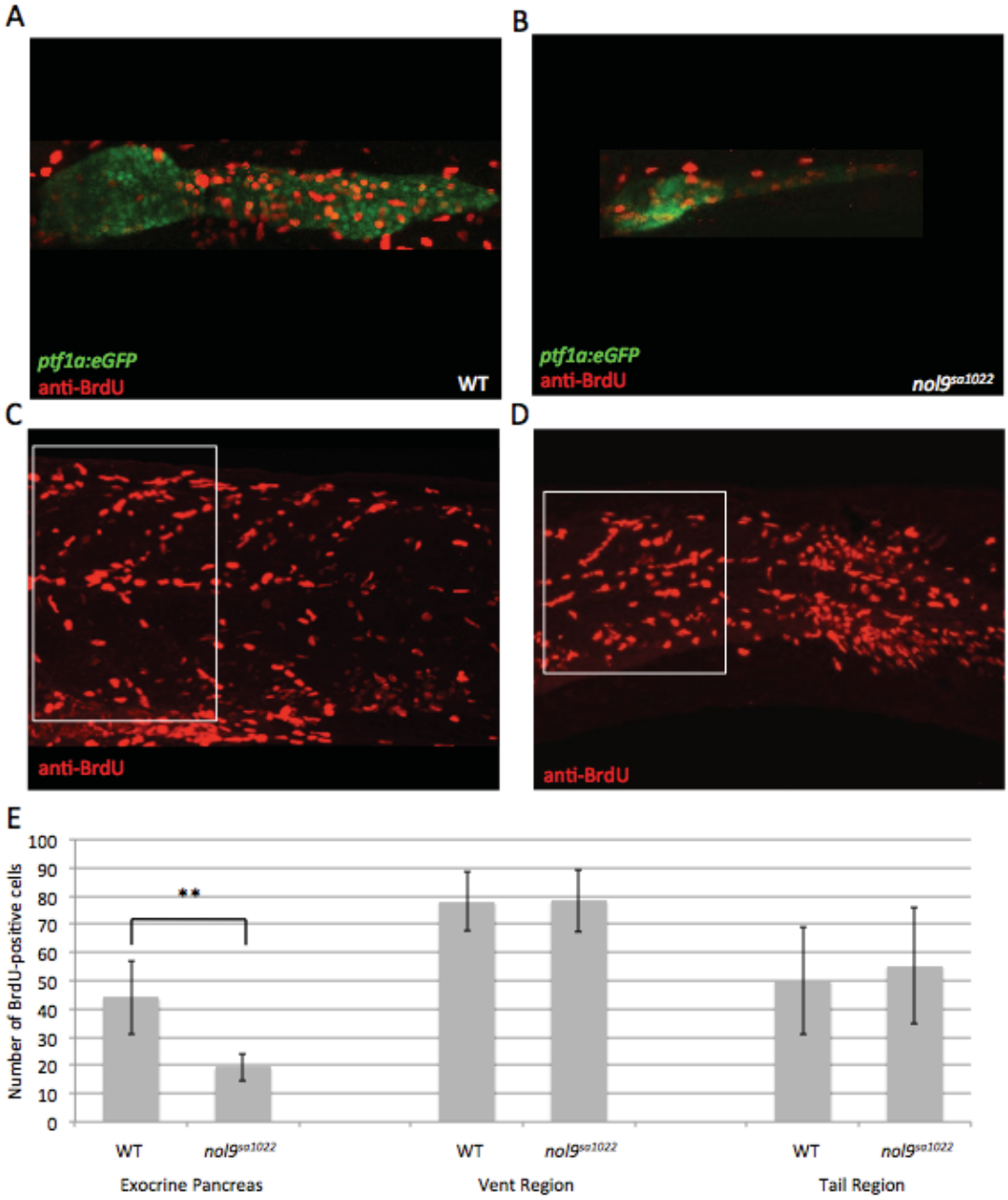

Figure 3-11 The cell proliferation of the exocrine pancreas of *nol9*^{sa1022} mutants is impaired. (A-D) Representative maximum intensity projection images of a z series of confocal sections through 4 d.p.f. larvae from an incross of *Tg(ins:mCherry)*^{jh2}*;Tg(ptf1a:EGFP)*^{jh1}*;nol9*$^{sa1022/+}$ expressing only EGFP and subjected to BrdU incorportation assay. (A-B) The number of BrdU-positive cells is smaller in *nol9*^{sa1022} mutants (B) compared to wild-type siblings (A). (C-D) Representative maximum intensity projection images of confocal stacks of the spinal cord region (boxed area) above the vent (C) and near the tail (D) where the number of BrdU-positive cells was counted. (E) Graph showing that the number of BrdU-positive cells in the exocrine pancreas of *nol9*^{sa1022} mutants (n=9) is statistically significantly smaller than that of wild-type siblings (n=7). The number of BrdU-positive cells in the spinal cord region above the vent and near the tail is similar in both *nol9*^{sa1022} mutants (n=3 for both regions) and wild-type siblings (n=3 for vent region and n=6 for tail region). Data is represented as the mean ± SD, Student's *t*-test **p<0.01. (WT) wild-type.

3.2.11 The pancreas of *nol9*^{sa1022} mutants do not show increased cell death

In addition to impaired cell proliferation, an increase in cell death could also contribute to the expansion defect of the exocrine pancreas in *nol9*^{sa1022} mutants. Therefore, cell death was studied using the terminal deoxynucleotidyl transferase dUTP nick end labelling (TUNEL) staining on 4 d.p.f. larvae from an incross of *Tg(ins:mCherry)*^{jh2}*;Tg(ptf1a:EGFP)*^{jh1}*;nol9*$^{sa1022/+}$ expressing only EGFP and not mCherry (Figure 3-12, Section 2.4.5). There were no tetramethylrhodamine (TMR)-labelled apoptotic cells in the pancreas of *nol9*^{sa1022} mutants (n=8) and wild-type siblings (n=9) (Figure 3-12 A). The mean number of apoptotic cells in the tails of *nol9*^{sa1022} mutants and wild-type siblings were not statistically significantly different, 14 and 11.4 respectively (Student's *t*-test, p = 0.179) (Figure 3-12 B, C). This experiment demonstrates that increase in cell death does not contribute to the expansion defect of the exocrine pancreas in *nol9*^{sa1022} mutants.

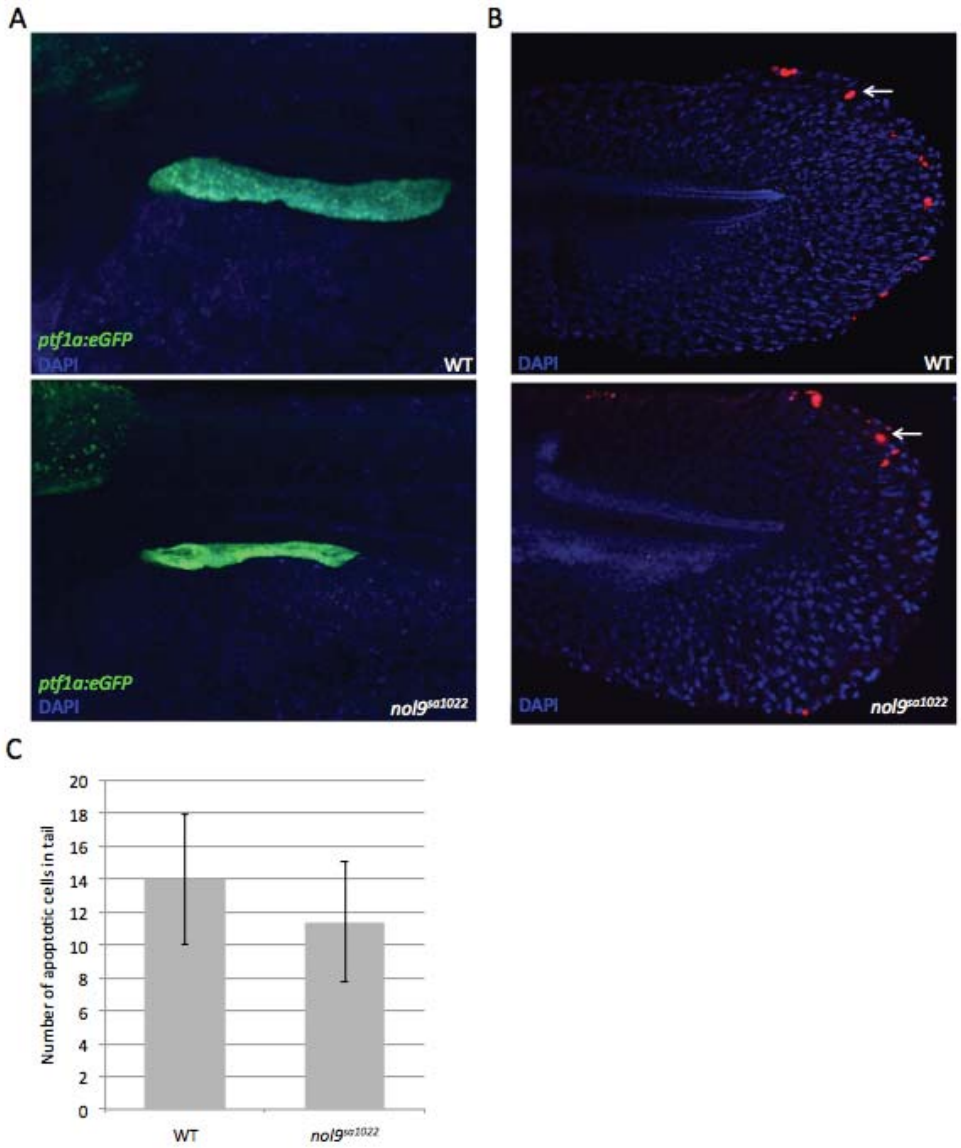

Figure 3-12 The exocrine pancreas of *nol9*^{sa1022} mutants do not show an increase in cell death. (A-B) Maximum intensity projection images of a z series of confocal sections through 4 d.p.f. larvae from an incross of *Tg(ins:mCherry)*^{jh2}*;Tg(ptf1a:EGFP)*^{jh1}*;nol9*$^{sa1022/+}$ expressing only EGFP and subjected to TUNEL and DAPI staining. (A) There are no TMR-labelled apoptotic cells in *ptf1a*-expressing exocrine pancreas of *nol9*^{sa1022} mutants and wild-type siblings. (B) The tails of *nol9*^{sa1022} mutants and wild-type siblings have apoptotic cells (arrow). (C) The mean number of apoptotic cells in the tails of *nol9*^{sa1022} mutants (n=8) is not statistically significantly different from those of wild-type siblings (n=9). Data is represented as the mean ± SD. (WT) wild-type.

3.2.12 Development of the jaw cartilage and erythrocyte is normal in *nol9*^{sa1022} mutants

Craniofacial dysmorphology is a common feature of ribosomopathies (Narla and Ebert, 2010) and previously described zebrafish mutants in genes *rbm19* (Mayer and Fishman, 2003), *def* (Chen et al., 2005), *pwp2h* (Boglev et al., 2013) and *nom1* (Qin et al., 2014) all exhibit abnormal craniofacial development. At 5 d.p.f., there were no major differences between the jaw of *nol9*^{sa1022} mutants and wild-type siblings under a dissecting microscope. To characterise the jaw of *nol9*^{sa1022} mutants further, 5 d.p.f. *nol9*^{sa1022} mutants and wild-type siblings were subjected to Alcian blue staining that labels acidic polysaccharides present in cartilages (Section 2.4.2). In zebrafish, the pharyngeal cartilage consists of seven pharyngeal arches: the anterior two form the jaw whilst the posterior five form the gill structures (Neuhauss et al., 1996). All the jaw cartilage elements were present and appeared normal in *nol9*^{sa1022} mutants (n=23) and wild-type siblings (n=54) (Figure 3-13 A). They include the first phargyngeal arch derivatives, Meckel's cartilage and palatoquadrate, the second pharyngeal arch derivative ceratohyal, and the third and seventh pharyngeal arches, namely the five ceratobranchials (Figure 3-13 A). This data suggests that *nol9*^{sa1022} mutants have normal jaw and branchial arch structures and that *nol9* is not required for craniofacial development.

A haematological phenotype such as anaemia is a shared clinical feature of ribosomopathies (Narla and Ebert, 2010). In both teleosts and mammals, haematopoiesis occurs in four sequential waves. The first two primitive waves produce transient precursors giving rise to embryonic macrophages and erythrocytes whilst the next two definitive waves consist of multipotent progenitors of adult cell types including firstly the erythromyeloid progenitors (EMPs) that will give rise to erythroid and myeloid lineages and then the multipotent haematopoietic stem cells (HSCs) which can produce all adult haematopoietic cell types and self renew (Stachura and Traver, 2011). The haemotopoietic cells of the definitive wave first appear around 26 h.p.f. in the aorta-gonad-mesonephros region and later seed the caudal hematopoietic tissue, where they expand and differentiate (Bertrand et al., 2010). Definitive erythrocytes derived from haematopoietic stem cells appear in the caudal haematopoietic tissue at 3 d.p.f. and slowly replace primitive erythrocytes in circulation (Chen and Zon, 2009). The formation of erythrocytes during early development was studied in *nol9*^{sa1022} mutants to investigate whether *nol9*^{sa1022} mutants also exhibited an anaemic

phenotype. All offspring from an incross of *nol9*$^{sa1022/+}$ zebrafish showed normal blood circulation in the heart and tail at 3 d.p.f. and 5 d.p.f. under the dissecting microscope. All 3 d.p.f. offspring showed a similar area of primitive erythrocytes that were stained with o-dianisidine; 18 out of the 70 zebrafish studied were *nol9*^{sa1022} mutants (Figure 3-13 B, Section 2.4.7). At 5 d.p.f., the presence of haemoglobin-containing erythrocytes was evident in both *nol9*^{sa1022} mutants (n=18) and wild-type siblings (n=51) (Figure 3-13 C). These results indicate that *nol9* is not required for the production of primitive erythrocytes during early development in zebrafish.

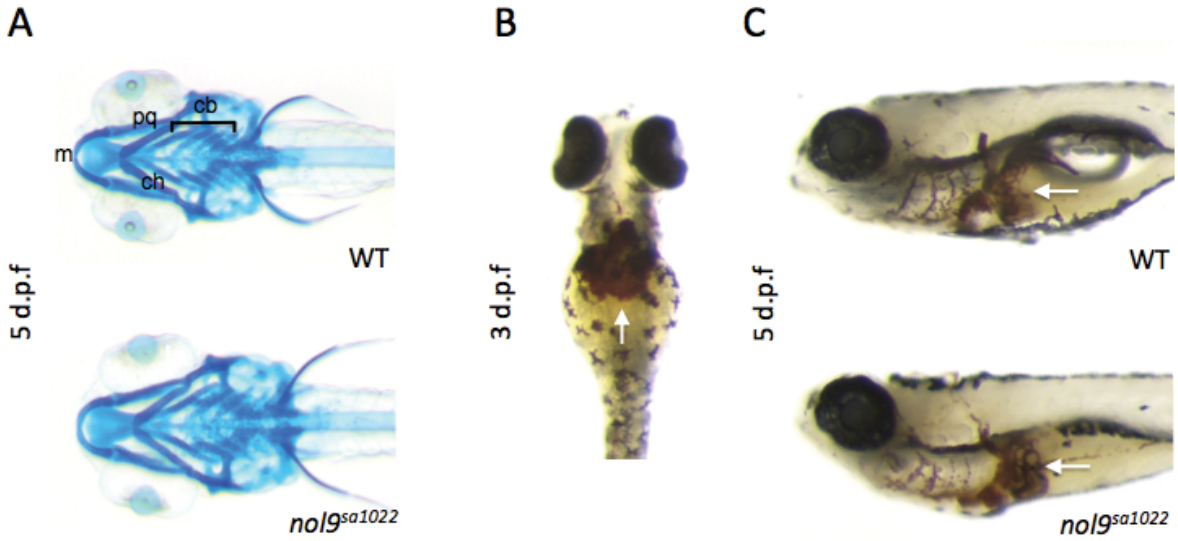

Figure 3-13 Development of jaw cartilage and erythrocyte is normal in *nol9*^{sa1022} mutants. (A) Ventral view with anterior to the left. Alcian blue staining revealed the normal formation of the jaw cartilage elements Meckel's (m), palatoquadrate (pq), ceratohyal (ch) and ceratobranchial (cb) in both *nol9*^{sa1022} mutants and wild-type siblings. (B) Ventral view with anterior to the top. Representative image of all 3 d.p.f. offspring from an incross of *nol9*$^{sa1022/+}$ labelling haemoglobin-containing erythrocytes (arrow). (C) Left side view of 5 d.p.f. wild-type and *nol9*^{sa1022} mutants showing the presence of erythrocytes (arrow) stained with o-dianisidine. (WT) wild-type; (m) meckel's; (pq) palatoquadrate; (ch) ceratohyal; (cb) ceratobranchials.

3.2.13 Developmental expression pattern of *nol9*

The defects in *nol9*^{sa1022} mutants were restricted to specific tissues despite the gene's crucial role in ribosome biogenesis, a process that is required in all tissues. In order to explain the tissue specificity of the phenotype, the expression of *nol9* during development was investigated. RNA-seq data from Ensembl revealed that *nol9* is maternally expressed at the 2-cell stage, and is also expressed at the different developmental stages studied 1, 2, 3 and 5 d.p.f. (Collins et al., 2012; Harvey et al., 2013). In order to examine the expression patterns of *nol9* during development, whole mount *in situ* hybridisation (WISH) was carried out using DIG-labelled RNA probe against *nol9* mRNA on PTU-treated wild-type zebrafish at different stages of development (Section 2.3.2). There was strong expression of *nol9* at 3 hours post fertilisation (h.p.f.), (Figure 3-14 A) and by 1 d.p.f., *nol9* was ubiquitously expressed with high levels detected in the head, eye and notochord (Figure 3-14 B). At 3 d.p.f., the expression became restricted to specific organs namely pancreas, liver, intestine and head (Figure 3-14 C) and this expression pattern continued to 4 d.p.f. (Figure 3-14 D). At 5 d.p.f., *nol9* was still strongly expressed in the digestive organs and was also expressed in the otic vesicles (Figure 3-14 E). The expression data reveals that *nol9* is initially ubiquitously expressed but then becomes restricted to specific organs including the pancreas, liver and intestine.

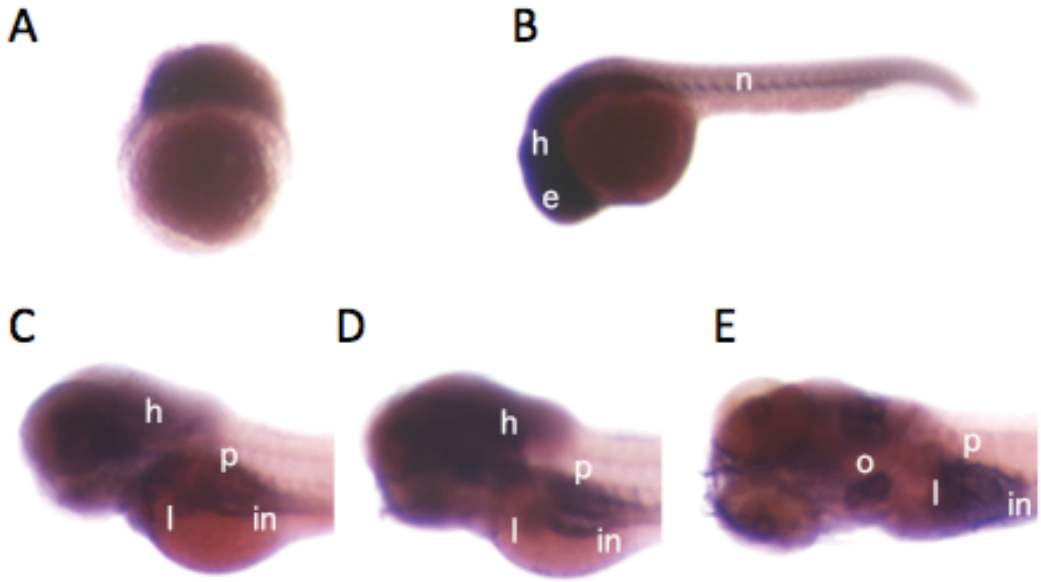

Figure 3-14 Developmental expression pattern of *nol9*. (A) Lateral view of 3 h.p.f. embryo showing strong *nol9* expression. (B-E) Lateral view with anterior to the left. (B) At 1 d.p.f., *nol9* is ubiquitously expressed with strong expression in the head, notochord and eye. (C-D) At 3 d.p.f. (C) and 4 d.p.f. (D), expression of *nol9* is apparent in the head, liver, pancreas and intestine. (E) At 5 d.p.f., *nol9* is strongly expressed in the digestive organs and also in the otic vesicles. (h) head; (n) notochord; (e) eye; (p) pancreas; (l) liver; (in) intestine; (o) otic vesicles.

3.2.14 The processing of 28S rRNA is impaired in *nol9*^{sa1022} mutants

Previous work demonstrated that human NOL9 protein is required for rRNA processing and more specifically for the generation of 5.8S and 28S rRNAs (Heindl and Martinez, 2010). To investigate whether Nol9 plays a similar role in zebrafish, incrosses of *Tg(ins:mCherry)*^{jh2}*;Tg(ptf1a:EGFP)*^{jh1}*;nol9*$^{sa1022/+}$ were phenotyped at 5 d.p.f based on the size of the *ptf1a*-expressing region. Northern blot analysis was carried out in collaboration with Dr Tobias Fleischmann on RNA of *nol9*^{sa1022} mutants and wild-type siblings from two biological replicates using a probe designed against the sequence spanning the 5.8S and Internal Transcriped Spacer (ITS)-2 (Sections 2.2 and 2.5.1) (Figure 3-15 A). RNAse H was used to digest a region of ~ 400 nucleotides (nts) from the start of the 28S rRNA sequence to distinguish between the different precursors that generate the mature 5.8S and 28S rRNAs Figure 3-15). Figure 3-15 A shows a schematic of rRNA processing including some of the different rRNA intermediates (Azuma et al., 2006). In the digested RNA from *nol9*^{sa1022} mutants, a band of 1000 nts displayed increased signal compared to that of digested RNA from wild-type siblings. This band corresponds to rRNA intermediate A (Figure 3-15 A, B). Additionally, two smaller bands of ~ 700 nts had signal of higher intensity in *nol9*^{sa1022} mutants RNA compared to those of wild-type RNA. These two bands correspond to rRNA intermediates B and C (Figure 3-15 A, B). The intensity of the 5.8S bands appeared similar in *nol9*^{sa1022} mutants and wild-type siblings. These data suggest that there is an accumulation of rRNA intermediates that generate 5.8S and 28S rRNA in *nol9*^{sa1022} mutants.

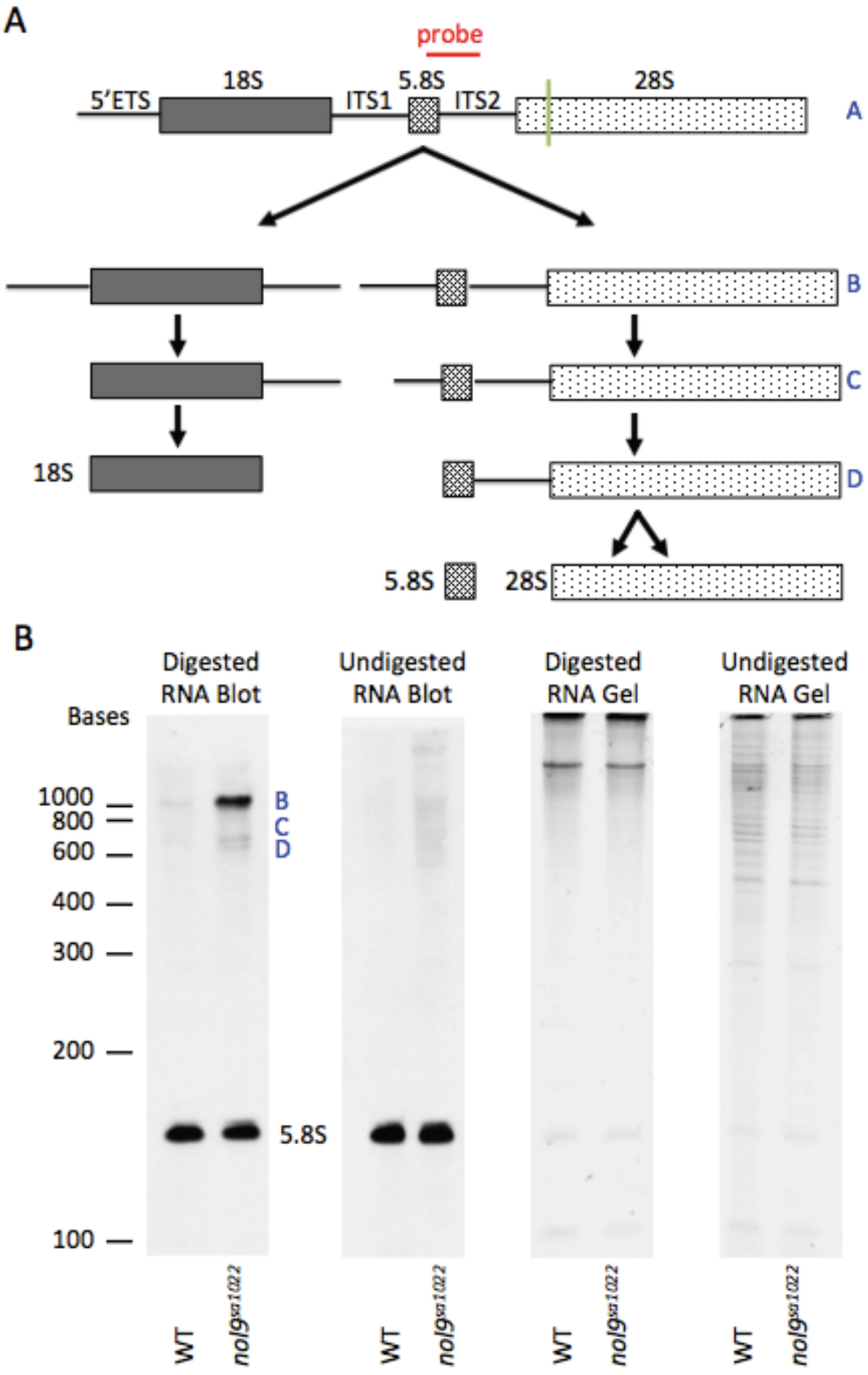

Figure 3-15 rRNA processing is impaired in *nol9*^{sa1022} mutants. (A) Schematic representation of the rRNA processing pathway. The site of hybridisation of the 5.8S-ITS2 probe (red) and the site where RNA was digested (green) are indicated. (B) Representative Northern blot analysis of RNA isolated from 5 d.p.f. *nol9*^{sa1022} mutants and wild-type siblings using the 5.8S-ITS2 probe to detect rRNA processing intermediates (blue). In the digested RNA blot, there is a marked increase in rRNA intermediate A of 1000 nts and an increase in rRNA intermediates B and C of ~ 700 nts in *nol9*^{sa1022} mutants compared to wild-type siblings. There was no apparent difference in the 5.8S band between in *nol9*^{sa1022} mutants compared to wild-type siblings. The RNA gel shows that equal amounts of RNA was loaded in *nol9*^{sa1022} mutants compared to wild-type siblings (WT) wild-type.

To determine if the ratio of 28S to 18S was altered in *nol9*^{sa1022} mutants RNA was compared on a bioanalyser (Section 2.2 and 2.5.1). The level of mature 28S rRNA in *nol9*^{sa1022} mutants was reduced compared to wild-type siblings, whereas levels of mature 18S rRNA were similar (Figure 3-16 A). These differences altered the 28S/18S rRNA ratio, which was 1.78 in *nol9*^{sa1022} RNA compared to 1.93 in wild-type siblings (Paired Student's *t*-test, 0.0371) (Figure 3-16 B). This data suggests that the processing of 28S rRNA and not 18S rRNA is impaired in *nol9*^{sa1022} mutants. Collectively the Northern blot and bioanalyser results demonstrate that the processing of 28S rRNA is impaired in *nol9*^{sa1022} mutants and that the function of Nol9 is conserved from human to zebrafish.

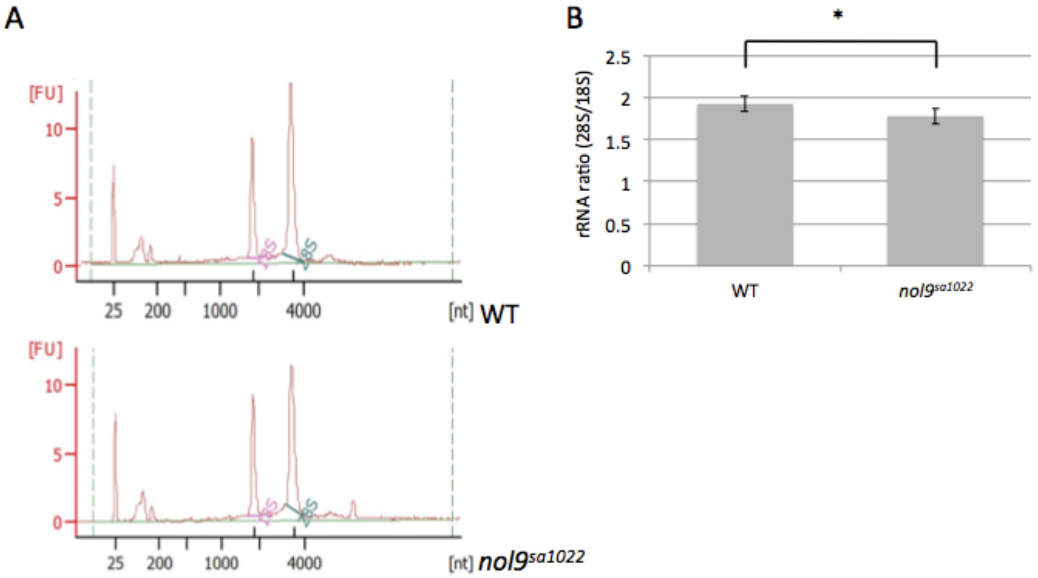

Figure 3-16 The processing of 28S rRNA is impaired in *nol9*^{sa1022} mutants. (A-B) Bioanalyser analysis of total RNA isolated from 5 d.p.f. *nol9*^{sa1022} mutants and wild-type siblings from an incross of *nol9*$^{sa1022/+}$ adults. (A) Representative images of bioanalyser analysis showing a reduction in levels of 28S rRNA but not 18S rRNA in *nol9*^{sa1022} mutants compared to wild-type siblings. (B) The relative rRNA ratio (28S/18S) is statistically significantly smaller in *nol9*^{sa1022} mutants compared to wild-type siblings. Data is representative of four biological replicates as the mean ± SD, Paired Student's *t*-test *p<0.05.

3.2.15 Formation of 60S ribosomal subunit is impaired in *nol9*^{sa1022} mutants

To investigate the effect of the deficiency of Nol9 on ribosome biogenesis, incrosses of *Tg(ins:mCherry)*^{jh2}*;Tg(ptf1a:EGFP)*^{jh1}*;nol9*$^{sa1022/+}$ were phenotyped at 5 d.p.f. based on the size of the *ptf1a*-expressing region. Polysome fractionation was carried out in collaboration with Dr Felix Weis; extracts were prepared from 50 phenotypic and non-phenotypic larvae and the ribosomal subunits were fractionated on sucrose density gradients (Section 2.5.2). The peaks corresponding to the 60S subunits and 80S monosomes in the lysate from *nol9*^{sa1022} mutants are distinctly smaller compared to those in the lysate from wild-type siblings (Figure 3-17). Additionally there are fewer and smaller peaks corresponding to the polysome in the lysate from *nol9*^{sa1022} mutants compared to the lysate from wild-type siblings. In contrast, the peak corresponding to the 40S subunit in the lysate from *nol9*^{sa1022} mutants is larger than that in the lysate from wild-type siblings. This data suggests that the *nol9* mutation affects the formation of the 60S ribosomal subunit and is consistent with the function of Nol9 in processing of 28S rRNA.

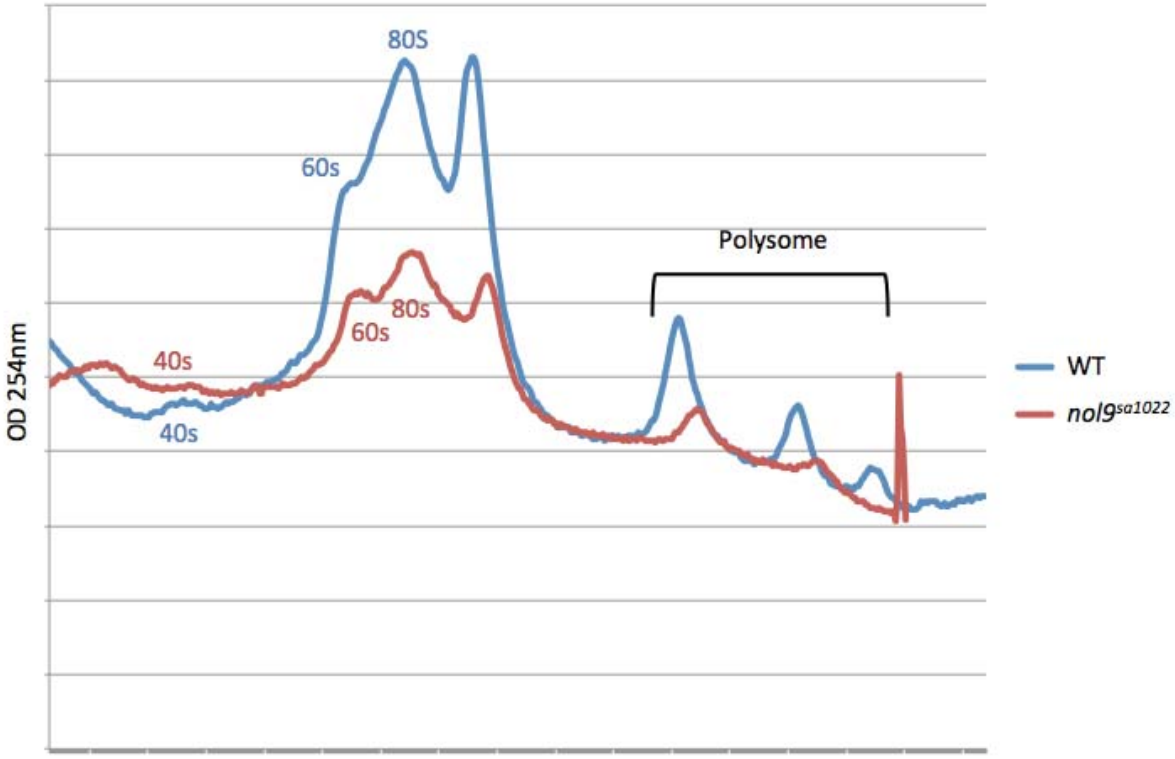

Figure 3-17 60S subunit formation is impaired in *nol9*^{sa1022} mutants. Polysome fractionation analysis performed on *nol9*^{sa1022} mutants and wild-siblings at 5 d.p.f. demonstrating reduced levels of 60S ribosomal subunits, 80S monosomes and polysomes and increased levels of 40S ribosomal subunits in *nol9*^{sa1022} mutants compared to wild-type siblings.

3.3 Discussion

The *nol9*^{sa1022} mutant exhibits a hypoplastic phenotype in digestive organs affecting the pancreas, liver and intestine, and an uninflated swim bladder, whilst the development of other organs appears unaffected. The zebrafish Nol9 protein is indispensable for life as the *nol9*^{sa1022} larvae die before 10 d.p.f.

In humans, the NOL9 protein is required for cleavage at the ITS2 region to generate 5.8S and 28S rRNAs of the large ribosomal subunit (Heindl and Martinez, 2010). The experiments carried out in this study demonstrate that the *nol9*^{sa1022} mutants displayed an accumulation of rRNA intermediates that generate the 5.8S and 28S rRNAs, an increase in the levels of 28S rRNA and reduced levels of 60S ribosomal subunits. These results are consistent with the function of human NOL9 protein. Since the *nol9*^{sa1022} mutation is a nonsense mutation at amino acid 195 in exon 2, it was presumed that this would result in a loss of Nol9 protein. The protein levels in *nol9*^{sa1022} mutants were not tested as commercial antibodies that cross-reacted with zebrafish Nol9 could not be found. The zebrafish Nol9 only shares 34% and 36% identity with human and mouse NOL9.

The development of the pancreas, liver and intestine in *nol9*^{sa1022} mutants proceed normally until 3 d.p.f. but at 4 d.p.f. the digestive organs of *nol9*^{sa1022} mutants are smaller compared to wild-type siblings. The phenotype of *nol9*^{sa1022} is highly reminiscent of other zebrafish mutants of genes encoding rRNA processing proteins namely *nil per os* (*npo*), mutated in gene *RNA binding protein 19* (*rbm19*) (Mayer and Fishman, 2003), *digestive expansion factor* (*def*) (Chen et al., 2005), *titania* (*tti*), mutated in *periodic tryptophan protein 2 homolog* (*pwp2h*) (Boglev et al., 2013) and *nucleolar protein with MIF4G domain 1* (*nom1*) (Qin et al., 2014). Nevertheless, the development of digestive organs in *npo*, *def* and *nom1* were impaired before 3.5 d.p.f. (Chen et al., 2005; Mayer and Fishman, 2003). Using organ-specific markers, we demonstrated that fully differentiated cells were still present in the pancreas and intestine of *nol9*^{sa1022} mutants. This is similar to the *def* and *nom1* mutants where cellular differentiation proceeds in the pancreas, intestine and liver and the *tti* mutant that had fully differentiated intestinal goblet cells (Boglev et al., 2013; Chen et al., 2005). Conversely, cytodifferentiation of the intestine and liver in *npo* mutant were inhibited. It will be interesting to determine whether cellular differentiation proceeds normally in the liver of *nol9*^{sa1022} mutants by doing *in situ hybridisation* with probes against markers of liver

differentiation including *ceruloplasmin* (*cp*) and *fatty acid binding protein 1* (*fabp1*) (Her et al., 2003; Korzh et al., 2001). The *npo*, *def*, *tti* and *nom1* mutants all had additional morphological defects including abnormal jaws, branchial arches and smaller head and eyes (Boglev et al., 2013; Chen et al., 2005; Mayer and Fishman, 2003; Qin et al., 2014). In general, the phenotype of *nol9*^{sa1022} mutants is subtler than the previously described *npo*, *def*, *tti* and *nom1*.

A closer examination of pancreas development in *nol9*^{sa1022} mutants revealed that pancreatic duct formation is impaired. On the other hand, the endocrine cells of the pancreas are formed and fully differentiated and *insulin*-expressing cells of the secondary islets are present in *nol9*^{sa1022} mutants at similar numbers as wild-type siblings. Both pancreatic ducts and secondary islets arise from pancreatic Notch-responsive cells (PNCs) that together with *ptf1a*-expressing cells are derived from the ventral bud (Wang et al., 2011). Hence the pancreatic defect in the *nol9*^{sa1022} mutants is not restricted to a specific cell lineage but instead it is possible that cells that are proliferating at a higher rate are affected by defects in ribosome biogenesis. A more detailed study of secondary islet formation is required where the nascent and other mature endocrine cells (α- and δ-cells) of secondary islets are examined. Also, it will be interesting to investigate the formation of pancreatic ducts and secondary islets in the other rRNA processing mutants, *npo*, *def*, *tti* and *nom1*.

The hypoplastic phenotype of digestive organs of *nol9*^{sa1022} mutants could be due to cell proliferation arrest or increased cell death. The *nol9*^{sa1022} mutants have an increased proportion of cells arrested at the G1 phase implicating defects in cell proliferation. BrdU-labelling revealed that the proliferation rate of the exocrine pancreas of *nol9*^{sa1022} mutants is reduced while the TUNEL assay did not detect an increase in cell death in *nol9*^{sa1022} mutants. These results are in agreement with those of previously reported rRNA processing mutants: the *def* and *tti* mutant larvae showed compromised cell proliferation in digestive organs and in the *nom1* mutant larvae, cell proliferation of the exocrine pancreas was impaired. There was no obvious increase in cell death in all three mutants whilst cell proliferation and cell death were not measured in the *npo* mutant (Boglev et al., 2013; Chen et al., 2005; Mayer and Fishman, 2003; Qin et al., 2014). Future work to help explain the phenotype of the *nol9*^{sa1022} mutants will include studying the cell proliferation of the endocrine pancreas, liver and intestine. Recently, it was discovered that autophagy is induced in intestinal epithelial cells of *tti* mutant to prolong the cell survival and lifespan of the mutant larva (Boglev et al., 2013).

Additionally, red blood cells of zebrafish mutants with deficiency in *ribosomal protein S7* (*rps7*) showed increased autophagy (Heijnen et al., 2014). Studies to determine whether the pancreas, liver and intestine of *nol9*^{sa1022} mutants undergo autophagy will be critical and may corroborate the idea that autophagy is a general response mechanism to ribosomal stress.

The tissue-specific defects resulting from mutations in a gene that is involved in a ubiquitous process could be attributed to the preferential expression of that gene in the tissues affected. The developmental expression pattern of *nol9* follows that of ribosomal biogenesis genes *npo*, *def*, *tti*, *nom1* and multiple *ribosomal protein L* (*rpl*) (Boglev et al., 2013; Chen et al., 2005; Mayer and Fishman, 2003; Provost et al., 2013; Qin et al., 2014). After an initial widespread expression in early embryos, *nol9* and other ribosomal biogenesis genes become increasingly restricted to specific organs including the pancreas, liver and intestine starting from 2 to 3 d.p.f. These organs are amongst the most rapidly proliferating tissues at 3 d.p.f. (de Jong-Curtain et al., 2009). The main hypothesis to explain the tissue specific phenotype of a ubiquitously expressed gene is that wild-type mRNA and/or protein deposited by the heterozygous mother support the development until about 3 d.p.f. (Boglev et al., 2013). Thereafter, rapidly dividing tissues that require large numbers of ribosomes for protein synthesis exhaust the maternally derived wild-type mRNA resulting in a tissue-specific phenotype. This hypothesis however may be an oversimplification since the head of *nol9*^{sa1022} mutants is normal despite *nol9* being highly expressed in the head at 3-4 d.p.f. and the dorsal midbrain and hindbrain proliferating rapidly at 3 d.p.f. (de Jong-Curtain et al., 2009). Therefore, other possibilities that can also contribute to the defects specific to the digestive organs should be considered including Nol9 having digestive organ-specific functions in ribosome biogenesis.

In some ribosomopathies, patients suffer from haematological abnormalities including anaemia (Narla and Ebert, 2010). In 3 d.p.f. and 5 d.p.f. *nol9*^{sa1022} mutants, the blood circulation appeared normal and primitive erythrocytes were present. However, the definitive waves of haematopoiesis that comprise of progenitors of adult cell types in *nol9*^{sa1022} mutants may still be affected. Future work will include analysis of haematopoietic stem cells of the definitive wave by carrying out *in situ hybridisation* using probes against c-*myeloblastosis oncogene* (*c-myb*) and *runt-related transcription factor 1* (*runx1*) (de Jong and Zon, 2005). In addition, the differentiation potential of haematopoietic cells in *nol9*^{sa1022} mutants will be investigated using probes against *recombination activating gene 1* (*rag1*) and *haemoglobin*

alpha embryonic 1 (*hbae1*), markers of differentiated lymphocytes and erythrocytes respectively (de Jong and Zon, 2005). It will be interesting to examine haematopoiesis in adult *nol9*$^{sa1022/+}$ fish since mice heterozygous for the Rpl24 gene, encoding 60S ribosomal protein L24, are characterised by impaired haematopoietic stem cell function due to inefficient protein synthesis (Signer et al., 2014).

The yeast orthologues of *def* and *pwp2h, UTP25* and *PWP2* are both components of the small-subunit (SSU) processome (Bernstein et al., 2007; Charette and Baserga, 2010; Dosil and Bustelo, 2004; Goldfeder and Oliveira, 2010). The SSU processome is a large ribonucleoprotein complex that comprises of the U3 small nucleolar RNA (snoRNA) and at least 43 proteins and is required for biogenesis of the 18S rRNA of the small ribosomal subunit (Bernstein and Baserga, 2004; Dragon et al., 2002). NOM1 and Mrd1p, the yeast orthologue of *npo* are also required for 18S pre-rRNA processing (Alexandrov et al., 2011; Jin et al., 2002). Comparatively, human mutations in *Cirhin*, the homologue of a component of the SSU processome complex, *UTP4* cause liver failure in children, a condition known as North American Indian childhood cirrhosis (NAICC) (Chagnon et al., 2002). *NOL11*, another SSU processome component and an interaction partner for *hUTP4*/Cirhin, is also implicated in the pathogenesis of NAICC (Freed et al., 2012). In addition, exocrine pancreatic dysfunction is one of the clinical features of Shwachman-Diamond syndrome, an inherited bone marrow failure syndrome caused by mutations in *sbds* (Boocock et al., 2003). Although SBDS is a multifunctional protein, its function in the maturation and export of the 60S ribosomal subunit could be instrumental in producing the exocrine pancreatic phenotype (Finch et al., 2011; Menne et al., 2007; Wong et al., 2011b). In general, defective 18S rRNA processing proteins CIRHIN, Def, Pwp2h, Nom1, Npo and large ribosomal subunit biogenesis protein SBDS all result in failure of digestive organs, revealing that digestive organs are particularly sensitive to mutations that impair ribosome production. Therefore it will be unsurprising if digestive organ failure is found to be a regular feature of newly discovered ribosomopathies. Mutations in human *NOL9* have not yet been reported and it is difficult to predict the clinical features of the patients. Nevertheless the loss of function of *nol9* in zebrafish suggests that the human condition could also be characterised by impaired function of digestive organs whereas craniofacial and/or skeletal defects are less likely to be present.

The *nol9*^{sa1022} mutant is the first zebrafish ribosomal biogenesis mutant to be described with morphological defects present only in digestive organs. Studying this mutant further will help elucidate the indispensable role of Nol9 in expansion growth of digestive organs and also facilitate our understanding of the puzzling phenomenon of tissue-specificity resulting from impaired ribosome biogenesis in zebrafish and in ribosomopathies.

Chapter 4 Characterisation of *las1l*^{sa674} mutants

4.1 Introduction

In the previous chapter, Nol9 was identified as playing a role in pancreas development in zebrafish. In this chapter, I aimed to investigate whether any Nol9-interacting proteins had a similar function to Nol9. A literature search revealed that the nucleolar protein LAS1-like (LAS1L) forms a complex with proteins Nucleolar Protein 9 (NOL9), SUMO1/sentrin/SMT3 specific peptidase 3 (SENP3), Proline, glutamic acid and leucine rich protein 1 (PELP1), Testis expressed 10 (TEX10) and WD repeat domain 18 (WDR18) (Castle et al., 2012). LAS1L and its associated proteins are involved in processing of the pre-rRNA internal transcribed spacer 2 region to produce 28S rRNA (Castle et al., 2012; Castle et al., 2010). Las1, the yeast orthologue of LAS1L, was initially found to be involved in cell morphogenesis and also to play a conserved role in processing of rRNAs of the large ribosomal subunit (Castle et al., 2013; Doseff and Arndt, 1995). Recently, Butterfield *et al.* described a patient with a spinal muscular atrophy with respiratory distress (SMARD) phenotype and identified a de novo mutation in *LAS1L* (Butterfield et al., 2014). The authors knocked down *las1l* in zebrafish by morpholino resulting in disruption of peripheral nerve and muscle architecture and early lethality of the embryos (Butterfield et al., 2014). There are currently no reports of studies of LAS1L in mice. The Zebrafish Mutation Project was searched for disruptive mutations in *las1l*, *senp3a*, *senp3b*, *PELP1*, *tex10* and *wdr18*, zebrafish orthologues of *LAS1L*, *SENP3*, *PELP1*, *TEX10* and *WDR18*. At the time of the search, a nonsense allele was identified for *las1l* (*las1l*^{sa674}), whereas alleles of *senp3a*, *senp3b*, *PELP1*, *tex10* and *wdr18* had not yet been found.

The *las1l* gene has three Zv9 Ensembl transcripts: las1l-001, las1l-201 and las1l-202 (Figure 4-1 A). The longest transcript las1l-001 is comprised of 2642 bases and has 13 exons encoding a protein of 580 amino acids. The las1l-201 and las1l-202 are two shorter transcripts comprising of 942 and 567 bases encoding a protein of 314 and 189 amino acids, respectively. The Las1l protein of human (ENSP00000363944), mouse (ENSMUSP00000078901) and zebrafish (ENSDARP00000121984) are conserved especially

in the *Las1* domain (Figure 4-1 B). The zebrafish Las1l has 37% and 38% amino acid residues that are identical to the human and mouse Las1l respectively. The *las1l*^{sa674} has a G to T base change in exon 11 of the transcript las1l-001 converting the amino acid 475 from a glutamic acid (GAG) into a stop codon (TAG) (Figure 4-1 A, B).

In order to determine whether Las1l has a similar function to Nol9 in zebrafish development, I aimed to characterise the *las1l*$^{sa674/sa674}$ mutant (abbreviated as *las1l*^{sa674}) by first identifying any gross morphological defects that may be present in *las1l*^{sa674} mutant, focusing on the digestive organs since they are hypoplastic in *nol9*^{sa1022} mutant. Secondly, I aimed to determine whether the pancreatic defects of *las1l*^{sa674} mutant were comparable to those of the *nol9*^{sa1022} mutant by identifying the stage at which pancreas development is impaired. Thirdly, I analysed cell death in *las1l*^{sa674} mutant in order to investigate whether increased cell death could contribute to the phenotype. Lastly, I examined the jaw morphology and erythrocyte development of *las1l*^{sa674} mutant to determine whether they were normal and similar to the *nol9*^{sa1022} mutant.

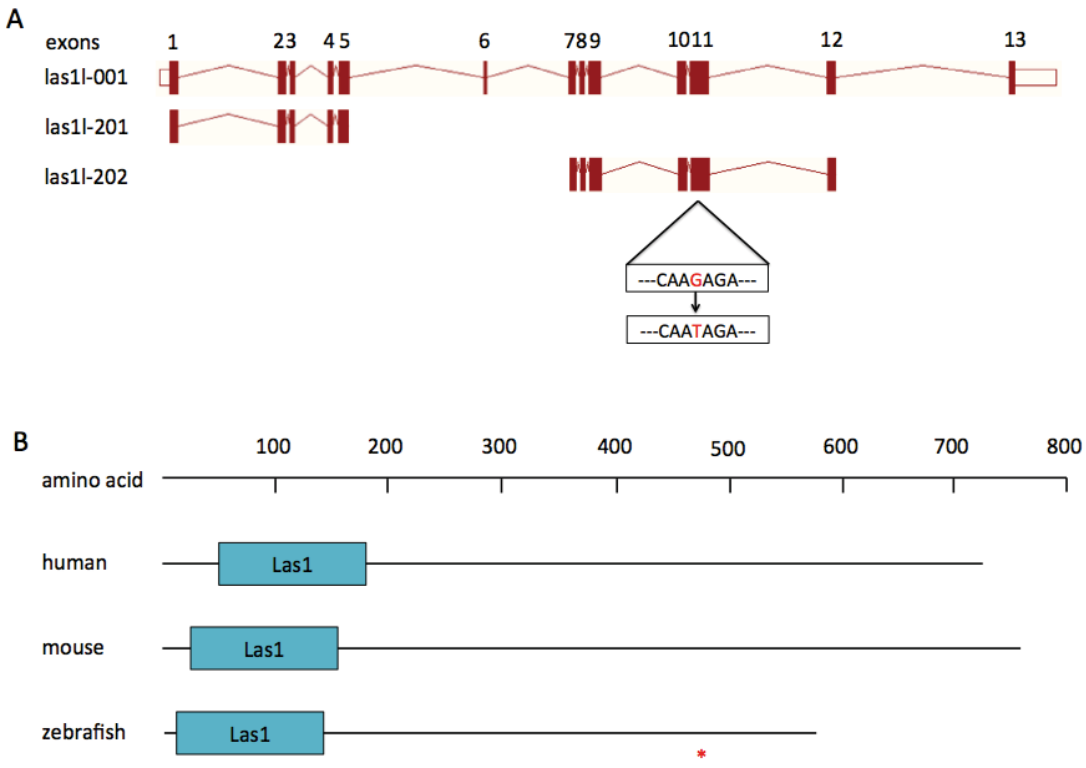

Figure 4-1 Diagram of *las1l* gene and Las1l protein. (A) The zebrafish *las1l* gene has three Ensembl transcripts las1l-001, las1l-201 and las1l-202. The *las1l*^{sa674} is a nonsense mutation in exon 11 of transcript las1l-001 converting the codon GAG (Glutamic acid) into TAG (stop codon). The diagrams were taken from Ensembl. Exons are shown as boxes and introns are shown as lines. (B) The human, mouse and zebrafish Las1l proteins are conserved. Boxes show the protein domains and * indicate the location of the *las1l*^{sa674} mutation.

4.2 Results

4.2.1 Gross morphology of *las1l*^{sa674} mutants

The *las1l*^{sa674} mutants, similarly to *nol9*^{sa1022} mutants, appeared normal up to 4 days post fertilisation (d.p.f.). However at 5 d.p.f., they could be distinguished from wild-type siblings under a dissecting microscope (Figure 4-2). The *las1l*^{sa674} mutants had fewer intestinal folds and appeared to have a slightly smaller liver and pancreas compared to wild-type siblings and approximately half of the 5 d.p.f. *las1l*^{sa674} mutants failed to inflate their swim bladder. The morphology of the head, eyes, jaw, size and body shape of *las1l*^{sa674} mutants were indistinguishable from that of wild-type siblings.

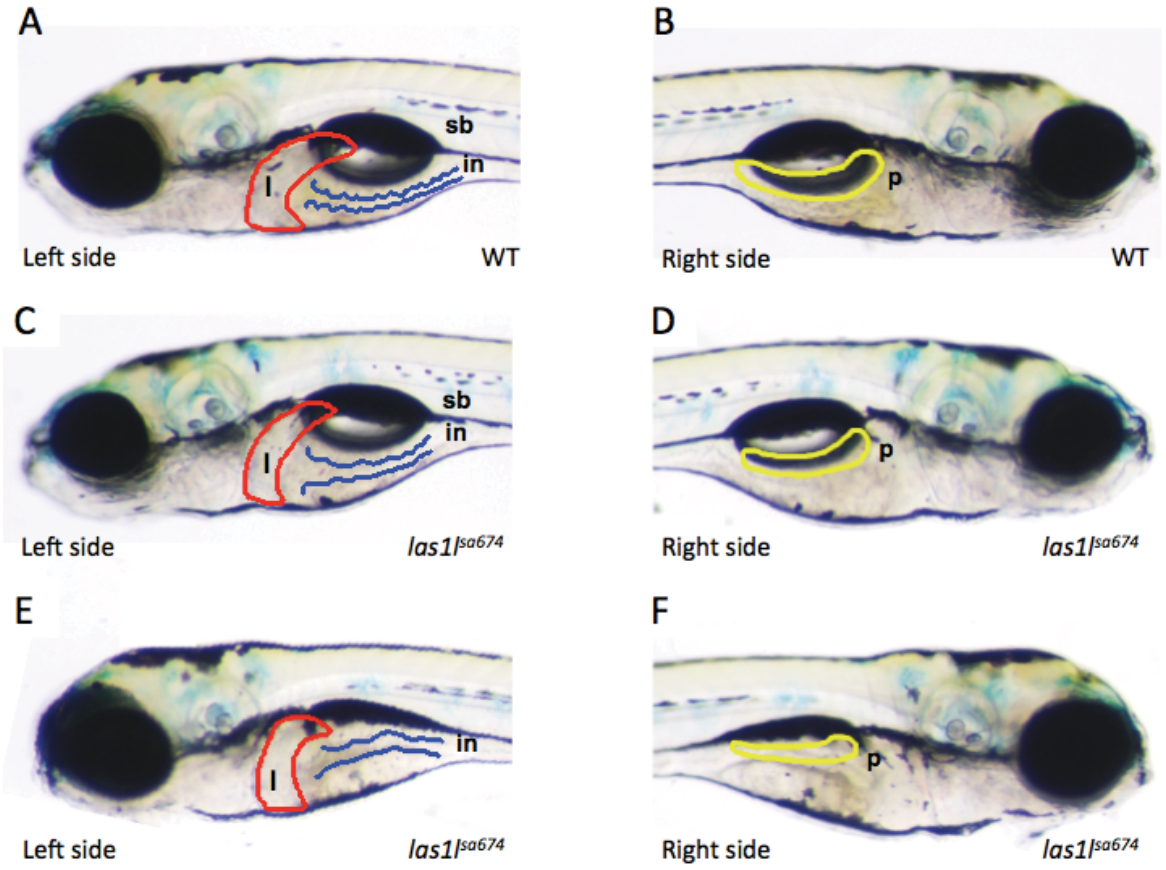

Figure 4-2 The digestive organs of *las1l*^{sa674} mutants are less developed than wild-type siblings. (A-F) Bright-field images of 5 d.p.f. wild-type and *las1l*^{sa674} mutant larvae. (A,C,E) Left side view of wild-type (A) and *las1l*^{sa674} mutants with (C) or without (E) swim bladder showing that the *las1l*^{sa674} mutants have fewer intestinal folds (in; blue) and smaller liver (l; red) compared to wild-type siblings. Swim bladder (sb) is present (C) or absent (E) in *las1l*^{sa674} mutants. (B,D,F) Right side view of wild-type (B) and *las1l*^{sa674} mutants with (D) or without (F) swim bladder showing that *las1l*^{sa674} mutants have a smaller pancreas (p; yellow) compared to wild-type siblings. (WT) wild-type; (l) liver; (in) intestine; (sb) swim bladder; (p) pancreas.

4.2.2 The *las1l*^{sa674} mutants have smaller exocrine pancreas

The pancreas of *las1l*^{sa674} mutants appeared smaller than wild-type siblings under the dissecting microscope. To determine whether *las1l*^{sa674} is causative of the phenotype, offspring from incrosses of F3 *las1l*$^{sa674/+}$ were phenotyped at 5 d.p.f. based on the size of the pancreas under the dissecting microscope and subsequently genotyped (Section 2.1.2). All phenotypic larvae were *las1l*$^{sa674/sa674}$ (n=16) and all non-phenotypic larvae were either *las1l*$^{sa674/+}$ (n=34) or *las1l*$^{+/+}$ (n=16) (Figure 4-3). This data suggests that the *las1l*^{sa674} mutation causes a smaller pancreas and that the phenotype follows a Mendelian pattern of recessive inheritance.

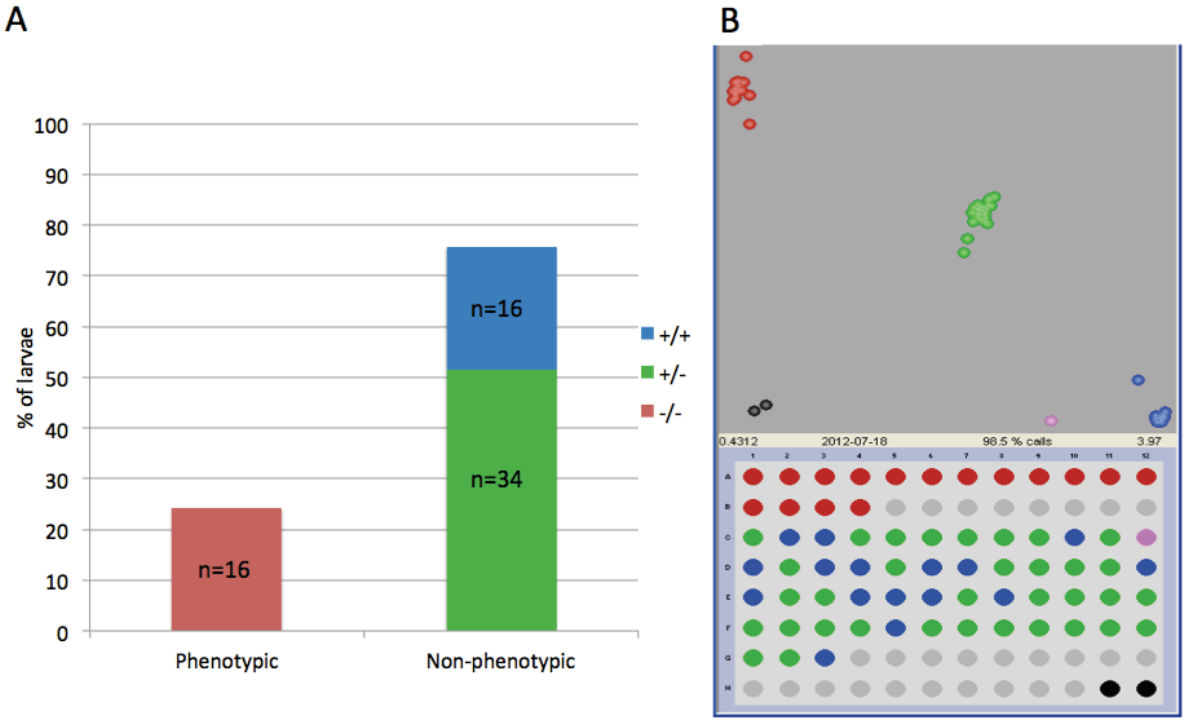

Figure 4-3 The *las1l*^{sa674} mutation is causative of a small pancreas phenotype. (A) Graph showing the percentage of phenotypic and non-phenotypic larvae that are homozygous mutant (-/-; red), heterozygous (+/-; green) and homozygous wild-type (+/+; blue) for *las1l*^{sa674} mutation. (B) KASPar genotyping image. Phenotypic larvae are in the first two rows and non-phenoytpic larvae are in the subsequent five rows. The genotype of homozygous mutant, heterozygous and homozygous wild-type are shown as red, green and blue dots respectively. Pink are uncalled genotypes.

In order to facilitate the study of pancreas development in *las1l*^{sa674} mutants, the F3 *las1l*$^{sa674/+}$ were outcrossed to the transgenic line *Tg(ins:mCherry)*^{jh2}*;Tg(ptf1a:EGFP)*^{jh1} (Pisharath et al., 2007) that express mCherry in the pancreatic islet and EGFP in the exocrine pancreas. Offspring from an incross of *Tg(ins:mCherry)*^{jh2}*;Tg(ptf1a:EGFP)*^{jh1}*;las1l*$^{sa674/+}$ were phenotyped at either 2 d.p.f., 3 d.p.f., 4 d.p.f. or 5 d.p.f. and subsequently genotyped for the *las1l*^{sa674} mutation (Section 2.1.2). At 2 d.p.f., all the embryos had formed an *insulin*-expressing pancreatic islet enclosed by *ptf1a*-expressing tissue. Of the 18 embryos studied, eight were *las1l*^{sa674} mutants (Figure 4-4 A). At 3 d.p.f., the *ptf1a*-expressing region had expanded posteriorly and the *insulin*-positive area had increased in size in all 19 offspring, six of which were *las1l*^{sa674} mutants (Figure 4-4 B). At 4 d.p.f., *las1l*^{sa674} mutants (n=6) could be distinguished from wild-type siblings (n=37) by appearing to have a smaller area of *ptf1a*-expressing cells whilst the *insulin*-positive area appeared similar in size in mutants and wild-type siblings (Figure 4-4 C). At 5 d.p.f., the *ptf1a*-expressing tissue of *las1l*^{sa674} mutants (n=10) appeared smaller than that of wild-type siblings (n=40) whereas the area expressing *insulin* in both mutants and wild-type siblings appeared similar in size (Figure 4-4 D). In both *las1l*^{sa674} mutants and wild-type siblings, the *ptf1a*-positive exocrine tissue had expanded compared to their size at 4 d.p.f. The volume of *ptf1a*-expressing region of *las1l*^{sa674} mutants and wild-type siblings were measured at 5 d.p.f. (Section 2.3.4). The mean volume of *ptf1a*-expressing region of *las1l*^{sa674} mutants (n=10) is statistically significantly smaller than that of wild-type siblings (n=11), 0.00065 mm^3 and 0.002 mm^3 respectively (Student's *t*-test, $p = 1.31 \times 10^{-10}$). These results indicate that the development of the exocrine, but not the *insulin*-positive area, is impaired in *las1l*^{sa674} mutants and that the exocrine pancreas fails to expand normally in *las1l*^{sa674} mutants after 3 d.p.f.

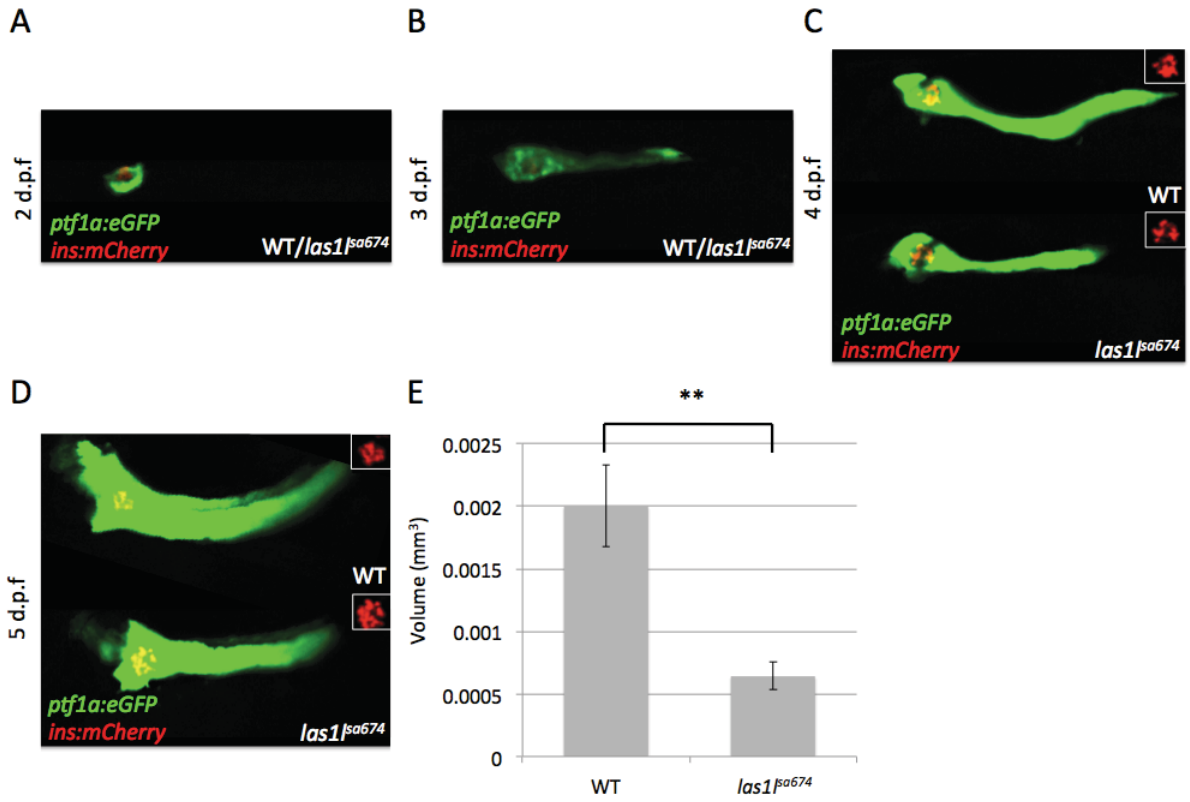

Figure 4-4 Expansion of the exocrine pancreas is impaired in *las1l*^{sa674} mutants. (A-D) Confocal images of 2 d.p.f. to 5 d.p.f offspring from an incross of *Tg(ins:mCherry)*^{jh2}*;Tg(ptf1a:EGFP)*^{jh1}*;las1l*$^{sa674/+}$. (A) Representative image of 2 d.p.f. embryo showing *insulin*-positive pancreatic islet surrounded by *ptf1a*-positive exocrine pancreas. (B) Representative image of 3 d.p.f. embryo showing that the *ptf1a*-positive region has grown. (C-D) At 4 d.p.f. (C) and 5 d.p.f. (D), the *ptf1a*-expressing exocrine pancreas is smaller in *las1l*^{sa674} mutants (upper image) compared to wild-type siblings (lower image) whereas the *insulin*-expressing pancreatic islet (shown in boxed area) is similar in size in *las1l*^{sa674} mutants and wild-type siblings. (E) The volume of *ptf1a*-expressing region of *las1l*^{sa674} mutants (n=10) is significantly smaller than wild-type siblings (n=11). Data is represented as the mean ± SD, Student's *t*-test **p<0.01. (WT) wild-type.

4.2.3 The pancreas of *las1l*^{sa674} mutants do not show increased cell death

The expansion defect of the exocrine pancreas of *las1l*^{sa674} mutants could be explained by increased cell death and/or impaired cell proliferation. The cell death of 4 d.p.f. larvae from an incross of *Tg(ins:mCherry)*^{jh2}*;Tg(ptf1a:EGFP)*^{jh1}*;las1l*$^{sa674/+}$ expressing only EGFP but not mCherry was investigated using TUNEL staining (Figure 4-5) (Section 2.4.5). There were no Tetramethylrhodamine (TMR)-labelled apoptotic cells detected in the pancreas of *las1l*^{sa674} mutants (n=9) or wild-type siblings (n=12). However, the tails of *las1l*^{sa674} mutants and wild-type siblings had a similar mean number of apoptotic cells 5 and 4.6 respectively (Student's *t*-test, $p = 0.50$). These results suggest that the pancreas phenotype of *las1l*^{sa674} mutants does not result from an increase in cell death.

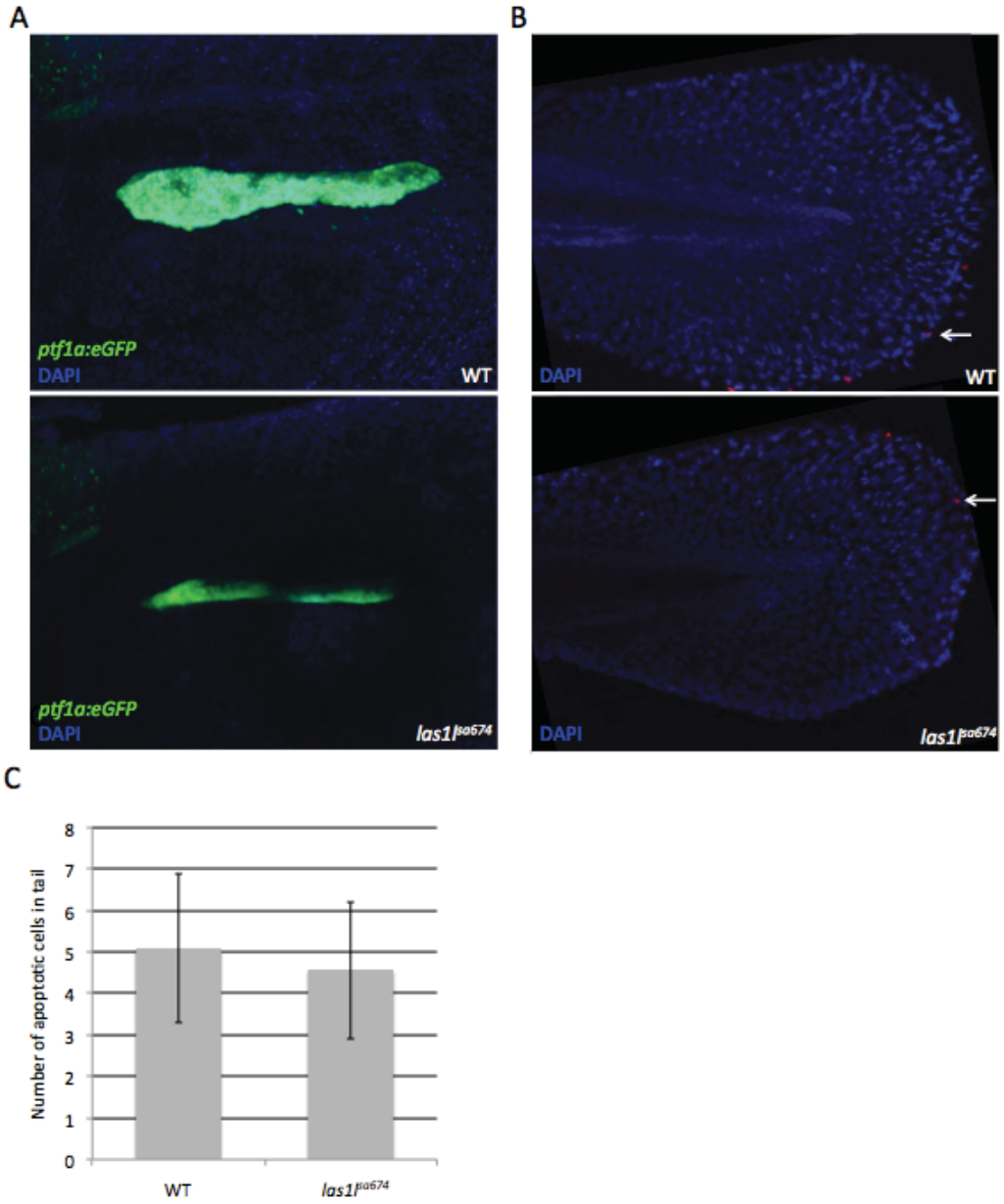

Figure 4-5 The exocrine pancreas of *las1l*^{sa674} mutants do not show increased cell death. (A-B) Maximum intensity projection images of a z series of confocal sections through 4 d.p.f. *las1l*^{sa674} mutant and wild-type zebrafish. Larvae were produced from an incross of *Tg(ins:mCherry)*^{jh2}*;Tg(ptf1a:EGFP)*^{jh1}**;***las1l*$^{sa674/+}$ but expressed only EGFP and subjected to TUNEL and DAPI staining. (A) There are no TMR-labelled apoptotic cells in *ptf1a*-expressing exocrine pancreas of *las1l*^{sa674} mutants and wild-type siblings. (B) Both *las1l*^{sa674} mutants and wild-type siblings have TMR-labelled apoptotic cells (white arrow) in their tails. (C) The number of apoptotic cells in the tails of *las1l*^{sa674} mutants (n=9) and wild-type siblings (n-12) is not statistically significantly different. (WT) wild-type.

4.2.4 Development of the jaw cartilage and erythrocyte is normal in *las1l*^{sa674} mutants

The development of the jaws of *las1l*^{sa674} mutants was investigated since craniofacial defects are common features of ribosomopathies (Narla and Ebert, 2010) and rRNA processing zebrafish mutants displayed jaw defects (Boglev et al., 2013; Chen et al., 2005; Mayer and Fishman, 2003; Qin et al., 2014). At 5 d.p.f., the jaws of *las1l*^{sa674} mutants were indistinguishable to those of wild-type siblings under a dissecting microscope. Alcian blue staining revealed that in *las1l*^{sa674} mutants (n=16) and wild-type siblings (n=43), all the jaw cartilage elements were present, including the Meckel's, palatoquadrate, certohyal and the five ceratobranchial cartilage (Figure 4-6 A) (Section 2.4.6). These results suggest that *las1l*, similarly to *nol9* is not required for jaw development in zebrafish.

The formation of erythrocytes in *las1l*^{sa674} mutants was examined to determine whether *las1l*^{sa674} mutants had erythropoietic defects that are common clinical features of ribosomopathies (Narla and Ebert, 2010). The blood circulation in the heart and tail of all offspring from an incross of *las1l*$^{sa674/+}$ zebrafish was normal at 3 d.p.f. and 5 d.p.f. under the dissecting microscope. O-dianisidine staining revealed that all 3 d.p.f. offspring (n=47) showed a similar area of primitive erythrocytes (Figure 4-6 B) (Section 2.4.7). At 5 d.p.f., haemoglobin-containing erythrocytes were present in both *las1l*^{sa674} mutants (n=16) and wild-type siblings (n=48) (Figure 4-6 C). This data indicates that *las1l*, like *nol9* is not required for the formation of erythrocytes during early development.

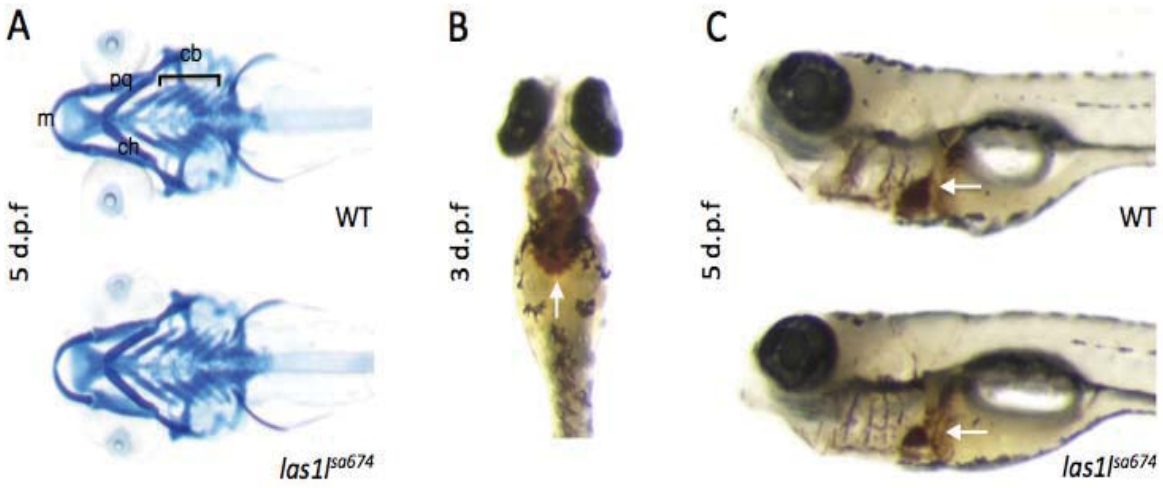

Figure 4-6 Development of the jaw cartilage and erythrocytes are normal in *las1l*^{sa674} mutants. (A) Ventral view with anterior to the left. All the jaw cartilage elements including Meckel's (m), palatoquadrate (pq), ceratohyal (ch) and ceratobranchial cartilage (cb) are present in 5 d.p.f. *las1l*^{sa674} mutants and wild-type siblings as revealed by Alcian blue staining. (B) Ventral view with anterior to the top. Representative image of all 3 d.p.f. embryo from an incross of *las1l*$^{sa654/+}$ stained with o-dianisidine to label haemoglobin-containing erythrocytes (arrow). (C) Left side view of 5 d.p.f. *las1l*^{sa674} mutants and wild-type siblings showing erythrocytes stained with o-dianisidine (arrow). (WT) wild-type; (m) Meckel's; (pq) palatoquadrate; (ch) ceratohyal; (cb) ceratobranchials.

4.3 Discussion

The human LAS1-like (LAS1L) protein is required for cell proliferation and ribosome biogenesis and forms a nucleolar complex with NOL9, PELP1, TEX10, WDR18 and SENP3 (Castle et al., 2012; Castle et al., 2010). All of these proteins are required for the efficient processing of the pre-rRNA internal transcribed spacer-2 (ITS-2) region, maturation of the 28S rRNA and 60S ribosomal subunit synthesis (Castle et al., 2012; Castle et al., 2010). In this project, the *las1l*^{sa674} mutant has been characterised to determine whether Las1l, a Nol9-interacting protein has a similar function to Nol9 during zebrafish development.

The *las1l*^{sa674} mutant displayed underdeveloped digestive organs at 5 d.p.f although the defects appeared to be less severe than those of *nol9*^{sa1022} mutant under the dissecting microscope. Further characterisation of the *las1l*^{sa674} mutant pancreas revealed that the expansion defect of the exocrine pancreas first became apparent between 3 d.p.f. and 4 d.p.f., as was the case for the *nol9*^{sa1022} mutant. At 5 d.p.f., the mean volume of the exocrine pancreas of the *las1l*^{sa674} mutant (0.00065 mm^3) was statistically significantly smaller than that of wild-type siblings (0.0020 mm^3), and nominally larger than that of the *nol9*^{sa1022} mutant (volume=0.0005 mm^3, Student's *t*-test, $p = 0.02$). There was no statistically significant difference in the pancreatic volume of wild-type siblings of *las1l*^{sa674} and *nol9*^{sa1022} mutant (Student's *t*-test, $p = 0.52$). Similarly to *nol9*^{sa1022} mutants, there was no increase in cell death in the pancreas of *las1l*^{sa674} mutants. This suggests that the phenotype is likely to result from impaired cell proliferation as is the case in *nol9*^{sa1022} mutants and this is currently under investigation. The exocrine pancreas of the *las1l*^{sa674} mutant unlike that of the *nol9*^{sa1022} mutant continued to expand after 3 d.p.f. This raises an important question of whether the exocrine pancreas of *las1l*^{sa674} mutant is able to recover from the expansion growth defect.

Recently, a mutation in *LAS1L* has been reported to cause a congenital lethal motor neuron disease (Butterfield et al., 2014). This study however has a major weakness: only one patient was identified as having a mutation in *LAS1L* despite attempts to find additional probands with mutations in the same gene. The pathogenicity of the *LAS1L* mutation is supported by morpholino knockdown of *las1l* in zebrafish that resulted in embryos displaying small malformed brain, shorter necrotic tail, disrupted architecture of peripheral nerve and muscle and early lethality at 24 h.p.f. (Butterfield et al., 2014). The phenotype described in the paper is in contrast with that of the *las1l*^{sa674} mutant where only defects in digestive

organs were observed. There are a number of reasons that could explain this discrepancy. Firstly, *las1l* knockdown was achieved using a translation-blocking morpholino and a splice blocking morpholino that induces skipping of exon 10 whereas the *las1l*^{sa674} mutation is in exon 11. The *las1l* morphants may have less functional Las1l protein than the *las1l*^{sa674} mutants resulting in a more a severe dysmorphic phenotype in the morphants. The expression of Las1l protein in *las1l*^{sa674} mutants is ongoing. Secondly, knocking down *las1l* using morpholinos might have resulted in off-target effects that contribute at least in part to the phenotype described (Robu et al., 2007). Indeed the suppression of the toxic effects of morpholinos by p53 inhibition has not been reported although the phenotype was consistent when using two independent morpholinos and partial rescue was achieved with wild-type but not mutant *LAS1L* RNA (Butterfield et al., 2014). In order to resolve this discrepancy, future work could include generating a zebrafish mutant with the exact mutation from the patient in the equivalent residue in zebrafish via TALENs or CRISPR/Cas technology and examining the axon and muscle development in that mutant.

In general, the phenotype of *las1l*^{sa674} mutant appeared to be less severe than that of *nol9*^{sa1022} mutant. This may be caused by: firstly, the Las1l protein in *las1l*^{sa674} mutant still retaining some functionality particularly since the conserved domain Las1 is encoded by amino acids 12 to 158 and the *lasl*^{sa674} mutation is in amino acid 475. To test this hypothesis, *las1l* function can be disrupted through the generation of a second *las1l* allele with a mutation before or within the Las1 domain using TALENs or CRISPR/Cas technology. Secondly, the requirement of Las1l for expansion of the exocrine pancreas in zebrafish may be less than that of Nol9 although both NOL9 and LAS1L human proteins have been found to be crucial for ribosome biogenesis and cell proliferation (Castle et al., 2012; Castle et al., 2010; Heindl and Martinez, 2010). Thirdly, the maternally deposited supplies of wild-type *nol9* mRNA and/or protein in highly proliferative organs may be exhausted before that of *las1l* mRNA resulting in a more severe phenotype in *nol9*^{sa1022} mutant.

A crucial component of the future work constitutes confirming the role of Las1l in the production of mature 28S rRNA and assembly of 60S ribosomal subunits in zebrafish. The study of *las1l*^{sa674} mutant has not been as detailed as that of *nol9*^{sa1022} mutant due to time constraints. Additional work on the *las1l*^{sa674} mutant should comprise of detailed characterisation of the digestive organs including examining endoderm formation, gut looping, formation of the liver and pancreatic primordia, organ expansion and differentiation

so that comparisons can be drawn between *nol9*^{sa1022} and *las1l*^{sa674} mutant. It would also be interesting to see whether formation of endocrine cells and secondary islets proceed normally as is the case in *nol9*^{sa1022} mutant. These data should help to answer whether Nol9 and Las1l have the same function in zebrafish development. Moreover, the cooperative actions of Nol9 and Las1l proteins can be studied in a *nol9*^{sa1022};*las1l*^{sa674} mutant that we have already generated. We suspect that the combined loss of *nol9* and *las1l* will have an additive effect on digestive organ development. In addition, the developmental expression of *las1l* will be an important aspect to explore. If its expression follows that of *nol9*, *npo*, *def*, *tti*, *nom1* and several *ribosomal protein L* (*rpl*) (Boglev et al., 2013; Chen et al., 2005; Mayer and Fishman, 2003; Provost et al., 2013; Qin et al., 2014), i.e. initially ubiquitously expressed and subsequently preferentially expressed in digestive organs, this will help explain the tissue-specificity of the phenotype observed.

Only the *las1l*^{sa674} mutant was studied since at the time, no other mutants of the other proteins in the complex had been identified. Future directions will include investigating whether Senp3a, Senp3b, Pelp1, Tex10 and Wdr18 have a similar function to Nol9 and Las1l in zebrafish development. At the time of writing, nonsense and/or essential splice site mutations in *senp3b*, *pelp1* and *wdr18* have been identified in ZMP and insertional mutants for *senp3a*, *senp3b* and *wdr18* are also available. These mutants could be studied, complemented with generation of *tex10* mutants to determine whether each of these proteins is involved in expansion growth of digestive organs or development of other organs. In zebrafish, *wdr18* morpholino knock-down experiments showed that Wdr18 is required for the formation of Kupffer's vesicle and for left-right asymmetry (Gao et al., 2011). The morphants displayed a randomised distribution of visceral organs, with the positions of the pancreas and liver either reversed or showing pancreas duplication when the liver was on the opposite position (Gao et al., 2011). Although the expansion growth of the digestive organs has not been studied in the *wdr18* morphants, this study raises the important question of whether proteins of the aforementioned nucleolar protein complex are involved in the regulation of body asymmetry. It is also worth exploring the combined loss of proteins in the complex by incrossing the different mutant lines and transiently knocking down specific genes. This will enhance our knowledge of the role of these proteins in zebrafish development and indicate whether the proteins have synergistic or opposing actions to each other.

Human conditions with mutations in *NOL9*, *SENP3*, *PELP1*, *TEX10* or *WDR18* remain to be identified. Since the function of Nol9 and Las1l have only been described in ribosome biogenesis (Castle et al., 2012; Castle et al., 2010; Heindl and Martinez, 2010) and we have shown that *nol9* and *las1l* zebrafish mutants have comparable digestive-organ specific phenotype, it is possible that mutations in *NOL9* and *LAS1L* in humans will result in a similar disease phenotype. If the congenital lethal motor neuron disease is not actually caused by LAS1L for reasons previously mentioned, we could predict from the zebrafish mutant data that the human condition will likely be characterised by digestive organ failure while craniofacial defects will less likely be present since *las1l*^{sa674} mutant does not have defects in jaw development. Here we found that the blood circulation of *las1l*^{sa674} mutant was normal and that primitive erythrocytes were present at 3 d.p.f. and 5 d.p.f. However, the *las1l*^{sa674} mutant may still have defects in the definitive waves of haematopoiesis comprising of multipotent progenitors of adult cell types. This is currently being explored and therefore it is difficult at present to speculate on the haematopoietic defects if any exist in the human condition. Some of these Las1l-interacting proteins have additional functions to the 28S pre-rRNA processing: PELP1 acts as a transcription coregulator of nuclear hormone receptors (Choi et al., 2004; Vadlamudi et al., 2001) and Wdr18 has an important role in zebrafish development (Gao et al., 2011). Consequently the clinical features resulting from mutations in these proteins will probably not be restricted to digestive organ failure.

The *las1l*^{sa674} mutant, like the *nol9*^{sa1022} mutant, exhibits defects in expansion growth of the exocrine pancreas. This indicates that Las1l and Nol9 have a similar function in zebrafish development and further supports the role of this 28S rRNA processing complex in zebrafish pancreas development.

Chapter 5 Analysis of mRNA expression profiles of *nol9*^{sa1022}, *las1l*^{sa674}, *tti*^{s450} and *set*^{s453} mutants

5.1 Introduction

The expression of mRNA determines the functional and physiological status of a cell, tissue or organism. The study of transcripts by mRNA expression has proved to be a powerful tool to uncover genes of unknown function and coordinate activities of genes in different biological processes, such as in developmental processes and genetic disorders (Ko, 2001; Smith and Greenfield, 2003). Various platforms have been used to study zebrafish mRNA expression profiles, including the most commonly used DNA microarray (Smith and Greenfield, 2003). This technique can detect thousands of zebrafish transcripts by measuring the intensity of signal produced by hybridisation of cDNA to probes attached to a solid surface. It has successfully identified, amongst others, gene clusters at distinct developmental stages (Mathavan et al., 2005), liver-enriched genes in adult zebrafish (Cheng et al., 2006), genes enriched in the gastrointestinal tract at various developmental stages (Stuckenholz et al., 2009) and genes enriched in *def* mutant (Chen et al., 2005) and in *sbds* knockdown (Provost et al., 2012). A second technology, serial analysis of gene expression (SAGE) (Velculescu et al., 1995), has been used only in a handful of studies in zebrafish, including the analysis of mRNA expression of ovarian follicles (Knoll-Gellida et al., 2006) and livers of male and female zebrafish (Zheng et al., 2013). This method can discover new genes through better quantification of transcription levels compared to microarray analysis but is more expensive (Ibrahim et al., 2005; van Ruissen et al., 2005). RNA-sequencing (RNA-seq) technology has now become the state-of-art method for studying mRNA expression (Wang et al., 2009). The technique involves converting an RNA population into a library containing cDNA fragments that have adapters attached to one or both ends (Wang et al., 2009). The molecules are then subjected to sequencing in a high-throughput manner to produce short sequences from one or both ends and the reads are either assembled *de novo* or aligned to a reference genome or transcripts (Wang et al., 2009). A genome-scale transcription map is

produced and can inform on the gene expression levels and transcriptional structure (Wang et al., 2009). Compared to the DNA microarray, RNA-seq can profile RNA transcript abundance more accurately and within a greater dynamic range, can detect novel transcripts, and can characterise and monitor alternatively spliced transcripts and non-coding RNAs (Marioni et al., 2008). It has been used in various studies including zebrafish mRNA expression at various developmental stages (Vesterlund et al., 2011; Yang et al., 2013), small RNA expression during early development (Wei et al., 2012), mRNA expression profiling of a zebrafish model of Diamond-Blackfan anemia (Jia et al., 2013) and transcriptome analyses of zebrafish mutants genes in *RNA-binding region (RNP1, RRM) containing 3* (*rnpc3*) (Markmiller et al., 2014) and *nom1* mutants (Qin et al., 2014).

Differential Expression Transcript Counting Technique (DeTCT) is a high-throughput mRNA expression profiling technique developed by John Collins (unpublished). It produces count data by tag sequencing the 3' end of transcripts from strand-specific Illumina libraries that have been enriched for short fragments adjacent to the polyA tail. DeTCT is used in the Sanger ZMP to determine the mRNA expression profiles of phenotypic ZMP mutants that are associated with an allele (Kettleborough et al., 2013). The DeTCT pipeline starts with RNA extraction of mutants and wild-type siblings. In brief, the library preparation (described in detail in Section 2.6.1) consists of annealing the poly(T) primer to pull down poly(A) transcripts (Figure 2-1). A first partial Illumina adapter is ligated to the 5' end of the transcripts. Subsequently, an oligonucleotide comprising of a second partial Illumina adapter, a six base index tag, four random bases and 14 T bases is ligated to the 3' end of the transcripts. The RNA ligated to the Illumina adapters is reverse transcribed and is amplified using full-length primers to produce libraries. The DeTCT libraries are subjected to paired-end sequencing on an Illumina HiSeq 2000. The sequencing data produces two sets of reads, the read 1 contains the random bases, the index tag, 14 T bases and the remaining is transcript-specific sequence whereas the read 2 is entirely transcript-specific sequence. The first step of the differential expression analysis is to differentiate between the different libraries by using their unique index tag on read 1 and to remove non-species sequences (Figure 5-1) (Section 2.6.2). Subsequently, Burrow-Wheeler Alignment (BWA) tool is used to align the sequencing reads to the Zv9 genome assembly independently of the known gene annotation (Li and Durbin, 2009). The random bases of read 1 are then used to remove PCR duplicates to reduce the effects of PCR amplification bias introduced during library preparation. The abundance of read 2 is counted where reads accumulate across all libraries

and is attached to the 3' end of regions defined using read 1. DESeq (Anders and Huber, 2010) is then used to determine the genomic regions that show significant differential transcript abundance and the Ensembl annotation is used to match the 3' end of transcripts identified by read 1. Lastly, a gene list of differentially expressed genes is produced filtered on the DESEq adjusted *p*-value and the distance to the nearest Ensembl gene.

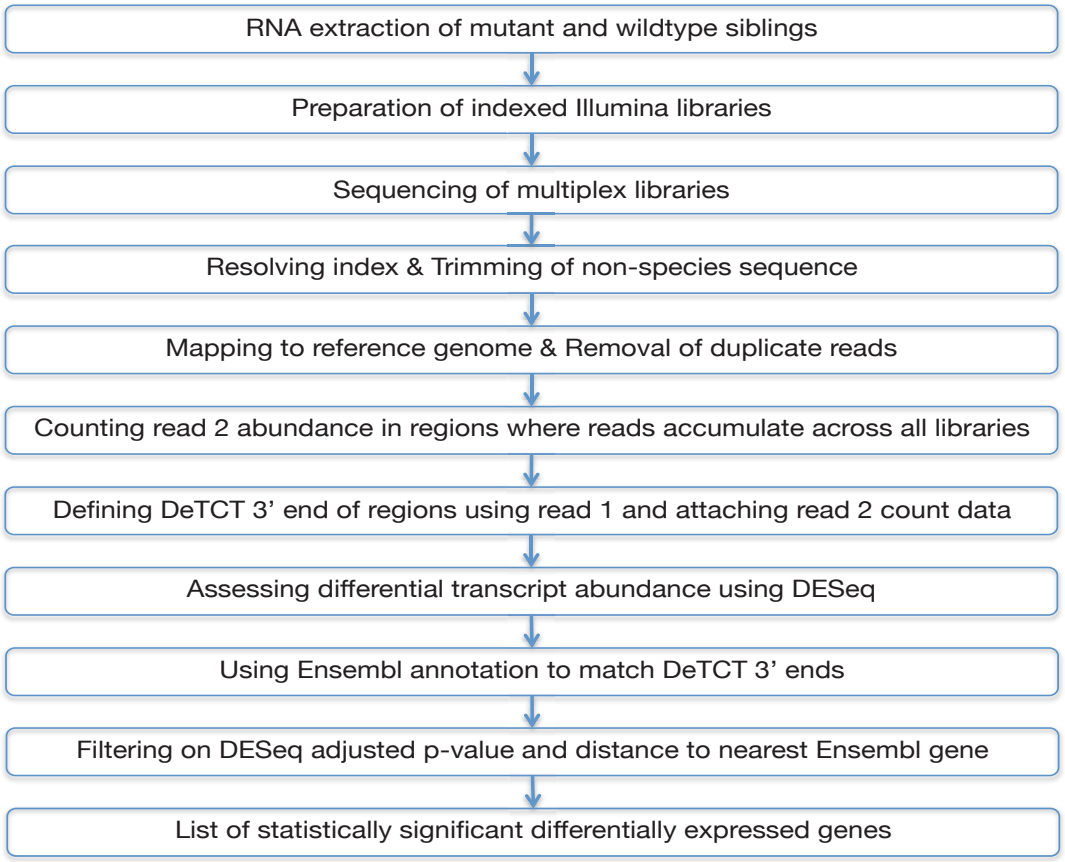

Figure 5-1 Differential Expression Transcript Counting Technique (DeTCT) pipeline. RNA of mutants and wild-type siblings is extracted and used for preparation of indexed Illumina libraries that are sequenced by paired-end Illumina HiSeq. Two sets of reads are produced: read 1 consists of random bases, index tag, 14 T bases and the remainder is transcript-specific sequence whilst read 2 is entirely transcript-specific sequence. The index of each library is resolved by using its unique tag and non-species sequences are trimmed. The sequencing reads are mapped to the reference genome by BWA and duplicate reads are removed by using the random bases. The abundance of read 2 is counted where reads accumulate across all libraries. The 3' end of regions is defined using read 1 and the count data is attached. DESeq is used to assess the differential transcript abundance and Ensembl annotation is used to match DeTCT 3' ends. The list is filtered based on the DESeq adjusted *p*-value and distance of transcript to the nearest Ensembl gene to produce a list of statistically significant differentially expressed genes.

Compared to RNA-seq, DeTCT provides a higher dynamic range for the same amount of sequence data since each transcript is sampled only once, and the total number of reads is not dominated by long or highly expressed transcripts (John Collins, personal communication). In addition, the library preparation of DeTCT is faster and less expensive than that of RNA-seq. With DeTCT, it is easier to locate un-annotated regions of the genome that show differential transcript abundance and identify previously unknown transcripts.

In order to provide a better understanding of the function of *nol9* and *las1l* in zebrafish development, we investigated the mRNA expression profiles of *nol9*^{sa1022} and *las1l*^{sa674} mutants using DeTCT with the goal of identifying genes and pathways that, when altered, can contribute to the phenotype of these mutants. In addition, the mRNA expression profiles of two mutants *tti*^{s450} and *set*^{s453} were also examined. Since *tti*^{s450} and *set*^{s453} mutants also have a mutation in rRNA processing genes and display similar phenotypic defects to *nol9*^{sa1022} and *las1l*^{sa674} mutants, comparisons of their expression profiles can help to uncover shared pathways and decipher the molecular basis of developmental defects of zebrafish rRNA processing mutants.

5.2 Results

5.2.1 The mRNA expression profile of *nol9*^{sa1022} mutants

In this experiment, six pairs of *nol9*$^{sa1022/+}$ zebrafish were incrossed and for each pair, 25 phenotypically mutant and 25 wild-type siblings were collected at 5 d.p.f. for RNA extraction (Section 2.2). Library preparation was carried out on the 12 samples (six mutant and six wild-type pools) and the 12 libraries were sequenced on one single lane of Illumina HiSeq 2000 (Section 2.6.1). Dr Ian Sealy carried out the bioinformatic analysis on the sequence data including resolving the index of each library, trimming of non-zebrafish sequence, mapping to reference genome and removal of duplicate reads. Table 5-1 shows the number and percentage of reads mapped for each pairs of mutant and wild-type siblings and the complexity of each library, i.e. the estimated number of unique molecules in each library. Since the library complexity is similar for each sample, all the six biological replicates were included for the next step in DeTCT analysis.

Sample	Reads			Estimated number of unique molecules
	Mapped	Total	% Mapped	
Mutant 1	22,762,654	28,952,219	78.62	1,323,614,272
Wild-type 1	23,844,191	28,708,629	83.06	1,209,790,911
Mutant 2	20,371,319	26,035,334	78.24	943,296,898
Wild-type 2	23,979,267	30,791,253	77.88	1,231,014,078
Mutant 3	23,579,438	30,153,578	78.20	1,418,214,013
Wild-type 3	22,151,787	27,007,284	82.02	1,236,748,436
Mutant 4	20,806,364	26,820,920	77.58	1,180,581,745
Wild-type 4	18,931,237	26,063,887	72.63	1,565,331,425
Mutant 5	18,006,129	25,116,115	71.69	1,180,950,054
Wild-type 5	18,009,362	24,359,753	73.93	943,381,713
Mutant 6	21,268,436	26,122,043	81.42	1,235,860,145
Wild-type 6	22,246,054	27,863,509	79.84	1,561,066,036
Average	21,329,686.5	27,332,877	77.93	1,252,487,477
Stdev	2,153,066	1,990,773	3.60	197,681,535

Table 5-1 Number and percentage of mapped reads for each sample of *nol9*^{sa1022} mutants and wild-type siblings and the estimated number of unique molecules in each library. (Stdev) Standard deviation.

The differential transcript abundance analysis was carried out using a DESeq-based pipeline written by Dr James Morris and Dr Ian Sealy (Anders and Huber, 2010) (Section 2.6.2). DESeq allows differential expression analysis by using a method based on negative binomial distribution and uses a shrinkage estimator for variance of the distribution (Anders and Huber, 2010). The list of differentially expressed regions has been filtered to include only regions that are within 100 bases of the nearest 3' end Ensembl gene. At a 5% false discovery

rate (FDR) when Benjamini-Hochberg multiple testing adjustment (Benjamini Y and Hochberg Y, 1995) was used, the number of differentially expressed regions within 100 bases to the nearest 3' end Ensembl gene was 599 corresponding to 566 unique genes. The *nol9*^{sa1022} mutant had significantly fewer transcripts than wild-type siblings in 231 of these genes, with a log2 fold change ranging from -0.69 to -4.59, but had significantly more transcripts than wild-type siblings in the remaining 335 genes, with a log2 fold change ranging from 0.70 to 5.59.

The most statistically significant differentially expressed genes in *nol9*^{sa1022} mutants with the minimum *p*-value accepted by the DESeq-based pipeline (an adjusted *p*-value of less than $1x10^{-16}$) are shown in Table 5-2 and Table 5-3. The downregulated genes, with a negative log2 fold change of mutant over wild-type siblings, include several genes that are specifically expressed in the liver (*fabp10a*), intestine (*fabp2*) and pancreas (*try* and *ela3l*) of 5 d.p.f. zebrafish larvae (Table 5-2). The eye-specific gene, *galectin related inter-fiber protein* (*grifin*) showed the biggest fold change in expression in mutants compared to wild-type siblings. Also, the gene *nol9* was downregulated with a log2 fold change of -1.16 at an adjusted *p*-value of 0.0127. This data suggests that that we can detect differential expression of tissue-specific genes and that the number of *nol9* transcripts is reduced in *nol9*^{sa1022} mutants. The upregulated genes, with a positive log2 fold change of mutant over wild-type siblings, include the tumour suppressor *tp53*, indicating that the Tp53 signalling pathway may contribute to the phenotypic defects of *nol9*^{sa1022} mutants. Also, it was found that the expression of *senp3b* that encodes a protein that in humans interact with NOL9, was upregulated with a log2 fold change of 1.14 at an adjusted *p*-value of $1.13x10^{-5}$ whereas no changes were detected in the transcript abundance of the other genes encoding NOL9-interacting proteins including *las1l*, *senp3a*, *tex10* and *wdr18* at an adjusted *p*-value of 0.05 (Refer to Appendix Table A - 1). This suggests that loss of *nol9* is affecting the expression of at least another gene involved in ribosome biogenesis.

Genome location	Strand	Distance to Ensembl Gene (bp)	Gene name	Gene description	Log2 fold change (*nol9*^{sa1022}/wild-type)
3:41780644	-1	1	*grifin*	*galectin related inter-fiber protein*	-4.39
12:34101458	-1	3	*ENPP7 (3 of 4)*	*ectonucleotide pyrophosphatase/phosphodiesterase 7*	-4.15
23:25084905	1	20	*olfml3a*	*olfactomedin-like 3a*	-3.60
21:9817926	1	62	*cel.2*	*carboxyl ester lipase, tandem duplicate 2*	-3.50
9:1035571	1	85	*slc15a1a*	*solute carrier family 15 (oligopeptide transporter), member 1a*	-3.46
20:25564364	-1	84	*cyp2ad2*	*cytochrome P450, family 2, subfamily AD, polypeptide 2*	-2.88
17:27320149	1	7	*ctsl.1*	*cathepsin L.1*	-2.76
2:38720820	-1	54	*rbp2b*	*retinol binding protein 2b, cellular*	-2.59
24:4835110	-1	1	*cpb1*	*carboxypeptidase B1 (tissue)*	-2.54
1:60218572	1	5	*cyp3a65*	*cytochrome P450, family 3, subfamily A, polypeptide 65*	-2.41
2:16581399	-1	3	*tfa*	*transferrin-a*	-2.40
5:27756150	-1	0	*ela3l*	*elastase 3 like*	-2.40
7:36516813	-1	4	*zgc:112160*	*zgc:112160*	-2.39
20:35506189	1	0	*mep1a.1*	*meprin A, alpha.1*	-2.28
16:56122673	1	1	*fabp10a*	*fatty acid binding protein 10a, liver basic*	-2.26
4:21594158	-1	4	*cd36*	*CD36 antigen*	-2.16
8:52652107	1	91	*msmbl*	*microseminoprotein, beta-like*	-2.12
22:17813696	-1	1	*gpx4a*	*glutathione peroxidase 4a*	-1.89
16:27320046	-1	1	*try*	*trypsin*	-1.82
1:24708924	1	51	*fabp2*	*fatty acid binding protein 2, intestinal*	-1.76

Table 5-2 List of the most statistically significant genes in *nol9*^{sa1022} mutants with an adjusted *p*-value of less than 1x10^{-16} sorted from the biggest to the smallest negative fold change.
The genome location, the strand direction, the distance to the nearest Ensembl gene, the gene name and description and the fold change of mutant over wild-type sibling are shown.

Genome location	Strand	Distance to Ensembl Gene (bp)	Gene name	Gene description	Log2 fold change (*nol9*^{sa1022}/wild-type)
5:45468027	-1	88	*BDP1 (2 of 2)*	*B double prime 1, subunit of RNA polymerase III transcription initiation factor IIIB*	2.75
3:21453661	-1	6	*tcap*	*titin-cap (telethonin)*	2.42
25:34827000	-1	2	*RPS27L*	*ribosomal protein S27-like*	2.42
2:167259	-1	1	*igfbp1b*	*insulin-like growth factor binding protein 1b*	2.19
20:7033441	1	1	*igfbp1a*	*insulin-like growth factor binding protein 1a*	2.10
5:25766741	1	1	*tp53*	*tumor protein p53*	2.08

Table 5-3 List of the most statistically significant genes in *nol9*^{sa1022} mutants with an adjusted *p*-value less than 1x10^{-16} sorted from the biggest to the smallest positive fold change. The genome location, the strand direction, the distance to the nearest Ensembl gene, the gene name and description and the fold change of mutant over wild-type sibling are shown.

5.2.2 Enriched Gene Ontology categories in *nol9*^{sa1022} mutants

Given the long list of differentially expressed genes in *nol9*^{sa1022} mutants, it is difficult to infer the biology underlying the *nol9*^{sa1022} phenotype. In order to enhance the interpretation of such list, functional analysis of the differentially expressed genes is an important step. The topGO package provides tools to test for enrichment of Gene Ontology (GO) terms by taking into account the relationships between the different GO terms (Alexa et al., 2006). Dr Ian Sealy carried out the functional analysis using the *elim* method that iteratively removes all the genes that are mapped to a significantly enriched node from more general terms (Alexa et al., 2006) (Section 2.6.4). The Kolmogorov-Smirnov (K-S)-like test statistic (Subramanian et al., 2005) was used to score for the significance of the Gene Ontology term (Alexa et al., 2006). The enrichment analysis for Gene Ontology categories cellular component, molecular function and biological process was produced (Ashburner et al., 2000; Harris et al., 2004). Since a multiple testing adjustment procedure was not carried out, a K-S value of 0.01 was used as an arbitrary threshold, which is a compromise between sensitivity and specificity. The genes displaying altered expression in *nol9*^{sa1022} mutants were markedly enriched for genes assigned to the cellular component categories ‘nucleolus’, ‘cytoplasm’, ‘proteasome core complex’, ‘ribonucleoprotein complex’, ‘proteasome complex’, ‘mitochondrion’ and ‘ribosome’ (Figure 5-2). For the molecular function categories, the enriched terms were ‘RNA binding’, ‘serine-type endopeptidase activity’, ‘translation initiation factor activity’, ‘DNA-directed RNA polymerase activity’ and ‘RNA methyltransferase activity’ (Figure 5-3). The most significantly enriched biological terms included ‘rRNA processing’, ‘tRNA aminoacylation for protein translation’, ‘mRNA processing’, ‘translational initiation’, ‘proteolysis’, ‘ribosome biogenesis’ ‘tRNA processing’, ‘translation’, ‘hematopoiesis’, ‘cell cycle’ and ‘digestive tract development’ (Figure 5-4). However, the other GO terms that described the digestive system namely the ‘exocrine pancreas development’, ‘pancreas development’, endocrine pancreas development’, ‘liver development’,’ digestive system development’ and ‘digestive tract morphogenesis’ were not statistically significantly enriched in *nol9*^{sa1022} mutants using a K-S cut off value of 0.01 (Refer to Appendix Table A - 2).

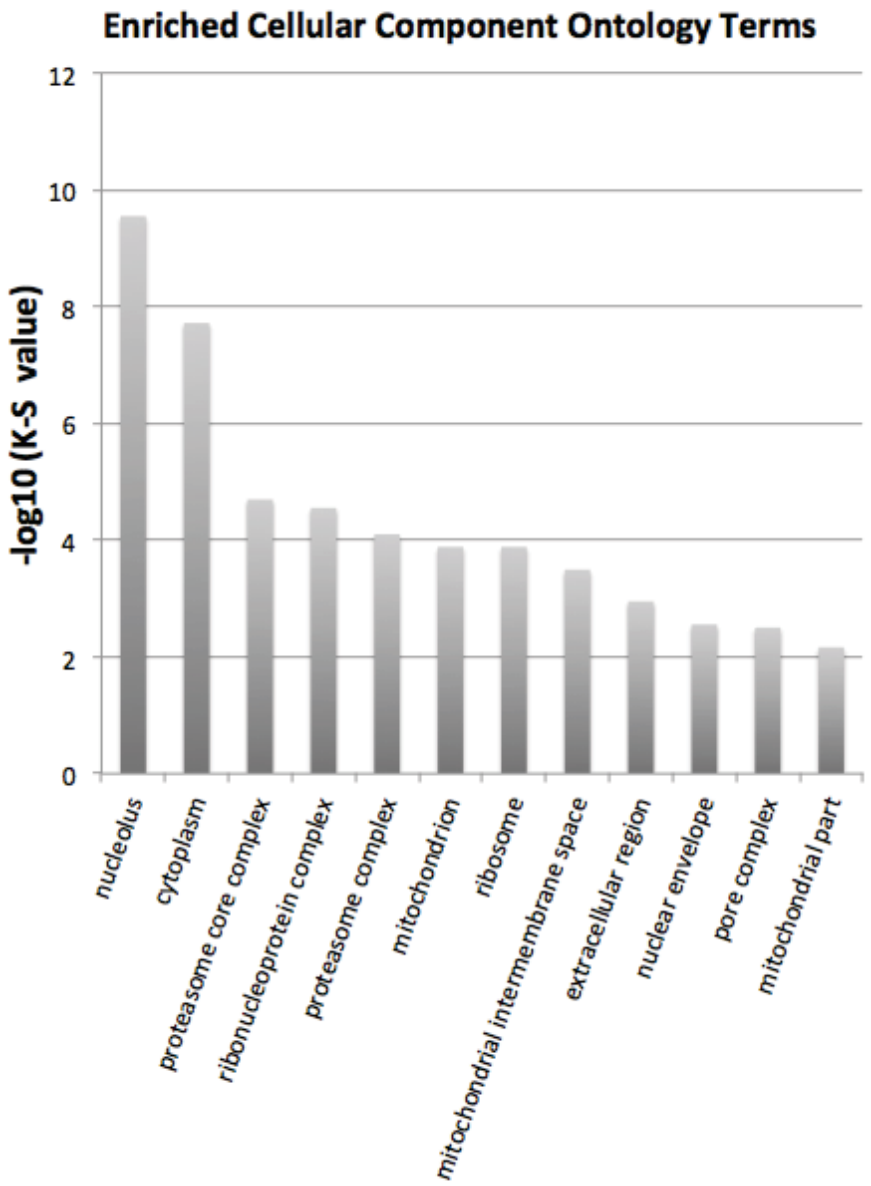

Figure 5-2 The enriched cellular component ontology terms in *nol9*^{sa1022} mutants at statistical significance of K-S value less than 0.01 (-log10 (K-S value) greater than 2.0).

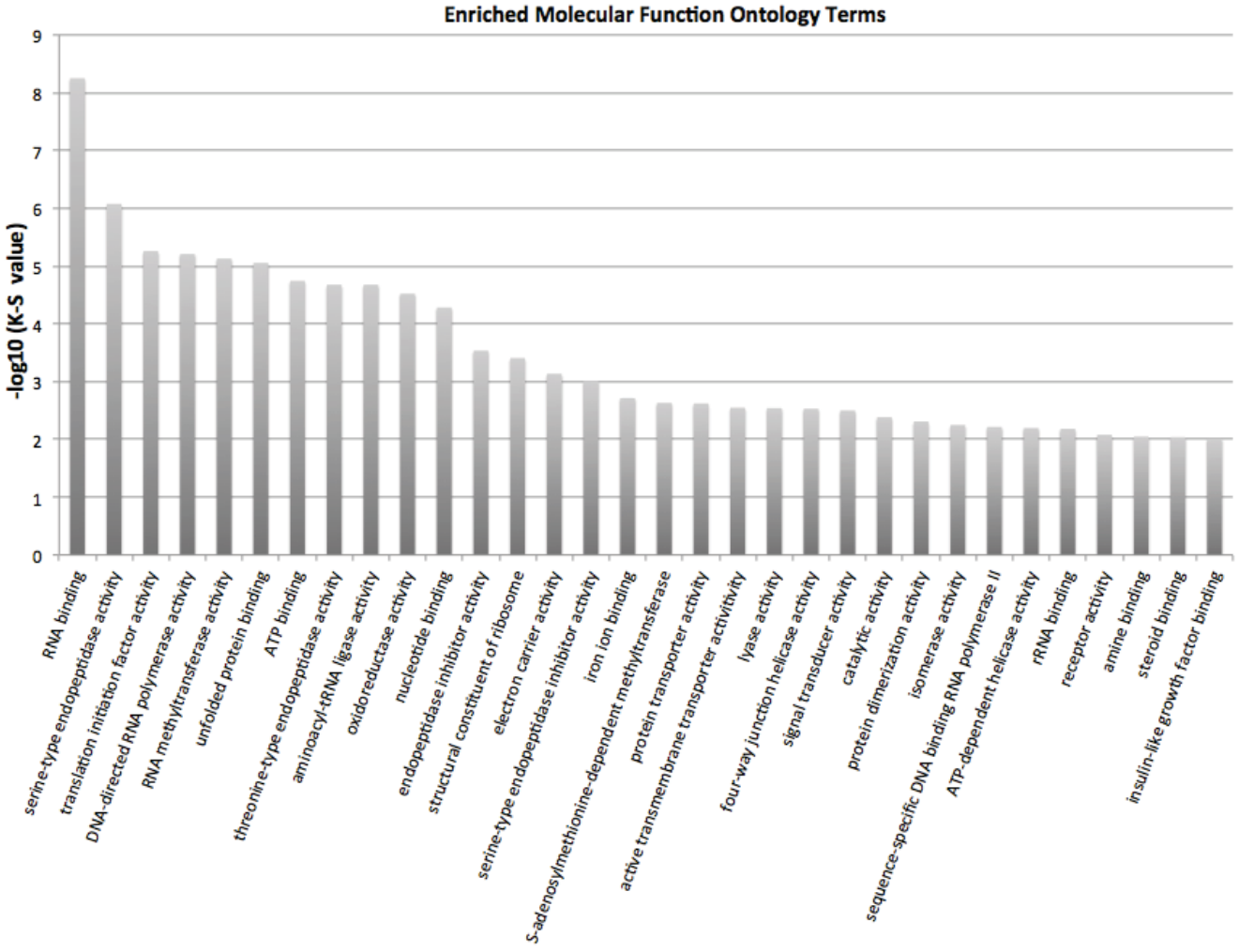

Figure 5-3 The enriched molecular function ontology terms in *nol9*^{sa1022} mutants at statistical significance of K-S value less than 0.01 (-log10 (K-S value) greater than 2.0).

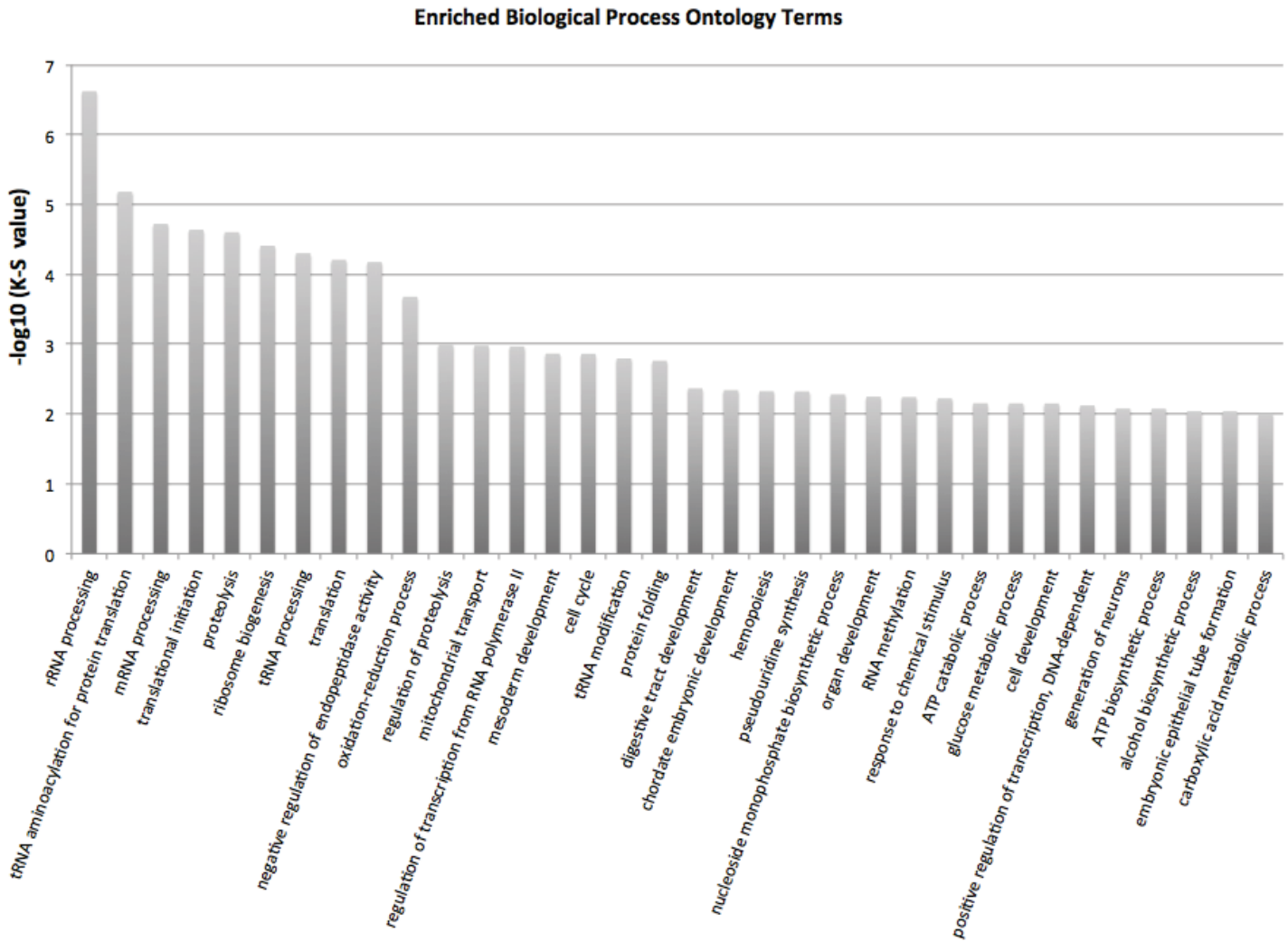

Figure 5-4 The enriched biological process ontology terms in *nol9*^{sa1022} mutants at statistical significance of K-S value less than 0.01 (log10(K-S value) greater than 2.0).

5.2.3 Enriched KEGG pathways in *nol9*^{sa022} mutants

In order to identify active pathways that differ between *nol9*^{sa1022} mutants and wild-type siblings, I explored the Database for Annotation, Visualization and Integrated Discovery (DAVID) (Dennis et al., 2003; Huang da et al., 2009b). DAVID provides different data mining tools that combine functionally descriptive information with graphic displays for large lists of genes and proteins (Dennis et al., 2003; Huang da et al., 2009b). *KeggCharts*, one of the analysis modules, ascribes genes to the Kyoto Encyclopedia of Genes and Genomes (KEGG) metabolic processes (Dennis et al., 2003; Huang da et al., 2009a; Kanehisa and Goto, 2000). The previously described list of 566 unique differentially expressed genes that were statistically significant (at an adjusted *p*-value of less than 0.05, after Benjamini-Hochberg multiple testing adjustment) was compared against a list of 11,170 unique genes that were assayed in this experiment (Section 2.6.5). The DAVID *KeggCharts* was able to provide information for only 131 of the 566 differentially expressed genes tested. At a false discovery rate of 5% after adjustment for multiple testing with the procedure of Benjamini and Hochberg (Benjamini Y and Hochberg Y, 1995), the enriched KEGG terms were 'Aminoacyl-tRNA biosynthesis', 'Steroid biosynthesis', 'Pyrimidine metabolism', 'PPAR signalling pathway' and 'RNA polymerase' (Table 5-4). All of the genes assigned to the 'Aminoacyl-tRNA biosynthesis' and 'RNA polymerase' KEGG pathways, and most of the genes assigned to the 'Pyrimidine metabolism' category, were upregulated in *nol9*^{sa1022} mutants compared to wild-type siblings (Refer to Appendix Table A - 3, Table A - 4, Table A - 5). This data is consistent with the functional analysis results using topGO and reveals an upregulation of genes involved in the transcription and translation in *nol9*^{sa1022} mutants. Interestingly, the KEGG term 'p53 signaling pathway' was also enriched in *nol9*^{sa1022} mutants, albeit only at a 10% false discovery rate (FDR) using Benjamini-Hochberg procedure. All the differentially expressed genes belonging to the 'p53 signalling pathway' are upregulated in *nol9*^{sa1022} mutants compared to wild-type siblings, including *tp53*, *mdm2*, *ccng1*, *cdkn1a*, *gadd45a*, *cycsb*, *casp8* and *baxa* (Table 5-5). These results again highlight the Tp53 signalling pathway as a potential important contributor to the *nol9*^{sa1022} mutant phenotype.

KEGG Term	Genes		Fold Enrichment	*p*-value	Adjusted *p*-value (Benjamini-Hochberg)
	#	%			
Aminoacyl-tRNA biosynthesis	12	2.40	7.71	9.25×10^{-8}	8.33×10^{-6}
Steroid biosynthesis	6	1.20	11.18	7.96×10^{-5}	0.003577288
Pyrimidine metabolism	12	2.40	3.61	3.04×10^{-4}	0.00907344
PPAR signalling pathway	9	1.80	4.53	5.31×10^{-4}	0.011874735
RNA polymerase	6	1.20	6.57	0.001446115	0.025712569
Drug metabolism	6	1.20	5.32	0.004006265	0.058437616
p53 signalling pathway	8	1.60	3.31	0.008468176	0.103574559
Purine metabolism	11	2.20	2.23	0.021887645	0.220397219

Table 5-4 The enriched KEGG terms of differentially expressed genes of *nol9*^{sa1022} mutants at a statistical significance of *p*-value less than 0.05 using a modified Fisher's exact test. The KEGG term, the number of genes involved in the terms and the percentage of involved genes over total number of genes, the fold enrichment, the *p*-value and the adjusted *p*-value using Benjamini-Hochberg procedure are shown.

Gene Name	Gene Description	Adjusted *p*-value (Benjamini–Hochberg)	Log2 fold change (*nol9*^{sa1022}/wild-type)
tp53	*tumor protein p53*	$<1 \times 10^{-16}$	2.08
mdm2	*transformed 3T3 cell double minute 2 homolog (mouse)*	2.72×10^{-10}	1.94
ccng1	*cyclin G1*	5.92×10^{-8}	1.29
cdkn1a	*cyclin-dependent kinase inhibitor 1A*	0.000938222	1.32
gadd45aa	*growth arrest and DNA-damage-inducible, alpha, a*	0.001929604	1.02
cycsb	*cytochrome c, somatic b*	0.003997489	0.84
casp8	*caspase 8, apoptosis-related cysteine peptidase*	0.021165876	1.24
baxa	*bcl2-associated X protein, a*	0.028395958	0.98

Table 5-5 The differentially expressed genes belonging to the KEGG term 'p53 signalling pathway'. The gene name and description, the adjusted *p*-value and the fold change of mutant over wild-type siblings are shown.

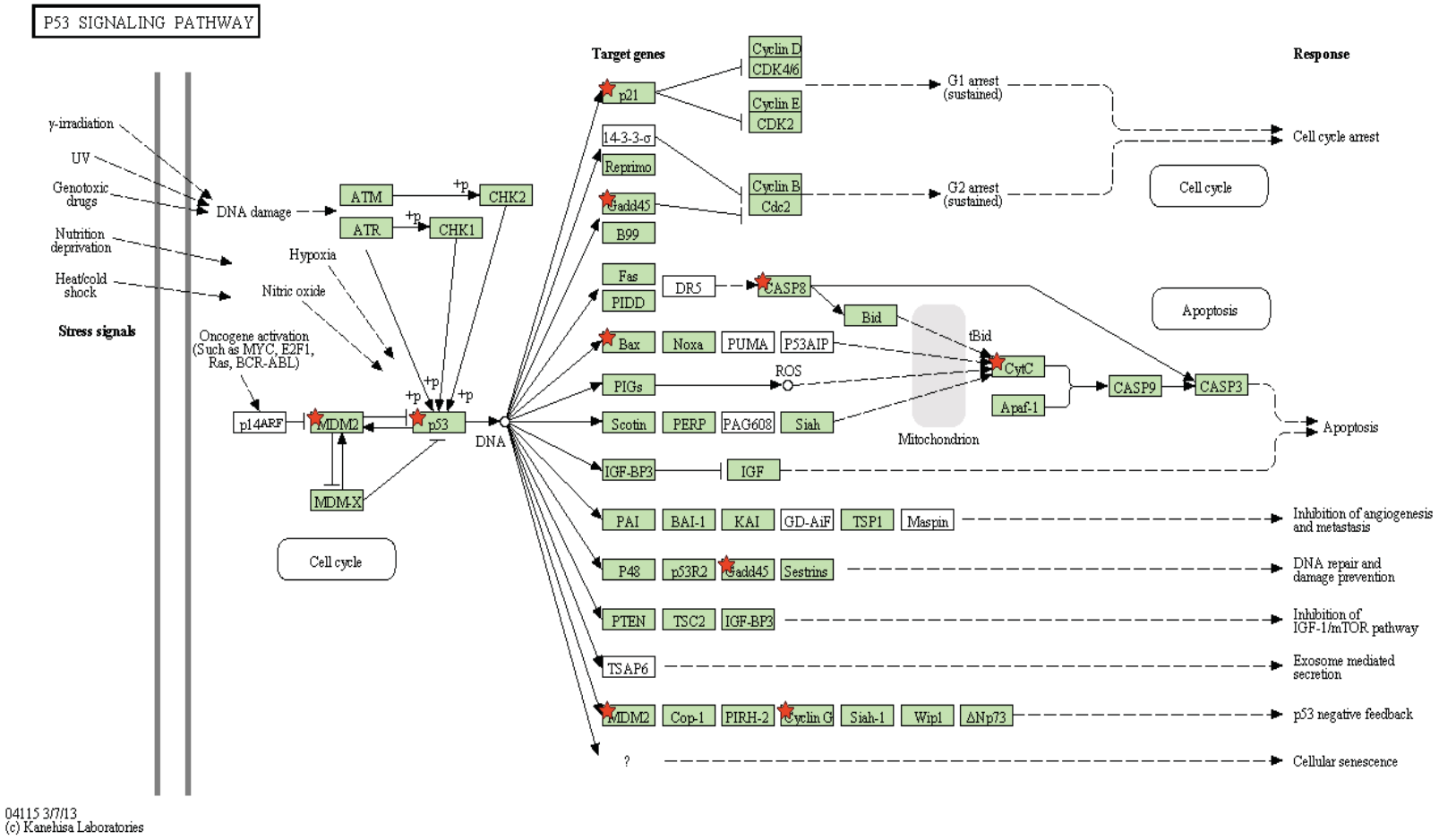

Figure 5-5 KEGG Tp53 signalling pathway in zebrafish. Boxes are gene products and red stars indicate genes that are upregulated in *nol9*^{sa1022} mutants compared to wild-type siblings. Taken from KEGG Pathway Database.

5.2.4 The small pancreas phenotype of *nol9^{sa1022}* mutant is Tp53-independent

The Tp53 pathway has been shown to mediate the response following nucleolar stress and is responsible for many of the clinical features of ribosomopathies by causing perturbations in tissue homeostasis (Fumagalli and Thomas, 2011; Holmberg Olausson, 2012). Moreover, depletion of *NOL9* in HCT116 colon carcinoma cells by RNAi results in Tp53-dependent G1 cell-cycle arrest, stabilisation of Tp53 and increased levels of its transcriptional target *p21* (Castle et al., 2012). Furthermore, we found that many genes involved in the Tp53 signalling pathway are upregulated in *nol9^{sa1022}* mutants. In order to investigate whether the phenotype of *nol9^{sa1022}* mutant is dependent on Tp53 signalling, the *nol9$^{sa1022/+}$* line was outcrossed to the *tp53$^{zdf1/+}$* line (Berghmans et al., 2005). The *tp53^{zdf1}* carries a M214K missense mutation in the DNA-binding domain that ultimately interferes with activation of its target genes. The *nol9$^{sa1022/+}$;tp53$^{zdf1/+}$* zebrafish were incrossed and the 5 d.p.f. larvae were phenotyped, under the dissecting microscope, based on the size of their pancreas and genotyped for both *nol9^{sa1022}* and *tp53^{zdf1}* alleles (Figure 5-6 A) (Section 2.1.2). Out of the 165 larvae studied, 26% were *nol9$^{-/-}$* and phenotypic, 48% were *nol9$^{+/-}$* and non-phenotypic whilst 27% were *nol9$^{+/+}$* and non-phenotypic. The percentage of phenotypic larvae with genotypes *tp53$^{-/-}$*, *tp53$^{+/-}$* and *tp53$^{+/+}$* were 25%, 52% and 23% respectively. For the 121 non-phenotypic larvae, 19% were *tp53$^{-/-}$*, 55% were *tp53$^{+/-}$* and 26% were *tp53$^{+/+}$*. These results indicate that it was not possible to distinguish among *nol9^{sa1022}* mutants with different *tp53* genotypes suggesting that the small pancreas phenotype of *nol9^{sa1022}* mutants is Tp53-independent. In order to confirm this, the *nol9$^{sa1022/+}$;tp53$^{zdf1/+}$* zebrafish were outcrossed to the transgenic line *Tg(ins:mCherry)^{jh2};Tg(ptf1a:EGFP)^{jh1}* and 5 d.p.f. larvae from an incross of *Tg(ins:mCherry)^{jh2};Tg(ptf1a:EGFP)^{jh1};nol9$^{sa1022/+}$;tp53$^{zdf1/+}$* were genoptyped and the volume of *ptf1a*-expressing region of larvae with genotype *nol9$^{+/+}$;tp53$^{+/+}$*, *nol9$^{+/+}$;tp53$^{-/-}$*, *nol9$^{-/-}$;tp53$^{+/+}$*and *nol9$^{-/-}$;tp53$^{-/-}$* fish was measured (Figure 5-6 B, C) (Sections 2.1.2 and 2.3.4). The *ptf1a*-expressing region of larvae with genotypes *nol9$^{-/-}$;tp53$^{+/+}$* and *nol9$^{-/-}$;tp53$^{-/-}$* appeared similar in size and were both smaller than the *ptf1a*-expressing region of larvae with genotypes *nol9$^{+/+}$;tp53$^{-/-}$* and *nol9$^{-/-}$;tp53$^{+/+}$* which were comparable (Figure 5-6 B). The mean volume of the *ptf1a*-expressing region of *nol9$^{+/+}$;tp53$^{+/+}$* (n=5), *nol9$^{+/+}$;tp53$^{-/-}$* (n=6), *nol9$^{-/-}$;tp53$^{+/+}$* (n=8) and *nol9$^{-/-}$;tp53$^{-/-}$* (n=11) is 0.00157 mm^3, 0.00126 mm^3, 0.000345 mm^3 and 0.000328 mm^3 respectively. The difference between the mean pancreatic volume of larvae with genotypes *nol9$^{+/+}$;tp53$^{+/+}$* and *nol9$^{-/-}$;tp53$^{+/+}$*, *nol9$^{+/+}$;tp53$^{+/+}$* and *nol9$^{-/-}$;tp53$^{-/-}$*, *nol9$^{+/+}$;tp53$^{-/-}$* and *nol9$^{-/-}$;tp53$^{+/+}$*, *nol9$^{+/+}$;tp53$^{-/-}$* and *nol9$^{-/-}$;tp53$^{-/-}$* was statistically significant

(Student's *t*-test, $p = 2.76\text{x}10^{-6}$, $p = 2.72\text{x}10^{-8}$, $p = 2.46\text{x}10^{-7}$ and $p = 1.17\text{x}10^{-9}$ respectively) (Figure 5-6 C). This data substantiates the hypothesis that the exocrine pancreas phenotype is independent of the Tp53 signalling pathway.

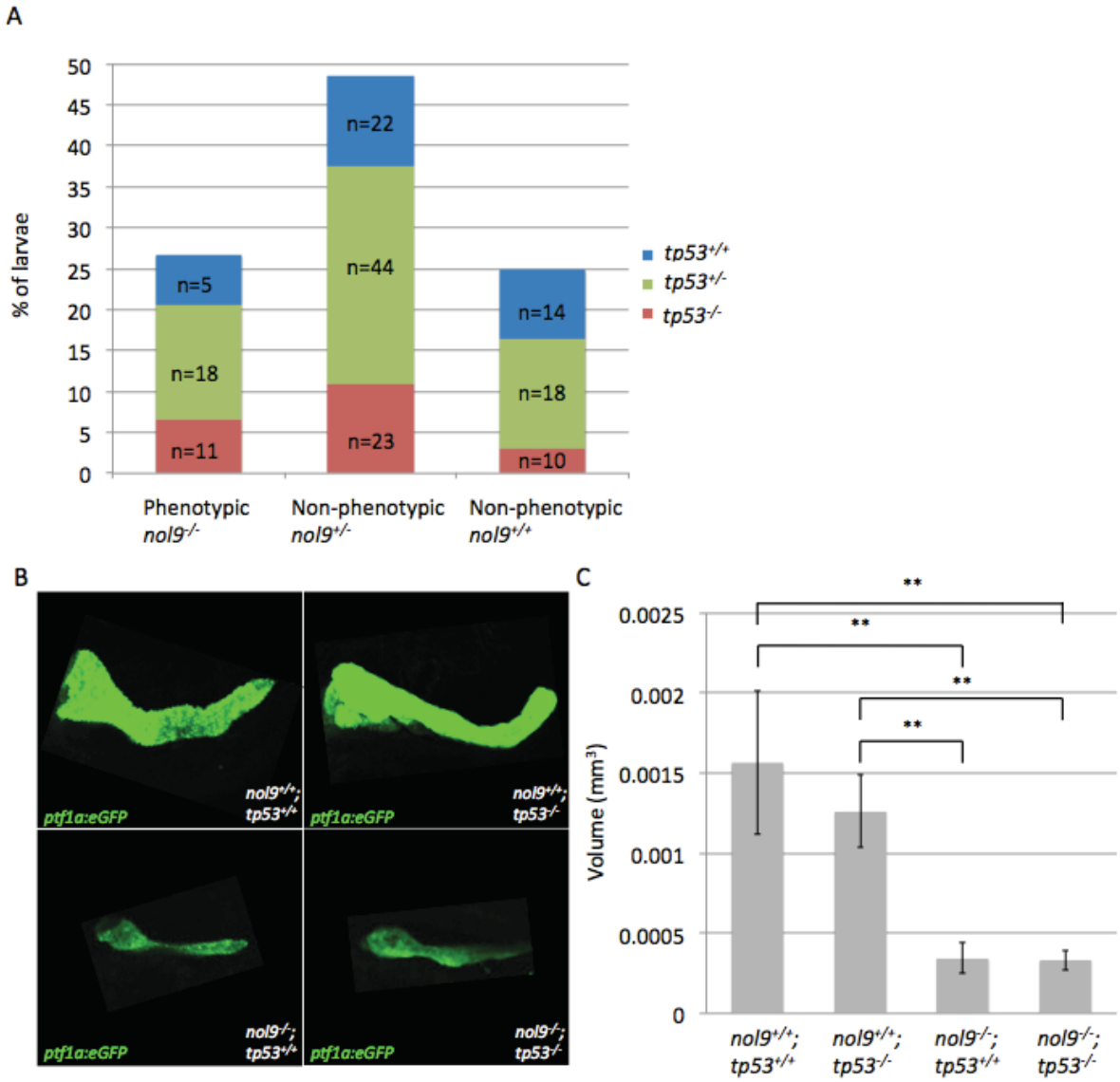

Figure 5-6 The exocrine pancreas phenotype of *nol9*^{sa1022} mutant is independent of Tp53 signalling pathway. (A) Graph showing the percentage of 5 d.p.f. phenotypic (*nol9*$^{-/-}$) and non-phenotypic (*nol9*$^{+/-}$ or *nol9*$^{+/+}$) larvae from an incross of *nol9*$^{sa1022/+}$;*tp53*$^{zdf1/+}$ zebrafish that are *tp53*$^{-/-}$ (red), *tp53*$^{+/-}$ (green) or *tp53*$^{+/+}$ (blue). (B) Representative maximum intensity projection images of confocal stacks of 5 d.p.f. larvae from an incross of *Tg(ins:mCherry)*^{jh2};*Tg(ptf1a:EGFP)*^{jh1};*nol9*$^{sa1022/+}$; *tp53*$^{zdf1/+}$ showing that the *ptf1a*-expressing region in *nol9*$^{-/-}$;*tp53*$^{+/+}$ and *nol9*$^{-/-}$;*tp53*$^{-/-}$ is comparable and is smaller than that in *nol9*$^{+/+}$;*tp53*$^{+/+}$ and *nol9*$^{+/+}$;*tp53*$^{-/-}$ which appear similar. (C) Graph showing that the mean volume of the *ptf1a*-expressing region in *nol9*$^{-/-}$;*tp53*$^{+/+}$ (n=8) and *nol9*$^{-/-}$;*tp53*$^{-/-}$ (n=11) is statistically significantly smaller than that in *nol9*$^{+/+}$;*tp53*$^{+/+}$ (n=5) and *nol9*$^{+/+}$;*tp53*$^{-/-}$ (n=6). Data is represented as the mean ± SD, Student's *t*-test ** $p < 0.01$.

5.2.5 The mRNA expression profile of *las1l*^{sa674} mutants

We found in Chapter 4 that the *las1l*^{sa674} mutant has similar defects to *nol9*^{sa1022} mutant, and hence we decided to also study the mRNA expression profile of *las1l*^{sa674} by DeTCT. In this experiment, six pairs of *las1l*$^{sa674/+}$ zebrafish were incrossed and for each pair, 25 mutant and 25 wild-type siblings were collected at 5 d.p.f. for RNA extraction (Section 2.2). Only the phenotypic larvae with an inflated swim bladder were collected as their pancreatic size could be assayed with more confidence therefore increasing the accuracy in differentiating between *las1l*^{sa674} mutants and wild-type siblings. Library preparation was carried out on the 12 samples but as one of the libraries failed, the biological replicate pair containing that failed library was excluded from further analysis. Therefore, only 10 libraries were sequenced on one single lane of Illumina HiSeq (Section 2.6.1). The sequence data analysis was carried out by Dr Ian Sealy (Section 2.6.2). Table 5-6 shows the number and percentage of mapped reads for each biological replicate and the library complexity, i.e. the estimated number of unique molecules in each library. All five biological replicates were used for differential transcript abundance using the DESeq-based pipeline written by Dr James Morris and Dr Ian Sealy since the library complexity is similar (Anders and Huber, 2010) (Section 2.6.2).

Sample	Reads			Estimated number of unique molecules
	Mapped	Total	% Mapped	
Mutant 1	26,979,522	36,397,692	74.12	1,846,656,917
Wild-type 1	21,611,207	27,836,272	77.64	1,422,215,600
Mutant 2	25,531,558	33,358,031	76.54	1,117,281,160
Wild-type 2	27,104,447	35,712,462	75.90	1,259,084,206
Mutant 3	26,949,361	34,128,699	78.96	1,166,856,015
Wild-type 3	24,172,449	33,228,696	72.75	1,597,497,227
Mutant 4	25,194,438	33,558,009	75.08	1,591,174,952
Wild-type 4	29,615,352	38,097,154	77.74	1,047,899,549
Mutant 5	19,475,812	24,877,809	78.29	1,064,422,212
Wild-type 5	24,893,796	31,197,807	79.79	1,179,672,647
Average	25,152,794.2	32,839,263.1	76.68	1,329,276,049
Stdev	2,910,369.913	3,975,929.983	2.23	271,785,213.7

Table 5-6 Number and percentage of mapped reads for each sample of *las1l*^{sa674} mutants and wild-type siblings and the estimated number of unique molecules in each library. (Stdev) Standard deviation.

The output of differentially expressed regions was filtered to include only the regions that are within 100 bases to the nearest 3' end Ensembl gene. At a 5% FDR, after adjusting for multiple testing using Benjamini-Hochberg procedure (Benjamini Y and Hochberg Y, 1995), the genes showing differential expression are *grifin*, *RPS27L*, *tp53*, *zgc:153846* and *zgc:136461* (7). The genes that were downregulated in *las1l*^{sa647} mutants compared to wild-type siblings were *zgc:136461*, an orthologue of a human gene *chymotrypsinogen B1* (*CTRB1*) that is expressed specifically in the pancreas, the eye lens genes *grifin* and the zebrafish orthologue of human crystallin, gamma D, *zgc:153846*. These results indicate that the differential expression of pancreatic and eye-specific genes is being detected in *las1l*^{sa674} mutants. Additionally there were no significant changes in transcript abundance of *las1l* and genes encoding proteins that interact with Las1l including *nol9*, *senp3a*, *senp3b*, *tex10* and *wdr18* in *las1l*^{sa674} mutants (Refer to Appendix Table A - 6).

Genome location	Strand	Adjusted *p*-value (Benjamini-Hochberg)	Distance to Ensembl Gene (bp)	Gene name	Gene description	Log2 fold change (*las1l*^{sa674}/wild-type)
3:41780644	-1	$2.27x10^{-9}$	1	*grifin*	*galectin related inter-fiber protein*	-2.235219873
25:34827000	-1	$3.64x10^{-5}$	2	*RPS27L*	*ribosomal protein S27-like*	1.588163195
5:25766741	1	0.000878724	1	*tp53*	*tumor protein p53*	1.479254501
9:23051646	1	0.001022345	3	*zgc:153846*	*zgc:153846*	-3.790242144
7:36524482	1	0.007348883	5	*zgc:136461*	*zgc:136461*	-1.528978382
24:4835110	-1	0.089208372	1	*cpb1*	*carboxypeptidase B1 (tissue)*	-1.103040368
16:27320046	-1	0.089208372	1	*try*	*trypsin*	-1.086928815
1:28031527	1	0.135826525	6	*cryaa*	*crystallin, alpha A*	-1.113336914
16:58404668	1	0.229527094	1	*nr0b2a*	*nuclear receptor subfamily 0, group B, member 2a*	1.279535082
16:31282459	1	0.299032485	0	*nes*	*nestin*	1.165607544
25:34827000	-1	0.343608453	2	*RPS27L*	*ribosomal protein S27-like*	1.276394309
14:23143173	1	0.344538274	5	*ccng1*	*cyclin G1*	1.00442056
4:5407050	1	0.39003004	2	*si:dkey-14d8.6*	*si:dkey-14d8.6*	-1.506566565
19:30471007	1	0.39003004	1	*serpina7*	*serpin peptidase inhibitor, clade A (alpha-1 antiproteinase, antitrypsin), member 7*	1.444459627
5:44068461	-1	0.448383904	0	*zgc:123103*	*zgc:123103*	0.988687546
7:27756150	-1	0.5250549	0	*ela3l*	*elastase 3 like*	-0.93154133
7:40027647	-1	0.558443494	2	*c6ast4*	*six-cysteine containing astacin protease 4*	-1.186117809
5:27756150	-1	0.826714077	0	*ela3l*	*elastase 3 like*	1.508652156
25:34827000	-1	0.826714077	2	*RPS27L*	*ribosomal protein S27-like*	-1.038784624
2:27549277	1	0.836122625	2	*sepp1b*	*selenoprotein P, plasma, 1b*	1.202330387
2:55854933	1	0.842020919	0	*calrl*	*calreticulin like*	1.100183091
1:11229671	1	0.973752112	0	*pla2g12a*	*phospholipase A2, group XIIA*	1.005701929

Table 5-7 List of differentially expressed genes in *las1l*^{sa674} mutants at adjusted *p*-value less than 1.0. The genome location, the strand direction, the adjusted *p*-value, the distance to the nearest Ensembl gene, the gene name and description and the fold change of mutant versus wild-type sibling are shown.

5.2.6 Enriched Gene Ontology categories in *las1l*^{sa674} mutants

There were only a small number of differentially expressed genes in *las1l*^{sa674} mutants that reached statistical significance at 5% FDR using Benjamini-Hochberg adjustment for multiple testing. To enhance the interpretation of such list, the topGO analysis was carried out on the differentially expressed genes of *las1l*^{sa674} mutants by Dr Ian Sealy using the *elim* method and the Kolmogorov-Smirnov (K-S)-like test statistic to score for GO enrichment (Alexa et al., 2006) (Section 2.6.4). At an arbitrary threshold of K-S value 0.01, the enriched GO cellular component terms were 'cytoplasm', 'cytoplasmic part', 'intracellular organelle', 'ribonucleoprotein complex' and nuclear terms 'nuclear lumen', 'nuclear membrane' and 'nucleus' (Figure 5-7). For the molecular function ontology categories, the most significant enriched terms were 'ATP binding', 'protein tyrosine kinase activity', 'nucleotide binding', 'structural molecule activity' and 'RNA binding' (Figure 5-8). The genes displaying altered expression were markedly enriched for the biological process categories 'regulation of transcription from RNA polymerase II promoter', 'mRNA processing', 'cell cycle', 'ATP biosynthetic process', 'regulation of transcription, DNA-dependent' and also 'pancreas development' and 'digestive tract development' (Figure 5-9). However, the additional GO terms describing the digestive system namely the 'liver development', 'endocrine pancreas development', 'digestive tract morphogenesis' and 'digestive system development' were not statistically significantly enriched in *nol9*^{sa1022} mutants using a K-S cut off value of 0.01 (Refer to Appendix Table A - 7).

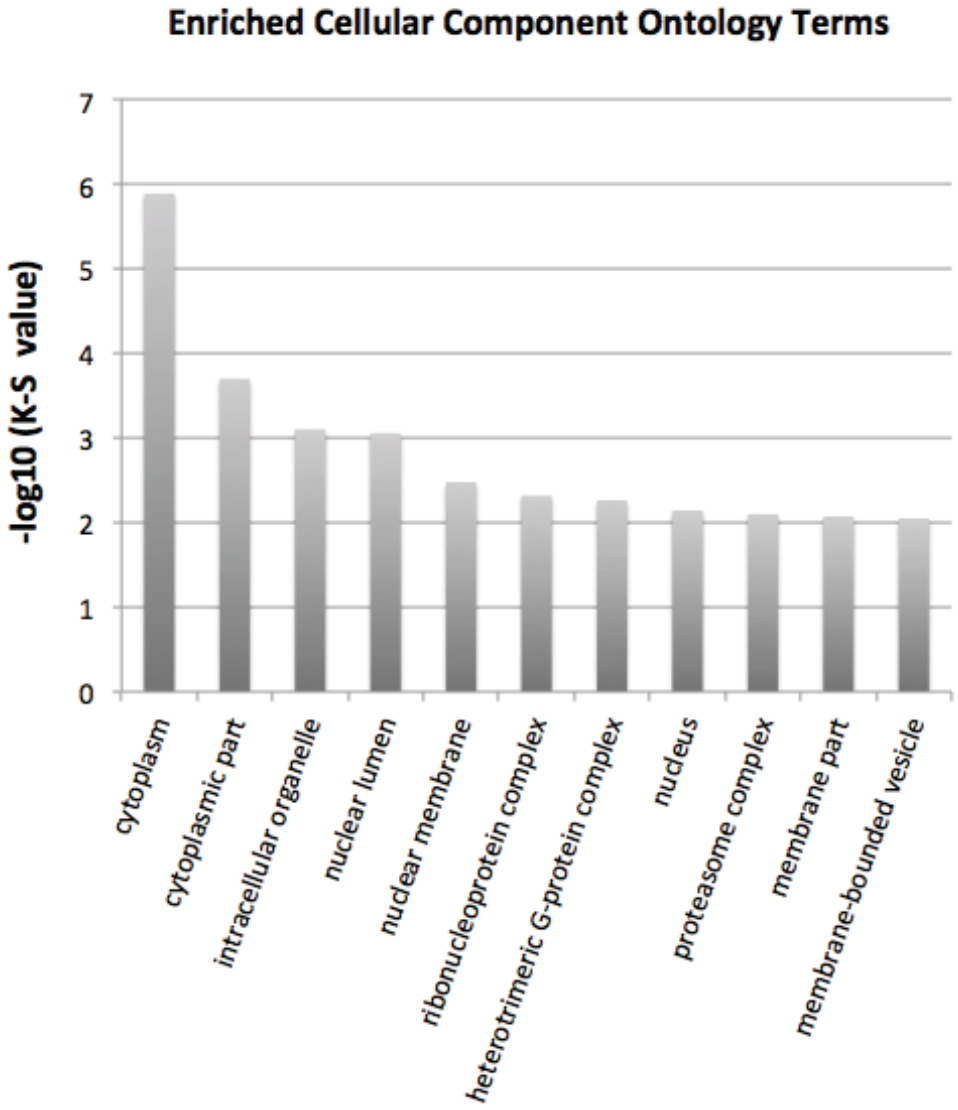

Figure 5-7 The enriched cellular component ontology terms in *las1l*^{sa674} mutants at statistical significance of K-S value less than 0.01 (-log10 (K-S value) greater than 2.0).

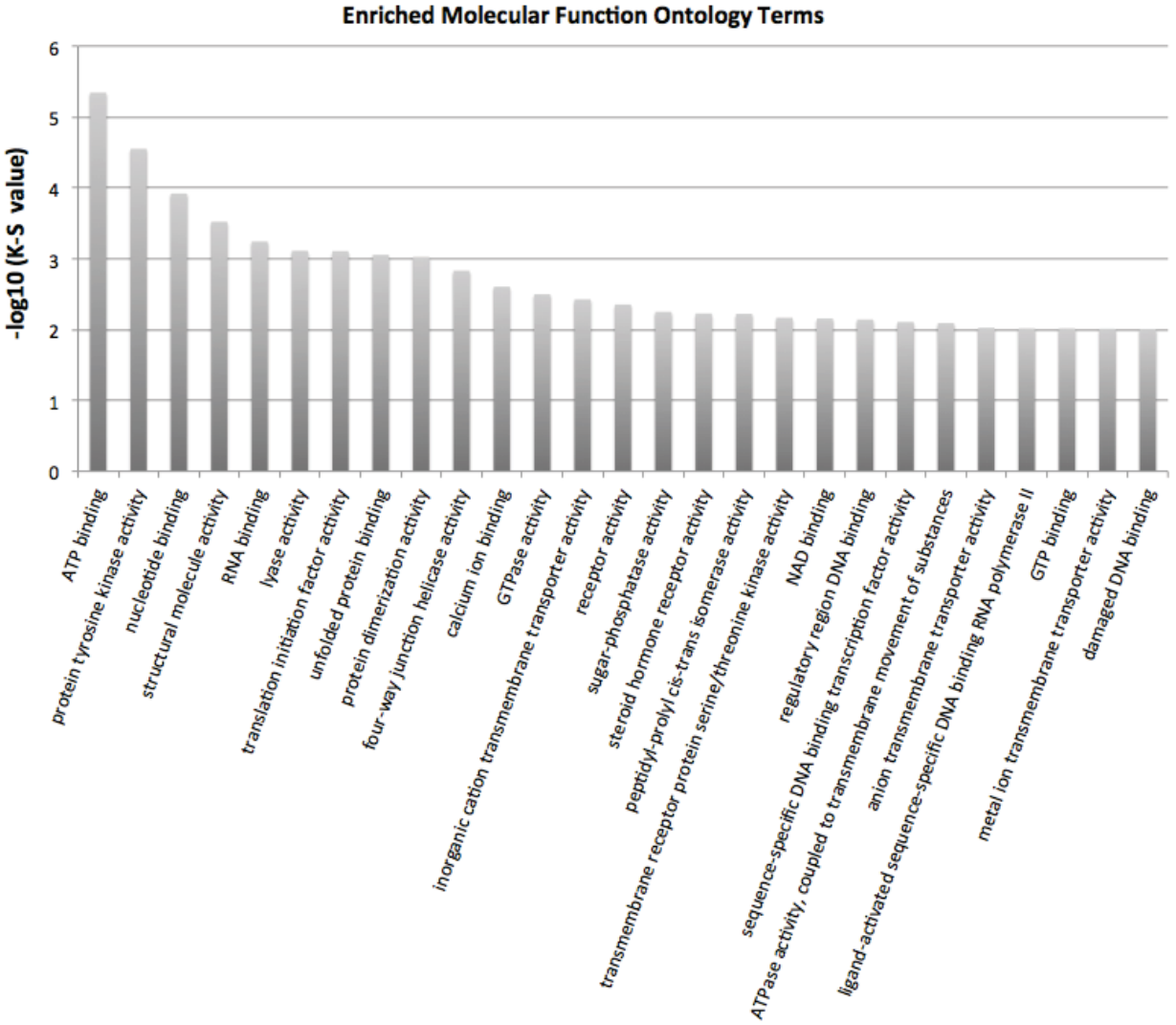

Figure 5-8 The enriched molecular function ontology terms in *las1l*^{sa674} mutants at statistical significance of K-S value less than 0.01 (-log10 (K-S value) greater than 2.0).

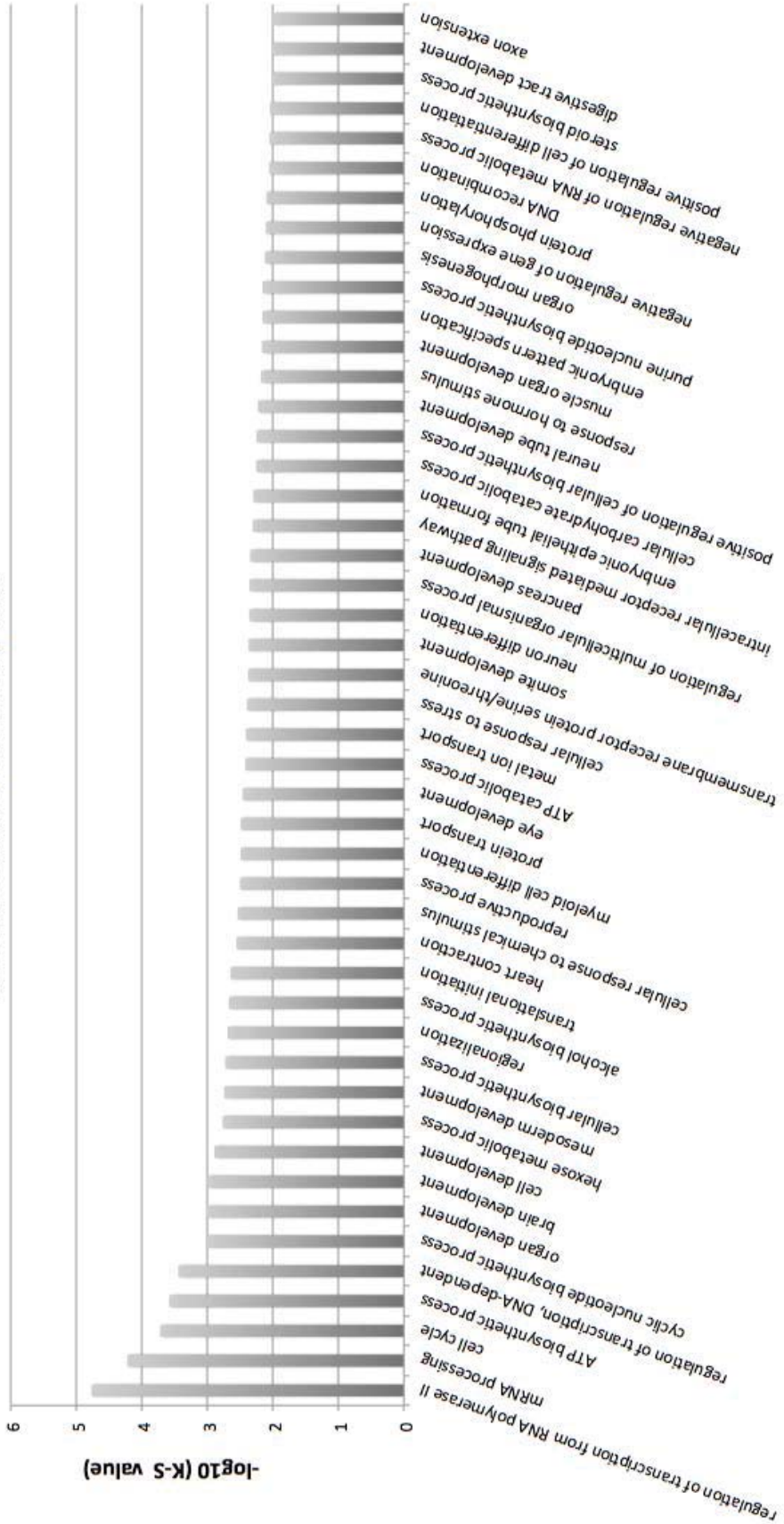

Figure 5-9 The enriched biological process ontology terms in *las11*^{sa674} mutants at statistical significance of K-S value less than 0.01 (-log10 (K-S value) greater than 2.0).

5.2.7 Comparison of the mRNA expression profiles of *nol9*^{sa1022}, *las1l*^{sa674}, *tti*^{s450} and *set*^{s453} mutants

Similarly to the *titania* (*tti*) mutant (described in Section 1.3.4), the *setebos* (*set*) mutant was also identified in the ENU mutagenesis Liver^{plus} screen that was carried out on a transgenic line that expresses GFP in the digestive organs (*Tg(XlEef1a1:GFP)*^{s854}) (Field et al., 2003b; Ng et al., 2005; Ober et al., 2006). The *setebos*^{s453} mutant is impaired in the development of many tissues including the intestine, exocrine pancreas, craniofacial cartilages, eye and brain (Dr Joan Heath, Personal Communication). It is mutated in the *nucleolar protein 8* (*nol8*) and exhibit defects in 28S rRNA processing and 60S ribosomal subunit biogenesis (unpublished). The *titania*^{s450} and *setebos*^{s453} mutants have similar phenotypes to *nol9*^{sa1022} and *las1l*^{sa674} mutants and the causative genes of those mutants play a similar role in rRNA processing. In order to help infer the underlying biology of the zebrafish rRNA processing mutants, I compared the mRNA expression profiles of these mutants to identify genes and pathways that may play an important role in the hypoplastic digestive organs of all four mutants.

Dr Joan Heath kindly provided the total RNA for mRNA expression profiling of *titania* and *setebos* mutants. For *titania* and *setebos*, library preparation was carried out on RNA of 12 biological replicates, i.e. 6 pairs of 25 mutants and 25 wild-type siblings (Section 2.6.1). For both *titania* and *setebos*, libraries of 3 biological replicates failed therefore only six libraries of each mutant were sequenced on a single Illumina HiSeq lane. Dr Ian Sealy carried out the analysis on the sequence data, which included resolving the index of each library, removal of non-species sequence, reference genome mapping, and removal of duplicate reads (Section 2.6.2). In order to compare the four mutants *tti*^{s450}, *set*^{453}, *nol9*^{sa1022} and *las1l*^{sa674}, three biological replicates were obtained for each mutant. As the total number of reads for the different libraries varied, each sample had to be normalised to a total read count of 26 M reads (the smallest number of reads across all samples from the different libraries) (Section 2.6.3). Subsequently, the duplicate reads were removed and differential transcript abundance was carried out for all four mutants using the DESeq-based pipeline (Sections 2.6.2 and 2.6.3).

For each mutant, only the differentially expressed regions within 100 bases to the nearest 3' end Ensembl gene were examined. The number of regions and genes that were significant at 5% FDR using a Benjamini-Hochberg adjustment (Benjamini Y and Hochberg Y, 1995) for each mutant is shown in Table 5-8.

Mutant	# differentially expressed regions	# differentially expressed genes	# differentially expressed genes upregulated in mutants vs wild-type siblings	# differentially expressed genes downregulated in mutants vs wild-type siblings
titania^{s450}	774	728	457	271
setebos^{s453}	651	607	363	244
nol9^{sa1022}	230	218	107	111
las1l^{sa674}	4	4	2	2

Table 5-8 The number of differentially expressed regions, genes and their direction of effect in *tti*^{s450}, *set*^{s453}, *nol9*^{sa1022} and *las1l*^{sa674} mutants.

The number of differentially expressed genes that are shared between *nol9*^{sa1022}, *tti*^{s450}, *set*^{453} and *las1l*^{sa674} mutants is shown in Figure 5-10. The two differentially expressed genes that were significant at a 5% FDR using the Benjamini-Hochberg procedure in all four mutants were *grifin* and *rps27.2*. RPS27L, the homologue of *rps27.2*, is a direct Tp53 inducible target and modulates the DNA damage response (He and Sun, 2007; Li et al., 2007). The *tti*^{s450}, *set*^{453} and *nol9*^{sa1022} mutants shared an additional 145 differentially expressed genes. Another 263 differentially expressed genes were shared between only the *tti*^{s450} and *set*^{453} mutants adding to a total of 401 differentially expressed genes shared between *tti*^{s450} and *set*^{453} mutants.

Figure 5-10 The number of differentially expressed genes that are significant at a 5% FDR using Benjamini-Hochberg procedure that are shared between *nol9*^{sa1022}, *tti*^{s450}, *set*^{s453}, and *las1l*^{sa674} mutants.

To identify the active pathways that are enriched in *tti*^{s450} and *set*^{453} mutants, the lists of 728 and 607 unique differentially expressed genes that were statistically significantly differentially expressed (an adjusted *p*-value of less than 0.05, after Benjamini-Hochberg multiple testing adjustment) in *tti*^{s450} and *set*^{453} mutants respectively were compared against a

list of unique genes that were assayed in this experiment (10527 and 10535 genes for *tti*^{s450} and *set*^{453} mutants respectively) using DAVID (Section 2.6.5). The DAVID *KeggCharts* provided information for 167 of the 730 differentially expressed genes and 146 of the 607 differentially expressed genes for *tti*^{s450} and *set*^{453} mutants respectively. In the Appendix Table A - 8 and Table A - 9 show the enriched KEGG terms of differentially expressed genes of *tti*^{s450} and *set*^{453} mutants at a statistical significance of *p*-value less than 0.05 using a modified Fisher's exact test. In all three mutants the enriched KEGG pathways were "Aminoacyl-tRNA biosynthesis", "RNA polymerase", "Steroid biosynthesis" and "PPAR signalling pathway".

The lists of differentially expressed genes for *tti*^{s450}, *set*^{453}, *nol9*^{sa1022} and *las1l*^{sa674} mutants were investigated for enrichment for GO terms using topGO and this analysis was carried out by Dr Ian Sealy (Alexa et al., 2006) (Section 2.6.4). The enriched GO terms at an arbitrary K-S value of 0.01 for categories cellular component, molecular function biological process of differentially expressed genes in *tti*^{s450} and *set*^{453} mutants are shown in the Appendix (Figure A - 1, Figure A - 2, Figure A - 3, Figure A - 4, Figure A - 5, Figure A - 6).

The enriched GO terms at an arbitrary K-S value of 0.01 of all four mutants were compared (Section 2.6.3). The GO cellular component categories that were enriched in all four mutants were 'cytoplasm' and 'proteasome complex'. The *tti*^{s450}, *set*^{453} and *nol9*^{sa1022} mutants also shared enrichment for the categories 'nucleolus', 'ribonucleoprotein complex' and 'mitochondrial intermembrane space'. For the molecular function ontology categories, the enriched terms in all four mutants were 'RNA binding', 'translation initiation factor activity', 'nucleotide binding' and 'unfolded protein binding'. The *tti*^{s450}, *set*^{453} and *nol9*^{sa1022} mutants additionally shared the categories 'aminoacyl-tRNA ligase activity', 'serine-type endopeptidase activity', 'endopeptidase inhibitor activity', 'DNA-directed RNA polymerase activity' and 'ATP-dependent helicase activity'. The biological process term enriched in all four mutants was 'translational initiation'. In addition, *tti*^{s450}, *set*^{453} and *nol9*^{sa1022} mutants also showed enrichment for terms 'rRNA processing', 'tRNA aminoacylation for protein translation' and 'ribosome biogenesis'.

Similarly to the *nol9*^{sa1022} and *las1l*^{sa674} mutants, the development of digestive organs of *tti*^{s450} and *set*^{453} mutants is impaired (Boglev et al., 2013). However, the GO terms associated with the digestive organs namely 'pancreas development', 'exocrine pancreas development' endocrine pancreas development', 'liver development',' digestive system

development', 'digestive tract development' and 'digestive tract morphogenesis' all had a K-S value greater than 0.01 in both *tti*^{s450} and *set*^{453} mutants (Refer to Appendix Table A - 10, Table A - 11). In addition to the digestive organ defects, the *tti*^{s450} and *set*^{453} mutants displayed other phenotypes including smaller eyes, head and craniofacial defects (Boglev et al., 2013). The differentially expressed genes in *tti*^{s450} and *set*^{453} mutants were not enriched in GO terms associated with the eye, brain, cartilage and skeletal muscle except for 'skeletal muscle tissue development' in *set*^{453} mutants (Refer to Appendix Table A - 10, Table A - 11). Moreover, autophagy was found to be upregulated in the intestinal epithelium of *tti*^{s450} and *set*^{453} mutants (Boglev et al., 2013). However, the GO term 'autophagy' was not enriched in *tti*^{s450}, *set*^{453}, *nol9*^{sa1022} or *las1l*^{sa674} mutants with K-S values of 0.80, 0.65, 0.15 and 0.11 respectively and none of the *autophagy-related genes* (*atg*) that were within 100 bases of the nearest 3' end Ensembl gene was statistically significantly differentially expressed in any of the four mutants (Refer to Appendix Table A - 12).

5.3 Discussion

In this chapter, the mRNA expression profiles of four different rRNA processing mutants *nol9*^{sa1022}, *las1l*^{sa674}, *tti*^{s450} and *set*^{453} were investigated using Differential Expression Transcript Counting Technique (DeTCT) in order to provide insight into the molecular basis of the phenotypes in these mutants.

The mRNA expression profiling of *nol9*^{sa1022} mutants revealed an increased expression of genes involved in ribosome biogenesis, rRNA processing, tRNA aminoacylation for protein translation and translational initiation. In comparison, the set of genes differentially expressed in the *las1l*^{sa674}, *tti*^{s450} and *set*^{453} mutants was enriched in ribosome- and translation-related functions. This agrees with the previously reported zebrafish loss of function model of SBDS in which differentially expressed genes showed enrichment in the GO categories 'ribosome biogenesis', 'rRNA processing' and 'translational initiation', and these trends were particularly robust amongst genes that showed upregulation in *sbds*-deficient embryos (Provost et al., 2012). In the *nom1* mutants also, differentially expressed genes were enriched in ribosome-related Gene Ontology categories (Qin et al., 2014). Provost *et al.* hypothesised that the increased expression of genes related to ribosome biogenesis and translation represents a mechanism by which cells compensate for the disruptions in ribosome assembly. Interestingly, there is a marked enrichment of upregulated genes belonging to the 'proteasome complex' in *nol9*^{sa1022}, *las1l*^{sa674}, *tti*^{s450} and *set*^{453} mutants, it is possible that this is due to cells trying to degrade unrequired or damaged proteins following nucleolar stress induced by impairments in rRNA processing.

As the mRNA expression analysis was carried out on RNA from pooled larvae of mutants or wild-type siblings, one concern of using this approach is its sensitivity in detecting tissue-specific changes. The *rps19*-deficient embryos are characterised by haematopoietic and developmental abnormalities similar to Diamond-Blackfan anaemia (Danilova et al., 2008; Uechi et al., 2008). RNA-seq on pooled embryos injected with *rps19* morpholino, *rps19* and *tp53* morpholino or control morpholino revealed that genes enriched in functions in haematological systems, skeletal and muscular disorders and nervous system development, showed significant differential expression between *rps19*-morphant and control embryos (Jia et al., 2013). This suggests that tissue-specific effects are still detectable when studying gene expression in pools of whole embryo mRNA. Our analysis of the differentially expressed

genes in *nol9*^{sa1022} and *las1l*^{sa674} mutants revealed an enrichment of genes associated with digestive system indicating that tissue-specific effects were also detectable in our system. In addition, genes that are specifically expressed by the liver, pancreas and intestine are amongst those that showed the most significant decrease in transcript abundance in *nol9*^{sa1022} mutants. This observation is consistent with the *nol9*^{sa1022} mutants having fewer transcripts specific to digestive organs due to the smaller size of the digestive organs in *nol9*^{sa1022} mutants compared to those in wild-type siblings.

The two rRNA processing mutants *titania* and *setebos* exhibit digestive organ defects, smaller eyes and head, craniofacial defects and autophagy was found to be increased in their intestinal epithelium (Boglev et al., 2013) (Dr Joan Heath, Personal Communication). The eye-specific gene *grifin* is amongst the genes that showed the most statistically significant decrease in transcript abundance in *nol9*^{sa1022}, *las1l*^{sa674}, *tti*^{s450} and *set*^{453} mutants. It would be interesting to confirm this result by examining the expression of *grifin* by *in situ* hybridisation and investigate whether rRNA processing genes play a role in eye development. The analysis of differentially expressed genes in *tti*^{s450} and *set*^{453} mutants did not detect any significant enrichment of GO terms associated with the digestive organs, eye, brain, cartilage, skeletal system and autophagy. There are a number of reasons to explain this: firstly, those particular tissue-specific changes cannot be distinguished in the RNA of whole larvae. Secondly, the mRNA expression analysis is being carried out on larvae at a stage when changes in the expression of genes associated with those organs and the autophagic process cannot be detected. It will be worth analysing the gene expression profiles of these mutants at a stage when the morphological defects begin to manifest, i.e. 3 d.p.f. for *tti*^{s450} and *set*^{453} mutants and 4 d.p.f. for *nol9*^{sa1022} and *las1l*^{sa674} mutants. Moreover, the examination of changes in the level and cellular localisation of proteins is critical to complement the gene expression analysis as changes in the latter do not always correlate with changes at the protein level. Protein levels can be ascertained through western blot analysis while antibody staining can reveal the localisation of proteins of interest. These will potentially provide insight into the activity of proteins and pathways and help understand the mechanisms underlying the defects in rRNA processing mutants.

Haematological defects are prevalent in ribosomopathies (Narla and Ebert, 2010). The knockdown of *sbds* in zebrafish causes loss of neutrophils and in a zebrafish model of Diamond Blackfan anemia, haematological abnormalities were present and differentially

expressed genes between *rps19*-morphant and control embryos were enriched in functions in haematological systems (Jia et al., 2013). The functional analysis of the mRNA expression profiles of *nol9*^{sa1022} and *las1l*^{sa674} mutants revealed that differentially expressed genes were enriched in the Gene Ontology term "hemopoiesis" in *nol9*^{sa1022} mutants and "myeloid cell differentiation" in *las1l*^{sa674} mutants. These observations suggest that *nol9*^{sa1022} and *las1l*^{sa674} mutants, similar to *sbds* and *rps19* morphants, may also have haematological defects and thus encourage a detailed examination of haematopoiesis in *nol9*^{sa1022} and *las1l*^{sa674} mutants.

The mRNA expression profiling of *las1l*^{sa674} mutants revealed only a handful of differentially expressed genes that reached statistical significance compared to *nol9*^{sa1022}, *tti*^{s450} and *set*^{453} mutants. This could be due to a less severe phenotype and therefore fewer differentially expressed genes compared to wild-type siblings. Similarly, the number of differentially expressed genes in *tti*^{s450} and *set*^{453} mutants was about three times more than the number of differentially expressed genes in *nol9*^{sa1022} mutants and could be due to additional morphological defects in *tti*^{s450} and *set*^{453} mutants. Several differentially expressed genes in *nol9*^{sa1022}, *tti*^{s450} and *set*^{453} mutants have not been previously characterised and future work will investigate their role in the rRNA processing mutants. Furthermore, in this experiment, the differentially expressed regions that are more than 100 bases from the nearest 3' end of an Ensembl annotated gene have been excluded from the analysis, but could potentially be of interest and explored in the future.

The tumor suppressor protein Tp53 is the principal guardian of the genome and of cell integrity (Lane, 1992). The gene expression analysis in *nol9*^{sa1022} mutants showed an increased expression of *tp53* and Tp53 target genes *mdm2*, *ccng1*, *cdkn1a*, *gadd45aa* and *baxa* (Tokino and Nakamura, 2000). Both Gadd45a and Cyclin G1 can induce cell cycle arrest at the G2/M phase whilst Cdkn1a is a cell cycle regulator at the G1/S phase and inhibits the activity of cyclin-CDK2, cyclin-CDK1 and cyclin-CDK4/6 complexes (Gartel and Radhakrishnan, 2005; Kimura et al., 2001; Rosemary Siafakas and Richardson, 2009). This increased expression of genes involved in cell cycle control could explain the cell cycle defects and impairments in cell proliferation that contribute to the exocrine pancreas phenotype in the *nol9*^{sa1022} mutants. Additionally, an increase in expression of genes involved in apoptosis including *baxa*, *casp8* and *cycsb* was observed (Kruidering and Evan, 2000; Liu et al., 1996; Oltvai et al., 1993) although an increase in apoptosis was not detected in *nol9*^{sa1022} mutants. Interestingly, *rps27.2*, the zebrafish orthologue of *RPS27L* was found to be

significantly upregulated in *nol9*^{sa1022}, *las1l*^{sa674}, *tti*^{s450} and *set*^{453} mutants. The *ribosomal protein S27-like* (*RPS27L*) gene is a Tp53 transcriptional target that determines cell fate in response to DNA damage (He and Sun, 2007; Li et al., 2007). *RPS27L* and *RPS27* form a complex with *MDM2* and inhibits Mdm2-mediated Tp53 ubiquitination thereby increasing the half-life and levels of the Tp53 protein (Xiong et al., 2011). It will be interesting to investigate whether Rps27.2 is involved in the mechanism responsible for the hypoplastic digestive organs of rRNA processing mutants. This can be achieved by studying the effects of knocking down *rps27.2* expression by morpholino and/or combined loss of function of *rps27.2* and *nol9.*

The disruption of ribosome biogenesis and/or nucleolar structure can activate a Tp53-dependent stress response (Holmberg Olausson, 2012). The two main models to explain the mechanism of activation of Tp53 are the stabilisation of Tp53 protein by default following disruption of nucleolar structure and/or function (Rubbi and Milner, 2003; Zauberman et al., 1995) and the inhibition of MDM2, a repressor of Tp53, by ribosomal proteins redistributed to the nucleoplasm after nucleolar disruption (Holmberg Olausson, 2012). Tp53 has been shown to be involved in the pathogenesis of ribosomopathies and ribosome biogenesis mutants. In the Treacher-Collins syndrome mouse model, reduction in expression of *Tp53* rescues craniofacial dysmorphology and in the zebrafish *wdr43* mutant that displays defects in early development in neural tube, eye, heart and pharyngeal arches and then in craniofacial cartilages, knockdown of *tp53* partially rescues the craniofacial defects (Jones et al., 2008; Zhao et al., 2014). In zebrafish *rpl11* and *rps29* mutants, inhibition of Tp53 partially rescues haematopoietic phenotypes in zebrafish *rpl11* and *rps29* mutants (Danilova et al., 2011; Taylor et al., 2012). In addition in the *def*^{hi429} mutant, where upregulation of Δ*113p53*, a shortened isoform and target gene of Tp53, induces the expression of Tp53 response genes, knockdown of *tp53* and Δ*113p53* partially rescues the mutant phenotype (Chen et al., 2009; Chen et al., 2005). In our study, the mean volume of 5 d.p.f. *nol9*$^{-/-}$*tp53*$^{+/+}$ and *nol9*$^{-/-}$*tp53*$^{-/-}$ larvae were not statistically significantly different meaning that the small exocrine pancreas phenotype of *nol9*^{sa1022} mutant was not rescued by Tp53 loss of function and suggests the involvement of a Tp53-independent mechanism. This result is comparable to the pancreatic defects of *sbds* deficient embryos and *pes*^{hi2Tg}, *rpl3*^{hi2437}, *rpl23a*^{hi2582}, and *rpl6*^{hi3655b} mutants also not being rescued by genetic loss of Tp53 (Provost et al., 2012; Provost et al., 2013). In addition, Tp53 loss of function does not abolish the induction of autophagy in the intestine of

tti^{s450} mutants even though the *tti*^{s450} larvae displayed increased transcription of the Tp53 target genes Δ*113p53*, *cdkn1a*, *ccng1* and *mdm2* (Boglev et al., 2013).

Tp53-independent mechanisms are thought to be involved in the pathogenesis of ribosmopathies and loss of Tp53 does not rescue the phenotypes completely in zebrafish *rps29, rpl11, wdr43* and *def*^{hi429} mutants (Chen et al., 2005; Danilova et al., 2011; Donati et al., 2012; Holmberg Olausson, 2012; Taylor et al., 2012; Zhao et al., 2014). Several Tp53-independent pathways that mediate the nucleolar stress response have been described and include an RPL11-dependent mechanism whereby inhibition of rRNA synthesis by POLR1A depletion impaired cell-cycle progression in Tp53-inactivated cancer cell lines by downregulation of the transcription factor E2F-1. RPL11 released after nucleolar stress, binds to MDM2 inactivating the E2F-1 stabilising function of MDM2 leading to a downregulation of E2F-1 protein and decreasing the expression of E2Fs target genes that are required for entry and progression at the S-phase (Donati et al., 2011). A second Tp53-independent mechanism is the downregulation of c-Myc in response to inhibition of ribosome biogenesis due to RPL11 binding to c-Myc and reducing its transcriptional activity. This results in reduced cell proliferation even in *tp53*-null cells (Dai et al., 2007). A third Tp53-independent mechanism involves the downregulation of PIM1 expression, caused by deficiency of ribosomal proteins or other ribosomal stressors, which results in stabilisation and activation of CDKN1B leading to cell-cycle arrest (Iadevaia et al., 2010). Other potential p53-independent mechanisms that have been put forward involve the Tp53-independent effects of MDM2 or p63 and p73, two members of the p53 superfamily although there are no studies to demonstrate that these mechanisms are nucleolar stress responses (Holmberg Olausson, 2012). Future work will include investigating whether any of these p53-independent mechanisms contribute to the hypoplastic digestive organs of *nol9*^{sa1022} mutants. Interestingly the expression of *mdm2*, *ccng1* and *cdkn1a* were not completely abolished in *tti*$^{-/-}$;*tp53*$^{-/-}$ mutants and those genes were in fact significantly upregulated in *tti*$^{-/-}$;*tp53*$^{-/-}$ mutants compared to *tti*$^{+/+}$;*tp53*$^{-/-}$ larvae. Furthermore, studying the mRNA expression profiles of *nol9*$^{-/-}$;*tp53*$^{-/-}$ mutants and *nol9*$^{-/-}$;*tp53*$^{+/+}$ mutants will help uncover genes that contribute to the phenotype of *nol9*^{sa1022} mutants in a Tp53-independent mechanism.

The mRNA expression analyses of *nol9*^{sa1022}, *las1l*^{sa674}, *tti*^{s450} and *set*^{453} mutants served as a discovery tool to identify alterations in genes and pathways in zebrafish rRNA processing mutants. Elucidating the mechanisms of nucleolar stress in the context of a whole

organism is critical to understanding the pathogenic mechanisms operating in ribosomopathies. In particular, determining the Tp53-independent stress pathways will benefit the development of treatments for ribosomopathies and cancers with defective Tp53.

Chapter 6 Discussion

In this thesis, I have characterised the phenotype of the loss-of-function *nol9*^{sa1022} zebrafish mutant and demonstrated that it exhibited defects in the development of the pancreas, liver and intestine. I further predicted that a loss-of-function mutation in *las1l*, a gene encoding a Nol9-interacting protein, would result in a similar phenotype to the *nol9*^{sa1022} mutant, which I confirmed upon morphological characterisation of the *las1l*^{sa674} zebrafish mutant. The mRNA expression profiles of *nol9*^{sa1022} and *las1l*^{sa674} mutant were then studied and compared to those of two other zebrafish rRNA processing mutants, *tti*^{s450} and *set*^{s453}, revealing shared genes and pathways that were differentially expressed in all four mutants. This chapter summarises the overall findings of the work and discusses the potential future directions for the project.

The purpose of my study was to determine the function of Nol9 in zebrafish pancreas development and would contribute to our expanding knowledge of ribosomal biogenesis mutants. In Chapter 3, I described the conserved function of Nol9 between human and zebrafish, observing that zebrafish Nol9 is also involved in the processing of the rRNA precursor molecules and formation of the large ribosomal subunit. The characterisation of the *nol9*^{sa1022} mutant showed that development of the exocrine pancreas, liver and intestine in these fish is impaired after 3 days post fertilisation (d.p.f.) whereas there were no other apparent morphological defects and the formation of the endocrine pancreas namely the pancreatic islets and the secondary islets was unaffected. In Chapter 4, I described morphological defects in the digestive organs and impaired exocrine pancreas development after 3 d.p.f. resulting from a disruptive mutation in the Nol9-interacting protein Las1l. Although a more detailed characterisation of the digestive organs of *las1l*^{sa674} mutant is required, the results strongly suggest a critical role for members of the Nol9-Las1l complex in the development of digestive organs in zebrafish. Previous studies have shown that Nol9 and Las1l are involved in processing of rRNAs of the large ribosomal subunit and are crucial for ribosome biogenesis (Castle et al., 2012; Castle et al., 2010; Heindl and Martinez, 2010). Our findings provide an additional link between functions in ribosomal biogenesis and digestive organ development (Boglev et al., 2013; Chen et al., 2005; Mayer and Fishman, 2003; Provost et al., 2012; Provost et al., 2013; Qin et al., 2014). Interestingly, we also found that the phenotype in *nol9*^{sa1022} mutants is milder, occurs later than *npo* and *def* mutants and does

not include jaw defects, in contrast to the *npo*, *def*, *tti* and *nom1* mutants. The possible reasons for an overall attenuated *nol9*^{sa1022} phenotype include a less critical role of *nol9* in ribosome biogenesis or a higher level of maternal mRNAs available. Further investigation into the protein activity and levels of the respective genes in each mutant and their effects on rRNA processing and ribosome biogenesis may provide greater insight into this area.

The tissue specificity of mutants of ribosomal biogenesis proteins and ribosomopathies is a puzzling phenomenon as these proteins are ubiquitously expressed and all cells and tissues require ribosomes for protein synthesis (Freed et al., 2010; McCann and Baserga, 2013; Narla and Ebert, 2010). The current hypothesis to explain the tissue-specific phenotype in zebrafish involves the exhaustion of maternally derived ribosomal biogenesis mRNA in tissues that are rapidly dividing and thus requiring large numbers of ribosomes. In Chapter 3, it was described that *nol9* is initially ubiquitously expressed and subsequently high level expression becomes restricted to highly proliferating organs including the pancreas, liver, intestine and head. This result agrees with the developmental expression pattern of previously published ribosomal biogenesis genes (Boglev et al., 2013; Chen et al., 2005; Mayer and Fishman, 2003; Provost et al., 2013; Qin et al., 2014). More research is needed to better understand the heightened sensitivity of digestive organs to mutations in ribosomal biogenesis genes. In particular, there are several hypotheses that can be explored; firstly, it is possible that a different spectrum of mRNAs is translated if the numbers of fully functional cytoplasmic ribosomes do not meet the cell's demand for protein synthesis. To test this possibility, the zebrafish ribosome biogenesis mutant lines could be crossed to a transgenic line e.g. (*Tg(XlEef1a1:GFP)*^{s854}) expressing GFP specifically in the digestive organs, sorting GFP+ and GFP- cells and subsequently studying their mRNA expression profiles (Ober et al., 2006; Stuckenholz et al., 2009). Secondly, Nol9 and other ribosomal biogenesis proteins can have tissue-specific interacting proteins and may have additional functions in digestive organs.

The mRNA expression profiles of *nol9*^{sa1022}, *las1l*^{sa674}, *tti*^{s450} and *set*^{s453} mutants were analysed and described in Chapter 5. The findings from this study are subject to two major limitations: firstly, whole zebrafish larvae were used for gene expression profiling potentially making it more difficult to detect tissue-specific changes and secondly, mRNA expression analysis was carried out on 5 d.p.f. larvae, at least one day after the impaired development of digestive organs first occurred. Despite these potential shortcomings, the study has found that

genes involved in cell cycle regulation were significantly upregulated in *nol9*^{sa1022} mutants, which is corroborated by the results from the cell cycle analysis that showed an increased number of cells at the G1 phase in these mutants and impaired cell proliferation of *ptf1a*-expressing cells in the exocrine pancreas. Altogether, these findings suggest that impaired cell proliferation contributes to the developmental defects of organs observed in *nol9*^{sa1022} mutants. An increase in cell death was not observed in *nol9*^{sa1022} mutants but functional analysis of the mRNA expression profiles of *nol9*^{sa1022} mutants revealed an upregulation of cell death genes. Since autophagy has been found to upregulated in the intestinal epithelium in *titania* and in red blood cells from *rps7*-deficient zebrafish embryos and DBA and SBDS patients, we surmise that autophagy also operates in *nol9*^{sa1022} mutants (Boglev et al., 2013; Heijnen et al., 2014). The study of the relationship between *nol9* function and autophagy will lead to a better understanding of autophagy as a cell survival mechanism that leads to defects in the development of digestive organs in *nol9*^{sa1022} mutants.

Another finding from the analysis of mRNA expression profiles in Chapter 5 was that genes belonging to the Tp53 signalling pathway are upregulated in *nol9*^{sa1022} mutants. This indicated that a Tp53-dependent mechanism could contribute to the developmental defects in the digestive system of *nol9*^{sa1022} mutants. This is consistent with the involvement of Tp53 in mediating clinical features of ribosomopathies in human, including the craniofacial dysmorphology in Treacher Collins syndrome (Jones et al., 2008), some of the red cell abnormalities in Diamond Blackfan anaemia (Boultwood et al., 2012), the macrocytic anaemia in 5q^{-} syndrome (Barlow et al., 2010) and the hepatobiliary dysfunction in North American Indian Childhood Cirrhosis (Wilkins et al., 2013). However, our study had shown that genetic loss of Tp53 did not rescue the small pancreas phenotype of *nol9*^{sa1022} mutants, confirming previous findings in some ribosome biogenesis zebrafish models and providing additional evidence for the involvement of Tp53-independent mechanisms in failed expansion of zebrafish exocrine pancreas following impairments in ribosome biogenesis (Boglev et al., 2013; Provost et al., 2012; Provost et al., 2013; Qin et al., 2014). Tp53-independent mechanisms have yet to be described in ribosomopathies. It is probable that the same Tp53-independent mechanism that is seen in the zebrafish rRNA processing mutants, also contributes to the exocrine pancreas defects in Shwachman-Bodian Diamond syndrome (SBDS) (Provost et al., 2012) and some of haematological defects in Diamond Blackfan anemia (Danilova et al., 2011; Jia et al., 2013; Song et al., 2014; Taylor et al., 2012). Future studies should concentrate on elucidating these Tp53-independent nucleolar stress pathways

as they will enhance our understanding of the pathogenic mechanisms of ribosomopathies. In addition such insights may influence the development of chemotherapeutic therapies since it is estimated that TP53 function is disrupted/lost in more than 50% of all human tumours (Soussi et al., 2000). The commonly used anti-cancer treatments induce cellular stress that activates TP53-mediated cell cycle arrest and/or death, and tumours with defective TP53 are less sensitive to those drug treatments than tumours with functioning TP53 (Harris, 1996). Studies on TP53-independent mechanisms could potentially identify new targets for chemotherapeutic applications.

The mammalian target of rapamycin (mTOR) complex can regulate ribosome biogenesis by promoting rDNA transcription and playing a role in rRNA processing (Iadevaia et al., 2012). Additionally it increases the preference of ribosome in translating terminal oligopyrimidine (5'-TOP) mRNAs including ribosomal biogenesis genes through phosphorylation of S6 kinase (S6K) 1, which in turns phosphorylates RPS6 (Jefferies et al., 1997; Mayer and Grummt, 2006; Reiter et al., 2004). Recently, Heijnen *et al*. reported a TOR-dependent increase in phosphorylation of S6K in human cells with RP loss and in RP-deficient zebrafish, a response that is triggered by reactive oxygen species (ROS) (Heijnen et al., 2014). Conversely, Boglev *et al.* found that autophagy induction in *tti*^{s450} is independent of mTOR (Boglev et al., 2013). Future directions for the project will include studying whether ROS and the mTOR pathway contribute to the exocrine pancreas defects in *nol9*^{sa1022} mutants.

The mRNA expression profiling revealed an enrichment of ribosome- and translation-related functions amongst genes that were significantly upregulated in *nol9*^{sa1022}, *las1l*^{sa674}, *tti*^{s450} and *set*^{s453} mutants, a result previously observed following knockdown of *sbds* and in *nom1* mutants (Provost et al., 2012; Qin et al., 2014). These findings further support the idea that a compensatory mechanism operates in cells following disruptions in ribosome biogenesis whereby cells attempt to increase the expression of genes involved in transcription and translation in order to fulfil the demands of rapidly proliferating tissues for protein synthesis (Provost et al., 2012). Further research is needed to determine the nature of this compensatory mechanism, more specifically how it is triggered, its effects on tissues and whether it is restricted to affected organs. Interestingly, this study revealed that genes functioning in haematopoiesis were differentially expressed in *nol9*^{sa1022} and *las1l*^{sa674} mutants. To our knowledge a role for an rRNA processing gene in haematopoiesis has not yet been described in zebrafish. A detailed examination of haematopoiesis in *nol9*^{sa1022} and

las1l^{sa674} mutants is currently being undertaken and can potentially provide insight into the process of haematopoiesis and the mechanisms operating in red blood cell defects in Diamond Blackfan anemia and 5q^{-} syndrome and neutropenia in Shwachman-Bodian-Diamond syndrome. In addition, it was found that the expression of the eye-specific gene *galectin related inter-fiber protein* is significantly downregulated in *nol9*^{sa1022}, *las1l*^{sa674}, *tti*^{s450} and *set*^{s453} mutants, although the gross morphology of the eye of *nol9*^{sa1022} and *las1l*^{sa674} mutants appeared normal. Further work needs to be done to establish whether the eye development of *nol9*^{sa1022} and *las1l*^{sa674} mutants is impaired.

Understanding the effects of aberrant ribosome biogenesis in an *in vivo* model is important to deciphering the underlying mechanisms of ribosomopathies and developing therapeutic treatments for these disorders. These studies may also benefit cancer research where there is a great deal of interest in developing therapeutics that target ribosome biogenesis in malignant cells (Drygin et al., 2010). An extensive knowledge of the molecular mechanisms following impaired ribosome biogenesis is required in order to safely modify them since targeting ribosome biogenesis could have devastating consequences and potentially result in changes in DNA regulation and/or mRNA translation patterns, eventually leading to an increased cancer risk (Holmberg Olausson, 2012).

This thesis has demonstrated that *nol9* and *las1l* are essential for normal exocrine pancreas development in zebrafish. Through this discovery, this work has provided a novel link between ribosome biogenesis and pancreas development, and helped to place the importance of rRNA processing proteins in a tissue-specific context. Further study of other Nol9 interacting proteins may help strengthen this link. The continued research on *nol9*^{sa1022} and *las1l*^{sa674} mutants will not only contribute to our knowledge of pancreas development and ribosomopathies but also contribute to the field of cancer and regeneration.

Bibliography

Abecasis, G.R., Altshuler, D., Auton, A., Brooks, L.D., Durbin, R.M., Gibbs, R.A., Hurles, M.E., McVean, G.A., 2010. A map of human genome variation from population-scale sequencing. Nature 467, 1061-1073.

Abecasis, G.R., Auton, A., Brooks, L.D., DePristo, M.A., Durbin, R.M., Handsaker, R.E., Kang, H.M., Marth, G.T., McVean, G.A., 2012. An integrated map of genetic variation from 1,092 human genomes. Nature 491, 56-65.

Agathon, A., Thisse, B., Thisse, C., 2001. Morpholino knock-down of antivin1 and antivin2 upregulates nodal signaling. Genesis 30, 178-182.

Ahlgren, U., Pfaff, S.L., Jessell, T.M., Edlund, T., Edlund, H., 1997. Independent requirement for ISL1 in formation of pancreatic mesenchyme and islet cells. Nature 385, 257-260.

Al-Dosari, M.S., Al-Muhsen, S., Al-Jazaeri, A., Mayerle, J., Zenker, M., Alkuraya, F.S., 2008. Johanson-Blizzard syndrome: report of a novel mutation and severe liver involvement. American journal of medical genetics. Part A 146A, 1875-1879.

Alexa, A., Rahnenfuhrer, J., Lengauer, T., 2006. Improved scoring of functional groups from gene expression data by decorrelating GO graph structure. Bioinformatics 22, 1600-1607.

Alexander, J., Rothenberg, M., Henry, G.L., Stainier, D.Y., 1999. casanova plays an early and essential role in endoderm formation in zebrafish. Developmental biology 215, 343-357.

Alexander, J., Stainier, D.Y., 1999. A molecular pathway leading to endoderm formation in zebrafish. Current biology : CB 9, 1147-1157.

Alexandrov, A., Colognori, D., Steitz, J.A., 2011. Human eIF4AIII interacts with an eIF4G-like partner, NOM1, revealing an evolutionarily conserved function outside the exon junction complex. Genes & development 25, 1078-1090.

Amsterdam, A., Burgess, S., Golling, G., Chen, W., Sun, Z., Townsend, K., Farrington, S., Haldi, M., Hopkins, N., 1999. A large-scale insertional mutagenesis screen in zebrafish. Genes & development 13, 2713-2724.

Amsterdam, A., Nissen, R.M., Sun, Z., Swindell, E.C., Farrington, S., Hopkins, N., 2004. Identification of 315 genes essential for early zebrafish development. Proceedings of the National Academy of Sciences of the United States of America 101, 12792-12797.

Amsterdam, A., Varshney, G.K., Burgess, S.M., 2011. Retroviral-mediated Insertional Mutagenesis in Zebrafish. Methods in cell biology 104, 59-82.

Anders, S., Huber, W., 2010. Differential expression analysis for sequence count data. Genome biology 11, R106.eerrrr

Anderson, K.R., Singer, R.A., Balderes, D.A., Hernandez-Lagunas, L., Johnson, C.W., Artinger, K.B., Sussel, L., 2011. The L6 domain tetraspanin Tm4sf4 regulates endocrine pancreas differentiation and directed cell migration. Development 138, 3213-3224.

Anderson, K.R., Torres, C.A., Solomon, K., Becker, T.C., Newgard, C.B., Wright, C.V., Hagman, J., Sussel, L., 2009a. Cooperative transcriptional regulation of the essential pancreatic islet gene NeuroD1 (beta2) by Nkx2.2 and neurogenin 3. The Journal of biological chemistry 284, 31236-31248.

Anderson, R.M., Bosch, J.A., Goll, M.G., Hesselson, D., Dong, P.D., Shin, D., Chi, N.C., Shin, C.H., Schlegel, A., Halpern, M., Stainier, D.Y., 2009b. Loss of Dnmt1 catalytic activity reveals multiple roles for DNA methylation during pancreas development and regeneration. Developmental biology 334, 213-223.

Andre, M., Ando, S., Ballagny, C., Durliat, M., Poupard, G., Briancon, C., Babin, P.J., 2000. Intestinal fatty acid binding protein gene expression reveals the cephalocaudal patterning during zebrafish gut morphogenesis. The International journal of developmental biology 44, 249-252.

Aoki, T.O., David, N.B., Minchiotti, G., Saint-Etienne, L., Dickmeis, T., Persico, G.M., Strahle, U., Mourrain, P., Rosa, F.M., 2002a. Molecular integration of casanova in the Nodal signalling pathway controlling endoderm formation. Development 129, 275-286.

Aoki, T.O., Mathieu, J., Saint-Etienne, L., Rebagliati, M.R., Peyrieras, N., Rosa, F.M., 2002b. Regulation of nodal signalling and mesendoderm formation by TARAM-A, a TGFbeta-related type I receptor. Developmental biology 241, 273-288.

Appel, B., Fritz, A., Westerfield, M., Grunwald, D.J., Eisen, J.S., Riley, B.B., 1999. Delta-mediated specification of midline cell fates in zebrafish embryos. Current biology : CB 9, 247-256.

Argenton, F., Zecchin, E., Bortolussi, M., 1999. Early appearance of pancreatic hormone-expressing cells in the zebrafish embryo. Mechanisms of development 87, 217-221.

Arkhipova, V., Wendik, B., Devos, N., Ek, O., Peers, B., Meyer, D., 2012. Characterization and regulation of the hb9/mnx1 beta-cell progenitor specific enhancer in zebrafish. Developmental biology 365, 290-302.

Armistead, J., Khatkar, S., Meyer, B., Mark, B.L., Patel, N., Coghlan, G., Lamont, R.E., Liu, S., Wiechert, J., Cattini, P.A., Koetter, P., Wrogemann, K., Greenberg, C.R., Entian, K.D., Zelinski, T., Triggs-Raine, B., 2009. Mutation of a gene essential for ribosome biogenesis, EMG1, causes Bowen-Conradi syndrome. American journal of human genetics 84, 728-739.

Armistead, J., Triggs-Raine, B., 2014. Diverse diseases from a ubiquitous process: the ribosomopathy paradox. FEBS letters 588, 1491-1500.

Artavanis-Tsakonas, S., Rand, M.D., Lake, R.J., 1999. Notch signaling: cell fate control and signal integration in development. Science 284, 770-776.

Ashburner, M., Ball, C.A., Blake, J.A., Botstein, D., Butler, H., Cherry, J.M., Davis, A.P., Dolinski, K., Dwight, S.S., Eppig, J.T., Harris, M.A., Hill, D.P., Issel-Tarver, L., Kasarskis, A., Lewis, S., Matese, J.C., Richardson, J.E., Ringwald, M., Rubin, G.M., Sherlock, G., 2000.

Gene ontology: tool for the unification of biology. The Gene Ontology Consortium. Nature genetics 25, 25-29.

Azuma, M., Toyama, R., Laver, E., Dawid, I.B., 2006. Perturbation of rRNA synthesis in the bap28 mutation leads to apoptosis mediated by p53 in the zebrafish central nervous system. The Journal of biological chemistry 281, 13309-13316.

Balciunas, D., Davidson, A.E., Sivasubbu, S., Hermanson, S.B., Welle, Z., Ekker, S.C., 2004. Enhancer trapping in zebrafish using the Sleeping Beauty transposon. BMC genomics 5, 62.

Barlow, J.L., Drynan, L.F., Hewett, D.R., Holmes, L.R., Lorenzo-Abalde, S., Lane, A.L., Jolin, H.E., Pannell, R., Middleton, A.J., Wong, S.H., Warren, A.J., Wainscoat, J.S., Boultwood, J., McKenzie, A.N., 2010. A p53-dependent mechanism underlies macrocytic anemia in a mouse model of human 5q- syndrome. Nature medicine 16, 59-66.

Ben-Shem, A., Garreau de Loubresse, N., Melnikov, S., Jenner, L., Yusupova, G., Yusupov, M., 2011. The structure of the eukaryotic ribosome at 3.0 A resolution. Science 334, 1524-1529.

Benjamini Y, Hochberg Y, 1995. Controllng the false discovery rate: a practical and powerful approach to multiple testing. J Roy Stat Soc B, 289-300.

Berghmans, S., Murphey, R.D., Wienholds, E., Neuberg, D., Kutok, J.L., Fletcher, C.D., Morris, J.P., Liu, T.X., Schulte-Merker, S., Kanki, J.P., Plasterk, R., Zon, L.I., Look, A.T., 2005. tp53 mutant zebrafish develop malignant peripheral nerve sheath tumors. Proceedings of the National Academy of Sciences of the United States of America 102, 407-412.

Bernstein, K.A., Baserga, S.J., 2004. The small subunit processome is required for cell cycle progression at G1. Molecular biology of the cell 15, 5038-5046.

Bernstein, K.A., Bleichert, F., Bean, J.M., Cross, F.R., Baserga, S.J., 2007. Ribosome biogenesis is sensed at the Start cell cycle checkpoint. Molecular biology of the cell 18, 953-964.

Bertrand, J.Y., Chi, N.C., Santoso, B., Teng, S., Stainier, D.Y., Traver, D., 2010. Haematopoietic stem cells derive directly from aortic endothelium during development. Nature 464, 108-111.

Betard, C., Rasquin-Weber, A., Brewer, C., Drouin, E., Clark, S., Verner, A., Darmond-Zwaig, C., Fortin, J., Mercier, J., Chagnon, P., Fujiwara, T.M., Morgan, K., Richter, A., Hudson, T.J., Mitchell, G.A., 2000. Localization of a recessive gene for North American Indian childhood cirrhosis to chromosome region 16q22-and identification of a shared haplotype. American journal of human genetics 67, 222-228.

Biemar, F., Argenton, F., Schmidtke, R., Epperlein, S., Peers, B., Driever, W., 2001. Pancreas development in zebrafish: early dispersed appearance of endocrine hormone expressing cells and their convergence to form the definitive islet. Developmental biology 230, 189-203.

Binot, A.C., Manfroid, I., Flasse, L., Winandy, M., Motte, P., Martial, J.A., Peers, B., Voz, M.L., 2010. Nkx6.1 and nkx6.2 regulate alpha- and beta-cell formation in zebrafish by acting on pancreatic endocrine progenitor cells. Developmental biology 340, 397-407.

Bjornson, C.R., Griffin, K.J., Farr, G.H., 3rd, Terashima, A., Himeda, C., Kikuchi, Y., Kimelman, D., 2005. Eomesodermin is a localized maternal determinant required for endoderm induction in zebrafish. Developmental cell 9, 523-533.

Blackburn, P.R., Campbell, J.M., Clark, K.J., Ekker, S.C., 2013. The CRISPR System-Keeping Zebrafish Gene Targeting Fresh. Zebrafish 10, 116-118.

Boglev, Y., Badrock, A.P., Trotter, A.J., Du, Q., Richardson, E.J., Parslow, A.C., Markmiller, S.J., Hall, N.E., de Jong-Curtain, T.A., Ng, A.Y., Verkade, H., Ober, E.A., Field, H.A., Shin, D., Shin, C.H., Hannan, K.M., Hannan, R.D., Pearson, R.B., Kim, S.H., Ess, K.C., Lieschke, G.J., Stainier, D.Y., Heath, J.K., 2013. Autophagy induction is a Tor- and Tp53-independent cell survival response in a zebrafish model of disrupted ribosome biogenesis. PLoS genetics 9, e1003279.

Bolze, A., Mahlaoui, N., Byun, M., Turner, B., Trede, N., Ellis, S.R., Abhyankar, A., Itan, Y., Patin, E., Brebner, S., Sackstein, P., Puel, A., Picard, C., Abel, L., Quintana-Murci, L., Faust, S.N., Williams, A.P., Baretto, R., Duddridge, M., Kini, U., Pollard, A.J., Gaud, C., Frange, P., Orbach, D., Emile, J.F., Stephan, J.L., Sorensen, R., Plebani, A., Hammarstrom, L., Conley, M.E., Selleri, L., Casanova, J.L., 2013. Ribosomal protein SA haploinsufficiency in humans with isolated congenital asplenia. Science 340, 976-978.

Bonafe, L., Schmitt, K., Eich, G., Giedion, A., Superti-Furga, A., 2002. RMRP gene sequence analysis confirms a cartilage-hair hypoplasia variant with only skeletal manifestations and reveals a high density of single-nucleotide polymorphisms. Clinical genetics 61, 146-151.

Boniface, E.J., Lu, J., Victoroff, T., Zhu, M., Chen, W., 2009. FlEx-based transgenic reporter lines for visualization of Cre and Flp activity in live zebrafish. Genesis 47, 484-491.

Boocock, G.R., Morrison, J.A., Popovic, M., Richards, N., Ellis, L., Durie, P.R., Rommens, J.M., 2003. Mutations in SBDS are associated with Shwachman-Diamond syndrome. Nature genetics 33, 97-101.

Boultwood, J., Pellagatti, A., Wainscoat, J.S., 2012. Haploinsufficiency of ribosomal proteins and p53 activation in anemia: Diamond-Blackfan anemia and the 5q- syndrome. Advances in biological regulation 52, 196-203.

Bowen, P., Conradi, G.J., 1976. Syndrome of skeletal and genitourinary anomalies with unusual facies and failure to thrive in Hutterite sibs. Birth defects original article series 12, 101-108.

Butterfield, R.J., Stevenson, T.J., Xing, L., Newcomb, T.M., Nelson, B., Zeng, W., Li, X., Lu, H.M., Lu, H., Farwell Gonzalez, K.D., Wei, J.P., Chao, E.C., Prior, T.W., Snyder, P.J., Bonkowsky, J.L., Swoboda, K.J., 2014. Congenital lethal motor neuron disease with a novel defect in ribosome biogenesis. Neurology 82, 1322-1330.

Campbell, L.J., Willoughby, J.J., Jensen, A.M., 2012. Two types of Tet-On transgenic lines for doxycycline-inducible gene expression in zebrafish rod photoreceptors and a gateway-based tet-on toolkit. PloS one 7, e51270.

Cano, D.A., Hebrok, M., Zenker, M., 2007. Pancreatic development and disease. Gastroenterology 132, 745-762.

Castle, C.D., Cassimere, E.K., Denicourt, C., 2012. LAS1L interacts with the mammalian Rix1 complex to regulate ribosome biogenesis. Molecular biology of the cell 23, 716-728.

Castle, C.D., Cassimere, E.K., Lee, J., Denicourt, C., 2010. Las1L is a nucleolar protein required for cell proliferation and ribosome biogenesis. Molecular and cellular biology 30, 4404-4414.

Castle, C.D., Sardana, R., Dandekar, V., Borgianini, V., Johnson, A.W., Denicourt, C., 2013. Las1 interacts with Grc3 polynucleotide kinase and is required for ribosome synthesis in Saccharomyces cerevisiae. Nucleic acids research 41, 1135-1150.

Chagnon, P., Michaud, J., Mitchell, G., Mercier, J., Marion, J.F., Drouin, E., Rasquin-Weber, A., Hudson, T.J., Richter, A., 2002. A missense mutation (R565W) in cirhin (FLJ14728) in North American Indian childhood cirrhosis. American journal of human genetics 71, 1443-1449.

Charette, J.M., Baserga, S.J., 2010. The DEAD-box RNA helicase-like Utp25 is an SSU processome component. RNA 16, 2156-2169.

Chen, A.T., Zon, L.I., 2009. Zebrafish blood stem cells. Journal of cellular biochemistry 108, 35-42.

Chen, J., Ng, S.M., Chang, C., Zhang, Z., Bourdon, J.C., Lane, D.P., Peng, J., 2009. p53 isoform delta113p53 is a p53 target gene that antagonizes p53 apoptotic activity via BclxL activation in zebrafish. Genes & development 23, 278-290.

Chen, J., Ruan, H., Ng, S.M., Gao, C., Soo, H.M., Wu, W., Zhang, Z., Wen, Z., Lane, D.P., Peng, J., 2005. Loss of function of def selectively up-regulates Delta113p53 expression to arrest expansion growth of digestive organs in zebrafish. Genes & development 19, 2900-2911.

Chen, S., Li, C., Yuan, G., Xie, F., 2007. Anatomical and histological observation on the pancreas in adult zebrafish. Pancreas 34, 120-125.

Chen, Y., Schier, A.F., 2001. The zebrafish Nodal signal Squint functions as a morphogen. Nature 411, 607-610.

Cheng, P.Y., Lin, C.C., Wu, C.S., Lu, Y.F., Lin, C.Y., Chung, C.C., Chu, C.Y., Huang, C.J., Tsai, C.Y., Korzh, S., Wu, J.L., Hwang, S.P., 2008. Zebrafish cdx1b regulates expression of downstream factors of Nodal signaling during early endoderm formation. Development 135, 941-952.

Cheng, W., Guo, L., Zhang, Z., Soo, H.M., Wen, C., Wu, W., Peng, J., 2006. HNF factors form a network to regulate liver-enriched genes in zebrafish. Developmental biology 294, 482-496.

Choi, Y.B., Ko, J.K., Shin, J., 2004. The transcriptional corepressor, PELP1, recruits HDAC2 and masks histones using two separate domains. The Journal of biological chemistry 279, 50930-50941.

Chung, W.S., Shin, C.H., Stainier, D.Y., 2008. Bmp2 signaling regulates the hepatic versus pancreatic fate decision. Developmental cell 15, 738-748.

Chung, W.S., Stainier, D.Y., 2008. Intra-endodermal interactions are required for pancreatic beta cell induction. Developmental cell 14, 582-593.

Cipolli, M., 2001. Shwachman-Diamond syndrome: clinical phenotypes. Pancreatology 1, 543-548.

Clark, K.J., Voytas, D.F., Ekker, S.C., 2011. A TALE of two nucleases: gene targeting for the masses? Zebrafish 8, 147-149.

Cmejla, R., Cmejlova, J., Handrkova, H., Petrak, J., Pospisilova, D., 2007. Ribosomal protein S17 gene (RPS17) is mutated in Diamond-Blackfan anemia. Human mutation 28, 1178-1182.

Collins, J.E., White, S., Searle, S.M., Stemple, D.L., 2012. Incorporating RNA-seq data into the zebrafish Ensembl genebuild. Genome research 22, 2067-2078.

Collombat, P., Hecksher-Sorensen, J., Broccoli, V., Krull, J., Ponte, I., Mundiger, T., Smith, J., Gruss, P., Serup, P., Mansouri, A., 2005. The simultaneous loss of Arx and Pax4 genes promotes a somatostatin-producing cell fate specification at the expense of the alpha- and beta-cell lineages in the mouse endocrine pancreas. Development 132, 2969-2980.

Collombat, P., Mansouri, A., Hecksher-Sorensen, J., Serup, P., Krull, J., Gradwohl, G., Gruss, P., 2003. Opposing actions of Arx and Pax4 in endocrine pancreas development. Genes & development 17, 2591-2603.

Collombat, P., Xu, X., Ravassard, P., Sosa-Pineda, B., Dussaud, S., Billestrup, N., Madsen, O.D., Serup, P., Heimberg, H., Mansouri, A., 2009. The ectopic expression of Pax4 in the mouse pancreas converts progenitor cells into alpha and subsequently beta cells. Cell 138, 449-462.

Culp, P., Nusslein-Volhard, C., Hopkins, N., 1991. High-frequency germ-line transmission of plasmid DNA sequences injected into fertilized zebrafish eggs. Proceedings of the National Academy of Sciences of the United States of America 88, 7953-7957.

Cvejic, A., Hall, C., Bak-Maier, M., Flores, M.V., Crosier, P., Redd, M.J., Martin, P., 2008. Analysis of WASp function during the wound inflammatory response--live-imaging studies in zebrafish larvae. Journal of cell science 121, 3196-3206.

Dai, M.S., Arnold, H., Sun, X.X., Sears, R., Lu, H., 2007. Inhibition of c-Myc activity by ribosomal protein L11. The EMBO journal 26, 3332-3345.

Dalgin, G., Ward, A.B., Hao le, T., Beattie, C.E., Nechiporuk, A., Prince, V.E., 2011. Zebrafish mnx1 controls cell fate choice in the developing endocrine pancreas. Development 138, 4597-4608.

Danilova, N., Sakamoto, K.M., Lin, S., 2008. Ribosomal protein S19 deficiency in zebrafish leads to developmental abnormalities and defective erythropoiesis through activation of p53 protein family. Blood 112, 5228-5237.

Danilova, N., Sakamoto, K.M., Lin, S., 2011. Ribosomal protein L11 mutation in zebrafish leads to haematopoietic and metabolic defects. British journal of haematology 152, 217-228.

Dauwerse, J.G., Dixon, J., Seland, S., Ruivenkamp, C.A., van Haeringen, A., Hoefsloot, L.H., Peters, D.J., Boers, A.C., Daumer-Haas, C., Maiwald, R., Zweier, C., Kerr, B., Cobo, A.M., Toral, J.F., Hoogeboom, A.J., Lohmann, D.R., Hehr, U., Dixon, M.J., Breuning, M.H., Wieczorek, D., 2011. Mutations in genes encoding subunits of RNA polymerases I and III cause Treacher Collins syndrome. Nature genetics 43, 20-22.

Davidson, A.E., Balciunas, D., Mohn, D., Shaffer, J., Hermanson, S., Sivasubbu, S., Cliff, M.P., Hackett, P.B., Ekker, S.C., 2003. Efficient gene delivery and gene expression in zebrafish using the Sleeping Beauty transposon. Developmental biology 263, 191-202.

Davuluri, G., Gong, W., Yusuff, S., Lorent, K., Muthumani, M., Dolan, A.C., Pack, M., 2008. Mutation of the zebrafish nucleoporin elys sensitizes tissue progenitors to replication stress. PLoS genetics 4, e1000240.

de Bruijn, E., Cuppen, E., Feitsma, H., 2009. Highly Efficient ENU Mutagenesis in Zebrafish. Methods Mol Biol 546, 3-12.

de Jong, J.L., Zon, L.I., 2005. Use of the zebrafish system to study primitive and definitive hematopoiesis. Annual review of genetics 39, 481-501.

de Jong-Curtain, T.A., Parslow, A.C., Trotter, A.J., Hall, N.E., Verkade, H., Tabone, T., Christie, E.L., Crowhurst, M.O., Layton, J.E., Shepherd, I.T., Nixon, S.J., Parton, R.G., Zon, L.I., Stainier, D.Y., Lieschke, G.J., Heath, J.K., 2009. Abnormal nuclear pore formation triggers apoptosis in the intestinal epithelium of elys-deficient zebrafish. Gastroenterology 136, 902-911.

de Pater, E., Clijsters, L., Marques, S.R., Lin, Y.F., Garavito-Aguilar, Z.V., Yelon, D., Bakkers, J., 2009. Distinct phases of cardiomyocyte differentiation regulate growth of the zebrafish heart. Development 136, 1633-1641.

Dennis, G., Jr., Sherman, B.T., Hosack, D.A., Yang, J., Gao, W., Lane, H.C., Lempicki, R.A., 2003. DAVID: Database for Annotation, Visualization, and Integrated Discovery. Genome biology 4, P3.

Devos, N., Deflorian, G., Biemar, F., Bortolussi, M., Martial, J.A., Peers, B., Argenton, F., 2002. Differential expression of two somatostatin genes during zebrafish embryonic development. Mechanisms of development 115, 133-137.

Dick, A., Mayr, T., Bauer, H., Meier, A., Hammerschmidt, M., 2000. Cloning and characterization of zebrafish smad2, smad3 and smad4. Gene 246, 69-80.

dilorio, P., Alexa, K., Choe, S.K., Etheridge, L., Sagerstrom, C.G., 2007. TALE-family homeodomain proteins regulate endodermal sonic hedgehog expression and pattern the anterior endoderm. Developmental biology 304, 221-231.

dilorio, P.J., Moss, J.B., Sbrogna, J.L., Karlstrom, R.O., Moss, L.G., 2002. Sonic hedgehog is required early in pancreatic islet development. Developmental biology 244, 75-84.

Dinman, J.D., Berry, M.J., 2007. Translational Control in Biology and Medicine. Cold Spring Harbor Laborator Press, New York.

Djiotsa, J., Verbruggen, V., Giacomotto, J., Ishibashi, M., Manning, E., Rinkwitz, S., Manfroid, I., Voz, M.L., Peers, B., 2012. Pax4 is not essential for beta-cell differentiation in zebrafish embryos but modulates alpha-cell generation by repressing arx gene expression. BMC developmental biology 12, 37.

Doherty, L., Sheen, M.R., Vlachos, A., Choesmel, V., O'Donohue, M.F., Clinton, C., Schneider, H.E., Sieff, C.A., Newburger, P.E., Ball, S.E., Niewiadomska, E., Matysiak, M., Glader, B., Arceci, R.J., Farrar, J.E., Atsidaftos, E., Lipton, J.M., Gleizes, P.E., Gazda, H.T., 2010. Ribosomal protein genes RPS10 and RPS26 are commonly mutated in Diamond-Blackfan anemia. American journal of human genetics 86, 222-228.

Donati, G., Brighenti, E., Vici, M., Mazzini, G., Trere, D., Montanaro, L., Derenzini, M., 2011. Selective inhibition of rRNA transcription downregulates E2F-1: a new p53-independent mechanism linking cell growth to cell proliferation. Journal of cell science 124, 3017-3028.

Donati, G., Montanaro, L., Derenzini, M., 2012. Ribosome biogenesis and control of cell proliferation: p53 is not alone. Cancer research 72, 1602-1607.

Dong, P.D., Munson, C.A., Norton, W., Crosnier, C., Pan, X., Gong, Z., Neumann, C.J., Stainier, D.Y., 2007. Fgf10 regulates hepatopancreatic ductal system patterning and differentiation. Nature genetics 39, 397-402.

Dong, P.D., Provost, E., Leach, S.D., Stainier, D.Y., 2008. Graded levels of Ptf1a differentially regulate endocrine and exocrine fates in the developing pancreas. Genes & development 22, 1445-1450.

Dooley, C.M., Scahill, C., Fenyes, F., Kettleborough, R.N., Stemple, D.L., Busch-Nentwich, E.M., 2013. Multi-allelic phenotyping - A systematic approach for the simultaneous analysis of multiple induced mutations. Methods.

Doseff, A.I., Arndt, K.T., 1995. LAS1 is an essential nuclear protein involved in cell morphogenesis and cell surface growth. Genetics 141, 857-871.

Dosil, M., Bustelo, X.R., 2004. Functional characterization of Pwp2, a WD family protein essential for the assembly of the 90 S pre-ribosomal particle. The Journal of biological chemistry 279, 37385-37397.

Dougan, S.T., Warga, R.M., Kane, D.A., Schier, A.F., Talbot, W.S., 2003. The role of the zebrafish nodal-related genes squint and cyclops in patterning of mesendoderm. Development 130, 1837-1851.

Dragon, F., Gallagher, J.E., Compagnone-Post, P.A., Mitchell, B.M., Porwancher, K.A., Wehner, K.A., Wormsley, S., Settlage, R.E., Shabanowitz, J., Osheim, Y., Beyer, A.L., Hunt, D.F., Baserga, S.J., 2002. A large nucleolar U3 ribonucleoprotein required for 18S ribosomal RNA biogenesis. Nature 417, 967-970.

Draptchinskaia, N., Gustavsson, P., Andersson, B., Pettersson, M., Willig, T.N., Dianzani, I., Ball, S., Tchernia, G., Klar, J., Matsson, H., Tentler, D., Mohandas, N., Carlsson, B., Dahl,

N., 1999. The gene encoding ribosomal protein S19 is mutated in Diamond-Blackfan anaemia. Nature genetics 21, 169-175.

Driever, W., Solnica-Krezel, L., Schier, A.F., Neuhauss, S.C., Malicki, J., Stemple, D.L., Stainier, D.Y., Zwartkruis, F., Abdelilah, S., Rangini, Z., Belak, J., Boggs, C., 1996. A genetic screen for mutations affecting embryogenesis in zebrafish. Development 123, 37-46.

Drygin, D., Rice, W.G., Grummt, I., 2010. The RNA polymerase I transcription machinery: an emerging target for the treatment of cancer. Annual review of pharmacology and toxicology 50, 131-156.

Du, A., Hunter, C.S., Murray, J., Noble, D., Cai, C.L., Evans, S.M., Stein, R., May, C.L., 2009. Islet-1 is required for the maturation, proliferation, and survival of the endocrine pancreas. Diabetes 58, 2059-2069.

Durie, P.R., 1996. Inherited and congenital disorders of the exocrine pancreas. The Gastroenterologist 4, 169-187.

Ebert, B.L., Pretz, J., Bosco, J., Chang, C.Y., Tamayo, P., Galili, N., Raza, A., Root, D.E., Attar, E., Ellis, S.R., Golub, T.R., 2008. Identification of RPS14 as a 5q- syndrome gene by RNA interference screen. Nature 451, 335-339.

Eisen, J.S., Smith, J.C., 2008. Controlling morpholino experiments: don't stop making antisense. Development 135, 1735-1743.

Emelyanov, A., Parinov, S., 2008. Mifepristone-inducible LexPR system to drive and control gene expression in transgenic zebrafish. Developmental biology 320, 113-121.

Eschrich, D., Buchhaupt, M., Kotter, P., Entian, K.D., 2002. Nep1p (Emg1p), a novel protein conserved in eukaryotes and archaea, is involved in ribosome biogenesis. Current genetics 40, 326-338.

Esni, F., Ghosh, B., Biankin, A.V., Lin, J.W., Albert, M.A., Yu, X., MacDonald, R.J., Civin, C.I., Real, F.X., Pack, M.A., Ball, D.W., Leach, S.D., 2004. Notch inhibits Ptf1 function and acinar cell differentiation in developing mouse and zebrafish pancreas. Development 131, 4213-4224.

Farrar, J.E., Nater, M., Caywood, E., McDevitt, M.A., Kowalski, J., Takemoto, C.M., Talbot, C.C., Jr., Meltzer, P., Esposito, D., Beggs, A.H., Schneider, H.E., Grabowska, A., Ball, S.E., Niewiadomska, E., Sieff, C.A., Vlachos, A., Atsidaftos, E., Ellis, S.R., Lipton, J.M., Gazda, H.T., Arceci, R.J., 2008. Abnormalities of the large ribosomal subunit protein, Rpl35a, in Diamond-Blackfan anemia. Blood 112, 1582-1592.

Favareto, F., Caprino, D., Micalizzi, C., Rosanda, C., Boeri, E., Mori, P.G., 1989. New clinical aspects of Pearson's syndrome. Report of three cases. Haematologica 74, 591-594.

Feil, R., Wagner, J., Metzger, D., Chambon, P., 1997. Regulation of Cre recombinase activity by mutated estrogen receptor ligand-binding domains. Biochemical and biophysical research communications 237, 752-757.

Feng, H., Langenau, D.M., Madge, J.A., Quinkertz, A., Gutierrez, A., Neuberg, D.S., Kanki, J.P., Look, A.T., 2007. Heat-shock induction of T-cell lymphoma/leukaemia in conditional Cre/lox-regulated transgenic zebrafish. British journal of haematology 138, 169-175.

Field, H.A., Dong, P.D., Beis, D., Stainier, D.Y., 2003a. Formation of the digestive system in zebrafish. II. Pancreas morphogenesis. Developmental biology 261, 197-208.

Field, H.A., Ober, E.A., Roeser, T., Stainier, D.Y., 2003b. Formation of the digestive system in zebrafish. I. Liver morphogenesis. Developmental biology 253, 279-290.

Finch, A.J., Hilcenko, C., Basse, N., Drynan, L.F., Goyenechea, B., Menne, T.F., Gonzalez Fernandez, A., Simpson, P., D'Santos, C.S., Arends, M.J., Donadieu, J., Bellanne-Chantelot, C., Costanzo, M., Boone, C., McKenzie, A.N., Freund, S.M., Warren, A.J., 2011. Uncoupling of GTP hydrolysis from eIF6 release on the ribosome causes Shwachman-Diamond syndrome. Genes & development 25, 917-929.

Fisher, S., Grice, E.A., Vinton, R.M., Bessling, S.L., Urasaki, A., Kawakami, K., McCallion, A.S., 2006. Evaluating the biological relevance of putative enhancers using Tol2 transposon-mediated transgenesis in zebrafish. Nature protocols 1, 1297-1305.

Flasse, L.C., Pirson, J.L., Stern, D.G., Von Berg, V., Manfroid, I., Peers, B., Voz, M.L., 2013. Ascl1b and Neurod1, instead of Neurog3, control pancreatic endocrine cell fate in zebrafish. BMC biology 11, 78.

Freed, E.F., Bleichert, F., Dutca, L.M., Baserga, S.J., 2010. When ribosomes go bad: diseases of ribosome biogenesis. Molecular bioSystems 6, 481-493.

Freed, E.F., Prieto, J.L., McCann, K.L., McStay, B., Baserga, S.J., 2012. NOL11, implicated in the pathogenesis of North American Indian childhood cirrhosis, is required for pre-rRNA transcription and processing. PLoS genetics 8, e1002892.

Freedman, S.D., Blanco, P., Shea, J.C., Alvarez, J.G., 2000. Mechanisms to explain pancreatic dysfunction in cystic fibrosis. The Medical clinics of North America 84, 657-664, x.

Fumagalli, S., Thomas, G., 2011. The role of p53 in ribosomopathies. Seminars in hematology 48, 97-105.

Gaiano, N., Allende, M., Amsterdam, A., Kawakami, K., Hopkins, N., 1996. Highly efficient germ-line transmission of proviral insertions in zebrafish. Proceedings of the National Academy of Sciences of the United States of America 93, 7777-7782.

Gallagher, J.E., Dunbar, D.A., Granneman, S., Mitchell, B.M., Osheim, Y., Beyer, A.L., Baserga, S.J., 2004. RNA polymerase I transcription and pre-rRNA processing are linked by specific SSU processome components. Genes & development 18, 2506-2517.

Gao, W., Xu, L., Guan, R., Liu, X., Han, Y., Wu, Q., Xiao, Y., Qi, F., Zhu, Z., Lin, S., Zhang, B., 2011. Wdr18 is required for Kupffer's vesicle formation and regulation of body asymmetry in zebrafish. PloS one 6, e23386.

Gartel, A.L., Radhakrishnan, S.K., 2005. Lost in transcription: p21 repression, mechanisms, and consequences. Cancer research 65, 3980-3985.

Gazda, H.T., Grabowska, A., Merida-Long, L.B., Latawiec, E., Schneider, H.E., Lipton, J.M., Vlachos, A., Atsidaftos, E., Ball, S.E., Orfali, K.A., Niewiadomska, E., Da Costa, L., Tchernia, G., Niemeyer, C., Meerpohl, J.J., Stahl, J., Schratt, G., Glader, B., Backer, K., Wong, C., Nathan, D.G., Beggs, A.H., Sieff, C.A., 2006. Ribosomal protein S24 gene is mutated in Diamond-Blackfan anemia. American journal of human genetics 79, 1110-1118.

Gazda, H.T., Preti, M., Sheen, M.R., O'Donohue, M.F., Vlachos, A., Davies, S.M., Kattamis, A., Doherty, L., Landowski, M., Buros, C., Ghazvinian, R., Sieff, C.A., Newburger, P.E., Niewiadomska, E., Matysiak, M., Glader, B., Atsidaftos, E., Lipton, J.M., Gleizes, P.E., Beggs, A.H., 2012. Frameshift mutation in p53 regulator RPL26 is associated with multiple physical abnormalities and a specific pre-ribosomal RNA processing defect in diamond-blackfan anemia. Human mutation 33, 1037-1044.

Gazda, H.T., Sheen, M.R., Vlachos, A., Choesmel, V., O'Donohue, M.F., Schneider, H., Darras, N., Hasman, C., Sieff, C.A., Newburger, P.E., Ball, S.E., Niewiadomska, E., Matysiak, M., Zaucha, J.M., Glader, B., Niemeyer, C., Meerpohl, J.J., Atsidaftos, E., Lipton, J.M., Gleizes, P.E., Beggs, A.H., 2008. Ribosomal protein L5 and L11 mutations are associated with cleft palate and abnormal thumbs in Diamond-Blackfan anemia patients. American journal of human genetics 83, 769-780.

Gelperin, D., Horton, L., Beckman, J., Hensold, J., Lemmon, S.K., 2001. Bms1p, a novel GTP-binding protein, and the related Tsr1p are required for distinct steps of 40S ribosome biogenesis in yeast. RNA 7, 1268-1283.

Georgala, P.A., Carr, C.B., Price, D.J., 2011. The role of Pax6 in forebrain development. Developmental neurobiology 71, 690-709.

Gittes, G.K., 2009. Developmental biology of the pancreas: a comprehensive review. Developmental biology 326, 4-35.

Glasgow, E., Tomarev, S.I., 1998. Restricted expression of the homeobox gene prox 1 in developing zebrafish. Mechanisms of development 76, 175-178.

Gnugge, L., Meyer, D., Driever, W., 2004. Pancreas development in zebrafish. Methods in cell biology 76, 531-551.

Godinho, L., Mumm, J.S., Williams, P.R., Schroeter, E.H., Koerber, A., Park, S.W., Leach, S.D., Wong, R.O., 2005. Targeting of amacrine cell neurites to appropriate synaptic laminae in the developing zebrafish retina. Development 132, 5069-5079.

Goessling, W., North, T.E., Lord, A.M., Ceol, C., Lee, S., Weidinger, G., Bourque, C., Strijbosch, R., Haramis, A.P., Puder, M., Clevers, H., Moon, R.T., Zon, L.I., 2008. APC mutant zebrafish uncover a changing temporal requirement for wnt signaling in liver development. Developmental biology 320, 161-174.

Goldfeder, M.B., Oliveira, C.C., 2010. Utp25p, a nucleolar Saccharomyces cerevisiae protein, interacts with U3 snoRNP subunits and affects processing of the 35S pre-rRNA. The FEBS journal 277, 2838-2852.

Golling, G., Amsterdam, A., Sun, Z., Antonelli, M., Maldonado, E., Chen, W., Burgess, S., Haldi, M., Artzt, K., Farrington, S., Lin, S.Y., Nissen, R.M., Hopkins, N., 2002. Insertional

mutagenesis in zebrafish rapidly identifies genes essential for early vertebrate development. Nature genetics 31, 135-140.

Gonzales, B., Henning, D., So, R.B., Dixon, J., Dixon, M.J., Valdez, B.C., 2005. The Treacher Collins syndrome (TCOF1) gene product is involved in pre-rRNA methylation. Human molecular genetics 14, 2035-2043.

Goobie, S., Popovic, M., Morrison, J., Ellis, L., Ginzberg, H., Boocock, G.R., Ehtesham, N., Betard, C., Brewer, C.G., Roslin, N.M., Hudson, T.J., Morgan, K., Fujiwara, T.M., Durie, P.R., Rommens, J.M., 2001. Shwachman-Diamond syndrome with exocrine pancreatic dysfunction and bone marrow failure maps to the centromeric region of chromosome 7. American journal of human genetics 68, 1048-1054.

Gradwohl, G., Dierich, A., LeMeur, M., Guillemot, F., 2000. neurogenin3 is required for the development of the four endocrine cell lineages of the pancreas. Proceedings of the National Academy of Sciences of the United States of America 97, 1607-1611.

Gripp, K.W., Curry, C., Olney, A.H., Sandoval, C., Fisher, J., Chong, J.X., Genomics, U.W.C.f.M., Pilchman, L., Sahraoui, R., Stabley, D.L., Sol-Church, K., 2014. Diamond-Blackfan anemia with mandibulofacial dystostosis is heterogeneous, including the novel DBA genes TSR2 and RPS28. American journal of medical genetics. Part A 164, 2240-2249.

Gritsman, K., Zhang, J., Cheng, S., Heckscher, E., Talbot, W.S., Schier, A.F., 1999. The EGF-CFC protein one-eyed pinhead is essential for nodal signaling. Cell 97, 121-132.

Haffter, P., Granato, M., Brand, M., Mullins, M.C., Hammerschmidt, M., Kane, D.A., Odenthal, J., van Eeden, F.J., Jiang, Y.J., Heisenberg, C.P., Kelsh, R.N., Furutani-Seiki, M., Vogelsang, E., Beuchle, D., Schach, U., Fabian, C., Nusslein-Volhard, C., 1996. The identification of genes with unique and essential functions in the development of the zebrafish, Danio rerio. Development 123, 1-36.

Halpern, M.E., Rhee, J., Goll, M.G., Akitake, C.M., Parsons, M., Leach, S.D., 2008. Gal4/UAS transgenic tools and their application to zebrafish. Zebrafish 5, 97-110.

Hans, S., Kaslin, J., Freudenreich, D., Brand, M., 2009. Temporally-controlled site-specific recombination in zebrafish. PloS one 4, e4640.

Hardy, M.E., Ross, L.V., Chien, C.B., 2007. Focal gene misexpression in zebrafish embryos induced by local heat shock using a modified soldering iron. Developmental dynamics : an official publication of the American Association of Anatomists 236, 3071-3076.

Harris, C.C., 1996. Structure and function of the p53 tumor suppressor gene: clues for rational cancer therapeutic strategies. Journal of the National Cancer Institute 88, 1442-1455.

Harris, M.A., Clark, J., Ireland, A., Lomax, J., Ashburner, M., Foulger, R., Eilbeck, K., Lewis, S., Marshall, B., Mungall, C., Richter, J., Rubin, G.M., Blake, J.A., Bult, C., Dolan, M., Drabkin, H., Eppig, J.T., Hill, D.P., Ni, L., Ringwald, M., Balakrishnan, R., Cherry, J.M., Christie, K.R., Costanzo, M.C., Dwight, S.S., Engel, S., Fisk, D.G., Hirschman, J.E., Hong, E.L., Nash, R.S., Sethuraman, A., Theesfeld, C.L., Botstein, D., Dolinski, K., Feierbach, B., Berardini, T., Mundodi, S., Rhee, S.Y., Apweiler, R., Barrell, D., Camon, E., Dimmer, E., Lee, V., Chisholm, R., Gaudet, P., Kibbe, W., Kishore, R., Schwarz, E.M., Sternberg, P., Gwinn,

M., Hannick, L., Wortman, J., Berriman, M., Wood, V., de la Cruz, N., Tonellato, P., Jaiswal, P., Seigfried, T., White, R., 2004. The Gene Ontology (GO) database and informatics resource. Nucleic acids research 32, D258-261.

Harrison, K.A., Thaler, J., Pfaff, S.L., Gu, H., Kehrl, J.H., 1999. Pancreas dorsal lobe agenesis and abnormal islets of Langerhans in Hlxb9-deficient mice. Nature genetics 23, 71-75.

Harscoet, E., Dubreucq, B., Palauqui, J.C., Lepiniec, L., 2010. NOF1 encodes an Arabidopsis protein involved in the control of rRNA expression. PloS one 5, e12829.

Harvey, S.A., Sealy, I., Kettleborough, R., Fenyes, F., White, R., Stemple, D., Smith, J.C., 2013. Identification of the zebrafish maternal and paternal transcriptomes. Development 140, 2703-2710.

Hatta, K., Kimmel, C.B., Ho, R.K., Walker, C., 1991. The cyclops mutation blocks specification of the floor plate of the zebrafish central nervous system. Nature 350, 339-341.

He, H., Sun, Y., 2007. Ribosomal protein S27L is a direct p53 target that regulates apoptosis. Oncogene 26, 2707-2716.

Heijnen, H.F., van Wijk, R., Pereboom, T.C., Goos, Y.J., Seinen, C.W., van Oirschot, B.A., van Dooren, R., Gastou, M., Giles, R.H., van Solinge, W., Kuijpers, T.W., Gazda, H.T., Bierings, M.B., Da Costa, L., MacInnes, A.W., 2014. Ribosomal protein mutations induce autophagy through S6 kinase inhibition of the insulin pathway. PLoS genetics 10, e1004371.

Heindl, K., Martinez, J., 2010. Nol9 is a novel polynucleotide 5'-kinase involved in ribosomal RNA processing. The EMBO journal 29, 4161-4171.

Heiss, N.S., Knight, S.W., Vulliamy, T.J., Klauck, S.M., Wiemann, S., Mason, P.J., Poustka, A., Dokal, I., 1998. X-linked dyskeratosis congenita is caused by mutations in a highly conserved gene with putative nucleolar functions. Nature genetics 19, 32-38.

Heller, R.S., Jenny, M., Collombat, P., Mansouri, A., Tomasetto, C., Madsen, O.D., Mellitzer, G., Gradwohl, G., Serup, P., 2005. Genetic determinants of pancreatic epsilon-cell development. Developmental biology 286, 217-224.

Heller, R.S., Stoffers, D.A., Liu, A., Schedl, A., Crenshaw, E.B., 3rd, Madsen, O.D., Serup, P., 2004. The role of Brn4/Pou3f4 and Pax6 in forming the pancreatic glucagon cell identity. Developmental biology 268, 123-134.

Henseleit, K.D., Nelson, S.B., Kuhlbrodt, K., Hennings, J.C., Ericson, J., Sander, M., 2005. NKX6 transcription factor activity is required for alpha- and beta-cell development in the pancreas. Development 132, 3139-3149.

Her, G.M., Chiang, C.C., Chen, W.Y., Wu, J.L., 2003. In vivo studies of liver-type fatty acid binding protein (L-FABP) gene expression in liver of transgenic zebrafish (Danio rerio). FEBS letters 538, 125-133.

Herbert, T.P., Proud, C.G., 2007. Translational Control In Biology and Medicine. Cold Spring Harbor Laboratory Press, New York.

Hesselson, D., Anderson, R.M., Stainier, D.Y., 2011. Suppression of Ptf1a activity induces acinar-to-endocrine conversion. Current biology : CB 21, 712-717.

Hildebrand, H., Borgstrom, B., Bekassy, A., Erlanson-Albertsson, C., Helin, I., 1982. Isolated co-lipase deficiency in two brothers. Gut 23, 243-246.

Hinits, Y., Osborn, D.P., Hughes, S.M., 2009. Differential requirements for myogenic regulatory factors distinguish medial and lateral somitic, cranial and fin muscle fibre populations. Development 136, 403-414.

Ho, R.K., Kane, D.A., 1990. Cell-autonomous action of zebrafish spt-1 mutation in specific mesodermal precursors. Nature 348, 728-730.

Holmberg Olausson, K.N., M.; Lindström, M.S., 2012. p53 -Dependent and -Independent Nucleolar Stress Responses. Cells 1, 774-798.

Howe, K., Clark, M.D., Torroja, C.F., Torrance, J., Berthelot, C., Muffato, M., Collins, J.E., Humphray, S., McLaren, K., Matthews, L., McLaren, S., Sealy, I., Caccamo, M., Churcher, C., Scott, C., Barrett, J.C., Koch, R., Rauch, G.J., White, S., Chow, W., Kilian, B., Quintais, L.T., Guerra-Assuncao, J.A., Zhou, Y., Gu, Y., Yen, J., Vogel, J.H., Eyre, T., Redmond, S., Banerjee, R., Chi, J., Fu, B., Langley, E., Maguire, S.F., Laird, G.K., Lloyd, D., Kenyon, E., Donaldson, S., Sehra, H., Almeida-King, J., Loveland, J., Trevanion, S., Jones, M., Quail, M., Willey, D., Hunt, A., Burton, J., Sims, S., McLay, K., Plumb, B., Davis, J., Clee, C., Oliver, K., Clark, R., Riddle, C., Eliott, D., Threadgold, G., Harden, G., Ware, D., Mortimer, B., Kerry, G., Heath, P., Phillimore, B., Tracey, A., Corby, N., Dunn, M., Johnson, C., Wood, J., Clark, S., Pelan, S., Griffiths, G., Smith, M., Glithero, R., Howden, P., Barker, N., Stevens, C., Harley, J., Holt, K., Panagiotidis, G., Lovell, J., Beasley, H., Henderson, C., Gordon, D., Auger, K., Wright, D., Collins, J., Raisen, C., Dyer, L., Leung, K., Robertson, L., Ambridge, K., Leongamornlert, D., McGuire, S., Gilderthorp, R., Griffiths, C., Manthravadi, D., Nichol, S., Barker, G., Whitehead, S., Kay, M., Brown, J., Murnane, C., Gray, E., Humphries, M., Sycamore, N., Barker, D., Saunders, D., Wallis, J., Babbage, A., Hammond, S., Mashreghi-Mohammadi, M., Barr, L., Martin, S., Wray, P., Ellington, A., Matthews, N., Ellwood, M., Woodmansey, R., Clark, G., Cooper, J., Tromans, A., Grafham, D., Skuce, C., Pandian, R., Andrews, R., Harrison, E., Kimberley, A., Garnett, J., Fosker, N., Hall, R., Garner, P., Kelly, D., Bird, C., Palmer, S., Gehring, I., Berger, A., Dooley, C.M., Ersan-Urun, Z., Eser, C., Geiger, H., Geisler, M., Karotki, L., Kirn, A., Konantz, J., Konantz, M., Oberlander, M., Rudolph-Geiger, S., Teucke, M., Osoegawa, K., Zhu, B., Rapp, A., Widaa, S., Langford, C., Yang, F., Carter, N.P., Harrow, J., Ning, Z., Herrero, J., Searle, S.M., Enright, A., Geisler, R., Plasterk, R.H., Lee, C., Westerfield, M., de Jong, P.J., Zon, L.I., Postlethwait, J.H., Nusslein-Volhard, C., Hubbard, T.J., Roest Crollius, H., Rogers, J., Stemple, D.L., 2013. The zebrafish reference genome sequence and its relationship to the human genome. Nature 496, 498-503.

Huang, C.J., Jou, T.S., Ho, Y.L., Lee, W.H., Jeng, Y.T., Hsieh, F.J., Tsai, H.J., 2005. Conditional expression of a myocardium-specific transgene in zebrafish transgenic lines. Developmental dynamics : an official publication of the American Association of Anatomists 233, 1294-1303.

Huang da, W., Sherman, B.T., Lempicki, R.A., 2009a. Bioinformatics enrichment tools: paths toward the comprehensive functional analysis of large gene lists. Nucleic acids research 37, 1-13.

Huang da, W., Sherman, B.T., Lempicki, R.A., 2009b. Systematic and integrative analysis of large gene lists using DAVID bioinformatics resources. Nature protocols 4, 44-57.

Huang, H., Liu, N., Lin, S., 2001. Pdx-1 knockdown reduces insulin promoter activity in zebrafish. Genesis 30, 134-136.

Huang, P., Zhu, Z., Lin, S., Zhang, B., 2012. Reverse genetic approaches in zebrafish. Journal of genetics and genomics = Yi chuan xue bao 39, 421-433.

Huang, W., Wang, G., Delaspre, F., Vitery Mdel, C., Beer, R.L., Parsons, M.J., 2014. Retinoic acid plays an evolutionarily conserved and biphasic role in pancreas development. Developmental biology 394, 83-93.

Hwang, W.Y., Fu, Y., Reyon, D., Maeder, M.L., Tsai, S.Q., Sander, J.D., Peterson, R.T., Yeh, J.R., Joung, J.K., 2013. Efficient genome editing in zebrafish using a CRISPR-Cas system. Nature biotechnology 31, 227-229.

Iadevaia, V., Caldarola, S., Biondini, L., Gismondi, A., Karlsson, S., Dianzani, I., Loreni, F., 2010. PIM1 kinase is destabilized by ribosomal stress causing inhibition of cell cycle progression. Oncogene 29, 5490-5499.

Iadevaia, V., Zhang, Z., Jan, E., Proud, C.G., 2012. mTOR signaling regulates the processing of pre-rRNA in human cells. Nucleic acids research 40, 2527-2539.

Ibrahim, A.F., Hedley, P.E., Cardle, L., Kruger, W., Marshall, D.F., Muehlbauer, G.J., Waugh, R., 2005. A comparative analysis of transcript abundance using SAGE and Affymetrix arrays. Functional & integrative genomics 5, 163-174.

Imrie, J.R., Fagan, D.G., Sturgess, J.M., 1979. Quantitative evaluation of the development of the exocrine pancreas in cystic fibrosis and control infants. The American journal of pathology 95, 697-708.

Indra, A.K., Warot, X., Brocard, J., Bornert, J.M., Xiao, J.H., Chambon, P., Metzger, D., 1999. Temporally-controlled site-specific mutagenesis in the basal layer of the epidermis: comparison of the recombinase activity of the tamoxifen-inducible Cre-ER(T) and Cre-ER(T2) recombinases. Nucleic acids research 27, 4324-4327.

Ip, W.F., Dupuis, A., Ellis, L., Beharry, S., Morrison, J., Stormon, M.O., Corey, M., Rommens, J.M., Durie, P.R., 2002. Serum pancreatic enzymes define the pancreatic phenotype in patients with Shwachman-Diamond syndrome. The Journal of pediatrics 141, 259-265.

Ivics, Z., Hackett, P.B., Plasterk, R.H., Izsvak, Z., 1997. Molecular reconstruction of Sleeping Beauty, a Tc1-like transposon from fish, and its transposition in human cells. Cell 91, 501-510.

Jackson, R.J., Hellen, C.U., Pestova, T.V., 2010. The mechanism of eukaryotic translation initiation and principles of its regulation. Nature reviews. Molecular cell biology 11, 113-127.

Jansen, G., Hazendonk, E., Thijssen, K.L., Plasterk, R.H., 1997. Reverse genetics by chemical mutagenesis in Caenorhabditis elegans. Nature genetics 17, 119-121.

Jefferies, H.B., Fumagalli, S., Dennis, P.B., Reinhard, C., Pearson, R.B., Thomas, G., 1997. Rapamycin suppresses 5'TOP mRNA translation through inhibition of p70s6k. The EMBO journal 16, 3693-3704.

Jia, Q., Zhang, Q., Zhang, Z., Wang, Y., Zhang, W., Zhou, Y., Wan, Y., Cheng, T., Zhu, X., Fang, X., Yuan, W., Jia, H., 2013. Transcriptome Analysis of the Zebrafish Model of Diamond-Blackfan Anemia from RPS19 Deficiency via p53-Dependent and -Independent Pathways. PloS one 8, e71782.

Jiang, Z., Song, J., Qi, F., Xiao, A., An, X., Liu, N.A., Zhu, Z., Zhang, B., Lin, S., 2008. Exdpf is a key regulator of exocrine pancreas development controlled by retinoic acid and ptf1a in zebrafish. PLoS biology 6, e293.

Jin, S.B., Zhao, J., Bjork, P., Schmekel, K., Ljungdahl, P.O., Wieslander, L., 2002. Mrd1p is required for processing of pre-rRNA and for maintenance of steady-state levels of 40 S ribosomal subunits in yeast. The Journal of biological chemistry 277, 18431-18439.

Jinek, M., Chylinski, K., Fonfara, I., Hauer, M., Doudna, J.A., Charpentier, E., 2012. A programmable dual-RNA-guided DNA endonuclease in adaptive bacterial immunity. Science 337, 816-821.

Jones, N.C., Lynn, M.L., Gaudenz, K., Sakai, D., Aoto, K., Rey, J.P., Glynn, E.F., Ellington, L., Du, C., Dixon, J., Dixon, M.J., Trainor, P.A., 2008. Prevention of the neurocristopathy Treacher Collins syndrome through inhibition of p53 function. Nature medicine 14, 125-133.

Jones, N.L., Hofley, P.M., Durie, P.R., 1994. Pathophysiology of the pancreatic defect in Johanson-Blizzard syndrome: a disorder of acinar development. The Journal of pediatrics 125, 406-408.

Jonsson, J., Carlsson, L., Edlund, T., Edlund, H., 1994. Insulin-promoter-factor 1 is required for pancreas development in mice. Nature 371, 606-609.

Kanehisa, M., Goto, S., 2000. KEGG: kyoto encyclopedia of genes and genomes. Nucleic acids research 28, 27-30.

Kawaguchi, Y., Cooper, B., Gannon, M., Ray, M., MacDonald, R.J., Wright, C.V., 2002. The role of the transcriptional regulator Ptf1a in converting intestinal to pancreatic progenitors. Nature genetics 32, 128-134.

Kawakami, K., 2007. Tol2: a versatile gene transfer vector in vertebrates. Genome biology 8 Suppl 1, S7.

Kawakami, K., Shima, A., Kawakami, N., 2000. Identification of a functional transposase of the Tol2 element, an Ac-like element from the Japanese medaka fish, and its transposition in the zebrafish germ lineage. Proceedings of the National Academy of Sciences of the United States of America 97, 11403-11408.

Kawakami, K., Takeda, H., Kawakami, N., Kobayashi, M., Matsuda, N., Mishina, M., 2004. A transposon-mediated gene trap approach identifies developmentally regulated genes in zebrafish. Developmental cell 7, 133-144.

Kelly, A., Hurlstone, A.F., 2011. The use of RNAi technologies for gene knockdown in zebrafish. Briefings in functional genomics 10, 189-196.

Kettleborough, R.N., Bruijn, E., Eeden, F., Cuppen, E., Stemple, D.L., 2011. High-throughput target-selected gene inactivation in zebrafish. Methods in cell biology 104, 121-127.

Kettleborough, R.N., Busch-Nentwich, E.M., Harvey, S.A., Dooley, C.M., de Bruijn, E., van Eeden, F., Sealy, I., White, R.J., Herd, C., Nijman, I.J., Fenyes, F., Mehroke, S., Scahill, C., Gibbons, R., Wali, N., Carruthers, S., Hall, A., Yen, J., Cuppen, E., Stemple, D.L., 2013. A systematic genome-wide analysis of zebrafish protein-coding gene function. Nature 496, 494-497.

Kikuchi, Y., Trinh, L.A., Reiter, J.F., Alexander, J., Yelon, D., Stainier, D.Y., 2000. The zebrafish bonnie and clyde gene encodes a Mix family homeodomain protein that regulates the generation of endodermal precursors. Genes & development 14, 1279-1289.

Kikuchi, Y., Verkade, H., Reiter, J.F., Kim, C.H., Chitnis, A.B., Kuroiwa, A., Stainier, D.Y., 2004. Notch signaling can regulate endoderm formation in zebrafish. Developmental dynamics : an official publication of the American Association of Anatomists 229, 756-762.

Kim, H.J., Sumanas, S., Palencia-Desai, S., Dong, Y., Chen, J.N., Lin, S., 2006. Genetic analysis of early endocrine pancreas formation in zebrafish. Mol Endocrinol 20, 194-203.

Kimmel, C.B., 1989. Genetics and early development of zebrafish. Trends in genetics : TIG 5, 283-288.

Kimmel, C.B., Ballard, W.W., Kimmel, S.R., Ullmann, B., Schilling, T.F., 1995. Stages of embryonic development of the zebrafish. Developmental dynamics : an official publication of the American Association of Anatomists 203, 253-310.

Kimmel, R.A., Onder, L., Wilfinger, A., Ellertsdottir, E., Meyer, D., 2011. Requirement for Pdx1 in specification of latent endocrine progenitors in zebrafish. BMC biology 9, 75.

Kimura, S.H., Ikawa, M., Ito, A., Okabe, M., Nojima, H., 2001. Cyclin G1 is involved in G2/M arrest in response to DNA damage and in growth control after damage recovery. Oncogene 20, 3290-3300.

Kinkel, M.D., Eames, S.C., Alonzo, M.R., Prince, V.E., 2008. Cdx4 is required in the endoderm to localize the pancreas and limit beta-cell number. Development 135, 919-929.

Kinkel, M.D., Prince, V.E., 2009. On the diabetic menu: zebrafish as a model for pancreas development and function. BioEssays : news and reviews in molecular, cellular and developmental biology 31, 139-152.

Knight, R.D., Mebus, K., d'Angelo, A., Yokoya, K., Heanue, T., Roehl, H., 2011. Ret signalling integrates a craniofacial muscle module during development. Development 138, 2015-2024.

Knoll-Gellida, A., Andre, M., Gattegno, T., Forgue, J., Admon, A., Babin, P.J., 2006. Molecular phenotype of zebrafish ovarian follicle by serial analysis of gene expression and proteomic profiling, and comparison with the transcriptomes of other animals. BMC genomics 7, 46.

Ko, M.S., 2001. Embryogenomics: developmental biology meets genomics. Trends in biotechnology 19, 511-518.

Korzh, S., Emelyanov, A., Korzh, V., 2001. Developmental analysis of ceruloplasmin gene and liver formation in zebrafish. Mechanisms of development 103, 137-139.

Kotani, T., Nagayoshi, S., Urasaki, A., Kawakami, K., 2006. Transposon-mediated gene trapping in zebrafish. Methods 39, 199-206.

Krapp, A., Knofler, M., Ledermann, B., Burki, K., Berney, C., Zoerkler, N., Hagenbuchle, O., Wellauer, P.K., 1998. The bHLH protein PTF1-p48 is essential for the formation of the exocrine and the correct spatial organization of the endocrine pancreas. Genes & development 12, 3752-3763.

Kressler, D., Hurt, E., Bassler, J., 2010. Driving ribosome assembly. Biochimica et biophysica acta 1803, 673-683.

Kruidering, M., Evan, G.I., 2000. Caspase-8 in apoptosis: the beginning of "the end"? IUBMB life 50, 85-90.

Lafontaine, D.L.J., Tollervey, D., 2006. Ribosomal RNA. In: eLS. John Wiley & Sons, Ltd: Chichester.

Lamont, R.E., Loredo-Osti, J., Roslin, N.M., Mauthe, J., Coghlan, G., Nylen, E., Frappier, D., Innes, A.M., Lemire, E.G., Lowry, R.B., Greenberg, C.R., Triggs-Raine, B.L., Morgan, K., Wrogemann, K., Fujiwara, T.M., Zelinski, T., 2005. A locus for Bowen-Conradi syndrome maps to chromosome region 12p13.3. American journal of medical genetics. Part A 132A, 136-143.

Lancman, J.J., Zvenigorodsky, N., Gates, K.P., Zhang, D., Solomon, K., Humphrey, R.K., Kuo, T., Setiawan, L., Verkade, H., Chi, Y.I., Jhala, U.S., Wright, C.V., Stainier, D.Y., Dong, P.D., 2013. Specification of hepatopancreas progenitors in zebrafish by hnf1ba and wnt2bb. Development 140, 2669-2679.

Landowski, M., O'Donohue, M.F., Buros, C., Ghazvinian, R., Montel-Lehry, N., Vlachos, A., Sieff, C.A., Newburger, P.E., Niewiadomska, E., Matysiak, M., Glader, B., Atsidaftos, E., Lipton, J.M., Beggs, A.H., Gleizes, P.E., Gazda, H.T., 2013. Novel deletion of RPL15 identified by array-comparative genomic hybridization in Diamond-Blackfan anemia. Human genetics 132, 1265-1274.

Lane, D.P., 1992. Cancer. p53, guardian of the genome. Nature 358, 15-16.

Langenau, D.M., Feng, H., Berghmans, S., Kanki, J.P., Kutok, J.L., Look, A.T., 2005. Cre/lox-regulated transgenic zebrafish model with conditional myc-induced T cell acute lymphoblastic leukemia. Proceedings of the National Academy of Sciences of the United States of America 102, 6068-6073.

Langenau, D.M., Keefe, M.D., Storer, N.Y., Guyon, J.R., Kutok, J.L., Le, X., Goessling, W., Neuberg, D.S., Kunkel, L.M., Zon, L.I., 2007. Effects of RAS on the genesis of embryonal rhabdomyosarcoma. Genes & development 21, 1382-1395.

Laue, K., Janicke, M., Plaster, N., Sonntag, C., Hammerschmidt, M., 2008. Restriction of retinoic acid activity by Cyp26b1 is required for proper timing and patterning of osteogenesis during zebrafish development. Development 135, 3775-3787.

Le, X., Langenau, D.M., Keefe, M.D., Kutok, J.L., Neuberg, D.S., Zon, L.I., 2007. Heat shock-inducible Cre/Lox approaches to induce diverse types of tumors and hyperplasia in transgenic zebrafish. Proceedings of the National Academy of Sciences of the United States of America 104, 9410-9415.

Lee, R.C., Feinbaum, R.L., Ambros, V., 1993. The C. elegans heterochronic gene lin-4 encodes small RNAs with antisense complementarity to lin-14. Cell 75, 843-854.

Leulliot, N., Bohnsack, M.T., Graille, M., Tollervey, D., Van Tilbeurgh, H., 2008. The yeast ribosome synthesis factor Emg1 is a novel member of the superfamily of alpha/beta knot fold methyltransferases. Nucleic acids research 36, 629-639.

Lewis, J.D., Tollervey, D., 2000. Like attracts like: getting RNA processing together in the nucleus. Science 288, 1385-1389.

Li, H., Arber, S., Jessell, T.M., Edlund, H., 1999. Selective agenesis of the dorsal pancreas in mice lacking homeobox gene Hlxb9. Nature genetics 23, 67-70.

Li, H., Durbin, R., 2009. Fast and accurate short read alignment with Burrows-Wheeler transform. Bioinformatics 25, 1754-1760.

Li, J., Tan, J., Zhuang, L., Banerjee, B., Yang, X., Chau, J.F., Lee, P.L., Hande, M.P., Li, B., Yu, Q., 2007. Ribosomal protein S27-like, a p53-inducible modulator of cell fate in response to genotoxic stress. Cancer research 67, 11317-11326.

Lin, S., Gaiano, N., Culp, P., Burns, J.C., Friedmann, T., Yee, J.K., Hopkins, N., 1994. Integration and germ-line transmission of a pseudotyped retroviral vector in zebrafish. Science 265, 666-669.

Lin, Y.Y., White, R.J., Torelli, S., Cirak, S., Muntoni, F., Stemple, D.L., 2011. Zebrafish Fukutin family proteins link the unfolded protein response with dystroglycanopathies. Human molecular genetics 20, 1763-1775.

Lipton, J.M., Ellis, S.R., 2009. Diamond-Blackfan anemia: diagnosis, treatment, and molecular pathogenesis. Hematology/oncology clinics of North America 23, 261-282.

Liu, J., Hunter, C.S., Du, A., Ediger, B., Walp, E., Murray, J., Stein, R., May, C.L., 2011. Islet-1 regulates Arx transcription during pancreatic islet alpha-cell development. The Journal of biological chemistry 286, 15352-15360.

Liu, J., Walp, E.R., May, C.L., 2012. Elevation of transcription factor Islet-1 levels in vivo increases beta-cell function but not beta-cell mass. Islets 4, 199-206.

Liu, J.M., Lipton, J.M., Ellis, S.R., 2013. Genetics of Ribosomopathies. In: eLS. John Wiley & Sons, Ltd: Chichester.

Liu, P.C., Thiele, D.J., 2001. Novel stress-responsive genes EMG1 and NOP14 encode conserved, interacting proteins required for 40S ribosome biogenesis. Molecular biology of the cell 12, 3644-3657.

Liu, X., Kim, C.N., Yang, J., Jemmerson, R., Wang, X., 1996. Induction of apoptotic program in cell-free extracts: requirement for dATP and cytochrome c. Cell 86, 147-157.

Ludwig, L.S., Gazda, H.T., Eng, J.C., Eichhorn, S.W., Thiru, P., Ghazvinian, R., George, T.I., Gotlib, J.R., Beggs, A.H., Sieff, C.A., Lodish, H.F., Lander, E.S., Sankaran, V.G., 2014. Altered translation of GATA1 in Diamond-Blackfan anemia. Nature medicine 20, 748-753.

Lunde, K., Belting, H.G., Driever, W., 2004. Zebrafish pou5f1/pou2, homolog of mammalian Oct4, functions in the endoderm specification cascade. Current biology : CB 14, 48-55.

Mack, D.R., Forstner, G.G., Wilschanski, M., Freedman, M.H., Durie, P.R., 1996. Shwachman syndrome: exocrine pancreatic dysfunction and variable phenotypic expression. Gastroenterology 111, 1593-1602.

Mahlaoui, N., Minard-Colin, V., Picard, C., Bolze, A., Ku, C.L., Tournilhac, O., Gilbert-Dussardier, B., Pautard, B., Durand, P., Devictor, D., Lachassinne, E., Guillois, B., Morin, M., Gouraud, F., Valensi, F., Fischer, A., Puel, A., Abel, L., Bonnet, D., Casanova, J.L., 2011. Isolated congenital asplenia: a French nationwide retrospective survey of 20 cases. The Journal of pediatrics 158, 142-148, 148 e141.

Manfroid, I., Delporte, F., Baudhuin, A., Motte, P., Neumann, C.J., Voz, M.L., Martial, J.A., Peers, B., 2007. Reciprocal endoderm-mesoderm interactions mediated by fgf24 and fgf10 govern pancreas development. Development 134, 4011-4021.

Manfroid, I., Ghaye, A., Naye, F., Detry, N., Palm, S., Pan, L., Ma, T.P., Huang, W., Rovira, M., Martial, J.A., Parsons, M.J., Moens, C.B., Voz, M.L., Peers, B., 2012. Zebrafish sox9b is crucial for hepatopancreatic duct development and pancreatic endocrine cell regeneration. Developmental biology 366, 268-278.

Marioni, J.C., Mason, C.E., Mane, S.M., Stephens, M., Gilad, Y., 2008. RNA-seq: an assessment of technical reproducibility and comparison with gene expression arrays. Genome research 18, 1509-1517.

Markmiller, S., Cloonan, N., Lardelli, R.M., Doggett, K., Keightley, M.C., Boglev, Y., Trotter, A.J., Ng, A.Y., Wilkins, S.J., Verkade, H., Ober, E.A., Field, H.A., Grimmond, S.M., Lieschke, G.J., Stainier, D.Y., Heath, J.K., 2014. Minor class splicing shapes the zebrafish transcriptome during development. Proceedings of the National Academy of Sciences of the United States of America 111, 3062-3067.

Marneros, A.G., 2013. BMS1 is mutated in aplasia cutis congenita. PLoS genetics 9, e1003573.

Martin, S.E., Caplen, N.J., 2007. Applications of RNA interference in mammalian systems. Annual review of genomics and human genetics 8, 81-108.

Mathavan, S., Lee, S.G., Mak, A., Miller, L.D., Murthy, K.R., Govindarajan, K.R., Tong, Y., Wu, Y.L., Lam, S.H., Yang, H., Ruan, Y., Korzh, V., Gong, Z., Liu, E.T., Lufkin, T., 2005.

Transcriptome analysis of zebrafish embryogenesis using microarrays. PLoS genetics 1, 260-276.

Matthews, R.P., Lorent, K., Manoral-Mobias, R., Huang, Y., Gong, W., Murray, I.V., Blair, I.A., Pack, M., 2009. TNFalpha-dependent hepatic steatosis and liver degeneration caused by mutation of zebrafish S-adenosylhomocysteine hydrolase. Development 136, 865-875.

Mavropoulos, A., Devos, N., Biemar, F., Zecchin, E., Argenton, F., Edlund, H., Motte, P., Martial, J.A., Peers, B., 2005. sox4b is a key player of pancreatic alpha cell differentiation in zebrafish. Developmental biology 285, 211-223.

Mayer, A.N., Fishman, M.C., 2003. Nil per os encodes a conserved RNA recognition motif protein required for morphogenesis and cytodifferentiation of digestive organs in zebrafish. Development 130, 3917-3928.

Mayer, C., Grummt, I., 2006. Ribosome biogenesis and cell growth: mTOR coordinates transcription by all three classes of nuclear RNA polymerases. Oncogene 25, 6384-6391.

McCallum, C.M., Comai, L., Greene, E.A., Henikoff, S., 2000. Targeted screening for induced mutations. Nature biotechnology 18, 455-457.

McCann, K.L., Baserga, S.J., 2013. Genetics. Mysterious ribosomopathies. Science 341, 849-850.

Menne, T.F., Goyenechea, B., Sanchez-Puig, N., Wong, C.C., Tonkin, L.M., Ancliff, P.J., Brost, R.L., Costanzo, M., Boone, C., Warren, A.J., 2007. The Shwachman-Bodian-Diamond syndrome protein mediates translational activation of ribosomes in yeast. Nature genetics 39, 486-495.

Metzger, D., Clifford, J., Chiba, H., Chambon, P., 1995. Conditional site-specific recombination in mammalian cells using a ligand-dependent chimeric Cre recombinase. Proceedings of the National Academy of Sciences of the United States of America 92, 6991-6995.

Meyer, A., Schartl, M., 1999. Gene and genome duplications in vertebrates: the one-to-four (-to-eight in fish) rule and the evolution of novel gene functions. Current opinion in cell biology 11, 699-704.

Mikkola, H.K., Orkin, S.H., 2005. Gene targeting and transgenic strategies for the analysis of hematopoietic development in the mouse. Methods in molecular medicine 105, 3-22.

Milewski, W.M., Duguay, S.J., Chan, S.J., Steiner, D.F., 1998. Conservation of PDX-1 structure, function, and expression in zebrafish. Endocrinology 139, 1440-1449.

Mirabello, L., Macari, E.R., Jessop, L., Ellis, S.R., Myers, T., Giri, N., Taylor, A.M., McGrath, K.E., Humphries, J.M., Ballew, B.J., Yeager, M., Boland, J.F., He, J., Hicks, B.D., Burdett, L., Alter, B.P., Zon, L., Savage, S.A., 2014. Whole-exome sequencing and functional studies identify RPS29 as a novel gene mutated in multicase Diamond-Blackfan anemia families. Blood 124, 24-32.

Misra, R.P., Duncan, S.A., 2002. Gene targeting in the mouse: advances in introduction of transgenes into the genome by homologous recombination. Endocrine 19, 229-238.

Molven, A., Wright, C.V., Bremiller, R., De Robertis, E.M., Kimmel, C.B., 1990. Expression of a homeobox gene product in normal and mutant zebrafish embryos: evolution of the tetrapod body plan. Development 109, 279-288.

Mudumana, S.P., Wan, H., Singh, M., Korzh, V., Gong, Z., 2004. Expression analyses of zebrafish transferrin, ifabp, and elastaseB mRNAs as differentiation markers for the three major endodermal organs: liver, intestine, and exocrine pancreas. Developmental dynamics : an official publication of the American Association of Anatomists 230, 165-173.

Muller, F., Blader, P., Rastegar, S., Fischer, N., Knochel, W., Strahle, U., 1999. Characterization of zebrafish smad1, smad2 and smad5: the amino-terminus of smad1 and smad5 is required for specific function in the embryo. Mechanisms of development 88, 73-88.

Mullins, M.C., Hammerschmidt, M., Haffter, P., Nusslein-Volhard, C., 1994. Large-scale mutagenesis in the zebrafish: in search of genes controlling development in a vertebrate. Current biology : CB 4, 189-202.

Narla, A., Ebert, B.L., 2010. Ribosomopathies: human disorders of ribosome dysfunction. Blood 115, 3196-3205.

Naya, F.J., Huang, H.P., Qiu, Y., Mutoh, H., DeMayo, F.J., Leiter, A.B., Tsai, M.J., 1997. Diabetes, defective pancreatic morphogenesis, and abnormal enteroendocrine differentiation in BETA2/neuroD-deficient mice. Genes & development 11, 2323-2334.

Naye, F., Voz, M.L., Detry, N., Hammerschmidt, M., Peers, B., Manfroid, I., 2012. Essential roles of zebrafish bmp2a, fgf10, and fgf24 in the specification of the ventral pancreas. Molecular biology of the cell 23, 945-954.

Neuhauss, S.C., Solnica-Krezel, L., Schier, A.F., Zwartkruis, F., Stemple, D.L., Malicki, J., Abdelilah, S., Stainier, D.Y., Driever, W., 1996. Mutations affecting craniofacial development in zebrafish. Development 123, 357-367.

Ng, A.N., de Jong-Curtain, T.A., Mawdsley, D.J., White, S.J., Shin, J., Appel, B., Dong, P.D., Stainier, D.Y., Heath, J.K., 2005. Formation of the digestive system in zebrafish: III. Intestinal epithelium morphogenesis. Developmental biology 286, 114-135.

Nguyen, A.T., Emelyanov, A., Koh, C.H., Spitsbergen, J.M., Parinov, S., Gong, Z., 2012. An inducible kras(V12) transgenic zebrafish model for liver tumorigenesis and chemical drug screening. Disease models & mechanisms 5, 63-72.

Ni, J., Clark, K.J., Fahrenkrug, S.C., Ekker, S.C., 2008. Transposon tools hopping in vertebrates. Briefings in functional genomics & proteomics 7, 444-453.

Nissim, S., Sherwood, R.I., Wucherpfennig, J., Saunders, D., Harris, J.M., Esain, V., Carroll, K.J., Frechette, G.M., Kim, A.J., Hwang, K.L., Cutting, C.C., Elledge, S., North, T.E., Goessling, W., 2014. Prostaglandin E2 regulates liver versus pancreas cell-fate decisions and endodermal outgrowth. Developmental cell 28, 423-437.

Noel, E.S., Casal-Sueiro, A., Busch-Nentwich, E., Verkade, H., Dong, P.D., Stemple, D.L., Ober, E.A., 2008. Organ-specific requirements for Hdac1 in liver and pancreas formation. Developmental biology 322, 237-250.

Nolan, P.M., Hugill, A., Cox, R.D., 2002. ENU mutagenesis in the mouse: application to human genetic disease. Briefings in functional genomics & proteomics 1, 278-289.

Nousbeck, J., Spiegel, R., Ishida-Yamamoto, A., Indelman, M., Shani-Adir, A., Adir, N., Lipkin, E., Bercovici, S., Geiger, D., van Steensel, M.A., Steijlen, P.M., Bergman, R., Bindereif, A., Choder, M., Shalev, S., Sprecher, E., 2008. Alopecia, neurological defects, and endocrinopathy syndrome caused by decreased expression of RBM28, a nucleolar protein associated with ribosome biogenesis. American journal of human genetics 82, 1114-1121.

Nüsslein-Volhard, C., Dahm, R., 2002. Zebrafish. Oxford University Press.

O'Donohue, M.F., Choesmel, V., Faubladier, M., Fichant, G., Gleizes, P.E., 2010. Functional dichotomy of ribosomal proteins during the synthesis of mammalian 40S ribosomal subunits. The Journal of cell biology 190, 853-866.

Ober, E.A., Verkade, H., Field, H.A., Stainier, D.Y., 2006. Mesodermal Wnt2b signalling positively regulates liver specification. Nature 442, 688-691.

Odenthal, J., Nusslein-Volhard, C., 1998. fork head domain genes in zebrafish. Development genes and evolution 208, 245-258.

Offield, M.F., Jetton, T.L., Labosky, P.A., Ray, M., Stein, R.W., Magnuson, M.A., Hogan, B.L., Wright, C.V., 1996. PDX-1 is required for pancreatic outgrowth and differentiation of the rostral duodenum. Development 122, 983-995.

Ohlsson, H., Karlsson, K., Edlund, T., 1993. IPF1, a homeodomain-containing transactivator of the insulin gene. The EMBO journal 12, 4251-4259.

Oleykowski, C.A., Bronson Mullins, C.R., Godwin, A.K., Yeung, A.T., 1998. Mutation detection using a novel plant endonuclease. Nucleic acids research 26, 4597-4602.

Oltvai, Z.N., Milliman, C.L., Korsmeyer, S.J., 1993. Bcl-2 heterodimerizes in vivo with a conserved homolog, Bax, that accelerates programmed cell death. Cell 74, 609-619.

Pack, M., Solnica-Krezel, L., Malicki, J., Neuhauss, S.C., Schier, A.F., Stemple, D.L., Driever, W., Fishman, M.C., 1996. Mutations affecting development of zebrafish digestive organs. Development 123, 321-328.

Pan, F.C., Wright, C., 2011. Pancreas organogenesis: from bud to plexus to gland. Developmental dynamics : an official publication of the American Association of Anatomists 240, 530-565.

Pan, X., Wan, H., Chia, W., Tong, Y., Gong, Z., 2005. Demonstration of site-directed recombination in transgenic zebrafish using the Cre/loxP system. Transgenic research 14, 217-223.

Panse, V.G., Johnson, A.W., 2010. Maturation of eukaryotic ribosomes: acquisition of functionality. Trends in biochemical sciences 35, 260-266.

Parinov, S., Kondrichin, I., Korzh, V., Emelyanov, A., 2004. Tol2 transposon-mediated enhancer trap to identify developmentally regulated zebrafish genes in vivo. Developmental dynamics : an official publication of the American Association of Anatomists 231, 449-459.

Park, S.W., Davison, J.M., Rhee, J., Hruban, R.H., Maitra, A., Leach, S.D., 2008. Oncogenic KRAS induces progenitor cell expansion and malignant transformation in zebrafish exocrine pancreas. Gastroenterology 134, 2080-2090.

Parrella, S., Aspesi, A., Quarello, P., Garelli, E., Pavesi, E., Carando, A., Nardi, M., Ellis, S.R., Ramenghi, U., Dianzani, I., 2014. Loss of GATA-1 full length as a cause of Diamond-Blackfan anemia phenotype. Pediatric blood & cancer 61, 1319-1321.

Parsons, M.J., Pisharath, H., Yusuff, S., Moore, J.C., Siekmann, A.F., Lawson, N., Leach, S.D., 2009. Notch-responsive cells initiate the secondary transition in larval zebrafish pancreas. Mechanisms of development 126, 898-912.

Patton, E.E., Zon, L.I., 2001. The art and design of genetic screens: zebrafish. Nature reviews. Genetics 2, 956-966.

Pauls, S., Zecchin, E., Tiso, N., Bortolussi, M., Argenton, F., 2007. Function and regulation of zebrafish nkx2.2a during development of pancreatic islet and ducts. Developmental biology 304, 875-890.

Pisharath, H., Rhee, J.M., Swanson, M.A., Leach, S.D., Parsons, M.J., 2007. Targeted ablation of beta cells in the embryonic zebrafish pancreas using E. coli nitroreductase. Mechanisms of development 124, 218-229.

Plasterk, R.H., 2002. RNA silencing: the genome's immune system. Science 296, 1263-1265.

Pogoda, H.M., Solnica-Krezel, L., Driever, W., Meyer, D., 2000. The zebrafish forkhead transcription factor FoxH1/Fast1 is a modulator of nodal signaling required for organizer formation. Current biology : CB 10, 1041-1049.

Popovic, M., Goobie, S., Morrison, J., Ellis, L., Ehtesham, N., Richards, N., Boocock, G., Durie, P.R., Rommens, J.M., 2002. Fine mapping of the locus for Shwachman-Diamond syndrome at 7q11, identification of shared disease haplotypes, and exclusion of TPST1 as a candidate gene. European journal of human genetics : EJHG 10, 250-258.

Popperl, H., Rikhof, H., Chang, H., Haffter, P., Kimmel, C.B., Moens, C.B., 2000. lazarus is a novel pbx gene that globally mediates hox gene function in zebrafish. Molecular cell 6, 255-267.

Poulain, M., Furthauer, M., Thisse, B., Thisse, C., Lepage, T., 2006. Zebrafish endoderm formation is regulated by combinatorial Nodal, FGF and BMP signalling. Development 133, 2189-2200.

Poulain, M., Lepage, T., 2002. Mezzo, a paired-like homeobox protein is an immediate target of Nodal signalling and regulates endoderm specification in zebrafish. Development 129, 4901-4914.

Powell, G.T., Wright, G.J., 2011. Jamb and jamc are essential for vertebrate myocyte fusion. PLoS biology 9, e1001216.

Prieto, J.L., McStay, B., 2007. Recruitment of factors linking transcription and processing of pre-rRNA to NOR chromatin is UBF-dependent and occurs independent of transcription in human cells. Genes & development 21, 2041-2054.

Provost, E., Wehner, K.A., Zhong, X., Ashar, F., Nguyen, E., Green, R., Parsons, M.J., Leach, S.D., 2012. Ribosomal biogenesis genes play an essential and p53-independent role in zebrafish pancreas development. Development 139, 3232-3241.

Provost, E., Weier, C.A., Leach, S.D., 2013. Multiple ribosomal proteins are expressed at high levels in developing zebrafish endoderm and are required for normal exocrine pancreas development. Zebrafish 10, 161-169.

Qin, W., Chen, Z., Zhang, Y., Yan, R., Yan, G., Li, S., Zhong, H., Lin, S., 2014. Nom1 mediates pancreas development by regulating ribosome biogenesis in zebrafish. PloS one 9, e100796.

Reim, G., Mizoguchi, T., Stainier, D.Y., Kikuchi, Y., Brand, M., 2004. The POU domain protein spg (pou2/Oct4) is essential for endoderm formation in cooperation with the HMG domain protein casanova. Developmental cell 6, 91-101.

Reiter, A.K., Anthony, T.G., Anthony, J.C., Jefferson, L.S., Kimball, S.R., 2004. The mTOR signaling pathway mediates control of ribosomal protein mRNA translation in rat liver. The international journal of biochemistry & cell biology 36, 2169-2179.

Reiter, J.F., Kikuchi, Y., Stainier, D.Y., 2001. Multiple roles for Gata5 in zebrafish endoderm formation. Development 128, 125-135.

Ridanpaa, M., van Eenennaam, H., Pelin, K., Chadwick, R., Johnson, C., Yuan, B., vanVenrooij, W., Pruijn, G., Salmela, R., Rockas, S., Makitie, O., Kaitila, I., de la Chapelle, A., 2001. Mutations in the RNA component of RNase MRP cause a pleiotropic human disease, cartilage-hair hypoplasia. Cell 104, 195-203.

Roberts, I.M., 1990. Disorders of the pancreas in children. Gastroenterology clinics of North America 19, 963-973.

Robu, M.E., Larson, J.D., Nasevicius, A., Beiraghi, S., Brenner, C., Farber, S.A., Ekker, S.C., 2007. p53 activation by knockdown technologies. PLoS genetics 3, e78.

Rodaway, A., Takeda, H., Koshida, S., Broadbent, J., Price, B., Smith, J.C., Patient, R., Holder, N., 1999. Induction of the mesendoderm in the zebrafish germ ring by yolk cell-derived TGF-beta family signals and discrimination of mesoderm and endoderm by FGF. Development 126, 3067-3078.

Rosemary Siafakas, A., Richardson, D.R., 2009. Growth arrest and DNA damage-45 alpha (GADD45alpha). The international journal of biochemistry & cell biology 41, 986-989.

Rotig, A., Bourgeron, T., Chretien, D., Rustin, P., Munnich, A., 1995. Spectrum of mitochondrial DNA rearrangements in the Pearson marrow-pancreas syndrome. Human molecular genetics 4, 1327-1330.

Rotig, A., Colonna, M., Bonnefont, J.P., Blanche, S., Fischer, A., Saudubray, J.M., Munnich, A., 1989. Mitochondrial DNA deletion in Pearson's marrow/pancreas syndrome. Lancet 1, 902-903.

Roy, S., Qiao, T., Wolff, C., Ingham, P.W., 2001. Hedgehog signaling pathway is essential for pancreas specification in the zebrafish embryo. Current biology : CB 11, 1358-1363.

Rubbi, C.P., Milner, J., 2003. Disruption of the nucleolus mediates stabilization of p53 in response to DNA damage and other stresses. The EMBO journal 22, 6068-6077.

Sander, M., Neubuser, A., Kalamaras, J., Ee, H.C., Martin, G.R., German, M.S., 1997. Genetic analysis reveals that PAX6 is required for normal transcription of pancreatic hormone genes and islet development. Genes & development 11, 1662-1673.

Sander, M., Sussel, L., Conners, J., Scheel, D., Kalamaras, J., Dela Cruz, F., Schwitzgebel, V., Hayes-Jordan, A., German, M., 2000. Homeobox gene Nkx6.1 lies downstream of Nkx2.2 in the major pathway of beta-cell formation in the pancreas. Development 127, 5533-5540.

Sankaran, V.G., Ghazvinian, R., Do, R., Thiru, P., Vergilio, J.A., Beggs, A.H., Sieff, C.A., Orkin, S.H., Nathan, D.G., Lander, E.S., Gazda, H.T., 2012. Exome sequencing identifies GATA1 mutations resulting in Diamond-Blackfan anemia. The Journal of clinical investigation 122, 2439-2443.

Schier, A.F., 2013. Genomics: Zebrafish earns its stripes. Nature 496, 443-444.

Serafimidis, I., Heximer, S., Beis, D., Gavalas, A., 2011. G protein-coupled receptor signaling and sphingosine-1-phosphate play a phylogenetically conserved role in endocrine pancreas morphogenesis. Molecular and cellular biology 31, 4442-4453.

Shaham, O., Menuchin, Y., Farhy, C., Ashery-Padan, R., 2012. Pax6: a multi-level regulator of ocular development. Progress in retinal and eye research 31, 351-376.

Sheldon, W., 1964. Congenital Pancreatic Lipase Deficiency. Archives of disease in childhood 39, 268-271.

Sheppard, D.N., Welsh, M.J., 1999. Structure and function of the CFTR chloride channel. Physiological reviews 79, S23-45.

Shu, X., Cheng, K., Patel, N., Chen, F., Joseph, E., Tsai, H.J., Chen, J.N., 2003. Na,K-ATPase is essential for embryonic heart development in the zebrafish. Development 130, 6165-6173.

Signer, R.A., Magee, J.A., Salic, A., Morrison, S.J., 2014. Haematopoietic stem cells require a highly regulated protein synthesis rate. Nature 509, 49-54.

Sirotkin, H.I., Gates, M.A., Kelly, P.D., Schier, A.F., Talbot, W.S., 2000. Fast1 is required for the development of dorsal axial structures in zebrafish. Current biology : CB 10, 1051-1054.

Sjolund, K., Haggmark, A., Ihse, I., Skude, G., Karnstrom, U., Wikander, M., 1991. Selective deficiency of pancreatic amylase. Gut 32, 546-548.

Slack, J.M., 1995. Developmental biology of the pancreas. Development 121, 1569-1580.

Smith, L., Greenfield, A., 2003. DNA microarrays and development. Human molecular genetics 12 Spec No 1, R1-8.

Solnica-Krezel, L., Schier, A.F., Driever, W., 1994. Efficient recovery of ENU-induced mutations from the zebrafish germline. Genetics 136, 1401-1420.

Song, B., Zhang, Q., Zhang, Z., Wan, Y., Jia, Q., Wang, X., Zhu, X., Leung, A.Y., Cheng, T., Fang, X., Yuan, W., Jia, H., 2014. Systematic transcriptome analysis of the zebrafish model of diamond-blackfan anemia induced by RPS24 deficiency. BMC genomics 15, 759.

Song, G., Li, Q., Long, Y., Gu, Q., Hackett, P.B., Cui, Z., 2012a. Effective gene trapping mediated by Sleeping Beauty transposon. PloS one 7, e44123.

Song, G., Li, Q., Long, Y., Hackett, P.B., Cui, Z., 2012b. Effective expression-independent gene trapping and mutagenesis mediated by Sleeping Beauty transposon. Journal of genetics and genomics = Yi chuan xue bao 39, 503-520.

Song, J., Kim, H.J., Gong, Z., Liu, N.A., Lin, S., 2007. Vhnf1 acts downstream of Bmp, Fgf, and RA signals to regulate endocrine beta cell development in zebrafish. Developmental biology 303, 561-575.

Sosa-Pineda, B., Chowdhury, K., Torres, M., Oliver, G., Gruss, P., 1997. The Pax4 gene is essential for differentiation of insulin-producing beta cells in the mammalian pancreas. Nature 386, 399-402.

Soussi, T., Dehouche, K., Beroud, C., 2000. p53 website and analysis of p53 gene mutations in human cancer: forging a link between epidemiology and carcinogenesis. Human mutation 15, 105-113.

Soyer, J., Flasse, L., Raffelsberger, W., Beucher, A., Orvain, C., Peers, B., Ravassard, P., Vermot, J., Voz, M.L., Mellitzer, G., Gradwohl, G., 2010. Rfx6 is an Ngn3-dependent winged helix transcription factor required for pancreatic islet cell development. Development 137, 203-212.

St-Onge, L., Sosa-Pineda, B., Chowdhury, K., Mansouri, A., Gruss, P., 1997. Pax6 is required for differentiation of glucagon-producing alpha-cells in mouse pancreas. Nature 387, 406-409.

Stachura, D.L., Traver, D., 2011. Cellular dissection of zebrafish hematopoiesis. Methods in cell biology 101, 75-110.

Stafford, D., Prince, V.E., 2002. Retinoic acid signaling is required for a critical early step in zebrafish pancreatic development. Current biology : CB 12, 1215-1220.

Stafford, D., White, R.J., Kinkel, M.D., Linville, A., Schilling, T.F., Prince, V.E., 2006. Retinoids signal directly to zebrafish endoderm to specify insulin-expressing beta-cells. Development 133, 949-956.

Stormon, M.O., Durie, P.R., 2002. Pathophysiologic basis of exocrine pancreatic dysfunction in childhood. Journal of pediatric gastroenterology and nutrition 35, 8-21.

Streisinger, G., Walker, C., Dower, N., Knauber, D., Singer, F., 1981. Production of clones of homozygous diploid zebra fish (Brachydanio rerio). Nature 291, 293-296.

Stuart, G.W., McMurray, J.V., Westerfield, M., 1988. Replication, integration and stable germ-line transmission of foreign sequences injected into early zebrafish embryos. Development 103, 403-412.

Stuckenholz, C., Lu, L., Thakur, P., Kaminski, N., Bahary, N., 2009. FACS-assisted microarray profiling implicates novel genes and pathways in zebrafish gastrointestinal tract development. Gastroenterology 137, 1321-1332.

Subramanian, A., Tamayo, P., Mootha, V.K., Mukherjee, S., Ebert, B.L., Gillette, M.A., Paulovich, A., Pomeroy, S.L., Golub, T.R., Lander, E.S., Mesirov, J.P., 2005. Gene set enrichment analysis: a knowledge-based approach for interpreting genome-wide expression profiles. Proceedings of the National Academy of Sciences of the United States of America 102, 15545-15550.

Summerton, J., 1999. Morpholino antisense oligomers: the case for an RNase H-independent structural type. Biochimica et biophysica acta 1489, 141-158.

Summerton, J., Weller, D., 1997. Morpholino antisense oligomers: design, preparation, and properties. Antisense & nucleic acid drug development 7, 187-195.

Sun, C., Woolford, J.L., Jr., 1994. The yeast NOP4 gene product is an essential nucleolar protein required for pre-rRNA processing and accumulation of 60S ribosomal subunits. The EMBO journal 13, 3127-3135.

Sun, C., Woolford, J.L., Jr., 1997. The yeast nucleolar protein Nop4p contains four RNA recognition motifs necessary for ribosome biogenesis. The Journal of biological chemistry 272, 25345-25352.

Sun, Z., Hopkins, N., 2001. vhnf1, the MODY5 and familial GCKD-associated gene, regulates regional specification of the zebrafish gut, pronephros, and hindbrain. Genes & development 15, 3217-3229.

Talwar, P.K., Jhingran, A.G., 1991. Inland Fishes of India and Adjacent Countries. Taylor & Francis.

Tao, T., Shi, H., Guan, Y., Huang, D., Chen, Y., Lane, D.P., Chen, J., Peng, J., 2013a. Def defines a conserved nucleolar pathway that leads p53 to proteasome-independent degradation. Cell research.

Tao, T., Shi, H., Huang, D., Peng, J., 2013b. Def functions as a cell autonomous factor in organogenesis of digestive organs in zebrafish. PloS one 8, e58858.

Taylor, A.M., Humphries, J.M., White, R.M., Murphey, R.D., Burns, C.E., Zon, L.I., 2012. Hematopoietic defects in rps29 mutant zebrafish depend upon p53 activation. Experimental hematology 40, 228-237 e225.

Tehrani, Z., Lin, S., 2011. Antagonistic interactions of hedgehog, Bmp and retinoic acid signals control zebrafish endocrine pancreas development. Development 138, 631-640.

The Treacher Collins Syndrome Collaborative Group, 1996. Positional cloning of a gene involved in the pathogenesis of Treacher Collins syndrome. The Treacher Collins Syndrome Collaborative Group. Nature genetics 12, 130-136.

Thiel, C.T., Horn, D., Zabel, B., Ekici, A.B., Salinas, K., Gebhart, E., Ruschendorf, F., Sticht, H., Spranger, J., Muller, D., Zweier, C., Schmitt, M.E., Reis, A., Rauch, A., 2005. Severely incapacitating mutations in patients with extreme short stature identify RNA-processing endoribonuclease RMRP as an essential cell growth regulator. American journal of human genetics 77, 795-806.

Thisse, B., Wright, C.V., Thisse, C., 2000. Activin- and Nodal-related factors control antero-posterior patterning of the zebrafish embryo. Nature 403, 425-428.

Thisse, C., Thisse, B., 2008. High-resolution in situ hybridization to whole-mount zebrafish embryos. Nature protocols 3, 59-69.

Thummel, R., Burket, C.T., Brewer, J.L., Sarras, M.P., Jr., Li, L., Perry, M., McDermott, J.P., Sauer, B., Hyde, D.R., Godwin, A.R., 2005. Cre-mediated site-specific recombination in zebrafish embryos. Developmental dynamics : an official publication of the American Association of Anatomists 233, 1366-1377.

Thummel, R., Burket, C.T., Hyde, D.R., 2006. Two different transgenes to study gene silencing and re-expression during zebrafish caudal fin and retinal regeneration. TheScientificWorldJournal 6 Suppl 1, 65-81.

Tiso, N., Filippi, A., Pauls, S., Bortolussi, M., Argenton, F., 2002. BMP signalling regulates anteroposterior endoderm patterning in zebrafish. Mechanisms of development 118, 29-37.

Tiso, N., Moro, E., Argenton, F., 2009. Zebrafish pancreas development. Molecular and cellular endocrinology 312, 24-30.

Tokino, T., Nakamura, Y., 2000. The role of p53-target genes in human cancer. Critical reviews in oncology/hematology 33, 1-6.

Townes, P.L., 1965. Trypsinogen Deficiency Disease. The Journal of pediatrics 66, 275-285.

Trede, N.S., Medenbach, J., Damianov, A., Hung, L.H., Weber, G.J., Paw, B.H., Zhou, Y., Hersey, C., Zapata, A., Keefe, M., Barut, B.A., Stuart, A.B., Katz, T., Amemiya, C.T., Zon, L.I., Bindereif, A., 2007. Network of coregulated spliceosome components revealed by zebrafish mutant in recycling factor p110. Proceedings of the National Academy of Sciences of the United States of America 104, 6608-6613.

Uechi, T., Nakajima, Y., Chakraborty, A., Torihara, H., Higa, S., Kenmochi, N., 2008. Deficiency of ribosomal protein S19 during early embryogenesis leads to reduction of erythrocytes in a zebrafish model of Diamond-Blackfan anemia. Human molecular genetics 17, 3204-3211.

Urnov, F.D., Rebar, E.J., Holmes, M.C., Zhang, H.S., Gregory, P.D., 2010. Genome editing with engineered zinc finger nucleases. Nature reviews. Genetics 11, 636-646.

Vadlamudi, R.K., Wang, R.A., Mazumdar, A., Kim, Y., Shin, J., Sahin, A., Kumar, R., 2001. Molecular cloning and characterization of PELP1, a novel human coregulator of estrogen receptor alpha. The Journal of biological chemistry 276, 38272-38279.

Valdez, B.C., Henning, D., So, R.B., Dixon, J., Dixon, M.J., 2004. The Treacher Collins syndrome (TCOF1) gene product is involved in ribosomal DNA gene transcription by interacting with upstream binding factor. Proceedings of the National Academy of Sciences of the United States of America 101, 10709-10714.

Van den Berghe, H., Cassiman, J.J., David, G., Fryns, J.P., Michaux, J.L., Sokal, G., 1974. Distinct haematological disorder with deletion of long arm of no. 5 chromosome. Nature 251, 437-438.

van Ruissen, F., Ruijter, J.M., Schaaf, G.J., Asgharnegad, L., Zwijnenburg, D.A., Kool, M., Baas, F., 2005. Evaluation of the similarity of gene expression data estimated with SAGE and Affymetrix GeneChips. BMC genomics 6, 91.

Varshney, G.K., Lu, J., Gildea, D.E., Huang, H., Pei, W., Yang, Z., Huang, S.C., Schoenfeld, D., Pho, N.H., Casero, D., Hirase, T., Mosbrook-Davis, D., Zhang, S., Jao, L.E., Zhang, B., Woods, I.G., Zimmerman, S., Schier, A.F., Wolfsberg, T.G., Pellegrini, M., Burgess, S.M., Lin, S., 2013. A large-scale zebrafish gene knockout resource for the genome-wide study of gene function. Genome research 23, 727-735.

Velculescu, V.E., Zhang, L., Vogelstein, B., Kinzler, K.W., 1995. Serial analysis of gene expression. Science 270, 484-487.

Verbruggen, V., Ek, O., Georlette, D., Delporte, F., Von Berg, V., Detry, N., Biemar, F., Coutinho, P., Martial, J.A., Voz, M.L., Manfroid, I., Peers, B., 2010. The Pax6b homeodomain is dispensable for pancreatic endocrine cell differentiation in zebrafish. The Journal of biological chemistry 285, 13863-13873.

Vesterlund, L., Jiao, H., Unneberg, P., Hovatta, O., Kere, J., 2011. The zebrafish transcriptome during early development. BMC developmental biology 11, 30.

Wallace, K.N., Pack, M., 2003. Unique and conserved aspects of gut development in zebrafish. Developmental biology 255, 12-29.

Wallace, K.N., Yusuff, S., Sonntag, J.M., Chin, A.J., Pack, M., 2001. Zebrafish hhex regulates liver development and digestive organ chirality. Genesis 30, 141-143.

Walsh, D., Mohr, I., 2011. Viral subversion of the host protein synthesis machinery. Nature reviews. Microbiology 9, 860-875.

Wan, H., Korzh, S., Li, Z., Mudumana, S.P., Korzh, V., Jiang, Y.J., Lin, S., Gong, Z., 2006. Analyses of pancreas development by generation of gfp transgenic zebrafish using an exocrine pancreas-specific elastaseA gene promoter. Experimental cell research 312, 1526-1539.

Wang, D., Jao, L.E., Zheng, N., Dolan, K., Ivey, J., Zonies, S., Wu, X., Wu, K., Yang, H., Meng, Q., Zhu, Z., Zhang, B., Lin, S., Burgess, S.M., 2007. Efficient genome-wide mutagenesis of zebrafish genes by retroviral insertions. Proceedings of the National Academy of Sciences of the United States of America 104, 12428-12433.

Wang, Y., Rovira, M., Yusuff, S., Parsons, M.J., 2011. Genetic inducible fate mapping in larval zebrafish reveals origins of adult insulin-producing beta-cells. Development 138, 609-617.

Wang, Z., Gerstein, M., Snyder, M., 2009. RNA-Seq: a revolutionary tool for transcriptomics. Nature reviews. Genetics 10, 57-63.

Warga, R.M., Nusslein-Volhard, C., 1999. Origin and development of the zebrafish endoderm. Development 126, 827-838.

Warner, J.R., Vilardell, J., Sohn, J.H., 2001. Economics of ribosome biosynthesis. Cold Spring Harbor symposia on quantitative biology 66, 567-574.

Waters, D.L., Dorney, S.F., Gaskin, K.J., Gruca, M.A., O'Halloran, M., Wilcken, B., 1990. Pancreatic function in infants identified as having cystic fibrosis in a neonatal screening program. The New England journal of medicine 322, 303-308.

Wei, C., Salichos, L., Wittgrove, C.M., Rokas, A., Patton, J.G., 2012. Transcriptome-wide analysis of small RNA expression in early zebrafish development. RNA 18, 915-929.

Wendik, B., Maier, E., Meyer, D., 2004. Zebrafish mnx genes in endocrine and exocrine pancreas formation. Developmental biology 268, 372-383.

Wienholds, E., van Eeden, F., Kosters, M., Mudde, J., Plasterk, R.H., Cuppen, E., 2003. Efficient target-selected mutagenesis in zebrafish. Genome research 13, 2700-2707.

Wightman, B., Ha, I., Ruvkun, G., 1993. Posttranscriptional regulation of the heterochronic gene lin-14 by lin-4 mediates temporal pattern formation in C. elegans. Cell 75, 855-862.

Wilfinger, A., Arkhipova, V., Meyer, D., 2013. Cell type and tissue specific function of islet genes in zebrafish pancreas development. Developmental biology 378, 25-37.

Wilkins, B.J., Lorent, K., Matthews, R.P., Pack, M., 2013. p53-mediated biliary defects caused by knockdown of cirh1a, the zebrafish homolog of the gene responsible for North American Indian Childhood Cirrhosis. PloS one 8, e77670.

Wong, A.C., Draper, B.W., Van Eenennaam, A.L., 2011a. FLPe functions in zebrafish embryos. Transgenic research 20, 409-415.

Wong, C.C., Traynor, D., Basse, N., Kay, R.R., Warren, A.J., 2011b. Defective ribosome assembly in Shwachman-Diamond syndrome. Blood 118, 4305-4312.

Xiong, X., Zhao, Y., He, H., Sun, Y., 2011. Ribosomal protein S27-like and S27 interplay with p53-MDM2 axis as a target, a substrate and a regulator. Oncogene 30, 1798-1811.

Yang, H., Zhou, Y., Gu, J., Xie, S., Xu, Y., Zhu, G., Wang, L., Huang, J., Ma, H., Yao, J., 2013. Deep mRNA sequencing analysis to capture the transcriptome landscape of zebrafish embryos and larvae. PloS one 8, e64058.

Yee, N.S., 2010. Zebrafish as a biological system for identifying and validating therapeutic targets and compounds. Drug Discovery in Pancreatic Cancer, 95-112.

Yee, N.S., Gong, W., Huang, Y., Lorent, K., Dolan, A.C., Maraia, R.J., Pack, M., 2007. Mutation of RNA Pol III subunit rpc2/polr3b Leads to Deficiency of Subunit Rpc11 and disrupts zebrafish digestive development. PLoS biology 5, e312.

Yee, N.S., Lorent, K., Pack, M., 2005. Exocrine pancreas development in zebrafish. Developmental biology 284, 84-101.

Yee, N.S., Yusuff, S., Pack, M., 2001. Zebrafish pdx1 morphant displays defects in pancreas development and digestive organ chirality, and potentially identifies a multipotent pancreas progenitor cell. Genesis 30, 137-140.

Yu, B., Mitchell, G.A., Richter, A., 2009. Cirhin up-regulates a canonical NF-kappaB element through strong interaction with Cirip/HIVEP1. Experimental cell research 315, 3086-3098.

Zamore, P.D., 2002. Ancient pathways programmed by small RNAs. Science 296, 1265-1269.

Zauberman, A., Flusberg, D., Haupt, Y., Barak, Y., Oren, M., 1995. A functional p53-responsive intronic promoter is contained within the human mdm2 gene. Nucleic acids research 23, 2584-2592.

Zecchin, E., Filippi, A., Biemar, F., Tiso, N., Pauls, S., Ellertsdottir, E., Gnugge, L., Bortolussi, M., Driever, W., Argenton, F., 2007. Distinct delta and jagged genes control sequential segregation of pancreatic cell types from precursor pools in zebrafish. Developmental biology 301, 192-204.

Zecchin, E., Mavropoulos, A., Devos, N., Filippi, A., Tiso, N., Meyer, D., Peers, B., Bortolussi, M., Argenton, F., 2004. Evolutionary conserved role of ptf1a in the specification of exocrine pancreatic fates. Developmental biology 268, 174-184.

Zenker, M., Mayerle, J., Lerch, M.M., Tagariello, A., Zerres, K., Durie, P.R., Beier, M., Hulskamp, G., Guzman, C., Rehder, H., Beemer, F.A., Hamel, B., Vanlieferinghen, P., Gershoni-Baruch, R., Vieira, M.W., Dumic, M., Auslender, R., Gil-da-Silva-Lopes, V.L., Steinlicht, S., Rauh, M., Shalev, S.A., Thiel, C., Ekici, A.B., Winterpacht, A., Kwon, Y.T., Varshavsky, A., Reis, A., 2005. Deficiency of UBR1, a ubiquitin ligase of the N-end rule pathway, causes pancreatic dysfunction, malformations and mental retardation (Johanson-Blizzard syndrome). Nature genetics 37, 1345-1350.

Zenker, M., Mayerle, J., Reis, A., Lerch, M.M., 2006. Genetic basis and pancreatic biology of Johanson-Blizzard syndrome. Endocrinology and metabolism clinics of North America 35, 243-253, vii-viii.

Zhang, S., Shi, M., Hui, C.C., Rommens, J.M., 2006. Loss of the mouse ortholog of the shwachman-diamond syndrome gene (Sbds) results in early embryonic lethality. Molecular and cellular biology 26, 6656-6663.

Zhao, C., Andreeva, V., Gibert, Y., LaBonty, M., Lattanzi, V., Prabhudesai, S., Zhou, Y., Zon, L., McCann, K.L., Baserga, S., Yelick, P.C., 2014. Tissue specific roles for the ribosome biogenesis factor Wdr43 in zebrafish development. PLoS genetics 10, e1004074.

Zheng, W., Xu, H., Lam, S.H., Luo, H., Karuturi, R.K., Gong, Z., 2013. Transcriptomic analyses of sexual dimorphism of the zebrafish liver and the effect of sex hormones. PloS one 8, e53562.

Zorn, A.M., Wells, J.M., 2009. Vertebrate endoderm development and organ formation. Annual review of cell and developmental biology 25, 221-251.

Appendices

Gene Name	Gene Description	Adjusted *p*-value (Benjamini–Hochberg)	Log 2 fold change (*nol9*^{sa1022}/wild-type)
nol9	*nucleolar protein 9*	0.0127	-1.16
senp3b	*SUMO1/sentrin/SMT3 specific peptidase 3b*	$1.13x10^{-5}$	1.14
las11	*LAS1-like (S. cerevisiae)*	1	-0.166935452
senp3a	*SUMO1/sentrin/SMT3 specific peptidase 3a*	1	0.098424375
tex10	*testis expressed 10*	1	0.451582269
wdr18	*WD repeat domain 18*	1	0.357977686

Table A - 1 The list of genes encoding proteins that interact with Nol9 in *nol9*^{sa1022} mutants. The gene name and description, the adjusted *p*-value and the fold change of mutant versus wild-type sibling are shown.

GO Term ID	Term	K-S value
GO:0048565	digestive tract development	0.0043
GO:0001889	liver development	0.02733
GO:0055123	digestive system development	0.04959
GO:0031017	exocrine pancreas development	0.11301
GO:0031016	pancreas development	0.14306
GO:0048546	digestive tract morphogenesis	0.29657
GO:0031018	endocrine pancreas development	0.47669

Table A - 2 The list of GO terms associated with the digestive organs in *nol9*^{sa1022} mutants. The GO Term ID and name and the K-S value using topGO are shown.

Gene Name	Gene Description	Adjusted *p*-value (Benjamini–Hochberg)	Log 2 fold change (*nol9*^{sa1022}/wild-type)
yars	*tyrosyl-tRNA synthetase*	$1.38x10^{-7}$	1.42
tars	*threonyl-tRNA synthetase*	$5.78x10^{-6}$	1.22
qars	*glutaminyl-tRNA synthetase*	$5.87x10^{-5}$	1.27
eprs	*glutamyl-prolyl-tRNA synthetase*	$8.17x10^{-5}$	1.17
iars	*isoleucyl-tRNA synthetase*	$8.35x10^{-5}$	1.28
kars	*lysyl-tRNA synthetase*	0.000389147	0.97
iars	*isoleucyl-tRNA synthetase*	0.000619223	1.48
hars	*histidyl-tRNA synthetase*	0.0007359	0.99
farsa	*phenylalanyl-tRNA synthetase, alpha subunit*	0.001796306	0.94
rars	*arginyl-tRNA synthetase*	0.005236793	0.89
farsb	*phenylalanyl-tRNA synthetase, beta subunit*	0.013378278	0.86
nars	*asparaginyl-tRNA synthetase*	0.028617189	0.81
larsb	*leucyl-tRNA synthetase b*	0.030845695	0.84

Table A - 3 The differentially expressed genes belonging to the KEGG term 'Aminoacyl-tRNA biosynthesis' in *nol9*^{sa1022} mutants. The gene name and description, the adjusted *p*-value and the fold change of mutant versus wild-type sibling are shown.

Gene Name	Gene Description	Adjusted *p*-value (Benjamini–Hochberg)	Log 2 fold change (*nol9*^{sa1022}/wild-type)
ctps1a	*CTP synthase 1a*	2.03×10^{-8}	1.57
POLR1D	*polymerase (RNA) I polypeptide D, 16kDa*	7.10×10^{-7}	1.56
cad	*carbamoyl-phosphate synthetase 2, aspartate transcarbamylase, and dihydroorotase*	2.77×10^{-5}	1.22
polr1c	*polymerase (RNA) I polypeptide C*	0.000232932	1.31
polr1e	*polymerase (RNA) I polypeptide E*	0.000331795	1.22
upp2	*uridine phosphorylase 2*	0.000487591	-1.37
POLR3D	*polymerase (RNA) III (DNA directed) polypeptide D, 44kDa*	0.00213729	1.09
znrd1	*zinc ribbon domain containing 1*	0.00557888	1.52
txnrd1	*thioredoxin reductase 1*	0.005973931	0.85
zgc:110540	*zgc:110540*	0.014289753	-0.87
polr1a	*polymerase (RNA) I polypeptide A*	0.036743601	0.90
umps	*uridine monophosphate synthetase*	0.044072318	1.05
znrd1	*zinc ribbon domain containing 1*	0.04613515	1.65

Table A - 4 The differentially expressed genes belonging to the KEGG term 'Pyrimidine metabolism in *nol9*^{sa1022} mutants.. The gene name and description, the adjusted *p*-value and the fold change of mutant versus wild-type sibling are shown.

Gene Name	Gene Description	Adjusted *p*-value (Benjamini–Hochberg)	Log 2 fold change (*nol9*^{sa1022}/wild-type)
POLR1D	*polymerase (RNA) I polypeptide D, 16kDa*	7.10×10^{-7}	1.56
polr1c	*polymerase (RNA) I polypeptide C*	0.000232932	1.31
polr1e	*polymerase (RNA) I polypeptide E*	0.000331795	1.22
POLR3D	*polymerase (RNA) III (DNA directed) polypeptide D, 44kDa*	0.00213729	1.09
znrd1	*zinc ribbon domain containing 1*	0.00557888	1.52
polr1a	*polymerase (RNA) I polypeptide A*	0.036743601	0.90
znrd1	*zinc ribbon domain containing 1*	0.04613515	1.65

Table A - 5 The differentially expressed genes belonging to the KEGG term 'RNA polymerase' in *nol9*^{sa1022} mutants. The gene name and description, the adjusted *p*-value and the fold change of mutant versus wild-type sibling are shown.

Gene Name	Gene Description	Adjusted *p*-value (Benjamini–Hochberg)	Log 2 fold change (*nol9*^{sa1022}/wild-type)
las11	*LAS1-like (S. cerevisiae)*	1	-0.448606006
nol9	*nucleolar protein 9*	1	0.229556284
senp3a	*SUMO1/sentrin/SMT3 specific peptidase 3a*	1	0.236577597
senp3b	*SUMO1/sentrin/SMT3 specific peptidase 3b*	1	0.273886684
tex10	*testis expressed 10*	1	0.070232461
wdr18	*WD repeat domain 18*	1	0.618400968

Table A - 6 The list of genes encoding proteins that interact with Las1l in *las1l*^{sa674} mutants. The gene name and description, the adjusted *p*-value and the fold change of mutant versus wild-type sibling are shown.

GO Term ID	Term	K-S value
GO:0031016	pancreas development	0.00447
GO:0048565	digestive tract development	0.00941
GO:0031017	exocrine pancreas development	0.0102
GO:0001889	liver development	0.0472
GO:0048546	digestive tract morphogenesis	0.13953
GO:0055123	digestive system development	0.25312
GO:0031018	endocrine pancreas development	0.28337

Table A - 7 The list of GO terms associated with the digestive organs in *las1l*^{sa674} mutants. The GO Term ID and name and the K-S value using topGO are shown.

KEGG Term	Genes		Fold Enrichment	*p*-value	Adjusted *p*-value (Benjamini-Hochberg)
	#	%			
Aminoacyl-tRNA biosynthesis	16	2.46	7.14	2.64×10^{-10}	2.77×10^{-8}
PPAR signaling pathway	11	1.69	3.72	4.08×10^{-4}	0.021191437
Steroid biosynthesis	6	0.92	6.82	9.34×10^{-4}	0.032179842
Pyrimidine metabolism	12	1.84	2.42	0.008207939	0.194544645
Glutathione metabolism	7	1.08	3.50	0.01145079	0.21482917
Purine metabolism	14	2.15	1.99	0.019360768	0.289748562
Steroid hormone biosynthesis	5	0.77	4.46	0.020533482	0.267438789
Drug metabolism	6	0.92	3.57	0.021400618	0.247182337
Spliceosome	15	2.30	1.86	0.025918624	0.263887035
RNA polymerase	5	0.77	3.92	0.032950845	0.296587998

Table A - 8 The enriched KEGG terms of differentially expressed genes of *tti*^{s450} mutants at a statistical significance of *p*-value less than 0.05 using a modified Fisher's exact test. The KEGG term, the number of genes involved in the terms and the percentage of involved genes over total number of genes, the fold enrichment, the *p*-value and the adjusted *p*-value using Benjamini-Hochberg procedure are shown.

KEGG Term	Genes		Fold Enrichment	*p*-value	Adjusted *p*-value (Benjamini-Hochberg)
	#	%			
Aminoacyl-tRNA biosynthesis	15	2.81	7.87	3.45×10^{-10}	3.38×10^{-8}
PPAR signaling pathway	11	2.06	4.58	6.45×10^{-5}	0.003154475
Steroid biosynthesis	7	1.31	8.26	6.99×10^{-5}	0.002281903
Glutathione metabolism	7	1.31	3.96	0.006238015	0.142136284
Retinol metabolism	6	1.13	4.05	0.012889366	0.22452057
Steroid hormone biosynthesis	5	0.94	5.06	0.013361798	0.197251552
Purine metabolism	13	2.44	2.09	0.017599578	0.220098841
RNA polymerase	5	0.94	4.16	0.026950046	0.284424572
p53 signaling pathway	8	1.50	2.52	0.034401259	0.316949433
Metabolism of xenobiotics by cytochrome P450	4	0.75	4.72	0.046546298	0.373189632

Table A - 9 The enriched KEGG terms of differentially expressed genes of *set*^{s453} mutants at a statistical significance of *p*-value less than 0.05 using a modified Fisher's exact test. The KEGG term, the number of genes involved in the terms and the percentage of involved genes over total number of genes, the fold enrichment, the *p*-value and the adjusted *p*-value using Benjamini-Hochberg procedure are shown.

GO Term ID	Term	K-S value
Digestive organs		
GO:0031017	exocrine pancreas development	0.04942
GO:0048546	digestive tract morphogenesis	0.05708
GO:0001889	liver development	0.10248
GO:0031018	endocrine pancreas development	0.22476
GO:0055123	digestive system development	0.30988
GO:0048565	digestive tract development	0.31777
GO:0031016	pancreas development	0.36157
Eye		
GO:0031076	embryonic camera-type eye development	0.19883
GO:0048596	embryonic camera-type eye morphogenesis	0.34133
GO:0048048	embryonic eye morphogenesis	0.64118
GO:0001754	eye photoreceptor cell differentiation	0.70683
GO:0048593	camera-type eye morphogenesis	0.72337
GO:0048592	eye morphogenesis	0.78997
GO:0042462	eye photoreceptor cell development	0.92979
GO:0043010	camera-type eye development	0.95017
GO:0001654	eye development	0.95104
GO:0060041	retina development in camera-type eye	0.96029
GO:0060042	retina morphogenesis in camera-type eye	0.98179
Brain		
GO:0030902	hindbrain development	0.3064
GO:0007420	brain development	0.6693
GO:0030900	forebrain development	0.87958
GO:0030901	midbrain development	0.893
Cartilage		
GO:0051216	cartilage development	0.12518
Skeletal		
GO:0001501	skeletal system development	0.0204
GO:0048706	embryonic skeletal system development	0.26733
GO:0060538	skeletal muscle organ development	0.29114
GO:0048704	embryonic skeletal system morphogenesis	0.29273
GO:0048705	skeletal system morphogenesis	0.41744
GO:0007519	skeletal muscle tissue development	0.48451
GO:0048741	skeletal muscle fiber development	0.75617

Table A - 10 The list of GO terms associated with the digestive organs, eye, brain, cartilage and skeletal muscle in *tti*^{s450} mutants. The GO Term ID and name and the K-S value using topGO are shown.

GO Term ID	Term	K-S value
Digestive organs		
GO:0048565	digestive tract development	0.02479
GO:0055123	digestive system development	0.02639
GO:0001889	liver development	0.17341
GO:0031016	pancreas development	0.19378
GO:0031017	exocrine pancreas development	0.27094
GO:0048546	digestive tract morphogenesis	0.28365
GO:0031018	endocrine pancreas development	0.31304
Eye		
GO:0001654	eye development	0.08402
GO:0042462	eye photoreceptor cell development	0.17352
GO:0048048	embryonic eye morphogenesis	0.18294
GO:0043010	camera-type eye development	0.22899
GO:0048592	eye morphogenesis	0.24795
GO:0001754	eye photoreceptor cell differentiation	0.26204
GO:0031076	embryonic camera-type eye development	0.46281
GO:0048596	embryonic camera-type eye morphogenesis	0.55498
GO:0048593	camera-type eye morphogenesis	0.64427
GO:0060041	retina development in camera-type eye	0.75822
GO:0060042	retina morphogenesis in camera-type eye	0.89389
Cartilage		
GO:0051216	cartilage development	0.27115
Skeletal		
GO:0007519	skeletal muscle tissue development	0.00688
GO:0001501	skeletal system development	0.03697
GO:0048741	skeletal muscle fiber development	0.04216
GO:0060538	skeletal muscle organ development	0.0603
GO:0048705	skeletal system morphogenesis	0.12181
GO:0048704	embryonic skeletal system morphogenesis	0.14073
GO:0048706	embryonic skeletal system development	0.17811

Table A - 11 The list of GO terms associated with the digestive organs, eye, brain, cartilage and skeletal muscle in *set*^{s453} mutants. The GO Term ID and name and the K-S value using topGO are shown.

Gene Name	Gene Description	Adjusted *p*-value (Benjamini–Hochberg)	Log 2 fold change (*nol9*^{sa1022}/wild-type)
tti^{s450} mutant			
atg16l1	*ATG16 autophagy related 16-like 1 (S. cerevisiae)*	0.388405483	0.746690463
atg4b	*ATG4 autophagy related 4 homolog B (S. cerevisiae)*	0.488785713	0.817575752
atg9a	*ATG9 autophagy related 9 homolog A (S. cerevisiae)*	0.611158802	-0.772274754
atg5	*ATG5 autophagy related 5 homolog (S. cerevisiae)*	0.788039883	0.513492925
atg9a	*ATG9 autophagy related 9 homolog A (S. cerevisiae)*	0.818836971	-0.470201462
atg4c	*autophagy-related 4C (yeast)*	0.876251962	-0.476068028
atg10	*ATG10 autophagy related 10 homolog (S. cerevisiae)*	0.982750495	0.153372409
atg13	*ATG13 autophagy related 13 homolog (S. cerevisiae)*	0.983675464	-0.049780343
set^{s453} mutant			
atg16l1	*ATG16 autophagy related 16-like 1 (S. cerevisiae)*	0.609960781	0.648996789
atg10	*ATG10 autophagy related 10 homolog (S. cerevisiae)*	0.81602828	0.940493174
atg5	*ATG5 autophagy related 5 homolog (S. cerevisiae)*	0.833919644	0.638757882
atg12	*ATG12 autophagy related 12 homolog (S. cerevisiae)*	0.994165769	0.652995621
atg4b	*ATG4 autophagy related 4 homolog B (S. cerevisiae)*	0.99897654	0.516784842
atg13	*ATG13 autophagy related 13 homolog (S. cerevisiae)*	0.999674861	0.226912478
atg4c	*autophagy-related 4C (yeast)*	0.999674861	-0.204736068
atg9a	*ATG9 autophagy related 9 homolog A (S. cerevisiae)*	0.999674861	0.217419046
atg9a	*ATG9 autophagy related 9 homolog A (S. cerevisiae)*	0.999674861	-0.630197512
nol9^{sa1022} mutant			
atg4b	*ATG4 autophagy related 4 homolog B (S. cerevisiae)*	1	-0.18992073
atg13	*ATG13 autophagy related 13 homolog (S. cerevisiae)*	1	0.190786591
atg16l1	*ATG16 autophagy related 16-like 1 (S. cerevisiae)*	1	0.249922058
atg10	*ATG10 autophagy related 10 homolog (S. cerevisiae)*	1	0.486924121
atg4c	*autophagy-related 4C (yeast)*	1	0.241821933
atg5	*ATG5 autophagy related 5 homolog (S. cerevisiae)*	1	0.174871634
atg9a	*ATG9 autophagy related 9 homolog A (S. cerevisiae)*	1	-0.212406566
atg9a	*ATG9 autophagy related 9 homolog A (S. cerevisiae)*	1	-0.095397584
las1l^{sa674} mutant			
atg4b	*ATG4 autophagy related 4 homolog B (S. cerevisiae)*	1	0.014990544
atg13	*ATG13 autophagy related 13 homolog (S. cerevisiae)*	1	0.137029624
atg16l1	*ATG16 autophagy related 16-like 1 (S. cerevisiae)*	1	0.112731025
atg4c	*autophagy-related 4C (yeast)*	1	0.599221648
atg9a	*ATG9 autophagy related 9 homolog A (S. cerevisiae)*	1	-0.081416492
atg10	*ATG10 autophagy related 10 homolog (S. cerevisiae)*	1	0.162001033
atg5	*ATG5 autophagy related 5 homolog (S. cerevisiae)*	1	0.152707837
atg9a	*ATG9 autophagy related 9 homolog A (S. cerevisiae)*	1	-0.755265462

Table A - 12 The list of *autophagy-related genes* (*atg*) in *nol9*^{sa1022}, *las1l*^{sa674}, *tti*^{s450} and *set*^{453} mutants. The gene name and description, the adjusted *p*-value and the fold change of mutant over wild-type sibling are shown.

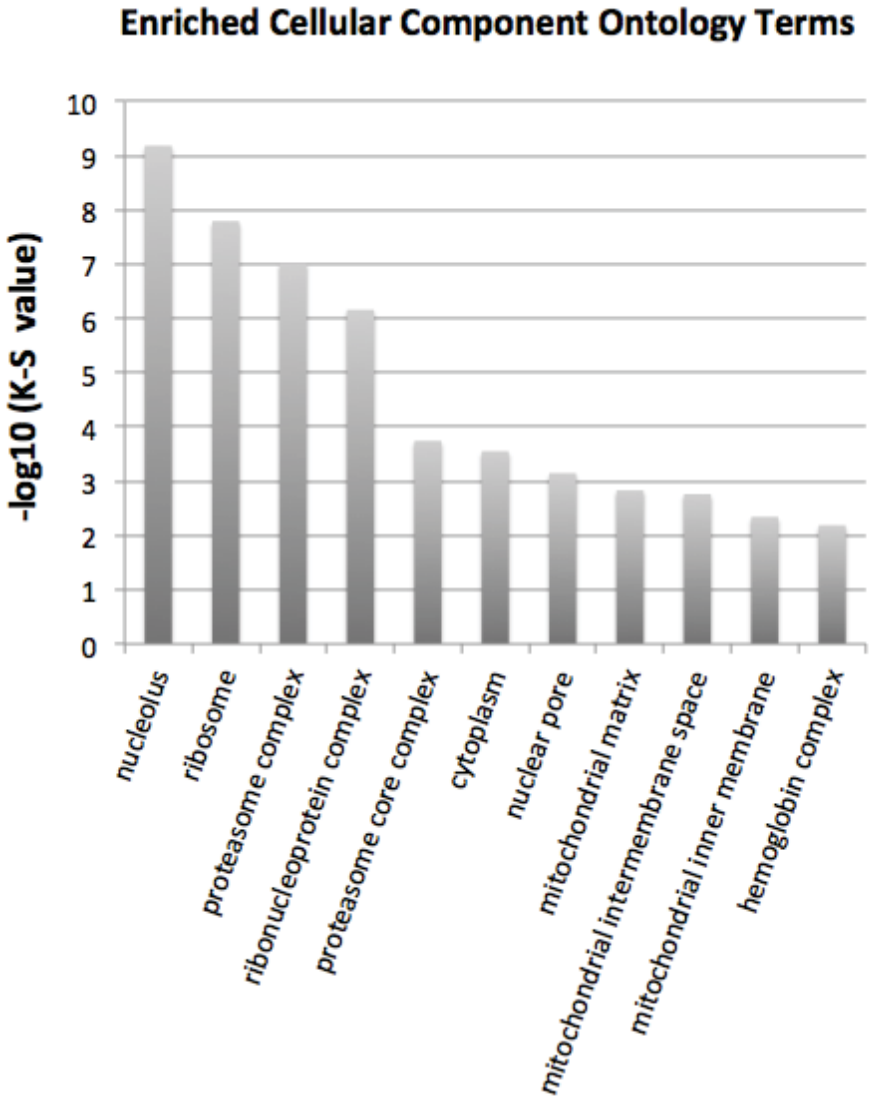

Figure A - 1 The enriched cellular component ontology terms in *tti*^{s450} mutants at statistical significance of K-S value less than 0.01 (-log10 (K-S value) more than 2.0).

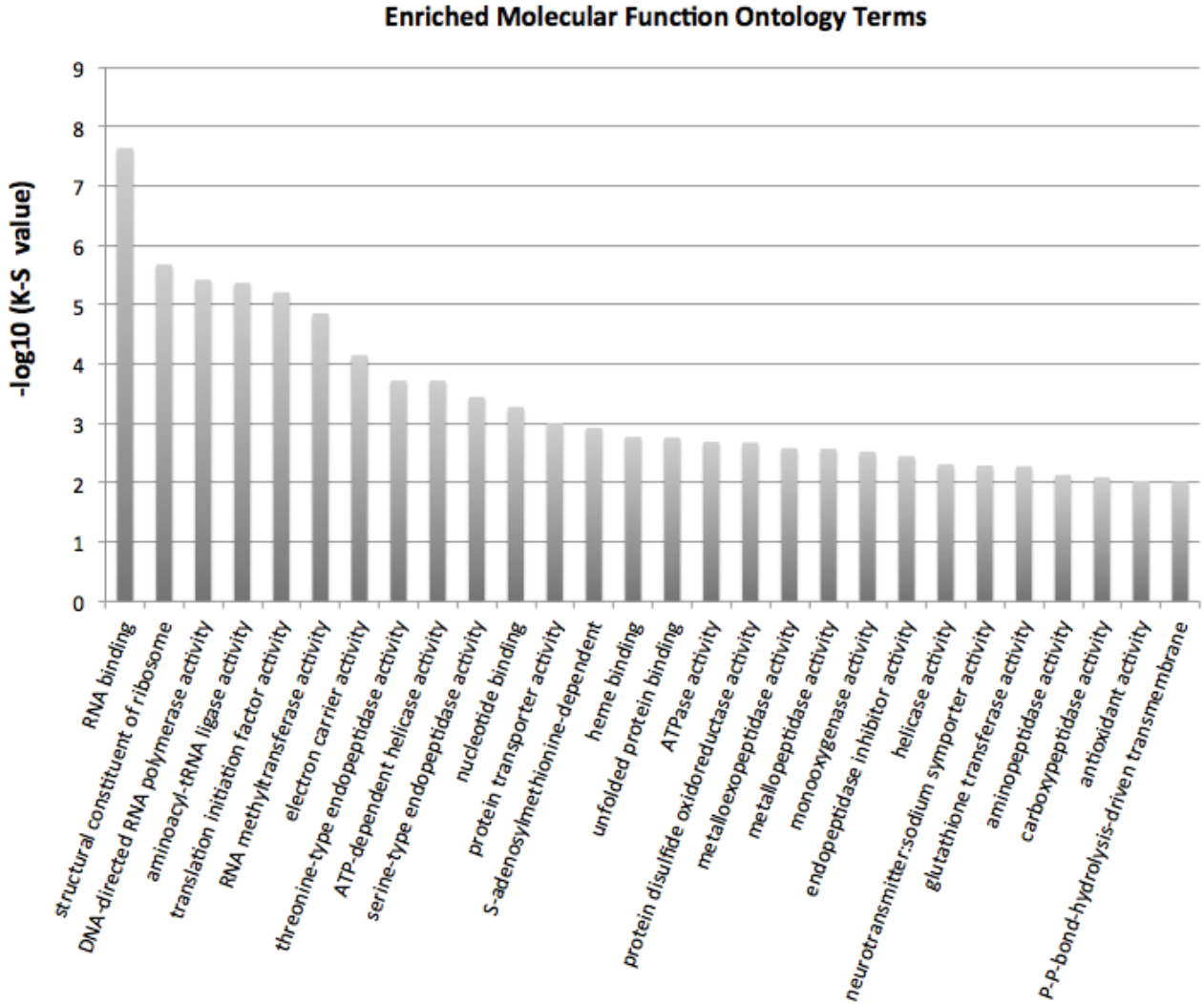

Figure A - 2 The enriched molecular function ontology terms in *tti*^{s450} mutants at statistical significance of K-S value less than 0.01 (-log10 (K-S value) more than 2.0).

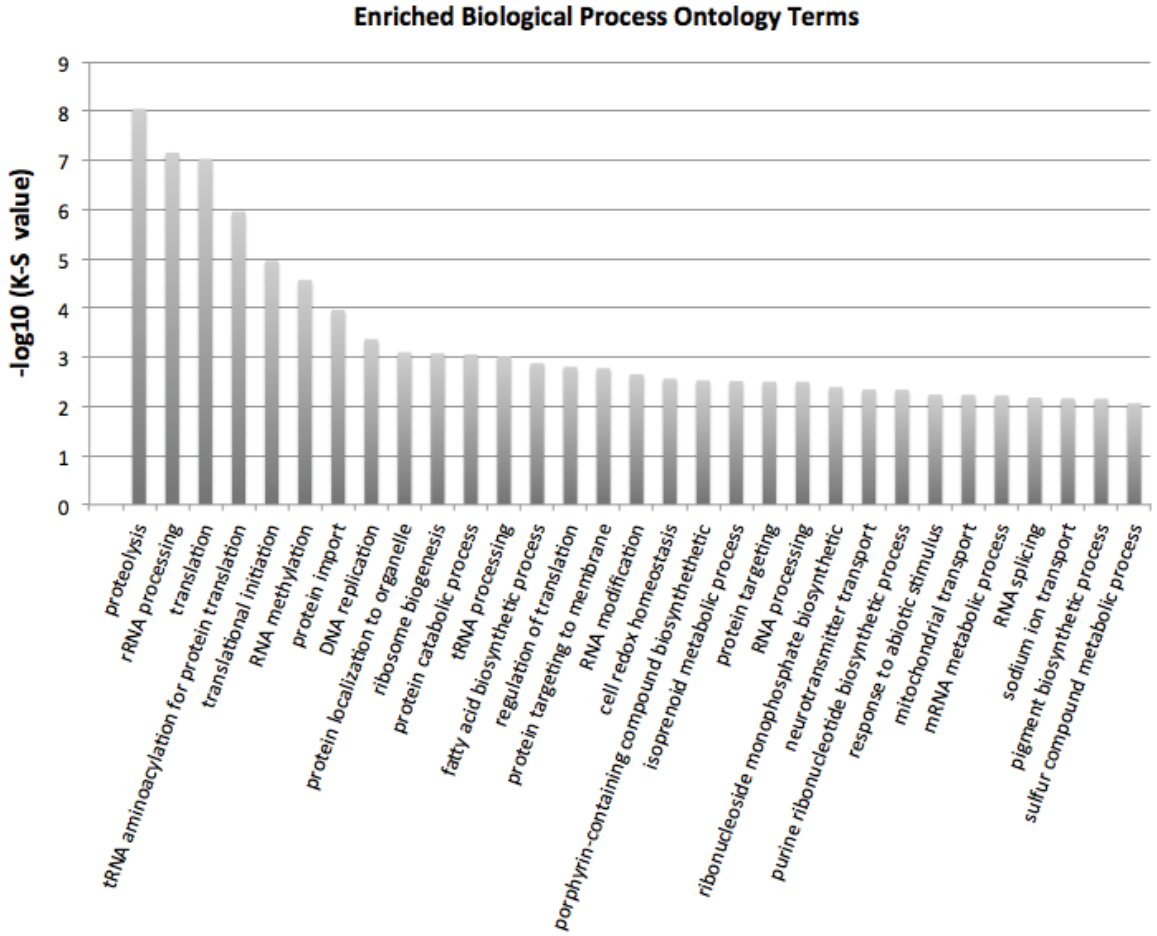

Figure A - 3 The enriched biological process ontology terms in *tti*^{s450} mutants at statistical significance of K-S value less than 0.01 (-log10 (K-S value) more than 2.0).

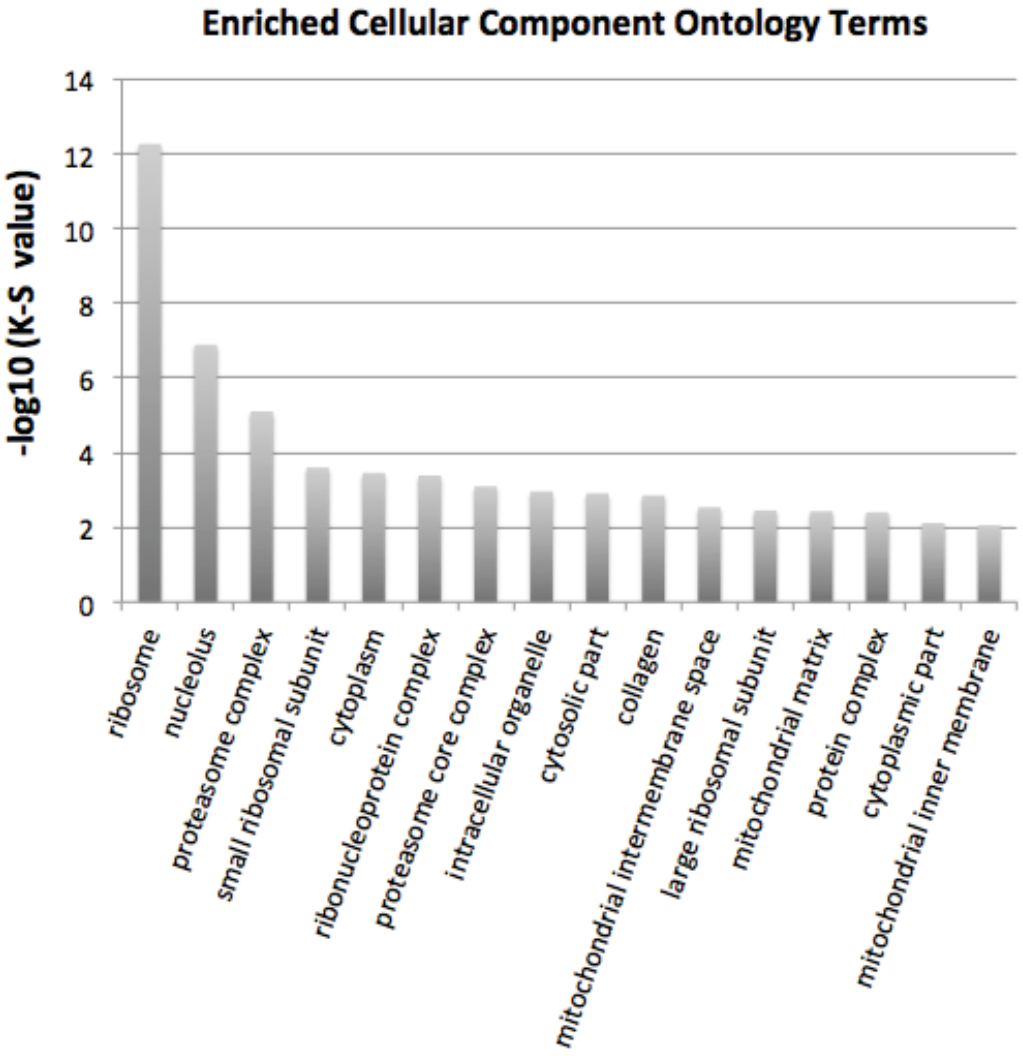

Figure A - 4 The enriched cellular component ontology terms in *set*^{s453} mutants at statistical significance of K-S value less than 0.01 (-log10 (K-S value) more than 2.0).

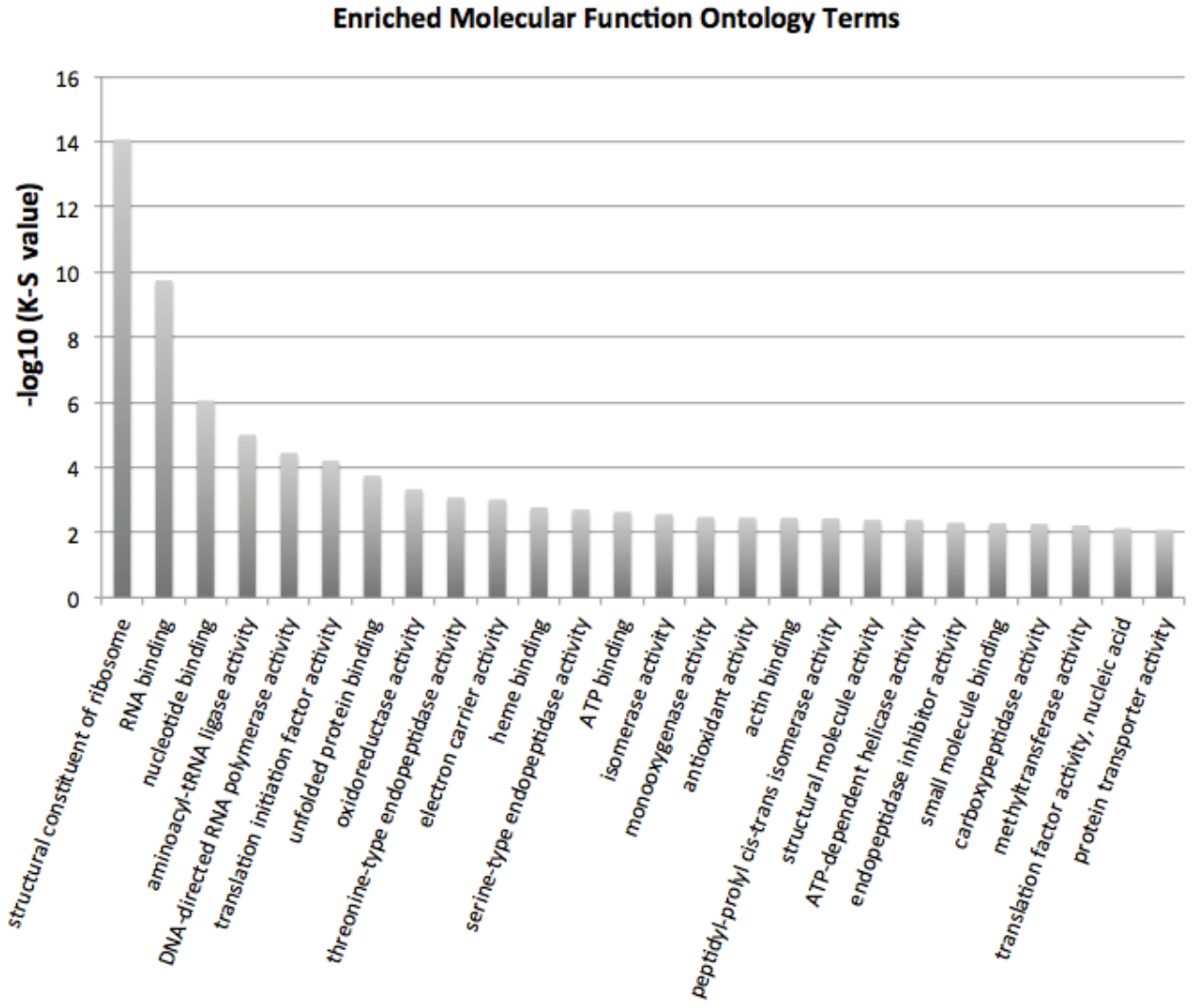

Figure A - 5 The enriched molecular function ontology terms in *set*^{s453} mutants at statistical significance of K-S value less than 0.01 (-log10 (K-S value) more than 2.0).

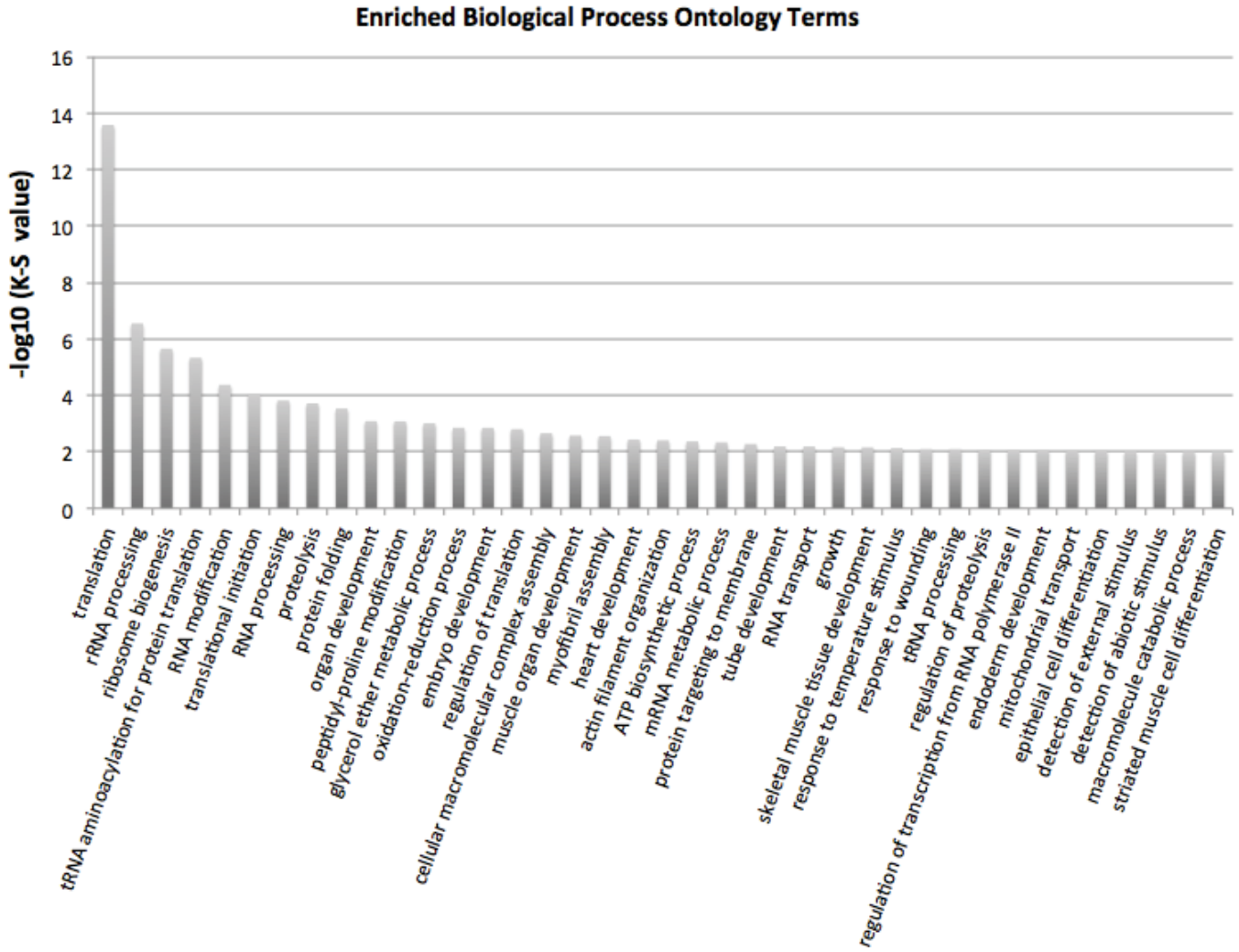

Figure A - 6 The enriched biological process ontology terms in *set*^{s453} mutants at statistical significance of K-S value less than 0.01 (-log10 (K-S value) more than 2.0